Improved Thermodynamic Modeling of Gas Hydrate Systems

by

Xin Chen

A thesis submitted in partial fulfillment of the requirements for the degree of

Doctor of Philosophy

in

Petroleum Engineering

Department of Civil and Environmental Engineering
University of Alberta

ABSTRACT

Natural gas hydrates are solid crystalline mixtures of water and small gas molecules that typically form at relatively low temperatures and moderate pressures. As a promising energy resource, the natural gas hydrates are discovered in many offshore and permafrost geological formations. Besides, the natural gas hydrates are also found to form in the pipelines located in cold areas and in the wellbores used in offshore petroleum industry, causing the flow assurance problems. The decomposition of in-situ hydrates during the exploitation process and the formation of hydrates in pipelines or wellbores will lead to a series of changes on the number of equilibrium phases and the phase compositions. How to accurately describe the phase behavior of natural gas hydrates plays a fundamentally important role in the accurate modeling of multiphase flow involving gas hydrates in both reservoirs and wellbores/pipelines. This study will start from developing improved thermodynamic frameworks that can improve the accuracy in modeling the phase behavior of reservoir fluids and gas hydrates. Then based on the improved thermodynamic models, we provide a reliable multiphase equilibrium calculation algorithm for gas hydrate systems.

As an efficient and reliable thermodynamic tool for modeling the multiphase behavior of reservoir fluids, cubic equation of state (CEOS) has been widely adopted in industrial simulators. However, most of the CEOS models cannot provide an accurate density prediction for the liquid phase. Although the temperature-volume-dependent volume translation (VT) is deemed as the most accurate method to correct the liquid density yielded by CEOS, the available VT-models do not fully exploit the potential of distance function and there is still a room for improving the prediction accuracy of saturated and single-phase liquid densities for water and hydrocarbons by VT-CEOS. Hence, this study proposes a series of improved VT-models to achieve more accurate

volumetric calculations for water, hydrocarbons and their mixtures. The absolute percentage deviations of the liquid molar volumes yielded by the newly-proposed VT-CEOSs for different compounds are usually lower than 1%.

In academia and industry, the van der Waals-Platteeuw (vdW-P) hydrate model is one of the most popular and classical hydrate-equilibrium calculation methods. Nevertheless, the hydrate equilibria of gas-mixture systems predicted by the vdW-P model are not as accurate as those predicted for pure-gas systems. In contrast to the previous studies that focused on the modifications of functional forms, the current study aims to provide new pragmatic strategies for tuning the gas-dependent parameters in the vdW-P hydrate model. A new procedure is developed for fitting the Kihara potential parameters in the vdW-P hydrate model using the experimental hydrate equilibrium data for both pure gases and binary-gas mixtures, considering the differences between hydrate structures I and II. As a result, the vdW-P model coupled with the newly fitted Kihara potential parameters performs well in gas hydrate equilibrium calculations and also properly detects the hydrate structure transition and cage occupancy behaviors.

Lastly, on the basis of the improved thermodynamic models, we develop an algorithm for multiphase equilibrium calculations in the presence of gas hydrates. The number of equilibrium phases that can be detected by this algorithm is up to four phases, i.e., a vapor phase, a hydrocarbon-rich liquid phase, an aqueous phase, and a gas hydrate phase. In this algorithm, a new criterion for determining the onset of hydrate dissociation is proposed based on van der Waals-Platteeuw model. To calculate the phase fractions and phase compositions, this new algorithm provides a series of material-balance equations involving hydrates. Example calculations demonstrate that this algorithm is capable of robustly conducting hydrate-inclusive multiphase equilibrium calculations for a given fluid at specified temperature and pressure.

PREFACE

A version of **Chapter 2** has been published as Chen, X. and Li, H. 2020. An Improved Volume-Translated SRK Equation of State Dedicated to More Accurate Determination of Saturated and Single-Phase Liquid Densities. Fluid Phase Equilibria, 521, 112724. Chen, X. is responsible for the theoretical development, simulation results, analysis, and manuscript composition. Li, H. is the supervisory author and gets involved in the concept formation, theoretical development, analysis, and manuscript composition.

A version of **Chapter 3** has been published as Chen, X. and Li, H. 2021. Improved Prediction of Saturated and Single-Phase Liquid Densities of Water through Volume-Translated SRK EOS. Fluid Phase Equilibria, 528, 112852. Chen, X. is responsible for the theoretical development, simulation results, analysis, and manuscript composition. Li, H. is the supervisory author and gets involved in the concept formation, theoretical development, analysis, and manuscript composition.

A version of **Chapter 4** has been published as Chen, X. and Li, H. 2022. New Pragmatic Strategies for Optimizing Kihara Potential Parameters Used in Van der Waals-Platteeuw Hydrate Model. Chemical Engineering Science, 248, 117213. Chen, X. is responsible for the theoretical development, simulation results, analysis, and manuscript composition. Li, H. is the supervisory author and gets involved in the concept formation, theoretical development, analysis, and manuscript composition.

A version of **Chapter 5** was submitted to Chemical Engineering Science for possible publication on June 25, 2022. Chen, X. is responsible for the theoretical development,

simulation results, analysis, and manuscript composition. Li, H. is the supervisory author and gets involved in the concept formation, theoretical development, analysis, and manuscript composition.

Chapter 1 summarizes the research background, problem statement, research objectives, and thesis structure. **Chapter 6** summarizes the conclusions reached in this thesis as well as the recommendations for future research. **Chapters 1** and **6** are originally written by Xin Chen and have never been published elsewhere.

DEDICATION

This dissertation is dedicated to my dearest parents: Mrs. Chongying Ni and Mr. Guoli Chen.

ACKNOWLEDGMENTS

I would like to express my appreciation to my supervisor Dr. Huazhou Li for his guidance towards my Ph.D. research and his assistance in preparing this thesis. I am also grateful to Dr. Yong Li, Dr. Tayfun Babadagli, Dr. Nobuo Maeda, Dr. Juliana Leung, Dr. Hao Zhang, and Dr. Yuanhang Chen for serving as my examination committee members as well as providing constructive comments/suggestions.

I would also like to thank the following individuals or organizations for their support during my Ph.D. program:

- The past and present group members in Dr. Li's research group.
- The China Scholarship Council (CSC) and the Natural Sciences and Engineering Research Council of Canada (NSERC) Discovery Grant for the financial support.
- All my friends and colleagues for their help.

TABLE OF CONTENTS

LIST OF TABLES

LIST OF FIGURES

CHAPTER 1 INTRODUCTION

1.1. Research Background

Natural gas hydrates are solid crystalline mixtures of water and small gas molecules. The gas molecules (guests) are encaged in the cavities (host) that are composed of hydrogen-bonded water molecules (Sloan, 2003). In general, natural gas contacting with sufficient water forms hydrate under relatively low temperatures and moderate pressures. Hence, natural gas hydrates can frequently appear in the pipelines located in cold areas and in the wellbores used in offshore petroleum industry, causing flow assurance problems. Besides, as a promising energy resource, natural gas hydrates are discovered in many offshore and permafrost geological formations. The decomposition of in-situ hydrates during the exploitation process and the formation of hydrates in pipelines or wellbores will lead to a series of changes on the number of equilibrium phases and the compositions in different phases. Thus, accurate modeling of gas hydrate equilibria is critical for describing multiphase flow involving gas hydrates, as it can provide insights for developing in-situ gas hydrates and preventing hydrate blockage in pipelines and wellbores.

In both academia and industry, the van der Waals and Platteeuw (vdW-P) model coupled with cubic equation of state (CEOS) is one of the most widely used methods for modeling the phase behavior of gas hydrate systems (van der Waals and Platteeuw, 1959; Medeiros et al., 2020). The vdW-P model can estimate the difference between the chemical potential of water in hydrate phase and that in ice or aqueous phase, helping to determine whether a hydrate phase appears. CEOSs serves as a reliable tool for describing the pressure-volume-temperature (PVT) relationships of fluids and calculating the fugacities of hydrate forming gases used in the vdW-P model.

Among the various robust CEOS models that have been developed in the past, Soave-Redlich-Kwong (SRK) EOS and Peng-Robinson (PR) EOS are the most widely used ones (Soave 1972; Peng and Robinson, 1976). However, most CEOSs cannot provide an accurate volumetric calculation for the liquid phase. Volume translation (VT) serves as a simple but effective technique to correct the liquid volume predicted by CEOS (Curtis and Michael, 2000). There are three types of VT models: 1) constant VT; 2) temperature-dependent VT; 3) temperature-volume-dependent VT. Constant VT is usually used to correct the volumes only at low temperatures but has poor performance near the critical region (Peneloux et al. 1989). Temperature-dependent VT can provide an accurate reproduction of saturated-liquid density over a wide temperature range, but the improvement on single-phase liquid density prediction is limited (Monnery et al., 1989; Ji and Lempe, 1997; Tsai and Chen, 1998; Lin et al., 2006; Shi et al., 2018). By introducing a volume-dependent distance function relating to the inverse of the isothermal compressibility, temperature-volume-dependent VT can acutely correct both the saturated and single-phase liquid volumes yielded by CEOS (Mathias et al., 1989; Chou and Prausnitz, 1989; Abudour et al., 2012). However, the performances of the available VT-EOSs in predicting the densities for water and water/hydrocarbons mixtures are barely satisfactory. In our view, there is still a room for further improving the prediction accuracy of liquid density by VT-EOS models.

Although the vdW-P model is a popular method to predict the thermodynamic properties of gas hydrates, the hydrate equilibrium calculations based on the vdW-P model may occasionally exhibit non-convergence problems (Klauda and Sandler, 2003; Meragawi et al., 2016; Hsieh et al., 2012). The contemporary research on hydrate equilibrium calculations emphasizes accuracy over robustness (Martin and Peters, 2009; Yoon et al., 2004). Moreover, the hydrate equilibria of gas-mixture systems predicted

by the vdW-P model are not as accurate as those predicted for pure-gas systems (Yoon et al., 2002; Sirino et al., 2018). For gas-mixture hydrates, the crystal structures may change in response to the changes of temperature, pressure, and gas composition. Previously, the gas-dependent parameters in vdW-P model were optimized solely on the basis of pure-gas-hydrate equilibrium data; their ability to reproduce gas-mixture-hydrate equilibria and structure transitions is overlooked (Sloan and Koh, 2008; Medeiros et al., 2020).

Two pivotal aspects should be addressed by multiphase equilibrium calculations: whether a mixture will actually split into two (or more) phases (i.e., stability test) and what the amounts and compositions of equilibrium phases are (i.e., flash calculation) (Curtis and Michael, 2000). Due to the appearance of a solid hydrate phase, the multiphase equilibrium predictions for water/hydrocarbons mixtures become more challenging. In 1989, Bishnoi et al. (1989) firstly proposed a multiphase equilibrium calculation algorithm for gas hydrate systems based on the concept of Gibbs free energy minimization. This algorithm combines the vdW-P hydrate model with the simultaneous stability analysis and flash calculation approach (Gupta, 1988). Later, Ballard and Sloan implemented this methodology in CSMGem, which was deemed as a start-of-the-art software for modeling the equilibria of gas hydrate systems (Ballard and Sloan, 2002 and 2004; Jager et al., 2003). However, these frameworks adopting the simultaneous stability and multiphase flash approach would encounter non-convergence problems at conditions close to the phase boundaries. Occasionally, even the credible software CSMGem cannot yield reliable multiphase equilibrium calculation results (Segtovich et al., 2016; Mahabadian et al., 2016).

Modeling the phase behavior of gas hydrate plays a fundamentally important role in the development of engineering techniques used for hydrate blockage prevention and

in-situ hydrate recovery. This research aims to improve the robustness and accuracy of thermodynamic frameworks in modeling the phase behavior of gas hydrate systems. The thesis research would start with developing a more accurate VT-CEOS for hydrocarbons and water. Next, this study would develop a new procedure for fitting Kihara potential parameters in the vdW-P hydrate model that can more accurately predict the gas-mixture hydrate equilibria. On the basis of the improved thermodynamic models, a robust vapor-liquid-aqueous-hydrate four-phase equilibrium calculation algorithm would be developed to more accurately determine the multiphase equilibria of gas hydrate systems at varied pressure and temperature conditions.

1.2. Problem Statements

The following technical problems are to be addressed in this thesis:

- Although the temperature-volume-dependent VT-model is deemed as the most accurate method to correct the liquid density yielded by CEOS (Young et al., 2017), there is still a room for improving the prediction accuracy of saturated and single-phase liquid densities of hydrocarbons by VT-EOS.
- Water, as a polar substance, is fundamentally different from hydrocarbons. It is necessary to develop an improved VT-EOS to further improve the prediction accuracy of densities of water and water/hydrocarbons mixtures over wide temperature/pressure ranges.
- The vdW-P model cannot converge occasionally. In some instances, it can also lead to significant errors in the calculations of gas-mixture-hydrate equilibria. The Kihara potential parameters are critical to the performance and reliability of vdW-P hydrate model. There are no specific guidelines established so far to guide the optimization of these gas-dependent parameters.

- Previous multiphase equilibrium calculations in the presence of hydrate phase usually employ the simultaneous approach that combines stability analysis and flash calculation. Although this approach can reduce computational cost, it is not a robust approach and may not converge at conditions close to phase boundaries. We need to improve the robustness and accuracy of multiphase equilibrium calculations for hydrate-inclusive systems.

1.3. Hypotheses

The following hypotheses are proposed in this thesis:

- The traditional temperature-volume-dependent VT-models with one fluid-dependent parameter do not fully exploit the potential of distance function. More fluid-dependent parameters adopted in VT-models may enable the distance function to acutely capture the variation of the residuals between measured molar volumes and calculated ones by CEOS. It is also possible to realize a good generalization of these fluid-dependent parameters for hydrocarbon species.
- The Kihara potential parameters play a vital role in the performance of the vdW-P hydrate model. The optimization of Kihara potential parameters with the consideration of hydrate structure transitions may improve its modeling accuracy of gas-mixture hydrate equilibria.
- The stage-wise multiphase equilibrium framework (i.e., a stability test is first conducted, followed by flash calculations if an instability is invoked) is more robust and accurate than the simultaneous approach. A multiphase equilibrium calculation algorithm for gas hydrate systems can be formulated in a stage-wise manner.

1.4. Research Objectives

The objective of this research is to improve multiphase equilibrium calculations for gas hydrate systems. In order to accomplish this general task, the short-term and long-term objectives are provided as follows:

The short-term objectives are:

- Improve the prediction accuracy of saturated and single-phase liquid densities for hydrocarbons yielded by CEOS through developing new temperature-volume-dependent volume translation models.
- Improve the liquid-density prediction accuracy for water and water/hydrocarbons mixtures through VT-EOS over wide temperature/pressure ranges.
- Improve the performance of the vdW-P hydrate model in modeling the gas-mixture hydrate equilibria.
- Develop a vapor-liquid-aqueous-hydrate four-phase equilibrium calculation algorithm.

The long-term objective is:

- Incorporate the improved thermodynamic models for fluid mixtures and gas hydrates as well as the related multiphase equilibrium calculation algorithms into wellbore/reservoir simulators and provide a theoretical guidance on the prevention of hydrate blockage and the development of gas hydrate resources.

1.5. Thesis Structure

This thesis is a paper-based thesis. Six chapters are presented in this thesis and organized as follows:

Chapter 1 introduces the basic research background, the problem statement and the major research objectives. In **Chapter 2**, an improved volume-translated EOS is

proposed to achieve more accurate volumetric calculations for various pure substances. A fairly good generalization of the fluid-dependent VT parameters can be achieved for hydrocarbons. In **Chapter 3**, a series of improved volume translation models have been proposed to achieve more accurate volumetric calculation for water with little additional computational cost. The newly developed VT-EOSs can also provide reliable volumetric predictions for water/hydrocarbons mixtures. In **Chapter 4**, a new procedure is developed for fitting the Kihara potential parameters in the vdW-P hydrate model by using the experimental hydrate equilibrium data for both pure gases and binary gas mixtures and considering the differences between hydrate structures I and II. The vdW-P model coupled by the newly fitted Kihara potential performs well in modeling the hydrate equilibria of gas mixtures and can properly detect the hydrate structure transition and cage occupancy behaviors. In **Chapter 5**, an algorithm for multiphase equilibrium calculations in the presence of gas hydrates is developed. Through point-to-point calculations, this algorithm can be used to plot pressure-temperature and pressure-composition phase diagrams for hydrate-inclusive systems. Finally, **Chapter 6** summarizes the conclusions reached in the thesis and the recommendations for future work.

References

Abudour, A.M., Mohammad, S.A., Robinson, R.L., Gasem, K.A.M., 2012. Volume-translated Peng-Robinson equation of state for saturated and single-phase liquid densities. Fluid Phase Equilib. 335: 74-87.

Ballard, A.L, Sloan, E.D. Jr., 2002. The next generation of hydrate prediction I. Hydrate standard states and incorporation of spectroscopy. Fluid Phase Equilib. 194-197: 371-383.

Ballard, A.L., Sloan, E.D. Jr., 2004. The next generation of hydrate prediction Part III. Gibbs energy minimization formalism. Fluid Phase Equilib. 218: 15-31.

Ballard, A.L., Sloan, E.D. Jr., 2004. The next generation of hydrate prediction IV. A comparison of available hydrate prediction programs. Fluid Phase Equilib. 216: 257-270.

Bishnoi, P.R., Gupta, A.K., Englezos, P., Kalogerakis, N., 1989. Multiphase equilibrium flash calculations for systems containing gas hydrates. Fluid Phase Equilib. 53: 97-104.

Belandria, V., Eslamimanesh, A., Mohammadi, A.H., Theveneau, P., Legendre, H., Richon, D., 2011. Compositional analysis and hydrate dissociation conditions measurements for carbon dioxide + methane + water system. Ind. Eng. Chem. Res. 50: 5783-5794.

Chou, G.F., Prausnitz, J.M., 1989. A phenomenological correction to an equation of state for the critical region. AIChE J. 35: 1487-1496.

Curtis, H.W., Michael, R.B., 2000. Phase Behavior. SPE Monograph Series 20.

Gupta, A.K., 1988. Steady state simulation of chemical processes. Ph.D. Thesis, University of Calgary, Calgary, Canada.

Hsieh, M.K., Ting, W.Y., Chen, Y.P., Chen, P.C., Lin, S.T., Chen, L.J., 2012. Explicit pressure dependence of the Langmuir adsorption constant in the van der Waals-Platteeuw model for the equilibrium conditions of clathrate hydrates. Fluid Phase Equilib. 325: 80-89.

Jager, M.D., Ballard, A.L., Sloan, E.D. Jr., 2003. The next generation of hydrate prediction II. Dedicated aqueous phase fugacity model for hydrate prediction. Fluid Phase Equilib. 211: 85-107.

Ji, W.R., Lempe, D.A., 1997. Density improvement of the SRK equation of state. Fluid Phase Equilib. 130: 49-63.

Klauda, J.B., Sandler, S.I., 2003. Phase behavior of clathrate hydrates: A model for single and multiple gas component hydrates. Chem. Eng. Sci. 58: 27-41.

Lin, H., Duan, Y.Y., Zhang, T., Huang, Z.M., 2006. Volumetric property improvement for the Soave-Redlich-Kwong equation of state. Ind. Eng. Chem. Res. 45: 1829-1839.

Mahabadian, M.A., Chapoy, A., Burgass, R., Tohidi, B., 2016. Development of a multiphase flash in presence of hydrates: Experimental measurements and validation with the CPA equation of state. Fluid Phase Equilib. 414: 117-132.

Martin, A., Peters, C.J., 2009. New thermodynamic model of equilibrium states of gas hydrates considering lattice distortion. J. Phys. Chem. C 113: 422-430.

Mathias, P.M., Naheiri, T., Oh, E.M., 1989. A density correction for the Peng-Robinson equation of state. Fluid Phase Equilib. 47: 77-87.

Meragawi, S.E., Diamantonis, N.I., Tsimpanogiannis, I.N., Economou, I.G., 2016. Hydrate-fluid phase equilibria modeling using PC-SAFT and Peng-Robinson equations of state. Fluid Phase Equilib. 413: 209-219.

Monnery, W.D., Svrcek, W.Y., Satyro, M.A., 1998. Gaussian-like volume shifts for the Peng-Robinson equation of state. Ind. Eng. Chem. Res. 37: 1663-1672.

Peneloux, A., Rauzy, E., Freze, R., 1982. A consistent correction for Redlich-Kwong-Soave volumes. Fluid Phase Equilib. 8: 7-23.

Peng, D.Y., Robinson, D.B., 1976. A new two-constant equation of state. Ind. Eng. Chem. Fundam. 15: 59-64.

Segtovich, I.S.V., Barreto, A.G. Jr., Tavares, F.W., 2016. Simultaneous multiphase flash and stability analysis calculations including hydrates. Fluid Phase Equilib. 413: 196-208.

Shi, J., Li, H., Pang, W., 2018. An improved volume translation strategy for PR EOS without crossover issue. Fluid Phase Equilib. 470: 164-175.

Sirino, T.H., Marcelino Neto, M.A., Bertoldi, D., Morales, R.E.M., Sum, A.K., 2018. Multiphase flash calculations for gas hydrates systems. Fluid Phase Equilib. 475: 45-63.

Sloan, E.D., 2003. Fundamental principles and applications of natural gas hydrates. Nature 426: 353-359.

Sloan, E.D., Koh, C.A., 2008. Clathrate hydrates of natural gases. CRC Press/Taylor & Francis.

Soave, G., 1972. Equilibrium constants from a modified Redlich-Kwong equation of state. Chem. Eng. Sci. 27: 1197-1203.

Tsai, J.C., Chen, Y.P., 1998. Application of a volume-translated Peng-Robinson equation of state on vapor-liquid equilibrium calculations. Fluid Phase Equilib. 145: 193-215.

van der Waals, J.D., 1873. Continuity of the gaseous and liquid state of matter. Ph.D. thesis, Leiden.

van der Waals, J.H., Platteeuw, J.C., 1959. Clathrate solutions. Adv. Chem. Phys. 2: 1-57.

Yoon, J.-H., Chun, M.-K., Lee, H., 2002. Generalized model for predicting phase behavior of clathrate hydrate. AIChE J. 48: 1317-1330.

Yoon, J.-H., Yamamoto, Y., Komai, T., Kawamura, T., 2004. PSRK method for gas hydrate equilibria: I. Simple and mixed hydrates. AIChE J. 50: 203-214.

CHAPTER 2 AN IMPROVED VOLUME-TRANSLATED SRK EOS DEDICATED TO MORE ACCURATE DETERMINATION OF SATURATED AND SINGLE-PHASE LIQUID DENSITIES

A version of this chapter has been published in *Fluid Phase Equilibria*

Abstract

Volume translation (VT) has been widely utilized to improve the liquid density (or volume) prediction by cubic equation of state (CEOS). Previous VT-models do not fully exploit the potential of distance function and there is still a room for improving the prediction accuracy of saturated and single-phase liquid densities by CEOS. In this study, we propose an improved volume translated Soave-Redlich-Kwong (VT-SRK) EOS to achieve more accurate volumetric calculations for various pure substances. The overall average absolute percentage deviations of the saturated and single-phase liquid molar volumes yielded by this VT-SRK EOS for 56 compounds are 0.61 and 0.84, respectively; these two errors are much lower than the counterparts provided by Abudour et al.'s VT-Peng-Robinson EOS (2012). A fairly good generalization of the fluid-dependent VT parameters can be achieved for hydrocarbons. Moreover, we extend the proposed VT-SRK EOS to mixtures through conventional mixing rules, finding that the proposed VT-SRK EOS provides reliable volume predictions for the hydrocarbon mixtures examined in this study.

2.1. Introduction

Since the proposal of van der Waals equation [1], cubic equation of state (CEOS) has been widely used to describe the relationship among pressure, volume, and temperature (PVT) of pure compounds and mixtures. In a simple form, CEOS serves as a fast and reliable tool for solving vapor/liquid equilibrium (VLE) problems [2]. However, most CEOSs cannot provide an accurate volumetric calculation for liquid phase. For example, coupled with updated Twu α-function [3], Peng-Robinson (PR) EOS [4] yields the mean absolute percentage errors (MAPEs) of 1.0%, 1.9%, 2.0%, respectively, in reproducing vapor pressure, enthalpy of vaporization and saturated-liquid heat capacity for more than 800 fluids, while Soave-Redlich-Kwong (SRK) EOS [5] yields 1.2%, 1.9%, 2.2%, respectively [6]. In contrast, the MAPEs in reproducing saturated-liquid density (under the reduced temperature T_r<0.9) for these 1721 fluids yielded by PR and SRK EOSs are 8.7% and 19.2%, respectively [6]. This indicates that although the available CEOSs can provide reliable predictions for many thermodynamic properties of various substances, they cannot offer accurate volumetric calculations. In order to overcome the limitations of two-parameter CEOS (SRK and PR), more compound-specific parameters have been proposed and incorporated into EOS, for example, Redlich-Kwong-Peng-Robinson (RKPR) EOS [7,8] with three parameters and Ghoderao-Dalvi-Narayan (GDN) EOS [9,10] with four parameters. These EOSs can slightly improve the accuracy of liquid-density determination but may lead to poorer performances on predicting other thermodynamic properties compared to classical SRK and PR EOSs [10].

Aiming to mitigate the overestimates of liquid volumes, Martin introduced the concept of volume translation (VT) in CEOS for the first time [11]. Then in 1982, Peneloux et al. suggested a constant volume correction in SRK EOS and the compound-

specific VT constant should exactly reproduce the measured saturated-liquid density at reduced temperature T_r=0.7 [12]. Such constant VT-model is still popular today and is recently applied to assess the liquid density of bitumen, refrigerant and supercritical carbon dioxide [13-16]. **Fig. 2-1** shows the needed volume shifts (i.e., the difference between the liquid molar volumes predicted by SRK EOS and the experimental values) for methane versus reduced temperature at saturation conditions and different single-phase reduced pressures. It can be obviously observed from the black line of **Fig. 2-1** that, instead of keeping a constant value, the needed volume shift at saturation conditions changes continuously versus temperature; because of this, the constant VT-model will give poor density predictions at temperatures away from T_r=0.7. Hence, some modified VT-models have been developed by considering the temperature dependence. Most of temperature-dependent VT-models adopt exponential-type functions [17-23], while Tsai and Chen's (1998) and Ji and Lempe's (1997) VT-models adopt power-law functions [24,25]. Moreover, a few linear temperature-dependent VT-models have been proposed to correct the liquid densities of hydrocarbons [26-28].

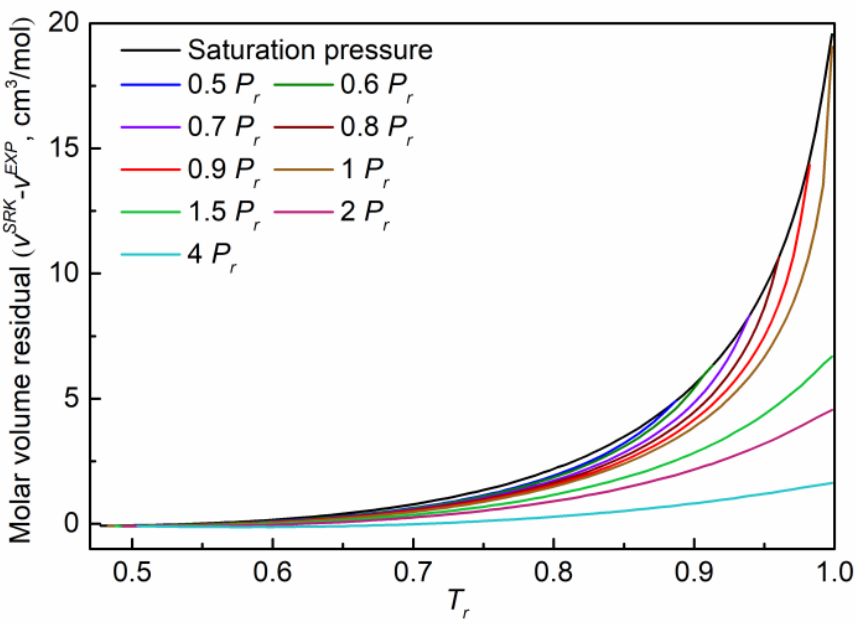

Fig. 2-1. The needed volume shifts in SRK EOS for methane versus reduced temperature at saturation conditions and different single-phase reduced pressures.

Fig. 2-1 also indicates that the needed volume shifts for single-phase liquid density depend on not only temperature but also volume itself, especially near the critical region. On this basis, Chou and Prausnitz [29] as well as Mathias et al. [30] defined a volume-dependent distance function (*d*) relating to the inverse of the isothermal compressibility and developed a novel type of both temperature- and volume-dependent VT-model. Later, Abudour et al. [31,32] and Frey et al. [33,34] modified Chou and Prausnitz's equation [29] and proposed improved VT-models for PR and SRK EOSs, respectively. It is reported that the overall average absolute percentage deviation (%AAD) of saturated-liquid density yielded by Abudour et al.'s VT-PR EOS for 65 fluids is 0.6 [31]. In contrast, putting more emphasis on the thermodynamic consistency of VT-models, Frey et al.'s VT-SRK EOS does not provide significant improvement on density predictions [33,34]. Hence, there is still a room for further improving the prediction accuracy of liquid density by VT-EOS.

Many models used to describe other fluid-properties heavily rely on density predictions, for example, viscosity, gas-liquid interfacial tension and solubility parameters [35-42]. Therefore, it is of critical importance to further improve the density-prediction accuracy over a wide temperature/pressure range. Some empirical correlations can help to determine the saturated-liquid densities but cannot conduct reliable calculations for single-phase liquid densities under different temperature/pressure conditions [43-46]. The Tait equation is one of famous equation of states to reproduce liquid density data through comparing with a reference condition [47]. Nevertheless, for some complicated mixtures, the reference densities would be hardly available, resulting in no reliance on Tait equation [48,49]. With the advent of

more advanced modeling techniques (such as perturbed chain-statistical associating fluid theory [50,51], multiparametric equations explicit in the Helmholtz free energy (including AGA 8 [52], GERG-2008 [53] and IAPWS-95 [54]), artificial neural network models [55] and molecular dynamics simulations [56]), there are more options for describing phase behavior of pure compounds and mixtures. But the traditional CEOSs have not been eclipsed by those new methods due to their concise form and low computational cost [57]. Similarly, volume translation is still a widely used technique in CEOS due to the advantages of higher accuracy but little additional computational cost.

SRK and PR EOSs are two of most commonly used CEOSs in academia and industry. These two CEOSs yield similar calculation errors in reproducing vapor pressure, enthalpy of vaporization and saturated-liquid heat capacity, but the density estimation yielded by SRK EOS is less accurate than that yielded by PR EOS [6,58]. Therefore, to some extent, development of VT models is more imperative for SRK EOS [59]. In this study, we propose an improved VT-model for SRK EOS in an attempt to accurately determine the saturated and single-phase liquid volumes. A database which includes the saturated and single-phase density data for 56 pure compounds has been complied; the three fluid-dependent parameters in the newly proposed VT-SRK EOS model have been optimized based on such density data for each compound. To make a fair comparison to the one of the best available VT-models (i.e., Abudour et al.'s VT-model [31]) in the literature [60,61], the VT parameter in Abudour et al.'s VT-model [31] is refitted based on the same group of density data. We compare the calculation accuracy for saturated and single-phase liquid molar volumes by the newly proposed VT-SRK EOS and the updated VT-PR EOS proposed by Abudour et al. [31] Efforts are also invested to generate a generalized VT-SRK EOS by developing generalized

expressions of the fluid-dependent VT parameters in the newly proposed VT-model. Finally, we extend this VT-model to mixtures via classical mixing rules and demonstrate the good performance of the newly proposed VT-SRK EOS in predicting the liquid-phase densities for several binary mixtures.

2.2. VT-SRK EOS and VT-PR EOS

Soave-Redlich-Kwong equation of state [5] is given as:

$$P^{SRK} = \frac{RT}{v^{SRK} - b^{SRK}} - \frac{a^{SRK}}{v^{SRK}\left(v^{SRK} + b^{SRK}\right)} \tag{2-1}$$

where P^{SRK} and v^{SRK} are the pressure and molar volume in SRK EOS, respectively, T is the temperature, R is the universal gas constant, a^{SRK} and b^{SRK} are the EOS parameters and in SRK EOS, they can be expressed as:

$$a^{SRK} = \frac{1}{9\left(\sqrt[3]{2} - 1\right)} \frac{R^2 T_c^2}{P_c} \alpha^{Twu}(T) \tag{2-2}$$

$$b^{SRK} = \frac{\sqrt[3]{2} - 1}{3} \frac{RT_c}{P_c} \tag{2-3}$$

where T_c and P_c are the experimental critical temperature and pressure, respectively. The term $\alpha(T)$ was firstly put forward by Soave [5] to improve VLE predictions and then modified by many researchers later on. In 2016, Le Guennec et al. [62] proposed a set of constraints for α-function to guarantee the safe property predictions for CEOSs in both subcritical and supercritical domains. Pina-Martinez et al. updated the Soave α-function and Twu α-function for over 1000 pure substances based on above constraints [6,58]. In the VT-SRK EOS model proposed in this study, the updated Twu α-function [3,6] is used because its good performances in reproducing thermodynamic properties:

$$\alpha^{Twu}(T) = T_r^{N(M-1)} \exp[L(1 - T_r^{MN})] \tag{2-4}$$

where T_r is the reduced temperature (i.e., $T_r = \frac{T}{T_c}$), L, M and N are compound-dependent parameters.

Based on Chou and Prausnitz [29], the dimensionless distance d^{SRK} in SRK EOS can be described by:

$$d^{SRK} = \frac{1}{RT_c}\left(\frac{\partial P^{SRK}}{\partial \rho^{SRK}}\right)_T = -\frac{v^{SRK^2}}{RT_c}\left(\frac{\partial P^{SRK}}{\partial v^{SRK}}\right)_T = \frac{v^{SRK^2}T}{T_c\left(v^{SRK}-b^{SRK}\right)^2} - \frac{a^{SRK}\left(2v^{SRK}+b^{SRK}\right)}{RT_c\left(v^{SRK}+b^{SRK}\right)^2} \quad (2\text{-}5)$$

Then they provided a temperature-volume-dependent VT-model containing d^{SRK} as:

$$v^{VTSRK} = v^{SRK} - c_1^{\,o} - \delta_c^{\,SRK}\left(\frac{0.35}{0.35+d^{SRK}}\right) \quad (2\text{-}6)$$

where v^{VTSRK} is the corrected molar volume after volume translation in SRK EOS, c_1^o is a substance-dependent parameter used for correcting the volumes remote from critical region and 0.35 is a universal constant determined by regressing density data for many substances. δ_c^{SRK} is the volume shift at critical temperature in SRK EOS:

$$\delta_c^{\,SRK} = \frac{RT_c}{P_c}\left(Z_c^{\,SRK} - Z_c\right) = v_c^{\,SRK} - v_c \quad (2\text{-}7)$$

where Z_c^{SRK} and v_c^{SRK} are the critical compressibility factor and critical molar volume in SRK EOS, Z_c and v_c are the experimental critical compressibility factor and critical molar volume, respectively.

In this study, we tried to promote the VT-model from the perspectives of possible generalization and improved calculation accuracy. At first, we updated Chou and Prausnitz's VT-model [29] and optimize the VT-parameter c_1' and c_2' in **Eq. 2-8** for n-alkanes,

$$v^{VTSRK} = v^{SRK} - c_1'\left(\frac{RT_c}{P_c}\right) - \delta_c^{SRK}\left(\frac{c_2'}{c_2' + d^{SRK}}\right) = v^{SRK} - c_1'\left(\frac{RT_c}{P_c}\right) - \delta_c^{SRK}\left(\frac{1}{1+\frac{d^{SRK}}{c_2'}}\right) \quad (2\text{-}8)$$

The optimized VT-parameters c_1' and c_2' in **Eq. 2-8** for n-alkanes are shown in **Fig. 2-2**. One may observe that, in general, both c_1' and c_2' exhibit a monotonic variation trend with the carbon number of n-alkanes: c_1' shows an increasing trend, while c_2' shows a decreasing trend. In addition, it can be seen from **Fig. 2-2** that the values of c_2' for most light n-alkanes are higher than 0.35, although 0.35 is a commonly adopted value in the literature. Thereby, it is necessary to honor the different c_2' values exhibited by different compounds.

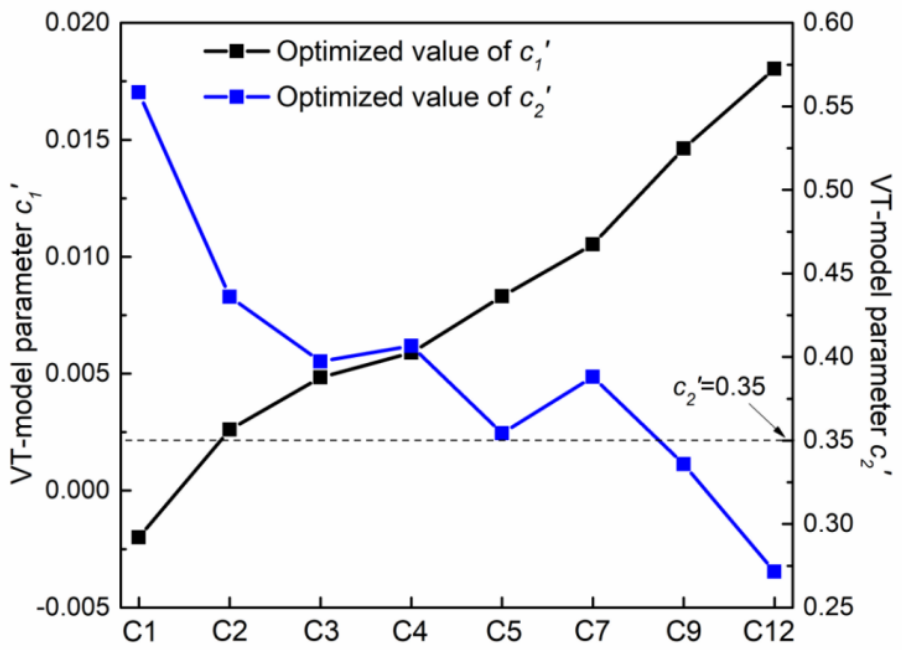

Fig. 2-2. Plots of optimized VT parameters in **Eq. 2-8** for n-alkanes.

The values of c_2' in **Eq. 2-8** can vary from one substance to another, which partially prompts us to further revise the third term (the term containing *d*) by recognizing its dependence on individual species. Based on this consideration, we add another

substance-dependent parameter to the above 2-parameter VT-model (**Eq. 2-8**) and propose a 3-parameter VT-model (**Eq. 2-9**) as follows:

$$v^{VTSRK} = v^{SRK} - c_1\left(\frac{RT_c}{P_c}\right) - \delta_c^{\ SRK}\left(\frac{1}{c_2 + c_3 d^{SRK}}\right) \tag{2-9}$$

where c_1, c_2 and c_3 are the fluid-dependent parameters.

We compare the average absolute percentage deviations (%AADs, determined by **Eq. 2-10**) in reproducing the saturated-liquid molar volumes for n-alkanes yielded by the 2-parameter VT-model (**Eq. 2-8**) and 3-parameter VT-model (**Eq. 2-9**):

$$\%AAD = \frac{100}{n}\sum_{i=1}^{n}\left|\frac{v^{VT} - v^{EXP}}{v^{EXP}}\right|_i \tag{2-10}$$

where n is the number of data points used, v^{VT} and v^{EXP} are the molar volume obtained by VT-EOS and the pseudo-experimental molar volume retrieved from National Institute of Standards and Technology (NIST) Web Thermo Tables (WTT) with the Version 2-2012-1-Pro [63], respectively.

As shown in **Fig. 2-3**, the 3-parameter VT-SRK EOS can provide more accurate volumetric predictions (lower %AADs) for all the n-alkanes used in this test than the 2-parameter VT-SRK EOS. This indicates that the two other fluid-dependent parameters (c_2 and c_3) adopted in the new VT-model enable the distance function (d) to acutely capture the variation of residuals between measured molar volumes and calculated ones by SRK EOS, resulting in improved density estimation. Based on the above preliminary results, we decide to extend the three-fluid-dependent-parameter VT-model (**Eq. 2-9**) to other compounds and compile a database containing the saturated and single -phase liquid density data for a diverse group of species.

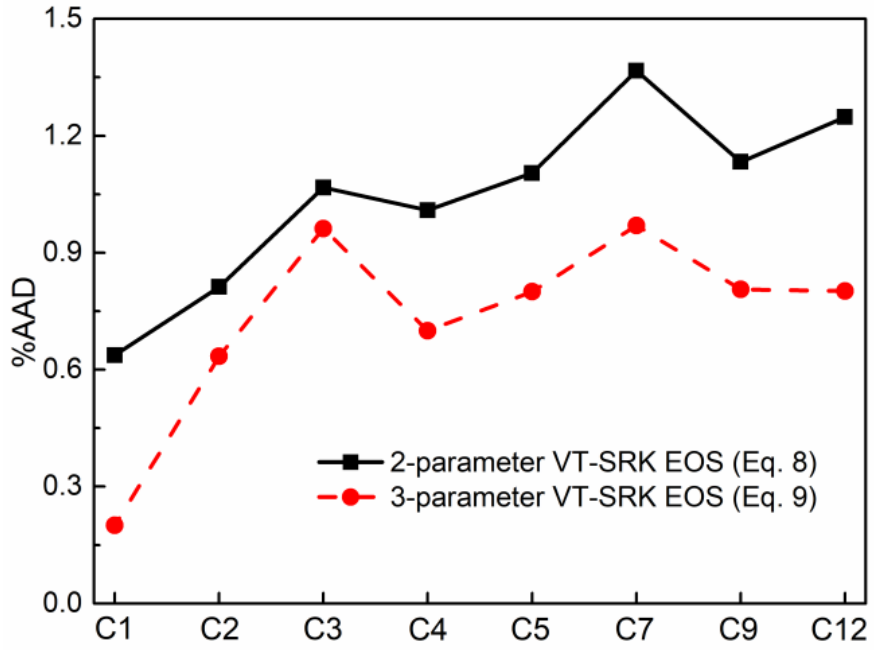

Fig. 2-3. Comparison of %AADs in reproducing the saturated liquid molar volumes of n-alkanes by 2-parameter VT-SRK EOS (**Eq. 2-8**) and 3-parameter VT-SRK EOS (**Eq. 2-9**).

In order to verify the accuracy of liquid volume predicted by this three-fluid-dependent-parameter VT-SRK EOS, a comparison to the existing VT-models is needed. In 2017, Young et al. [60] compared 8 different volume translation functions, finding that the VT-PR EOS proposed by Abudour et al. [31] exhibits the best performance for the saturated-liquid density prediction without causing PV isotherm crossing over a wide pressure/temperature range. Moreover, Matheis et al. [61] also proved that Abudour et al.'s VT-model [31] is superior to other VT-EOSs for real-gas density predictions. As such, we can deem Abudour et al.'s method [31] as the state-of-art VT-model for liquid density prediction and hence use their VT-model as a benchmark model in this study. It is noteworthy that Abudour et al.'s VT-model [31] is based on PR rather than SRK EOS. PR EOS [4] and Abudour et al.'s VT-model [31] are given as:

$$P^{PR} = \frac{RT}{v^{PR} - b^{PR}} - \frac{a^{PR}}{v^{PR}\left(v^{PR} + b^{PR}\right) + b^{PR}\left(v^{PR} - b^{PR}\right)} \tag{2-11}$$

$$v^{VTPR} = v^{PR} + cc - \delta_c^{PR}\left(\frac{0.35}{0.35 + d^{PR}}\right) \tag{2-12}$$

where P^{PR} and v^{PR} are the pressure and molar volume in PR EOS, respectively, a^{PR} and b^{PR} are the PR EOS parameters, d^{PR} is the dimensionless distance in PR EOS, δ_c^{PR} is the volume shift at critical temperature in PR EOS, v^{VTPR} is the corrected molar volume after volume translation in PR EOS, cc represents the corrected volumes far from critical region, and 0.35 is adopted as a universal constant for all compounds. a^{PR}, b^{PR}, d^{PR}, δ_c^{PR} and cc can be described by the following **Eqs. 2-13~2-17**.

$$a^{PR} = 0.457535\frac{R^2T_c^2}{P_c}\alpha^{Gasem}(T) \tag{2-13}$$

$$b^{PR} = 0.077796\frac{RT_c}{P_c} \tag{2-14}$$

$$d^{PR} = -\frac{v^{PR^2}}{RT_c}\left(\frac{\partial P^{PR}}{\partial v^{PR}}\right)_T = \frac{v^{PR^2}}{RT_c}\left[\frac{RT}{\left(v^{PR} - b^{PR}\right)^2} - \frac{2a^{PR}\left(v^{PR} + b^{PR}\right)}{\left(v^{PR^2} + 2b^{PR}v^{PR} - b^{PR^2}\right)^2}\right] \tag{2-15}$$

$$\delta_c^{PR} = \frac{RT_c}{P_c}\left(Z_c^{PR} - Z_c\right) = v_c^{PR} - v_c \tag{2-16}$$

$$cc = \left(\frac{RT_c}{P_c}\right)\left[cc_1 - \left(0.004 + cc_1\right)\cdot\exp\left(-2d^{PR}\right)\right] \tag{2-17}$$

where Z_c^{PR} and v_c^{PR} are the critical compressibility factor and critical molar volume in PR EOS, cc_1 is a compound-dependent parameter. **Eq. 2-17** is carefully designed to enable a good generalization of compound-dependent parameter cc_1. Although only containing one compound-dependent parameter, the form of Abudour et al. VT-model (**Eq. 2-17**) is more complicated than that proposed in our work (**Eq. 2-9**). This VT-PR EOS adopts the α-function proposed by Gasem et al. [64]

$$\alpha^{Gasem}(T) = \exp[\left(2 + 0.836T_r\right)\left(1 - T_r^{0.134+0.508\omega-0.0467\omega^2}\right)] \tag{2-18}$$

where ω is the acentric factor.

2.3. Database Used for Developing the Improved VT-SRK EOS

The saturated and single-phase density data for a total of 56 chemical compounds are compiled to form the database used for developing the improved VT-SRK EOS. 56 chemical compounds include 13 inorganics, 26 organic hydrocarbons, 12 oxy-organics and 5 fluorinated organics. **Table 2-1** presents the input compound properties in VT-EOS, including critical temperature, critical pressure, acentric factor, and critical compressibility factor. The compound-specific parameters c_1, c_2 and c_3 in the improved VT-model (**Eq. 2-9**) are determined through nonlinear regression over saturated-liquid molar volumes. The nonlinear regression is conducted by the iterative reweighted least squares algorithm. The temperature range of regression is from the minimum integer above the value of triple point temperature (with the unit of K) to the maximum integer below the critical temperature; the temperature step is 1 K. The pseudo-experimental saturated-liquid volumes used for fitting the VT-model parameters and compound properties are retrieved from the National Institute of Standards and Technology Web Thermo Tables with the Version 2-2012-1-Pro [63]. These pseudo-experimental liquid volumes were generated through some empirical correlations that well reproduce the available experimental data; these correlations are seldom adopted in industrial simulators for describing PVT behaviors of fluids due to their complicated functional forms.

Table 2-1. Physical properties of compounds considered in this study, the fitted parameters in the newly proposed VT-SRK EOS and the refitted parameter in VT-PR EOS proposed by Abudour et al. [31]

Category	Compound	T_c (K)	P_c (MPa)	ω	Z_c	Temperature range (K)	Number of data points	Parameters in the newly proposed VT-SRK EOS				Parameters in the updated VT-PR EOS proposed by Abudour et al. [31]*	
								c_1	c_2	c_3	R^2	cc_1	R^2
Inorganics	Sulfur dioxide	430.643	7.88	0.25545	0.26925	198~430	233	0.00951	0.99101	2.70124	0.99856	0.00244	0.98246

	Water	647.096	22.064	0.34429	0.22950	274~647	374	0.02425	1.30564	2.17549	0.99200	-0.01413	0.99230
	Carbon dioxide	304.128	7.377	0.22394	0.27493	217~304	88	0.00608	0.92912	2.65917	0.99846	0.00648	0.99465
	Nitrogen	126.192	3.3958	0.03723	0.28949	64~126	63	-0.00252	0.75199	2.19566	0.99873	0.01384	0.98815
	Oxygen	154.6	5.046	0.02207	0.29431	55~154	100	-0.00158	0.68002	1.98746	0.99707	0.01224	0.93915
	Argon	150.69	4.863	-0.00225	0.28958	84~150	67	-0.00314	0.76869	2.06605	0.99919	0.01425	0.99160
	Xenon	289.733	5.842	0.00366	0.28877	162~289	128	-0.00131	0.76413	2.00865	0.99964	0.01180	0.97486
	Fluorine	144.4	5.24	0.05095	0.27966	54~144	91	-0.00220	0.96291	2.70191	0.99686	0.01450	0.89021
	Carbon monoxide	132.9	3.498	0.04925	0.29187	69~132	64	-0.00210	0.76917	2.10916	0.99912	0.01338	0.99052
	Hydrogen sulfide	373.1	8.999	0.10044	0.28488	188~373	186	0.00144	0.97009	2.45887	0.99924	0.01075	0.95673
	Sulfur hexafluoride	318.723	3.755	0.21025	0.27887	224~318	95	0.00162	0.86167	2.23887	0.99858	0.00971	0.99026
	Ammonia	405.5	11.359	0.25593	0.25536	196~405	210	0.02004	1.14567	2.55131	0.99930	-0.00868	0.98093
	Carbonyl sulfide	378.77	6.369	0.09770	0.27300	135~378	244	0.00393	0.98471	2.87828	0.99744	0.00827	0.95058
Organic Hydrocarbons	Methane	190.564	4.5992	0.01140	0.28640	91~190	100	-0.00195	0.79540	2.13497	0.99895	0.01306	0.99152
	Ethane	305.322	4.872	0.09955	0.28001	91~305	215	0.00270	0.85431	2.59463	0.99482	0.00878	0.96398
	Propane	369.89	4.251	0.15212	0.27656	86~369	284	0.00492	0.89221	2.75570	0.98831	0.00658	0.92407
	Butane	425.12	3.796	0.20093	0.27390	135~425	291	0.00594	0.93036	2.60453	0.99414	0.00549	0.96178
	Pentane	469.66	3.369	0.25173	0.26474	144~469	326	0.00831	0.99529	3.00384	0.99336	0.00359	0.94913
	Hexane	507.79	3.042	0.30032	0.27872	178~507	330	0.00923	0.86394	2.07261	0.99103	0.00108	0.88977
	Heptane	541.2	2.774	0.34620	0.27467	183~540	358	0.01032	1.18249	2.08864	0.98586	0.00034	0.93543
	Octane	569.57	2.507	0.39436	0.26570	217~569	353	0.01226	1.19624	2.35762	0.99405	-0.00120	0.96706
	Nonane	594.55	2.28	0.44306	0.25487	220~594	375	0.01444	1.12707	2.66252	0.99470	-0.00301	0.97111
	Decane	617.7	2.101	0.48794	0.24982	244~617	374	0.01574	1.25347	3.03108	0.99438	-0.00359	0.93848
	Dodecane	658.1	1.82	0.57487	0.25015	264~658	395	0.01795	1.06434	3.48078	0.99481	-0.00551	0.95118
	Tridecane	675.89	1.67	0.60761	0.24020	268~675	408	0.02024	1.21436	3.36428	0.99527	-0.00785	0.94501
	Pentadecane	706.9	1.44	0.68240	0.22957	284~706	423	0.02334	1.19481	2.88678	0.99519	-0.01167	0.97598
	Hexadecane	722.24	1.43	0.73127	0.23861	292~722	431	0.02071	1.19303	3.43851	0.99330	-0.00809	0.93361
	Heptadecane	735.71	1.32	0.74951	0.23491	296~735	440	0.02339	1.25140	3.53867	0.99375	-0.01094	0.93147
	Eicosane	768.2	1.077	0.86873	0.22150	310~768	459	0.02930	1.38814	3.85212	0.99541	-0.01661	0.91442
	Isobutane	407.81	3.629	0.18358	0.27594	114~407	294	0.00554	0.89812	2.61896	0.99185	0.00587	0.94409
	2-Methylbutane	460.35	3.38	0.22767	0.27009	113~460	348	0.00688	0.89542	3.07548	0.98833	0.00484	0.92297
	2-Methylpentane	497.7	3.043	0.28000	0.27094	120~497	378	0.00841	0.97507	2.78662	0.98369	0.00297	0.91482
	Cyclohexane	553.64	4.075	0.20924	0.27301	280~553	274	0.00459	1.09262	2.21252	0.99695	0.00680	0.97233
	Cyclopropane	398.69	5.605	0.12875	0.26073	273~398	126	0.00490	1.23566	2.92174	0.99968	0.00958	0.82588
	Ethylene	282.35	5.0417	0.08652	0.28130	104~282	179	0.00228	0.84956	2.53781	0.99680	0.00930	0.97490
	Propylene	364.21	4.555	0.14607	0.27569	88~364	277	0.00592	0.87045	2.92556	0.98821	0.00578	0.92141
	Propyne	402.7	5.658	0.20244	0.27234	273~402	130	0.00695	1.06594	2.57349	0.99944	0.00551	0.99013
	Benzene	562.02	4.906	0.21081	0.26915	279~562	284	0.00680	1.00489	2.55901	0.99833	0.00503	0.98597
	Toluene	591.749	4.126	0.26567	0.26471	178~591	414	0.01024	1.05282	2.87184	0.99197	0.00149	0.94532
Oxy-organics	Methanol	513.38	8.22	0.56269	0.21926	176~513	338	0.02228	1.44952	2.62588	0.99512	-0.01070	0.95511
	Ethanol	515.4	6.3	0.63767	0.31531	250~513	264	0.01325	0.25264	0.45220	0.99942	-0.00855	0.94873
	1-Propanol	536.72	5.12	0.61448	0.25229	149~536	388	0.01316	1.14510	2.55041	0.99522	-0.00222	0.98001
	2-Propanol	508.27	4.75	0.66348	0.24716	186~508	323	0.01357	1.19815	2.58611	0.99690	-0.00227	0.98168
	1-Butanol	561.9	4.42	0.60088	0.26423	185~561	377	0.01119	1.06456	2.47778	0.99654	-0.00008	0.97681
	Isobutanol	548.9	4.299	0.57692	0.26092	172~548	377	0.01113	1.09706	2.37169	0.99678	-0.00037	0.98136

	Acetone	508.1	4.69	0.30625	0.23627	179~508	330	0.02162	1.17718	3.25112	0.99681	-0.00922	0.97917
	Butanone	536.45	4.172	0.32068	0.25645	187~536	350	0.01698	0.98991	2.19332	0.99649	-0.00690	0.92925
	2-Pentanone	561.42	3.73	0.34300	0.26886	254~561	308	0.01407	0.89416	1.79270	0.99824	-0.00498	0.85892
	Dimethyl ether	400.38	5.337	0.19607	0.26995	132~400	269	0.00751	1.07020	2.60559	0.99434	0.00409	0.94960
	1,1-dimethylethyl methyl ether	496.97	3.41	0.26535	0.27840	165~496	332	0.00720	0.90182	2.48625	0.99002	0.00422	0.93232
	Ethyl tert-butyl ether	509.4	2.97	0.32716	0.27750	180~509	330	0.00764	0.89895	2.48758	0.99359	0.00493	0.92900
Fluorinated Organics	Tetrafluoromethane	227.396	3.762	0.18184	0.27935	120~227	108	-0.00033	0.88355	2.27121	0.99909	0.01196	0.99324
	Difluoromethane	351.255	5.783	0.27699	0.24302	137~351	215	0.02192	1.19333	3.07950	0.99702	-0.00966	0.98597
	Fluoromethane	317.28	5.906	0.20110	0.24081	130~317	188	0.02006	1.26407	3.06178	0.99868	-0.00743	0.97897
	Hexafluoroethane	293.03	3.048	0.25664	0.28166	174~293	120	0.00207	0.83855	2.15993	0.99640	0.00895	0.96589
	Octafluoropropane	345.02	2.64	0.31712	0.27562	126~345	220	0.00457	0.96703	2.68244	0.98589	0.00707	0.92245

* This parameter in the VT-PR EOS proposed by Abudour et al. [31] has been refitted based on NIST data.

In order to make more reliable and objective comparisons, the parameter cc_1 in Abudour et al.'s VT-PR EOS [31] is refitted through the same database and fitting process. Note that some cc_1 refitted in this study for some compounds may be dramatically different from the original ones due to the different regression methods as well as different databases used. The correlation coefficient (R^2) can also be obtained during the fitting progress for the two VT-models. All the fitted compound-dependent parameters have been summarized in **Table 2-1**.

For all the substances listed in **Table 2-1** except water, the newly proposed VT-model yields higher R^2 than Abudour et al. VT-model [31]. Please note that all the R^2s yielded by this work are higher than 0.98 while those yielded by Abudour et al. VT-model for 2-pentanone, cyclopropane, hexane and fluorine are even less than 0.9. This demonstrates that the three fluid-dependent parameters adopted in this work enable the VT-model to acutely capture the needed volume shifts for various fluids.

2.4. Performance of Newly Proposed VT-SRK EOS in Reproducing Saturated and Single-Phase Liquid Molar Volumes for Pure Substances

In order to demonstrate the performance of the newly proposed VT method, we compare this VT-SRK EOS against Abudour et al.'s VT-PR EOS [31] in terms of %AADs (determined by **Eq. 2-10**) in reproducing both saturated and single-phase liquid molar volumes.

For the saturated-liquid molar volume, the data points used for %AAD calculation are consistent with those for parameter optimization. For the single-phase liquid molar volume, %AAD will be determined at different reduced pressures ($P_r = \frac{P}{P_c}$) and grouped into two categories, i.e., %AAD under subcritical pressures (P_r=0.1-1 with a step of 0.1) and %AAD under supercritical pressures (P_r=1.1, 1.2, 1.3, 1.4, 1.5, 2, 3 and 4). However, the starting temperatures at which the pseudo-experimental single-phase molar volumes can be retrieved from NIST WTT [63] for many compounds are obviously higher than the triple point temperatures. Hence, the lower temperature bound for %AAD calculations is set as the minimum integer in the available temperature range in NIST WTT [63]. Usually, under subcritical pressures, the maximum temperature used in the %AAD calculations for single-phase volume should be the maximum integer below the saturated temperature at a given reduced pressure, while under supercritical pressures, the maximum temperature should be the maximum integer below the critical temperature. Unfortunately, for a few compounds, NIST WTT [63] cannot provide the single-phase molar volumes at relatively high temperatures; hence, the maximum integer in the valid temperature range in NIST WTT [63] has been set as the upper temperature bound. The temperature step is set as 1 K for %AAD evaluations.

Table 2-2 lists the %AADs in saturated and single-phase liquid molar volumes predicted by this VT-SRK EOS and Abudour et al.'s VT-PR EOS [31]. As shown in **Table 2-2**, the newly proposed VT-SRK EOS yields lower %AADs in reproducing single-phase and saturated-liquid volumes for most compounds than Abudour et al.'s VT-PR EOS [31]. Only the %AADs for water, carbon dioxide and propyne yielded by this work are slightly higher than those yielded by Abudour et al.'s model [31]. But the density-prediction accuracy for water and carbon dioxide provided by the improved VT-SRK EOS should be still acceptable for chemical/petroleum engineering applications. The overall %AADs in the saturated and single-phase liquid molar volumes yielded by this VT-SRK EOS for 56 compounds are 0.61 and 0.84, respectively. By contrast, the overall %AADs obtained by Abudour et al.'s VT-PR EOS [31] are 1.36 and 1.45, which are fairly higher than those yielded by our VT-model. These calculation results indicate that the newly proposed VT-SRK EOS can generally provide a more accurate liquid volume prediction than Adudour et al.'s VT-PR EOS [31]. It is worthwhile of noting that the newly proposed VT-SRK EOS provides a %AAD of lower than 2.00 for single-phase and saturated-liquid volumes of all the compounds examined in this work. The above calculation results also demonstrate that, after incorporating the improved VT-model (**Eq. 2-9**), the SRK EOS could perform equally well or better in reproducing liquid densities than the best available versions of VT-PR EOS.

Table 2-2. Comparison of the calculation accuracy for saturated and single-phase liquid molar volumes yielded by the newly proposed VT-SRK EOS and the updated VT-PR EOS proposed by Abudour et al. [31]

Category	Compound	%AAD yielded by the newly proposed VT-SRK EOS				%AAD yielded by the updated VT-PR EOS proposed by Abudour et al. [31][b]			
		$\%AAD_{single}$[c]	$\%AAD_{sub}$[d]	$\%AAD_{sup}$[e]	$\%AAD_{sat}$[f]	$\%AAD_{single}$[c]	$\%AAD_{sub}$[d]	$\%AAD_{sup}$[e]	$\%AAD_{sat}$[f]
Inorganic	Sulfur dioxide	0.54	0.46	0.62	0.37	0.96	0.95	0.98	0.88
	Water	1.72	1.35	2.10	1.24	1.58	1.25	1.93	1.10

	Carbon dioxide	0.56	0.34	0.74	0.27	0.31	0.17	0.43	0.18
	Nitrogen	0.34	0.25	0.41	0.23	0.41	0.36	0.46	0.35
	Oxygen	0.58	0.52	0.64	0.43	0.85	0.81	0.88	0.87
	Argon	0.24	0.17	0.30	0.16	0.30	0.25	0.34	0.27
	Xenon	0.24	0.17	0.30	0.13	0.49	0.46	0.52	0.57
	Fluorine	0.53	0.46	0.59	0.41	1.03	1.03	1.03	1.25
	Carbon monoxide	0.36	0.27	0.45	0.19	0.44	0.39	0.50	0.33
	Hydrogen sulfide	0.33	0.28	0.39	0.20	0.59	0.60	0.58	0.69
	Sulfur hexafluoride	0.58	0.32	0.80	0.25	0.64	0.43	0.82	0.37
	Ammonia	0.42	0.29	0.55	0.24	0.66	0.61	0.71	0.74
	Carbonyl sulfide	0.61	0.53	0.69	0.43	1.21	1.19	1.23	1.22
Organic Hydrocarbons	Methane	0.28	0.22	0.33	0.20	0.37	0.34	0.41	0.33
	Ethane	0.84	0.76	0.92	0.63	1.29	1.25	1.32	1.12
	Propane	1.22	1.13	1.31	0.96	1.91	1.86	1.95	1.68
	Butane	1.00	0.89	1.12	0.73	1.51	1.44	1.58	1.27
	Pentane	1.07	0.96	1.20	0.80	1.81	1.75	1.88	1.62
	Hexane	1.19	1.07	1.32	0.90	1.66	1.57	1.77	1.69
	Heptane	1.25	1.13	1.38	0.97	1.63	1.54	1.73	1.37
	Octane	1.03	0.90	1.16	0.74	1.44	1.35	1.53	1.16
	Nonane	1.17	1.03	1.31	0.84	1.77	1.68	1.87	1.43
	Decane	1.10	0.96	1.26	0.80	1.87	1.82	1.92	1.82
	Dodecane	1.10	0.93	1.27	0.80	2.10	2.02	2.20	1.93
	Tridecane[a]	1.16	1.01	1.34	0.84	2.08	2.03	2.14	2.17
	Pentadecane[a]	1.28	1.30	1.24	1.07	3.23	3.24	3.22	1.89
	Hexadecane[a]	1.34	1.36	1.32	1.06	4.09	4.09	4.09	2.51
	Heptadecane[a]	1.40	1.31	1.50	1.03	4.15	4.17	4.13	3.07
	Eicosane[a]	1.05	0.94	1.18	0.81	2.47	2.47	2.47	2.75
	Isobutane	1.09	0.98	1.20	0.83	1.70	1.63	1.76	1.46
	2-Methylbutane	1.32	1.21	1.44	1.05	2.13	2.07	2.20	1.92
	2-Methylpentane	1.51	1.40	1.63	1.20	2.25	2.17	2.33	1.91
	Cyclohexane	0.66	0.49	0.83	0.39	0.81	0.70	0.91	0.67
	Cyclopropane	0.36	0.17	0.51	0.12	1.17	1.22	1.13	1.75
	Ethylene	0.67	0.58	0.76	0.48	1.02	0.98	1.06	0.89
	Propylene	1.21	1.12	1.31	0.99	1.96	1.92	2.00	1.77
	Propyne	0.56	0.31	0.78	0.17	0.48	0.38	0.57	0.44
	Benzene	0.63	0.48	0.78	0.38	0.88	0.79	0.96	0.69
	Toluene	1.18	1.06	1.30	0.88	1.87	1.81	1.93	1.66
Oxy-organics	Methanol	1.31	0.91	1.76	0.80	1.53	1.05	2.05	1.31
	Ethanol	0.66	0.31	1.03	0.21	4.70	4.74	4.65	6.51
	1-Propanol[a]	0.74	0.71	0.77	0.70	1.10	1.07	1.13	1.08
	2-Propanol[a]	0.67	0.48	0.89	0.41	0.97	0.68	1.30	0.81
	1-Butanol[a]	0.50	0.49	0.50	0.52	1.00	0.99	1.02	1.00
	Isobutanol[a]	0.36	0.40	0.32	0.49	0.59	0.58	0.60	0.92
	Acetone	0.78	0.66	0.90	0.62	1.46	1.51	1.42	1.54
	Butanone[a]	0.65	0.67	0.62	0.82	1.27	1.34	1.20	1.82
	2-Pentanone[a]	0.89	0.67	1.15	0.53	1.90	1.67	2.17	2.08
	Dimethyl ether	0.93	0.85	1.02	0.70	1.52	1.50	1.54	1.40

	1,1-dimethylethyl methyl ether[a]	1.12	0.91	1.36	0.89	1.34	1.20	1.51	1.46
	Ethyl tert-butyl ether[a]	1.16	0.86	1.51	0.75	1.41	1.24	1.61	1.58
Fluorinated Organics	Tetrafluoromethane	0.49	0.37	0.61	0.27	0.61	0.54	0.68	0.47
	Difluoromethane	0.63	0.52	0.74	0.50	1.18	1.20	1.17	1.18
	Fluoromethane	0.49	0.39	0.60	0.36	0.96	1.02	0.89	1.26
	Hexafluoroethane	0.46	0.28	0.62	0.22	0.60	0.47	0.73	0.56
	Octafluoropropane	1.39	1.24	1.55	1.02	1.85	1.75	1.97	1.54
Overall		0.84	0.71	0.97	0.61	1.45	1.38	1.52	1.36

[a] The maximum temperature at which the single-phase liquid densities can be retrieved from NIST database cannot reach the saturation condition.
[b] This parameter in the VT-PR EOS proposed by Abudour et al. [31] has been refitted based on NIST data.
[c] %AAD for single-phase liquid volume over the entire pressure range.
[d] %AAD for single-phase liquid volume under $P_r \leq 1$.
[e] %AAD for single-phase liquid volume under $P_r > 1$.
[f] %AAD for saturated-liquid volume.

In order to compare the calculation errors yielded by the newly proposed VT-SRK EOS and the Abudour et al. VT-PR EOS [31] against the uncertainty reported by NIST for pseudo-experimental liquid volumes, **Fig. 2-4** visually compares the uncertainty reported by NIST for pseudo-experimental liquid volumes of methane and dodecane against relative percentage deviation (%RD) in reproducing saturated-liquid molar volumes at different temperatures. The %RD at a given reduced temperature can be obtained by:

$$\%RD = 100 \times \left(\frac{v^{VT} - v^{EXP}}{v^{EXP}} \right) \tag{2-19}$$

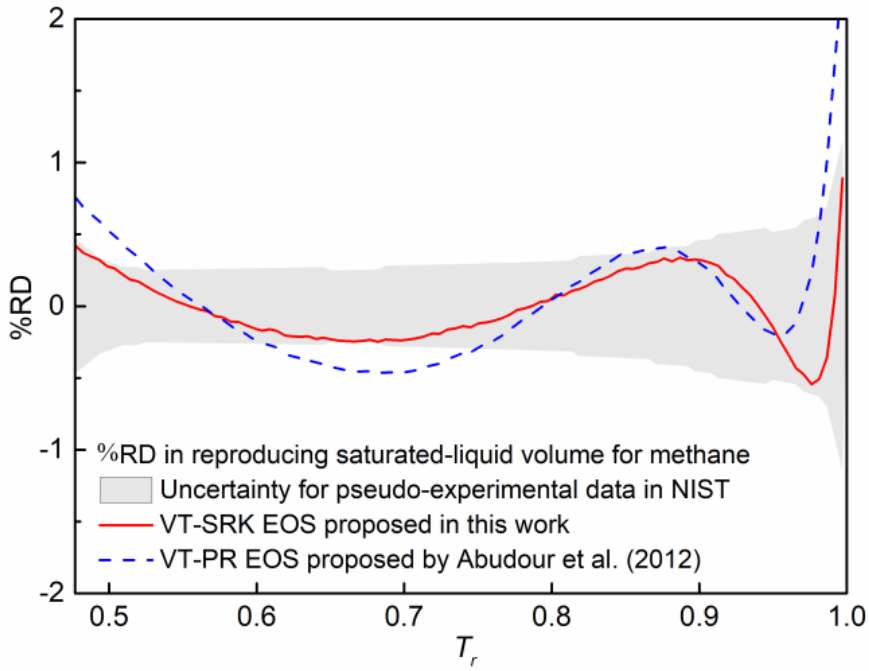

(a)

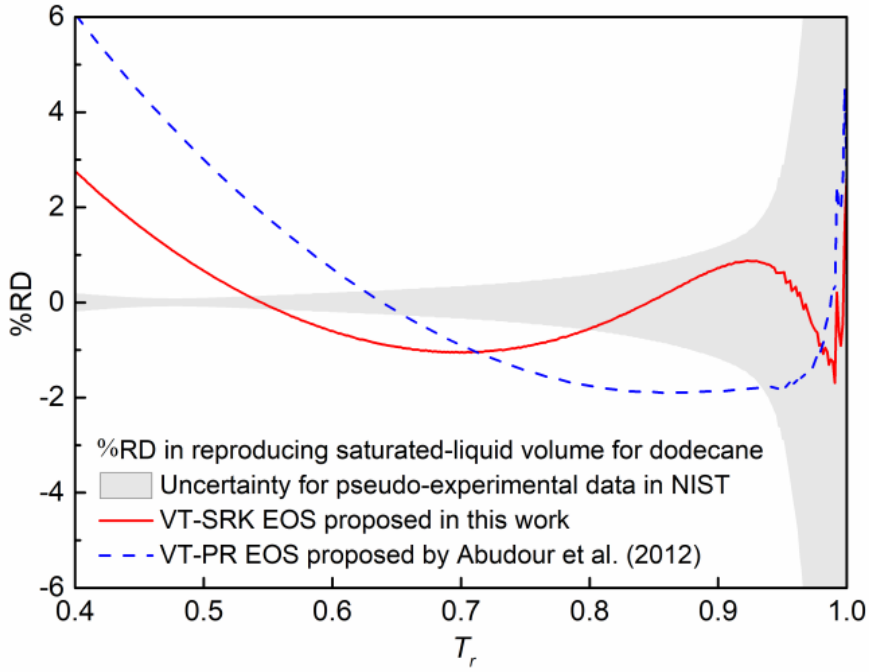

(b)

Fig. 2-4. Comparison of %RDs in reproducing the saturated-liquid molar volumes by the newly proposed VT-SRK EOS and the Abudour et al. VT-PR EOS [31] against the uncertainty reported by NIST [63] for pseudo-experimental liquid volumes: (a) methane and (b) dodecane.

As shown in **Fig. 2-4a**, at most temperature regions, the saturated-liquid volume %RDs for methane yielded by the newly proposed VT-SRK EOS are closer to

zero than those yielded by the Abudour et al. VT-PR EOS [31]. More importantly, all the %RDs for methane yielded by the improved VT-SRK EOS are within the area representing the uncertainty for pseudo-experimental data reported by NIST; the Abudour et al. VT-PR EOS [31] produces remarkably high %RDs near the critical temperature. Similarly, for dodecane (**Fig. 2-4b**), this improved VT-SRK EOS has a better performance on reproducing saturated-liquid density than the Abudour et al. VT-PR EOS [31]. The %RDs yielded by this work are close to the uncertainty for pseudo-experimental data over the low-temperature ranges but much lower than the uncertainty when T_r>0.80. This indicates that the improved VT-SRK EOS can provide more reliable saturated-volume calculations over the whole temperature range and may be possible to replace the available pseudo-experimental equation to reproduce the experimental liquid volumes.

Fig. 2-5 shows the %AADs in single-phase liquid volumes of methane and dodecane yielded by this work and Abudour et al.'s work [31] at different reduced pressures. Similar to the calculated saturated-liquid volume, for both methane and dodecane, the improved VT-model produces distinctly lower %AADs for single-phase liquid volumes than Abudour et al.'s model [31]. In particular, the %AADs yielded by our VT-SRK EOS appear to be much lower under subcritical pressures.

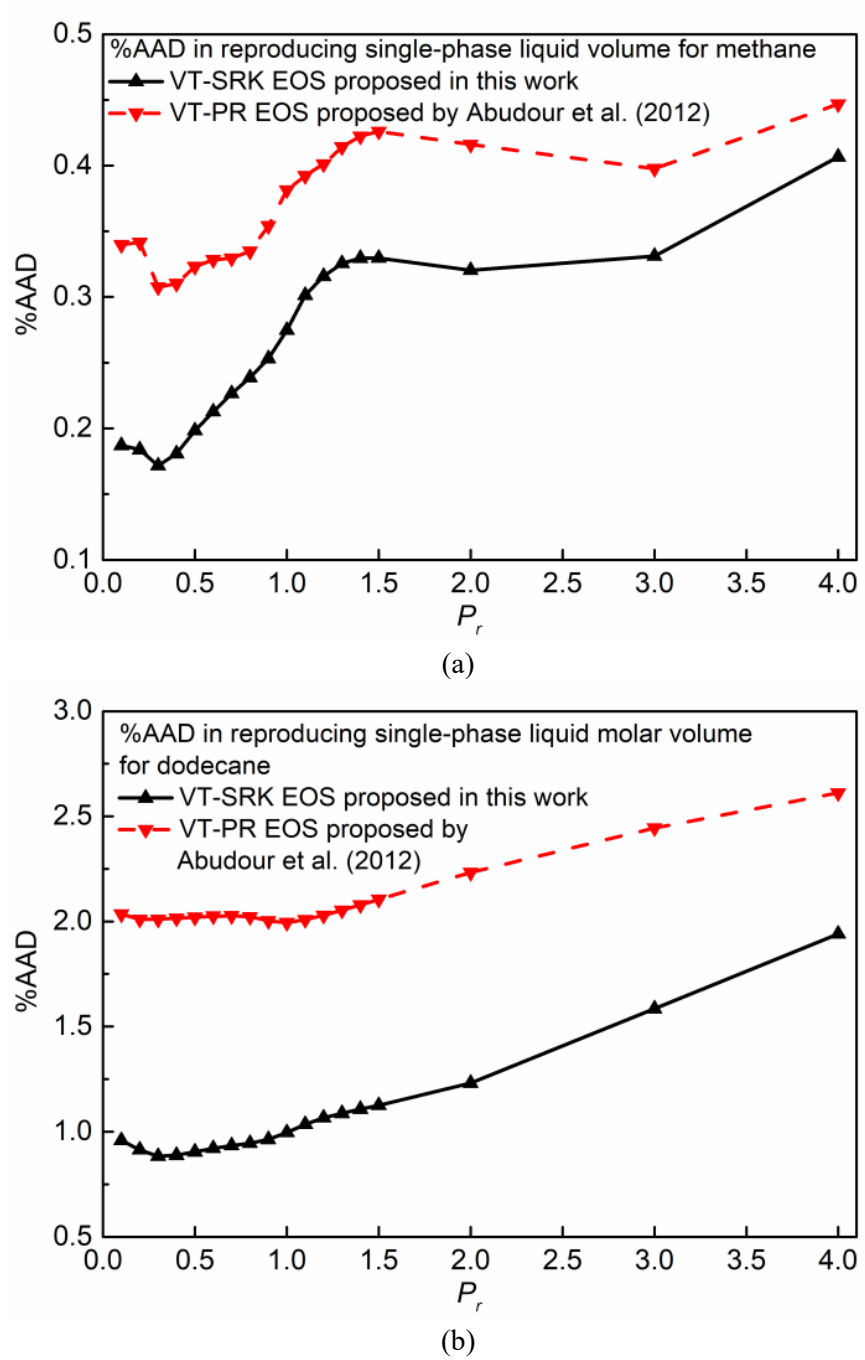

Fig. 2-5. Comparison of the %AADs in reproducing the single-phase liquid molar volumes by the newly proposed VT-SRK EOS and the updated VT-PR EOS proposed by Abudour et al. [31]: (a) methane and (b) dodecane.

Above evaluations about the liquid volume calculations are conducted under isobaric conditions. It is also necessary to consider the calculation accuracy of this improved VT-model in reproducing isothermal liquid volumes. Therefore, we compare the single-phase liquid molar volumes of methane and dodecane obtained by the newly

proposed VT-SRK EOS and the original SRK EOS [5] against the pseudo-experimental data reported by NIST [63] at given temperatures (T_r=0.5, 0.8, 0.99). The pressure rang is 0.01-5 P_r with a step of 0.01 P_r. As presented in **Fig. 2-6a**, both the newly proposed VT-SRK EOS and the original SRK EOS can provide reliable volumetric predictions for methane at a low reduced temperature (T_r=0.5). With the increasing temperatures, the original SRK EOS yields higher calculation errors on single-phase liquid volumes while the volume translated one can maintain satisfactory accuracy. For dodecane (**Fig. 2-6b**), the VT-model proposed in this work is able to significantly improve the isothermal volume calculations of SRK EOS at different given temperatures over the entire pressure range. In summary, the improved VT-SRK EOS can provide reliable volumetric calculations under both isobaric and isothermal processes.

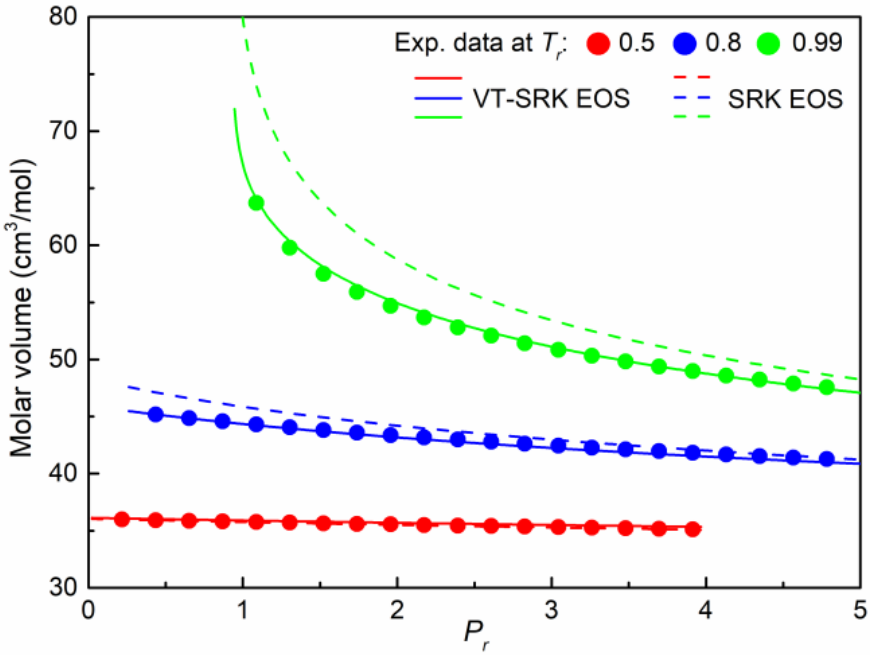

(a)

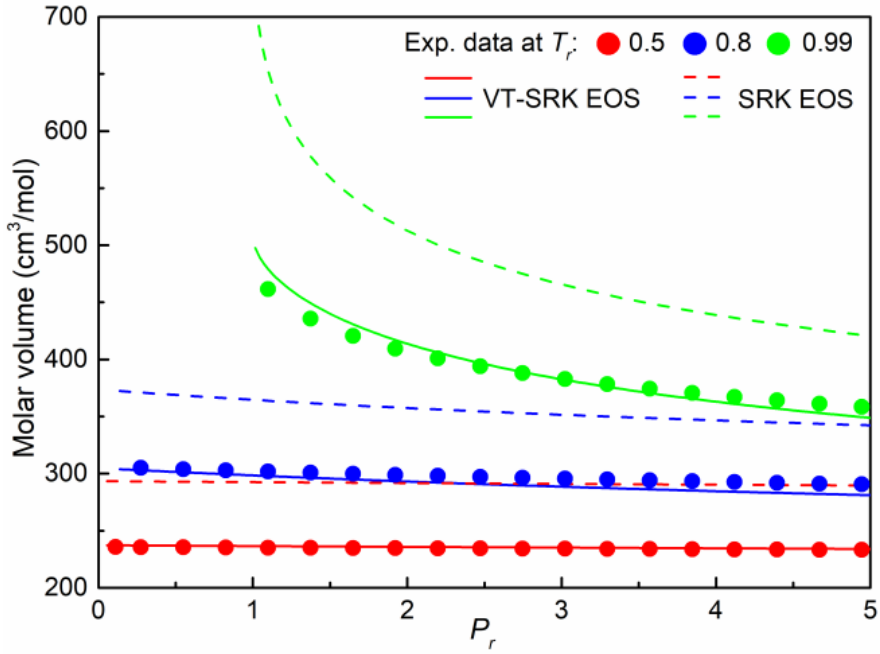

(b)

Fig. 2-6. Comparison of the single-phase liquid molar volumes under isothermal conditions yielded by the newly proposed VT-SRK EOS and the original SRK EOS [4] against the pseudo-experimental liquid volumes reported by NIST [63]: (a) methane and (b) dodecane.

Most temperature-dependent VT-model and temperature-volume-dependent VT-model can correct for the liquid density obtained by CEOS; but they might also alter some thermodynamic properties, resulting in thermodynamic inconsistency [65,66]. One of the thermodynamic inconsistency issues is that the pressure-volume (PV) isotherms at different temperatures for a given compound will intersect under supercritical pressures [66]. Thus, we need to check whether the newly proposed VT-model leads to PV isotherm crossover in a wide range of pressure and temperature. **Fig. 2-7** shows the PV curves of dodecane generated by the VT-SRK EOS (**Eq. 2-9**) at different reduced temperatures (T_r=0.5-3). In addition, we determine the maximum pressure below which there is no crossover in PV diagram based on the explicit criterion proposed by Shi and Li [67]:

$$D=\left(\frac{\partial v^{VTSRK}}{\partial T}\right)_P=\frac{RT}{P^{SRK}}\left(\frac{\partial Z^{SRK}}{\partial T}\right)_P+\frac{Z^{SRK}R}{P^{SRK}}-\frac{\partial[c(T)]}{\partial T}>0 \qquad (2\text{-}20)$$

where D is the first derivative of corrected molar volume with respect to temperature and the detailed derivation of D is presented in the previously published paper [67]. The value of D should be greater than zero if there is no crossover phenomenon. Z^{SRK} is the compressibility factor in SRK EOS, and $c(T)$ is given as:

$$c(T) = \Delta v = v^{SRK} - v^{VTSRK} = c_1\left(\frac{RT_c}{P_c}\right) + \sigma_c^{SRK}\left(\frac{1}{c_2 + c_3 d^{SRK}}\right) \tag{2-21}$$

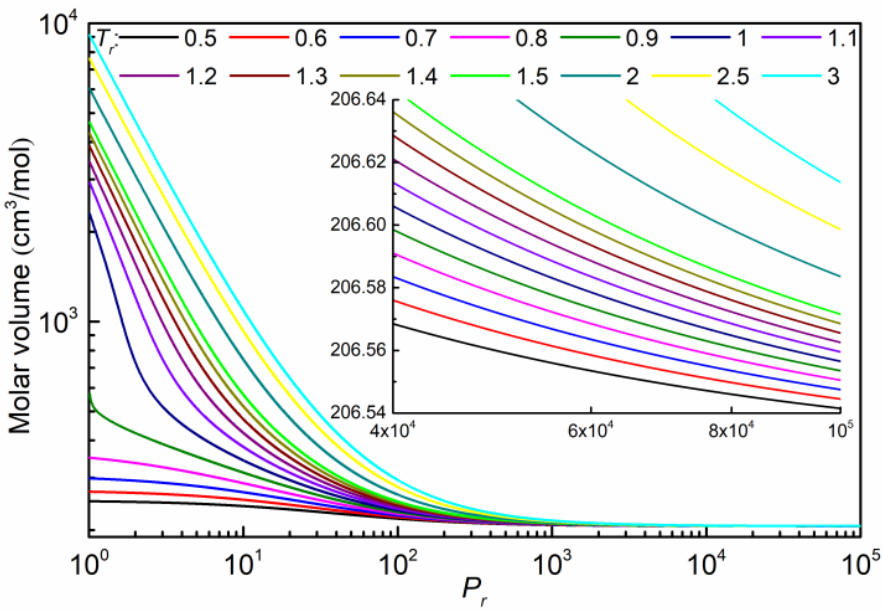

Fig. 2-7. PV diagrams for dodecane generated by the newly proposed VT-SRK EOS.

As seen in **Fig. 2-7**, the PV isotherms for dodecane at different reduced temperatures become closer with an increasing pressure but do not intersect with each other. Hence, we can draw a preliminary conclusion that the newly proposed VT-SRK EOS does not yield a crossover issue below 10^5 P_r. **Fig. 2-8** shows that the first derivative of corrected molar volume with respect to temperature (D) will continuously decrease with an increasing pressure at different temperatures. After approaching P_r=10^{16}, the values of D become less than zero under relatively low temperatures, indicating a crossover phenomenon. Therefore, the improved VT-SRK EOS is able to

provide volumetric calculations without causing the crossover phenomenon over a wide pressure range.

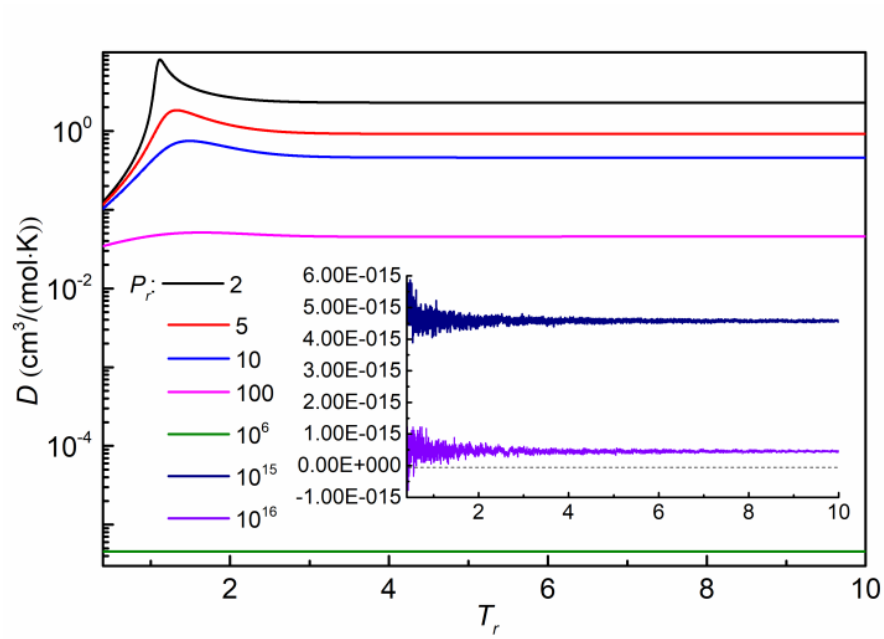

Fig. 2-8. Relationship between the first derivative of corrected molar volume for dodecane by the newly proposed VT-SRK EOS with respect to temperature (D) and reduced temperature (T_r) at different pressures.

2.5. Generalization of the Newly Proposed VT-SRK EOS

The generalization of the improved VT-EOS can be very useful since the specific parameters in VT-model are not available for other compounds that are absent in **Table 2-1**. However, due to the three fluid-dependent parameters adopted in the VT-model, this improved VT-SRK EOS becomes very sensitive to the individual compound and its generalization hardly reaches a compromise among the various substances from different categories. However, it might be possible to realize a better generalization only for a given subset of all the 56 compounds (such as organic hydrocarbons). Then we obtained linear regressions of c_1 versus acentric factor (ω) and c_2, c_3 versus critical compressibility factor (Z_c) for 26 organic hydrocarbons listed in **Table 2-1** and the results are presented in **Fig. 2-9**. For the sake of comparative analysis, the cc_1 in

Abudour et al.'s VT-model [31] for organic hydrocarbons has also been generalized versus critical compressibility factor Z_c and the results are shown in **Fig. 2-10**.

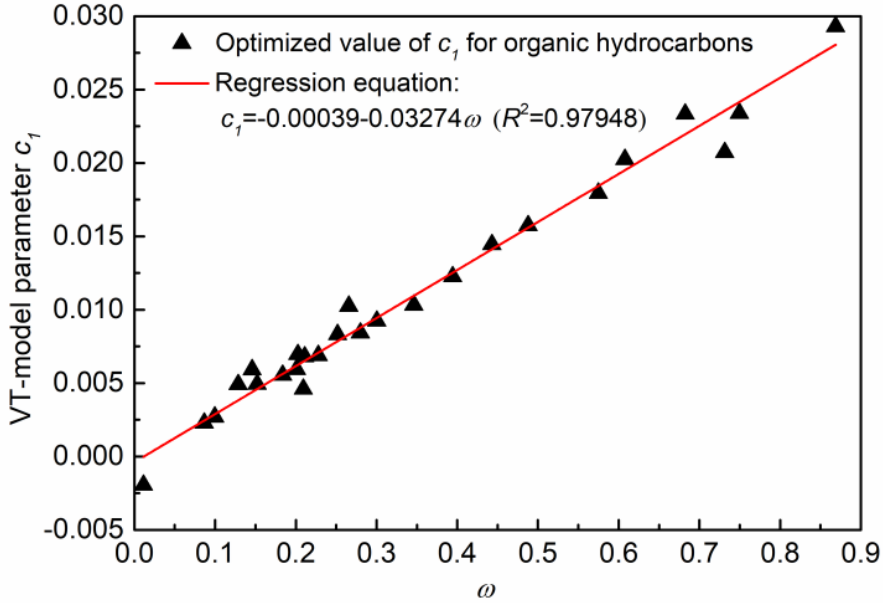

(a)

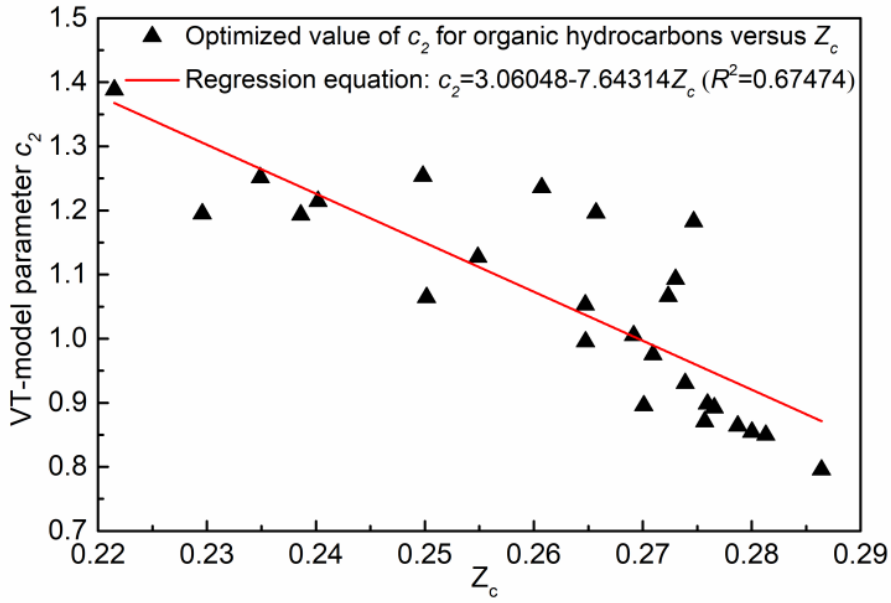

(b)

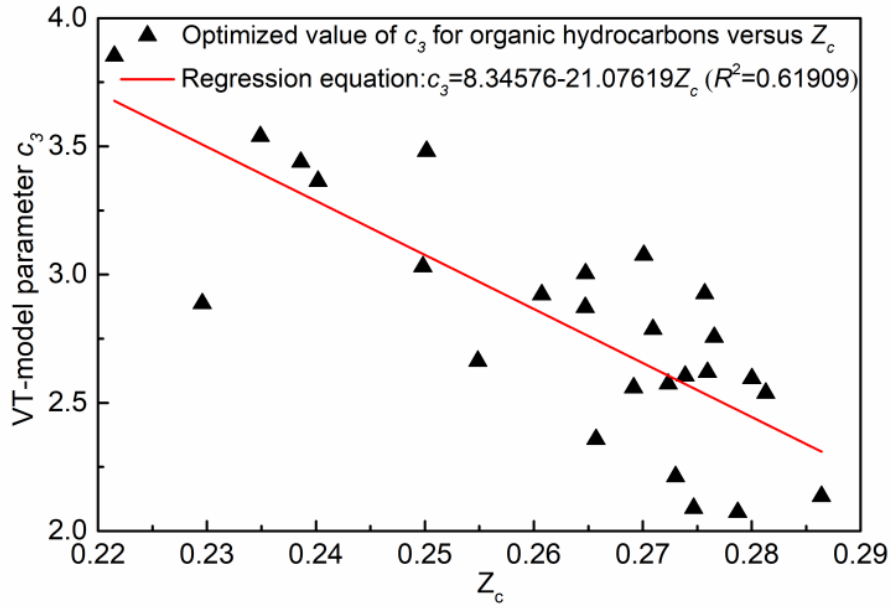

(c)

Fig. 2-9. Plots of optimized VT parameters in **Eq. 2-9** for the 26 organic hydrocarbons listed in **Table 2-1**: (a) c_1 versus acentric factor, (b) c_2 versus critical compressibility factor and (c) c_3 versus critical compressibility factor.

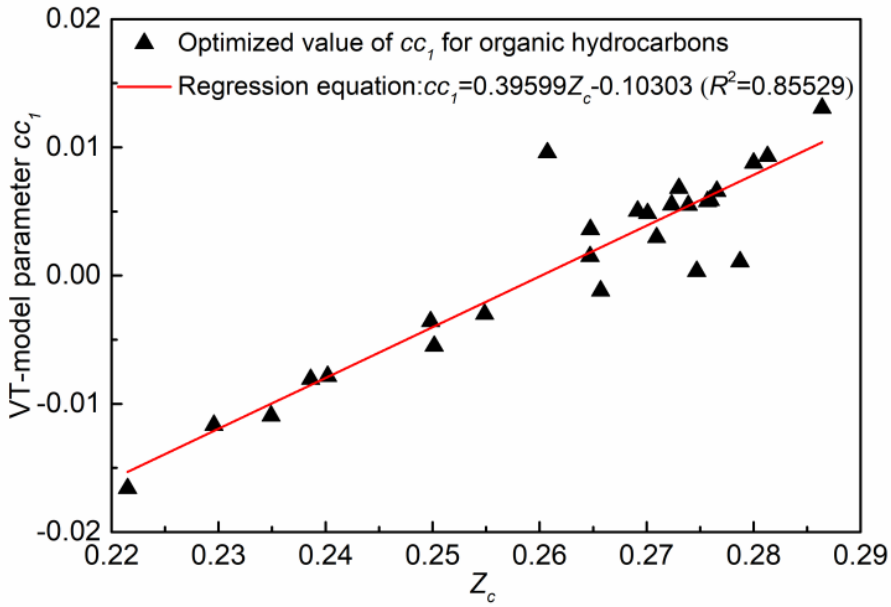

Fig. 2-10. Scattered plots of updated VT parameters in **Eq. 2-17** proposed by Abudour et al. [31] versus critical compressibility factor for the 26 organic hydrocarbons listed in **Table 2-1**.

Obviously, the c_1 values for organic hydrocarbons are well fitted to a regressed line (R^2=0.97948). Meanwhile, the c_2 and c_3 for organic hydrocarbons also clearly exhibit linear relationships with critical compressibility factor; the R^2s for regressing c_2

and c_3 are 0.67474 and 0.61909, respectively. These indicate an acceptable generalization of the VT-SRK EOS for hydrocarbons. The generalized VT-model parameters in SRK EOS are given as:

$$\begin{cases} c_1(\omega) = -3.90812\times10^{-4} + 0.03274\omega & (0.01140 < \omega < 0.86873) \\ c_2(Z_c) = 3.06048 - 7.64314Z_c & (0.22150 < Z_c < 0.28640) \\ c_3(Z_c) = 8.34576 - 21.07619Z_c & (0.22150 < Z_c < 0.28640) \end{cases} \quad (2\text{-}22)$$

The generalized VT-model parameter in PR EOS is given as:

$$cc_1(Z_c) = 0.39599Z_c - 0.10303 \qquad (0.22150 < Z_c < 0.28640) \quad (2\text{-}23)$$

Note that, in the generalized VT-SRK EOS, the original Twu α-function [3] presented in **Eq. 2-4** has also been replaced by the generalized version [68] shown below:

$$\alpha^{Twu}(T) = T_r^{2(M-1)} \exp[L(1 - T_r^{2M})] \quad (2\text{-}24)$$

where

$$\begin{cases} L(\omega) = 0.0611\omega^2 + 0.7535\omega + 0.1359 \\ M(\omega) = 0.1709\omega^2 - 0.2063\omega + 0.8787 \end{cases} \quad (2\text{-}25)$$

Table 2-3 compares the performances of our generalized VT-SRK EOS (**Eq. 2-22**) and the generalized VT-PR EOS proposed by Abudour et al. (**Eq. 2-23**) in reproducing saturated and single-phase liquid molar volumes. The overall %AADs for saturated and single-phase molar volumes yielded by our generalized VT-SRK EOS for 26 organic hydrocarbons are 1.18 and 1.31, respectively. These %AADs are higher than those yielded by the individualized version but still evidently lower than those yielded by generalized Abudour et al.'s VT-PR EOS (2.36 and 2.59). In addition, the %AADs for saturated and single-phase liquid volumes for all the 26 hydrocarbons obtained by

this generalized work are lower than 4.00 while those for hexane, heptane and cyclopropane obtained by Adudour et al.'s work [31] are over 5.00.

Table 2-3. Comparison of the calculation accuracy for saturated and single-phase liquid molar volume for organic hydrocarbons listed in **Table 2-1** by our generalized VT-SRK EOS (**Eq. 2-22**) and the generalized VT-PR EOS proposed by Abudour et al. (**Eq. 2-23**)

Compound	%AAD yielded by the generalized VT-SRK EOS				%AAD yielded by the generalized VT-PR EOS proposed by Abudour et al. [31][b]			
	$\%AAD_{single}$[c]	$\%AAD_{sub}$[d]	$\%AAD_{sup}$[e]	$\%AAD_{sat}$[f]	$\%AAD_{single}$[c]	$\%AAD_{sub}$[d]	$\%AAD_{sup}$[e]	$\%AAD_{sat}$[f]
Methane	1.37	1.36	1.38	1.12	2.15	2.19	2.10	1.98
Ethane	0.93	0.84	1.02	0.71	1.50	1.44	1.56	1.34
Propane	1.24	1.16	1.33	0.96	1.92	1.87	1.97	1.69
Butane	1.07	0.95	1.20	0.78	1.51	1.44	1.59	1.28
Pentane	1.04	0.94	1.15	0.79	2.31	2.18	2.44	2.11
Hexane	1.10	1.00	1.21	1.14	5.81	6.02	5.59	6.00
Heptane	1.16	1.03	1.29	1.01	5.30	5.53	5.06	5.25
Octane	0.92	0.81	1.03	0.84	3.39	3.59	3.18	3.35
Nonane	1.08	1.01	1.17	1.05	1.77	1.73	1.81	1.48
Decane	1.01	0.89	1.14	0.84	1.93	1.85	2.02	1.88
Dodecane	1.48	1.29	1.68	1.13	2.41	2.46	2.36	2.25
Tridecane[a]	0.99	0.89	1.12	1.00	2.07	2.02	2.13	2.17
Pentadecane[a]	3.46	3.52	3.38	3.00	2.60	2.61	2.58	1.96
Hexadecane[a]	2.72	2.67	2.78	3.26	3.48	3.47	3.48	2.52
Heptadecane[a]	1.62	1.52	1.75	1.19	3.28	3.27	3.28	2.73
Eicosane[a]	1.59	1.70	1.46	1.83	4.12	4.17	4.06	3.34
Isobutane	1.17	1.06	1.30	0.87	1.67	1.62	1.72	1.43
2-Methylbutane	1.56	1.44	1.70	1.25	2.29	2.20	2.39	2.08
2-Methylpentane	1.68	1.55	1.82	1.30	2.28	2.27	2.30	1.96
Cyclohexane	1.54	1.33	1.75	1.16	1.68	1.50	1.85	1.44
Cyclopropane	0.61	0.64	0.59	0.82	6.60	6.65	6.56	6.66
Ethylene	0.76	0.67	0.85	0.56	1.26	1.21	1.32	1.14
Propylene	1.31	1.28	1.33	1.18	1.94	1.92	1.97	1.74
Propyne	0.49	0.52	0.46	0.68	0.78	0.60	0.94	0.65
Benzene	0.58	0.49	0.68	0.50	1.51	1.38	1.63	1.28
Toluene	1.66	1.78	1.53	1.76	1.85	1.81	1.90	1.64
Overall	1.31	1.24	1.39	1.18	2.59	2.58	2.61	2.36

[a] The maximum temperature at which the single-phase liquid densities can be retrieved from NIST database cannot reach the saturation condition.
[b] The updated parameter within the VT-PR EOS proposed by Abudour et al. [31] for organic hydrocarbons listed in **Table 2-1** has been generalized.
[c] %AAD for single-phase liquid volume over the entire pressure range.
[d] %AAD for single-phase liquid volume under $P_r \leq 1$.
[e] %AAD for single-phase liquid volume under $P_r > 1$.
[f] %AAD for saturated-liquid volume.

For the sake of more reasonable validation, the calculation accuracy for saturated and single-phase liquid density of tetracosane, 1-butene and 2,3-dimethylpentane by

the generalized VT-SRK EOS have also been determined and compared with the counterpart by Adudour et al.'s VT-model [31]. These three hydrocarbons are randomly selected and not included in the database shown in **Table 2-1**. **Table 2-4** shows the physical properties of these three hydrocarbons as well as the calculation errors for saturated and single-phase liquid molar volumes yielded by our generalized VT-SRK EOS (**Eq. 2-22**) and the generalized Abudour et al.'s VT-PR EOS (**Eq. 2-23**). It can be clearly observed from **Table 2-4** that our generalized VT-SRK EOS yields lower %AADs for saturated and single-phase liquid molar volumes of the three hydrocarbons than the generalized Adudour et al.'s VT-PR EOS [31]. Overall, it can be concluded that the generalized VT-SRK EOS may not perform as well as the individualized version; but it is shown to be still quite reliable in predicting the liquid molar volumes for hydrocarbons.

Table 2-4. Physical properties for three randomly selected hydrocarbons and comparison of the calculation accuracy for saturated and single-phase liquid molar volume by our generalized VT-SRK EOS (**Eq. 2-22**) and the generalized VT-PR EOS proposed by Abudour et al. (**Eq. 2-23**)

Compound	T_c (K)	P_c (MPa)	ω	Z_c	%AAD yielded by the generalized VT-SRK EOS				%AAD yielded by the generalized VT-PR EOS proposed by Abudour et al. [31][b]			
					$\%AAD_{single}$[c]	$\%AAD_{sub}$[d]	$\%AAD_{sup}$[e]	$\%AAD_{sat}$[f]	$\%AAD_{single}$[c]	$\%AAD_{sub}$[d]	$\%AAD_{sup}$[e]	$\%AAD_{sat}$[f]
Tetracosane[a]	799.6	0.87	1.05756	0.20719	0.34	0.35	0.33	2.96	5.79	5.82	5.76	3.10
1-Butene	419.29	4.01	0.19237	0.27137	1.72	1.68	1.75	1.47	2.55	2.51	2.58	2.30
2,3-Dimethylpentane[a]	537.47	2.91	0.29481	0.25730	2.51	2.40	2.65	1.42	5.65	5.61	5.70	4.13

[a] The maximum temperature at which the single-phase liquid densities can be retrieved from NIST database cannot reach the saturation condition.
[b] The updated parameter within the VT-PR EOS proposed by Abudour et al. [31] for organic hydrocarbons listed in **Table 2-1** has been generalized.
[c] %AAD for single-phase liquid volume over the entire pressure range.
[d] %AAD for single-phase liquid volume under $P_r \leq 1$.
[e] %AAD for single-phase liquid volume under $P_r > 1$.
[f] %AAD for saturated-liquid volume.

2.6. Extension of the Newly Proposed VT-SRK EOS to Hydrocarbon Mixtures

Besides pure substances, it is of significance to provide accurate volume calculations for mixtures, especially for hydrocarbon mixtures that are commonly seen in petroleum industry. Hence, in this section, we demonstrate the performance of the

newly proposed VT-SRK EOS in reproducing liquid density of hydrocarbon mixtures with given compositions. The database of binary-mixture densities is shown in **Table 2-5**. The tested binary mixtures include three n-alkane mixtures, one cyclohexane-hexane mixture and one benzene-hexane mixture.

Table 2-5. Database of liquid densities of binary mixtures examined in this study.

System	Temperature range (K)	Pressure range (MPa)	Density range of liquid phase (g/cm^3)	Mole-fraction range of Compound (1) in liquid phase	Number of data points	Data source
Ethane(1)-Propane(2)	283.15-322.05	2.76-9.65	268.6-506.6	0.2991-0.9511	315	Parrish [72]
Propane(1)-Butane(2)	343.05-418.05	1.7237-4.292	251.4-455.6	0.1468-0.9258	62	Kay 1970 [73]
Pentane(1)-Hexane(2)	298.15-348.15	0.1-40	572.51-686.15	0.122-0.874	210	Pecar and Dolecek [74]
Cyclohexane(1)-Hexane(2)	298.15-473.15	0.1013	460.6-746	0.2039-0.8038	77	Beg et al. [75]
Benzene(1)-Hexane(2)	298.15-473.15	0.1013	469.4-816.8	0.2162-0.8153	77	Beg et al. [76]

The improved VT-model adopted in reproducing mixture volumes is the generalized version (**Eq. 2-22**). In order to extend CEOS to mixtures, we use the classical mixing rule to determine the values of EOS parameters (a_m and b_m) for mixtures as below [1,69],

$$a_m = \sum_i \sum_j x_i x_j a_{ij} \tag{2-26}$$

$$a_{ij} = \sqrt{a_i a_j}\left(1 - C_{ij}\right) \tag{2-27}$$

$$b_m = \sum_i \sum_j x_i x_j b_{ij} \tag{2-28}$$

$$b_{ij} = \frac{\left(b_i + b_j\right)}{2} \tag{2-29}$$

where the subscript i indicates the pure compound i in the mixture and the subscript m indicates the mixture. The C_{ij} in **Eq. 2-27** is the empirical "binary interaction parameters (BIP)" that is determined from experimental data. However, on the one hand, the mixtures adopted in this study are binary hydrocarbon systems, and BIP is generally more needed for the nonhydrocarbon-hydrocarbon systems. On the other hand, in 2013,

Abudour et al. [32] have proved that BIP increases the calculation accuracy of the bubble-point pressures for hydrocarbon mixtures, while it offers little improvement on the volumetric predictions yielded by VT-EOS. Thus we set C_{ij}=0 in this study.

The proposed VT-model for mixtures is shown as follows:

$$v_m^{VTSRK} = v_m^{SRK} - c_{1m}\left(\frac{RT_{cm}}{P_{cm}}\right) - \delta_{cm}^{SRK}\left(\frac{1}{c_{2m} + c_{3m} d_m^{SRK}}\right) \tag{2-30}$$

The VT-parameters for mixtures (c_{1m}, c_{2m} and c_{3m}) are determined according to the linear mixing rule proposed by Peneloux et al. [12] as:

$$c_{1m} = \sum_i x_i c_{1i} \quad c_{2m} = \sum_i x_i c_{2i} \quad c_{3m} = \sum_i x_i c_{3i} \tag{2-31}$$

The dimensionless distance function of mixture (d_m^{SRK}) and the volume shift of mixture at critical temperature ($\delta_{cm}^{\mathrm{SRK}}$) in SRK EOS are given as [32]:

$$d_m^{SRK} = -\frac{v_m^{SRK^2}}{RT_{cm}}\left(\frac{\partial P_m^{SRK}}{\partial v_m^{SRK}}\right)_T = \frac{v_m^{SRK^2} T}{T_{cm}\left(v_m^{SRK} - b_m^{SRK}\right)^2} - \frac{a_m^{SRK}\left(2v_m^{SRK} + b_m^{SRK}\right)}{RT_{cm}\left(v_m^{SRK} + b_m^{SRK}\right)^2} \tag{2-32}$$

$$\delta_{cm}^{SRK} = \frac{RT_{cm} Z_c^{SRK}}{P_{cm}} - v_{cm} \tag{2-33}$$

P_{cm} is the critical pressure of mixture and calculated through the correlation proposed by Aalto et al. [70]:

$$P_{cm} = \frac{(0.2905 - 0.085\omega_m) RT_{cm}}{v_{cm}} \tag{2-34}$$

where ω_m is the acentric factor of mixture and also calculated by linear mixing rule:

$$\omega_m = \sum_i x_i \omega_i \tag{2-35}$$

T_{cm} and v_{cm} are the critical temperature and critical volume of mixture, respectively, and they can be obtained according to the method proposed by Chueh and Prausnitz [71]:

$$T_{cm} = \sum_i \theta_i T_{ci} \tag{2-36}$$

$$v_{cm} = \sum_i \theta_i v_{ci} \tag{2-37}$$

where θ_i is the surface fraction of compound i:

$$\theta_i = \frac{x_i v_{ci}^{\frac{2}{3}}}{\sum_i x_i v_{ci}^{\frac{2}{3}}} \tag{2-38}$$

The above calculation method for P_{cm}, T_{cm}, ω_m and v_{cm} is essentially the same as the method adopted by Abudour et al. [32] Here, we will still use Abudour et al. VT-model as the benchmark model for comparison purpose. We calculate the densities of liquid mixtures with the given molar fractions through the proposed VT-SRK EOS, Abudour et al. VT-PR EOS, original SRK EOS and original PR EOS, respectively and calculation errors are summarized in **Table 2-6**. Overall, although the SRK EOS exhibits a much higher calculation error for mixture volumes (12.73 %AAD) than the PR EOS (4.05 %AAD), coupling the proposed VT-model to the SRK EOS leads to a dramatically lower %AAD (1.36 %AAD) than the VT-PR EOS proposed by Abudour et al. (2.52 %AAD). Moreover, the %AAD for each mixture yielded by the proposed VT-SRK EOS is also lower than that yielded by Abudour et al.'s VT-PR EOS, indicating a better performance of the proposed VT-SRK EOS model.

Table 2-6. Comparison of the average absolute percentage deviations (%AADs) for molar volumes of mixtures yielded by the original SRK EOS, the original PR EOS, the VT-SRK EOS proposed in this work and the VT-PR EOS proposed by Abudour et al. [31]

Mixtures	SRK EOS	VT-SRK EOS (This work)	PR EOS	VT-PR EOS (Abudour et al. [31])
Ethane(1)-Propane(2)	10.09	0.61	3.09	1.27
Propane(1)-Butane(2)	20.01	2.50	7.48	3.43
Pentane(1)-Hexane(2)	8.91	1.87	3.03	1.92
Cyclohexane(1)-Hexane(2)	12.01	1.10	3.56	3.05
Benzene(1)-Hexane(2)	12.64	0.70	3.07	2.94
Overall	12.73	1.36	4.05	2.52

To provide a more vivid comparison, we plot the volumes at the phase boundaries yielded by the newly proposed VT-SRK EOS, original SRK EOS and PR EOS against the experimental data for the propane-butane system in **Fig. 2-11** as well as the relative percentage deviations (%RDs) in reproducing single-phase liquid volumes at atmospheric pressure yielded by the proposed VT-SRK EOS and Abudour et al. VT-PR EOS for the benzene-hexane system in **Fig. 2-12**. As illustrated by **Fig. 2-11**, the VT-SRK EOS proposed in this work can more acutely simulate the volume change versus temperature than the original SRK and PR EOSs and improve the volume predictions for propane-butane system with different compositions. Similarly, **Fig. 2-12** shows that the proposed VT-SRK EOS can yield lower calculation errors of volumes for benzene-hexane system with different compositions than the Abudour et al. VT-PR EOS under different temperatures. In conclusion, the VT-model developed in this work improves the volume prediction not only for pure substances but also for hydrocarbon mixtures. It appears to be promising to employ the proposed VT-SRK EOS to achieve more accurate density estimation for complex reservoir fluids under varied temperature/pressure conditions.

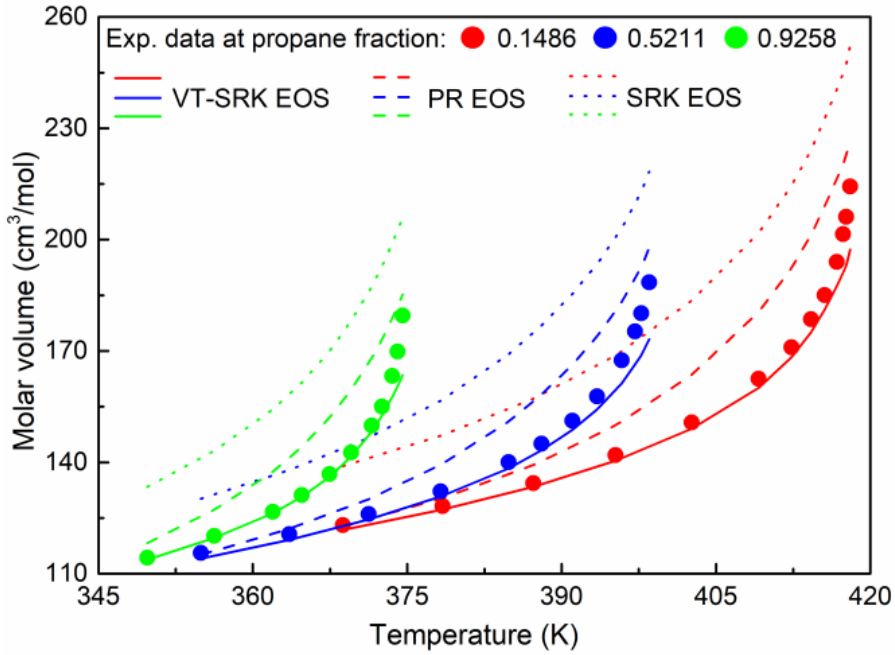

Fig. 2-11. Comparison of the molar volumes at the phase boundaries for propane(1)-butane(2) system yielded by the newly proposed VT-SRK EOS, original SRK EOS and PR EOS against experimental data [73].

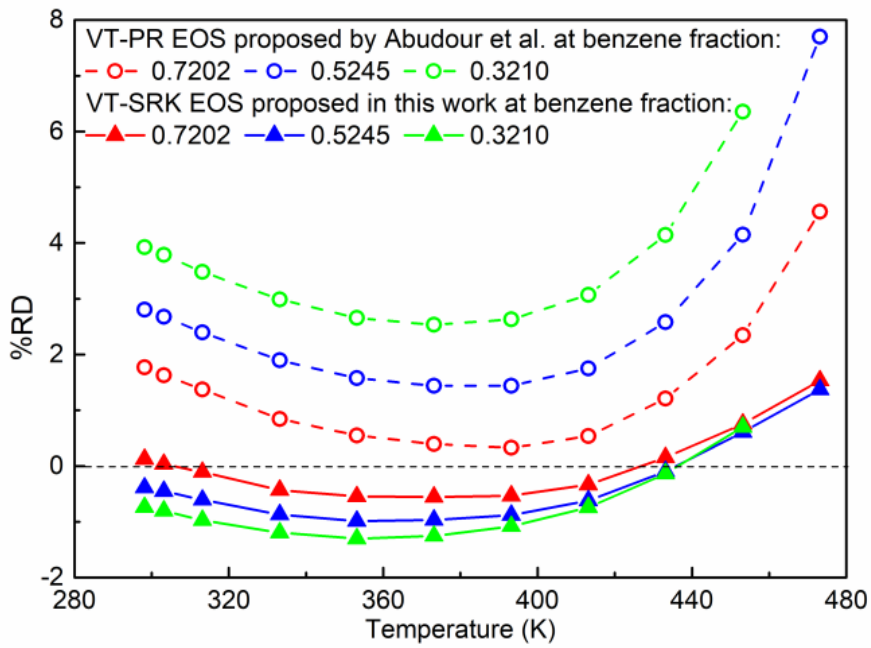

Fig. 2-12. Comparison of %RDs in reproducing molar volumes for benzene(1)-hexane(2) system at atmospheric pressure by the newly proposed VT-SRK EOS and the VT-PR EOS by Abudour et al. [31]

2.7. Conclusions

In this work, we develop an improved volume translation in SRK EOS that aims to significantly improve the calculation accuracy of saturated and single-phase liquid volumes. Compared to traditional one fluid-dependent parameter VT-model, the improved volume translation with three fluid-dependent parameters is more sensitive to distance function and precisely captures the needed volume shifts under different temperatures and pressures. We compile a database which includes the saturated and single-phase liquid density data for a diverse group of species (including 56 pure compounds); the three fluid-dependent parameters in VT-SRK EOS are optimally determined for each compound. The overall average absolute percentage deviations (%AADs) for the saturated and single-phase liquid volumes of 56 compounds obtained by the improved VT-SRK EOS are 0.61 and 0.84, respectively; these calculation errors are obviously lower than the counterparts yielded by updated Abudour et al.'s VT-PR EOS (i.e., 1.36 and 1.45). The proposed VT-SRK EOS is able to provide reliable volumetric calculation under both isobaric and isothermal processes and gives rise to the crossover of PV isotherms only under extremely high pressures. We also obtain a fairly good generalization of the VT-SRK EOS for organic hydrocarbons. The %AADs for saturated and single-phase molar volumes yielded by the generalized VT-SRK EOS for 26 hydrocarbons are 1.18 and 1.31, respectively, which are higher than those yielded by the individualized VT-SRK EOS but still evidently lower than those yielded by the generalized Abudour et al.'s VT-PR EOS (2.36 and 2.59). Finally, we extend the improved VT-model to mixtures through conventional mixing rules, demonstrating that the VT-SRK EOS also performs well in the density predictions for hydrocarbon mixtures examined in this study.

Acknowledgments

The authors greatly acknowledge a Discovery Grant from the Natural Sciences and Engineering Research Council (NSERC) of Canada to H. Li. X. Chen also greatly acknowledges the financial support provided by the China Scholarship Council (CSC) via a Ph.D. Scholarship (No.: 201806450029).

References

[1] J.D. van der Waals, Continuity of the gaseous and liquid state of matter, Ph.D. thesis, Leiden, 1873.

[2] H.W. Curtis, R.B. Michael, Phase behavior, SPE monograph series 20 (2000).

[3] C.H. Twu, D. Bluck, J.R. Cunningham, J.E. Coon, A cubic equation of state with a new alpha function and a new mixing rule, Fluid Phase Equilib. 69 (1991) 33-50, https://doi.org/10.1016/0378-3812(91)90024-2.

[4] D.Y. Peng, D.B. Robinson, A new two-constant equation of state, Ind. Eng. Chem. Fundam. 15 (1976) 59-64, https://doi.org/10.1021/i160057a011

[5] G. Soave, Equilibrium constants from a modified Redlich-Kwong equation of state, Chem. Eng. Sci. 27 (1972) 1197-1203, https://doi.org/10.1016/0009-2509(72)80096-4.

[6] A. Pina-Martinez, Y. Le Guennec, R. Privat, J. Jaubert, P.M. Mathias, Analysis of the combinations of property data that are suitable for a safe estimation of consistent Twu α-function parameters: Updated parameter values for the translated-consistent tc-PR and tc-RK cubic equations of state, J. Chem. Eng. Data 63 (2018) 3980-3988, https://doi.org/10.1021/acs.jced.8b00640.

[7] M. Cismondi, J. Cruz, M.J. Gomez, G.F. Montoya, Modelling the phase behavior of alkane mixtures in wide ranges of conditions: New parameterization and predictive correlations of binary interactions for the RKPR EOS, Fluid Phase Equilib. 403 (2015) 49-59, https://doi.org/10.1016/j.fluid.2015.06.005.

[8] N.G. Tassin, S.B.R. Reartes, M. Cismondi, New correlations for prediction of high-pressure phase equilibria of n-alkane mixtures with the RKPR EoS: Back from the use of l_{ij} (repulsive) interaction parameters, J. Chem. Eng. Data 64 (2019) 2093-2109, https://doi.org/10.1021/acs.jced.8b01050.

[9] P.N.P. Ghoderao, V.H. Dalvi, M. Narayan, A four-parameter cubic equation of state for pure compounds and mixtures, Chem. Eng. Sci. 190 (2018) 173-189, https://doi.org/10.1016/j.ces.2018.06.010.

[10] P.N.P. Ghoderao, V.H. Dalvi, M. Narayan, A four parameter cubic equation of state with temperature dependent covolume parameter, Chinese J. Chem. Eng. 27 (2019) 1132-1148, https://doi.org/10.1016/j.cjche.2018.08.013.

[11] J.J. Martin, Cubic equations of state-which? Ind. Eng. Chem. Fundam. 18 (1979) 81-97, https://doi.org/10.1021/i160070a001.

[12] A. Peneloux, E. Rauzy, R. Freze, A consistent correction for Redlich-Kwong-Soave volumes, Fluid Phase Equilib. 8 (1982) 7-23, https://doi.org/10.1016/0378-3812(82)80002-2.

[13] M.B. Dahbag, M. Zirrahi, H. Hassanzadeh, Solubility and liquid density of ammonia/athabasca bitumen mixtures at temperatures up to 463 K: Measurements and modeling, J. Chem. Eng. Data 64 (2019) 3592-3597, https://doi.org/10.1021/acs.jced.9b00356.

[14] T. Sun, A. Takbiri-Borujeni, H. Nourozieh, M. Gu, Application of Peng-Robinson equation of state for modelling the multiphase equilibrium properties in athabasca bitumen/ethane mixtures, Fuel 252 (2019) 439-447, https://doi.org/10.1016/j.fuel.2019.04.106.

[15] S.G. Cardoso, G.M.N. Costa, S.A.B. Vieira de Melo, Assessment of the liquid mixture density effect on the prediction of supercritical carbon dioxide volume expansion of organic solvents by Peng-Robinson equation of state, Fluid Phase Equilib. 425 (2016) 196-205, https://doi.org/10.1016/j.fluid.2016.06.006.

[16] I.H. Bell, J. Welliquet, M.E. Mondejar, A. Bazyleva, S. Quoilin, F. Haglind, Application of the group contribution volume translated Peng-Robinson equation of state to new commercial refrigerant mixtures, Int. J. Refrig. 103 (2019) 316-328, https://doi.org/10.1016/j.ijrefrig.2019.04.014.

[17] H. Lin, Y. Duan, Empirical correction to the Peng-Robinson equation of state for the saturated region, Fluid Phase Equilib. 233 (2005) 194-203, https://doi.org/10.1016/j.fluid.2005.05.008.

[18] H. Lin, Y. Duan, T. Zhang, Z.M. Huang, Volumetric property improvement for the Soave-Redlich-Kwong equation of state, Ind. Eng. Chem. Res. 45 (2006) 1829-1839, https://doi.org/10.1021/ie051058v.

[19] K. Magoulas, D. Tassios, Thermophysical properties of n-alkanes from C1 to C20 and their prediction for higher ones, Fluid Phase Equilib. 56 (1990) 119-140, https://doi.org/10.1016/0378-3812(90)85098-U.

[20] W.D. Monnery, W.Y. Svrcek, M.A. Satyro, Gaussian-like volume shifts for the Peng-Robinson equation of state, Ind. Eng. Chem. Res. 37 (1998) 1663-1672, https://doi.org/10.1021/ie970640j.

[21] M. Nazarzadeh, M. Moshfeghian, New volume translated PR equation of state for pure compounds and gas condensate systems, Fluid Phase Equilib. 337 (2013) 214-224, https://doi.org/10.1016/j.fluid.2012.10.003.

[22] J. Shi, H. Li, W. Pang, An improved volume translation strategy for PR EOS without crossover issue, Fluid Phase Equilib. 470 (2018) 164-175, https://doi.org/10.1016/j.fluid.2018.01.034.

[23] P. Watson, M. Cascella, D. May, S. Salerno, D. Tassios, Prediction of vapor pressures and saturated molar volumes with a simple cubic equation of state. 2. The Van der Waals-711 EOS, Fluid Phase Equilib. 27 (1986) 35-52, https://doi.org/10.1016/0378-3812(86)87039-X.

[24] W.R. Ji, D.A. Lempe, Density improvement of the SRK equation of state, Fluid Phase Equilib. 130 (1997) 49-63, https://doi.org/10.1016/S0378-3812(96)03190-1.

[25] J.C. Tsai, Y.P. Chen, Application of a volume-translated Peng-Robinson equation of state on vapor-liquid equilibrium calculations, Fluid Phase Equilib. 145 (1998) 193-215, https://doi.org/10.1016/S0378-3812(97)00342-7.

[26] H. Baled, R.M. Enick, Y. Wu, M.A. McHugh, W. Burgess, D. Tapriyal, B.D. Morreale, Prediction of hydrocarbon densities at extreme conditions using volume-translated SRK and PR equations of state fit to high temperature, high pressure PVT data, Fluid Phase Equilib. 317 (2012) 65-76, https://doi.org/10.1016/j.fluid.2011.12.027.

[27] H.B. De Sant'Ana, P. Ungerer, J.C. De Hemptinne, Evaluation of an improved volume translation for the prediction of hydrocarbon volumetric properties, Fluid Phase Equilib. 154 (1999) 193-204, https://doi.org/10.1016/S0378-3812(98)00441-5.

[28] H.B. De Sant'Ana, P. Ungerer, C. Batut, Measurement and prediction of volumetric and transport properties of reservoir fluids at high pressure, Oil Gas Sci. Tech. 53 (1998) 265-281, https://doi.org/10.2516/ogst:1998024.

[29] G.F. Chou, J.M. Prausnitz, A phenomenological correction to an equation of state for the critical region, AIChE J. 35 (1989) 1487-1496, https://doi.org/10.1002/aic.690350909.

[30] P.M. Mathias, T. Naheiri, E.M. Oh, A density correction for the Peng-Robinson equation of state, Fluid Phase Equilib. 47 (1989) 77-87, https://doi.org/10.1016/0378-3812(89)80051-2.

[31] A.M. Abudour, S.A. Mohammad, R.L. Robinson, K.A.M. Gasem, Volume-translated Peng-Robinson equation of state for saturated and single-phase liquid densities, Fluid Phase Equilib. 335 (2012) 74-87, https://doi.org/10.1016/j.fluid.2012.08.013.

[32] A.M. Abudour, S.A. Mohammad, R.L. Robinson, K.A.M. Gasem, Volume-translated Peng-Robinson equation of state for liquid densities of diverse binary mixtures, Fluid Phase Equilib. 349 (2013) 37-55, https://doi.org/10.1016/j.fluid.2013.04.002.

[33] K. Frey, J.W. Tester, M. Modell, Density-and-temperature-dependent volume translation for the SRK EOS: 1. Pure fluids, Fluid Phase Equilib. 279 (2009) 56-63, https://doi.org/10.1016/j.fluid.2009.02.005.K.

[34] K. Frey, M. Modell, J.W. Tester, Density-and-temperature-dependent volume translation for the SRK EOS: 2. Mixtures, Fluid Phase Equilib. 343 (2013) 13-23, https://doi.org/10.1016/j.fluid.2013.01.006.

[35] A. Cipollina, R. Anselmo, O. Scialdone, G. Filardo, A. Galia, Experimental P-T-ρ measurements of supercritical mixtures of carbon dioxide, carbon monoxide, and hydrogen and semiquantitative estimation of their solvent power using the solubility parameter concept, J. Chem. Eng. Data 52 (2007) 2291-2297, https://doi.org/10.1021/je700307r.

[36] C.M. Hansen, 50 years with solubility parameters-past and future, Prog. Org. Coat. 51 (2004) 77-84, https://doi.org/10.1016/j.porgcoat.2004.05.004.

[37] J. Jing, R. Yin, G. Zhu, J. Xue, S. Wang, S. Wang, Viscosity and contact angle prediction of low water-containing heavy crude oil diluted with light oil, J. Petrol. Sci. Eng. 176 (2019) 1121-1134, https://doi.org/10.1016/j.petrol.2019.02.012.

[38] S. Lee, M.C.H. Chien, A new multicomponent surface tension correlation based on scaling theory, presented at the SPE/DOE Fourth Symposium on Enhanced Oil Recovery, Tulsa Oklahoma, 15-18 April 1984, SPE-12643-MS, https://doi.org/10.2118/12643-MS.

[39] S.E. Quinones-Cisnero, C.K. Zeberg-Mikkelsen, E.H. Stenby, The friction theory for viscosity modeling: extension to crude oil systems, Chem. Eng. Sci. 56 (2001) 7007-7015, https://doi.org/10.1016/S0009-2509(01)00335-9.

[40] S. Verdier, D. Duong, S.I. Andersen, Experimental determination of solubility parameters of oils as a function of pressure, Energy Fuels 19 (2005) 1225-1229, https://doi.org/10.1021/ef049827v.

[41] C.K. Zeberg-Mikkelsen, Viscosity study of hydrocarbon fluids at reservoir conditions, Ph.D. thesis, Technical University of Denmark, 2001.

[42] D.S. Schechter, B. Guo, Parachors based on modern physics and their uses in IFT prediction of reservoir fluids, SPE Reservoir Eval. Eng. 1 (1998) 207-217, https://doi.org/10.2118/30785-PA.

[43] R.W. Hankinson, G.H. Thomson, A new correlation for saturated densities of liquids and their mixtures, AIChE J. 25 (1979) 653-663, https://doi.org/10.1002/aic.690250412.

[44] H.G. Rackett, Equation of state for saturated liquids, J. Chem. Eng. Data 15 (1970) 514-517, https://doi.org/10.1021/je60047a012.

[45] C.F. Spencer, R.P. Danner, Improved equation for prediction of saturated liquid density, J. Chem. Eng. Data 17 (1972) 236-241, https://doi.org/10.1021/je60053a012.

[46] G.H. Thomson, H.R. Brobst, R.W. Hankinson, An improved correlation for densities of compressed liquids and liquid mixtures, AIChE J. 28 (1982) 671-676, https://doi.org/10.1002/aic.690280420.

[47] J.H. Dymond, R. Malhotra, The Tait equation: 100 years on, Int. J. Thermophys. 9 (1988) 941-951, https://doi.org/10.1007/BF01133262.

[48] H. Hoang, G. Galliero, F. Montel, J. Bickert, Tait equation in the extended corresponding states framework: Application to liquids and liquid mixtures, Fluid Phase Equilib. 387 (2015) 5-11, https://doi.org/10.1016/j.fluid.2014.12.008.

[49] H. Hoang, G. Galliero, Predictive Tait equation for non-polar and weakly polar fluids: Applications to liquids and liquid mixtures, Fluid Phase Equilib. 425 (2016) 143-151, https://doi.org/10.1016/j.fluid.2016.05.026.

[50] J. Gross, G. Sadowski, Perturbed-chain SAFT: An equation of state based on a perturbation theory for chain molecules, Ind. Eng. Chem. Res. 40 (2001) 1244-1260, https://doi.org/10.1021/ie0003887.

[51] M. Ma, S. Chen, J. Abedi, Modeling the density, solubility and viscosity of bitumen/solvent systems using PC-SAFT, J. Petrol. Sci. Eng. 139 (2019) 1-12, https://doi.org/10.1016/j.petrol.2015.12.012.

[52] K.E. Starling, J.L. Savidge, Compressibility factors of natural gas and other related hydrocarbon gases, American Gas Association, Transmission Measurement Committee Report No. 8, 1992.

[53] O. Kunz, W. Wagner, The GERG-2008 wide-range equation of state for natural gases and other mixtures: An expansion of GERG-2004, J. Chem. Eng. Data 57 (2012) 3032-3091, https://doi.org/10.1021/je300655b.

[54] W. Wagner, A. Pruβ, The IAPWS formulation 1995 for the thermodynamic properties of ordinary water substance for general and scientific use, J. Phys. Chem. Ref. Data 31 (2002) 387-535, https://doi.org/10.1063/1.1461829.

[55] S. Laugier, F. Rivollet, D. Richon, New volume translation for cubic equations of state, Fluid Phase Equilib. 259 (2007) 99-104, https://doi.org/10.1016/j.fluid.2007.04.032.

[56] M. Knierbein, C. Held, C. Holzl, D. Horinek, M. Paulus, G. Sadowski, C. Sternemann, J. Nase, Density variations of TMAO solutions in the kilobar range: Experiments, PC-SAFT predictions, and molecular dynamics simulations, Biophys. Chem. 253 (2019) 106222, https://doi.org/10.1016/j.bpc.2019.106222.

[57] J.S. Lopez-Echeverry, S. Reif-Acherman, E. Araujo-Lopez, Peng-Robinson equation of state: 40 years through cubics, Fluid Phase Equilib. 447 (2017) 39-71, https://doi.org/10.1016/j.fluid.2017.05.007.

[58] A. Pina-Martinez, R. Privat, J. Jaubert, D.Y. Peng, Updated versions of the generalized Soave α-function suitable for the Redlich-Kwong and Peng-Robinson equations of state, Fluid Phase Equilib. 485 (2019) 264-269, https://doi.org/10.1016/j.fluid.2018.12.007.

[59] K.S. Pedersen, P.L. Christensen, J.A. Shaikh, Phase behavior of petroleum reservoir fluids, CRC Press, 2 edition, 2014.

[60] A.F. Young, F.L.P. Pessoa, V.R.R. Ahon, Comparison of volume translation and co-volume functions applied in the Peng-Robinson EoS for volumetric corrections, Fluid Phase Equilib. 435 (2017) 73-87, https://doi.org/10.1016/j.fluid.2016.12.016.

[61] J. Matheis, H. Muller, C. Lenz, M. Pfitzner, S. Hickel, Volume translation methods for real-gas computational fluid dynamics simulations, J. Supercrit. Fluid 107 (2016) 422-432, https://doi.org/10.1016/j.supflu.2015.10.004.

[62] Y. Le Guennec, S. Lasala, R. Privat, J.N. Jaubert, A consistency test for α-functions of cubic equations of state, Fluid Phase Equilib. 427 (2019) 513-538, https://doi.org/10.1016/j.fluid.2016.07.026.

[63] P.J. Linstrom, W.G. Mallard (Eds.), NIST Chemistry WebBook, NIST Standard Reference Database Number 69, National Institute of Standards and Technology, Gaithersburg, MD, 20899, http://webbook.nist.gov.

[64] K.A.M. Gasem, W. Gao, Z. Pan, R.L. Robinson Jr., A modified temperature dependence for the Peng-Robinson equation of state, Fluid Phase Equilib. 181 (2001) 113-125, https://doi.org/10.1016/S0378-3812(01)00488-5.

[65] J.N. Jaubert, R. Privat, Y. Le Guennec, L. Coniglio, Note on the properties altered by application of a Peneloux-type volume translation to an equation of state, Fluid Phase Equilib. 419 (2016) 88-95, https://doi.org/10.1016/j.fluid.2016.03.012.

[66] P.H. Salim, M.A. Trebble, A modified Trebble-Bishnoi equation of state: Thermodynamic consistency revisited, Fluid Phase Equilib. 65 (1991) 59-71, https://doi.org/10.1016/0378-3812(91)87017-4.

[67] J. Shi, H. Li, Criterion for determining crossover phenomenon in volume-translated equation of states, Fluid Phase Equilib. 430 (2016) 1-12, https://doi.org/10.1016/j.fluid.2016.09.017.

[68] C.H. Twu, A modified Redlich-Kwong equation of state for highly polar, supercritical systems, presented at the Proceedings of the International Symposium on Thermodynamics in Chemical Engineering and Industry, Beijing China, 30 May-2 June 1988.

[69] C. Tsonopoulos, J.L. Heidman, High-pressure vapor-liquid equilibria with cubic equation of state, Fluid Phase Equilib. 29 (1986) 391-411, https://doi.org/10.1016/0378-3812(86)85039-7.

[70] M. Aalto, K.I. Keskinen, J. Aittamaa, S. Liukkonen, An improved correlation for compressed liquid densities of hydrocarbons. Part 2. Mixtures, Fluid Phase Equilib. 114 (1996) 21-35, https://doi.org/10.1016/0378-3812(95)02824-2.

[71] P.L. Chueh, J.M. Prausnitz, Vapor-liquid equilibria at high pressures: Calculation of critical temperatures, volumes, and pressures of nonpolar mixtures, AIChE J. 13 (1967) 1107-1113, https://doi.org/10.1002/aic.690130613.

[72] W.R. Parrish, Compressed liquid densities of ethane-propane mixtures between 10 and 49°C at pressures up to 9.6 MPa, Fluid Phase Equilib. 18 (1984) 279-297, https://doi.org/10.1016/0378-3812(84)85012-8.

[73] W.B. Kay, Vapor-liquid equilibrium relations of binary systems. The propane-n-alkane systems. n-butane and n-pentane, J. Chem. Eng. Data 15 (1970) 46-52, https://doi.org/10.1021/je60044a026.

[74] D. Pecar, V. Dolecek, Isothermal compressibilities and isobaric expansibilities of pentane, hexane, heptane and their binary and ternary mixtures from density measurements, Fluid Phase Equilib. 211 (2003) 109-127, https://doi.org/10.1016/S0378-3812(03)00154-7.

[75] S.A. Beg, N.M. Tukur, D.K. Al-Harbi, Densities and excess volumes of cyclohexane + hexane between 298.15 K and 473.15 K, Fluid Phase Equilib. 113 (1995) 173-184, https://doi.org/10.1016/0378-3812(95)02794-4.

[76] S.A. Beg, N.M. Tukur, D.K. Al-Harbi, E.Z. Hamad, Densities and excess volumes of benzene + hexane between 298.15 and 473.15 K, J. Chem. Eng. Data 40 (1995) 74-78, https://doi.org/10.1021/je00017a016.

CHAPTER 3 IMPROVED PREDICTION OF SATURATED AND SINGLE-PHASE LIQUID DENSITIES OF WATER THROUGH VOLUME-TRANSLATED SRK EOS

A version of this chapter has been published in *Fluid Phase Equilibria*

Abstract

Available equation of states (EOSs) cannot well reconcile the calculation accuracy and the computational cost for reproducing liquid volumes of water. In this study, we propose a series of improved volume translated Soave-Redlich-Kwong (VT-SRK) EOSs to achieve more accurate volumetric calculation for water with little additional computational cost. The overall average absolute percentage deviation of the saturated liquid molar volume for water yielded by the proposed 4-parameter VT-SRK EOS is 0.26; this calculation error is much lower than the counterpart provided by our previously proposed 3-parameter VT-SRK EOS (1.24) and close to the uncertainty in the pseudo-experimental data reported by NIST (0.1%). After adopting the translated distance function, the proposed 5-parameter VT-SRK EOS provides a more accurate determination for the single-phase liquid volume of water over a wide temperature/pressure range and leads to the crossover of pressure-volume isotherms only at extremely high pressures. The proposed 4-parameter VT-SRK EOS also helps to improve the volumetric prediction for carbon dioxide, while the proposed 5-parameter VT-SRK EOS performs well in improving the density prediction for associating fluids. Moreover, we extend the proposed 5-parameter VT-SRK EOS to mixtures through conventional mixing rules, finding that the VT-SRK EOS provides reliable volume predictions for the aqueous solutions examined in this study.

Keywords: Water density; Volume translation; Equation of state; Aqueous solutions;

3.1. Introduction

Of all pure fluids, water (H_2O) is undoubtedly one of the most important and common substances in the natural world [1]. As a working fluid or solvent, water has been widely used in the industrialized world, such as bioengineering, petroleum engineering and chemical engineering [2-4]. Accurate prediction of water density is required in extensive technical applications. A huge number of water-density measurements have been conducted [5]. Many researchers developed empirical formulas for reproducing water density based on experimental data [6-13]. However, these empirical correlations are only applicable over a given range of temperature/pressure conditions and cannot be used for vapor/liquid equilibrium (VLE) calculations or determinations of other thermodynamic properties. In view of the multitude of applications and the scientific significance of water, it is critical to fully understand the thermodynamic properties of water over a wide pressure/temperature range [14,15]. Nevertheless, water is an intriguing liquid and exhibits numerous anomalies, such as denser liquid water than ice and supercooled water, due to its small molecular size, abundant hydrogen bonds, strong electrostatic interactions, high dielectric constant and diffusivity [2,16-18]. This also leads to different density-change rule of water from those of many simple liquids [5,19,20]. In consideration of intermolecular potential, molecular dynamics (MD) simulation serve as an effective tool for describing the thermodynamic behaviors of water [17,18,21-23]. However, available MD models emphasize on explaining the anomalous properties of water rather than providing accurate calculation of water density under different temperature/pressure conditions. The parametric equation of state is still the most popular method to determine thermodynamic properties of water [24].

Since the Helmholtz energy is dependent on density and temperature, a series of equation of states (EOSs) explicit in the Helmholtz free energy have been proposed [25-31]. In 1995, the International Association for the Properties of Water and Steam (IAPWS) recommended one of such models for reproducing the pressure-volume-temperature (PVT) and phase equilibrium behavior of H_2O due to the high accuracy and low uncertainty [31]. The advanced Helmholtz free energy model provided by Wagner and Pruβ is deemed as the best available EOS for accurate calculation of water density and adopted by the National Institute of Standards and Technology (NIST) Web Thermo Tables (WTT) to produce pseudo-experimental data of H_2O [31,32]. Although the uncertainty in reproducing density is generally less than 0.1%, Wagner and Pruβ's model possesses a really complicated function form and more than 50 parameters [29-31]. For a higher calculation efficiency, some thermodynamic models and modeling techniques have been developed, aiming to replace Wagner and Pruβ's formulation [33-36]. Unfortunately, those methods cannot reconcile the high prediction accuracy and the low computational cost.

So far, cubic equations of state (CEOS), for example, Soave-Redlich-Kwong (SRK) EOS and Peng-Robinson (PR) EOS, has gained wide popularity and been employed in many commercial thermodynamic packages because of its simplicity and engineering flexibility [38-40]. Note that CEOS has two drawbacks: 1) it is not well suited for associating fluids (including water); 2) it cannot provide an accurate volumetric calculation for liquid phase [40,41]. Consequently, the calculation errors for the saturated and single-phase liquid volumes of water yielded by SRK or PR EOS are usually higher than 10% [14]. On the basis of Helmholtz energy expressions accounting for the chain and association effects, Chapman et al. (1988, 1989, 1990) developed the statistical associating fluid theory (SAFT) EOS [42-44]. Later, combining with

perturbation theory, Gross and Sadowski (2001) proposed the perturbed chain statistical associating fluid theory (PC-SAFT) EOS, which is one of the most successful SAFT-type EOSs among the available modified versions [45]. Recently, incorporating associated reference perturbation theory (APT) into the generalized function of polar PC-SAFT EOS, Marshall (2018) provided an EOS dedicated to water [46,47]. Nevertheless, this EOS cannot accurately describe the thermodynamic properties of water near the critical region and the calculation deviation for saturated liquid density is about 1%, which is obviously higher than the uncertainties yielded by the Wagner and Pruβ's model (0.1%) and the original APT model (0.3%) [31,46-52]. Aiming to improve the CEOS performance for associating fluids, Kontogeorgis et al. (1996) introduced a cubic plus association (CPA) EOS through directly adding the association term taken from SAFT to the classical CEOS [48,53]. Although CPA EOSs are more concise than SAFT-type EOSs and more accurate than the original CEOSs for associating fluids, the up-to-date version still fails to provide reliable predictions for the thermodynamic properties of water at high temperatures and yields 1% calculation errors for water density, whose value is similar to the up-to-date SAFT-type EOS [46,53-58]. Other advanced cubic-like EOSs also offer little improvements on reproducing the volumetric/phase behaviors of water [14,59-62].

Volume translation (VT) acts as a simple but effective technique to correct the liquid volume predicted by CEOS [41]. There are three types of VT models: 1) constant VT; 2) temperature-dependent VT; 3) temperature-volume-dependent VT [62-72]. Constant VT is usually used to correct the volumes only at low temperatures but has poor performance near the critical region [62]. Temperature-dependent VT can provide an accurate reproduction for saturated-liquid density over a wide temperature range, but the improvement on single-phase liquid density prediction is barely satisfactory

[63-68]. By introducing a volume-dependent distance function relating to the inverse of the isothermal compressibility, temperature-volume-dependent VT can acutely correct both the saturated and single-phase liquid volumes yielded by CEOS [69-72]. The VT-models proposed by Abudour et al. (2012) and Chen and Li (2020) are two of the most accurate VT-models in the literature [71,72]. However, their calculation errors for water density are greater than 1%, which are dramatically higher than the uncertainty of the model recommended by IAPWS (0.1%) [31,32]. Lately, some researchers have attached constant VT-model to CPA and PC-SAFT EOSs to give more precise descriptions of the thermodynamic properties and phase behavior of water [73-77]. However, these modified EOSs cannot accurately predict the water density yet, especially under relatively high temperature/pressure conditions.

Volume translated EOS (VT-EOS) is still commonly used in commercial simulators due to the advantages of high accuracy but low computational cost [78]. Many models for reproducing physical and thermodynamic properties are highly dependent on the density yielded by VT-EOS [79-85]. In the light of the fundamental importance of water in different engineering disciplines (in particular, petroleum engineering), it is necessary to further improve the prediction accuracy for water density through VT-EOS over wide temperature/pressure ranges. Hence, in this study, we propose a series of VT-SRK EOSs dedicated to the accurate determination of saturated and single-phase density of water. The mathematical formulae of the proposed VT-models maintain succinct forms and are easy to use. It is hopeful that the calculation error for water yielded by these VT-SRK EOSs may approach the similar level of the uncertainty of the pseudo-experimental data reported by NIST. Moreover, the pressure-volume isotherm crossover issue caused by VT-SRK EOS for water has been checked according to the criterion proposed by Shi and Li [86]. We also evaluate the

performances of these newly proposed VT-SRK EOSs in volumetric calculations of other substances. Finally, we extend the newly proposed VT-model to mixtures via classical mixing rules and demonstrate their good performance in density prediction for aqueous solutions.

3.2. VT-SRK EOSs for Water

This study tries to develop more accurate VT-models for SRK EOS considering its wide use in industry but poor performance on predicting water density. SRK EOS is shown as [38]:

$$P = \frac{RT}{v-b} - \frac{a}{v(v+b)} \tag{3-1}$$

where v and P are the molar volume and pressure, respectively, R is the universal gas constant, T is the temperature, a and b are the EOS parameters and in SRK EOS, which are given as [38]:

$$a = \frac{1}{9\left(\sqrt[3]{2}-1\right)} \frac{R^2 T_c^2}{P_c} \alpha(T) \tag{3-2}$$

$$b = \frac{\sqrt[3]{2}-1}{3} \frac{RT_c}{P_c} \tag{3-3}$$

where T_c and P_c are the experimental critical temperature and pressure and, for water, their values are 647.096 K and 22.064 MPa (retrieved from NIST WTT), respectively. The Twu α-function (shown by **Eq. 3-4**) recently updated by Pina-Martinez et al. is adopted in this study [87,88]:

$$\alpha(T) = T_r^{N(M-1)} \exp[L(1-T_r^{MN})] \tag{3-4}$$

where T_r is the reduced temperature (i.e., $T_r = \frac{T}{T_c}$), L, M and N are compound-dependent parameters in Twu α-function. For water, the values of L, M and N are 0.4171, 0.8758 and 2.1818, respectively.

3.2.1 Previous VT-SRK EOSs

In 1989, Chou and Prausnitz [70] defined a volume-dependent distance function (d) relating to the inverse of the isothermal compressibility and proposed a temperature/volume-dependent VT-model as:

$$d = \frac{1}{RT_c}\left(\frac{\partial P}{\partial \rho}\right)_T = -\frac{v^2}{RT_c}\left(\frac{\partial P}{\partial v}\right)_T = \frac{v^2 T}{T_c(v-b)^2} - \frac{a(2v+b)}{RT_c(v+b)^2} \tag{3-5}$$

$$v^{VT} = v - c_1 - \delta_c\left(\frac{0.35}{0.35+d}\right) \tag{3-6}$$

where v^{VT} is the corrected molar volume after volume translation in SRK EOS, c_1 is a substance-dependent parameter used for correcting the volumes remote from critical region, and 0.35 is a universal constant determined by regressing density data of many substances. δ_c is the volume shift at critical temperature in SRK EOS:

$$\delta_c = \frac{RT_c}{P_c}\left(Z_c^{EOS} - Z_c\right) = v_c^{EOS} - v_c \tag{3-7}$$

where Z_c^{EOS} and v_c^{EOS} are the critical compressibility factor and critical molar volume in SRK EOS, Z_c and v_c are the experimental critical compressibility factor and critical molar volume, respectively.

One may easily observe that the Chou and Prausnitz's VT-model [70] only contains one substance-dependent parameter and we can replace the constant 0.35 by another substance-dependent parameter to further increase the calculation accuracy as,

$$v^{VT} = v - c_1\left(\frac{RT_c}{P_c}\right) - \delta_c\left(\frac{c_2}{c_2 + d}\right) = v - c_1\left(\frac{RT_c}{P_c}\right) - \delta_c\left(\frac{1}{1 + \frac{d}{c_2}}\right) \tag{3-8}$$

Furthermore, in our previous study [72], we proposed an improved 3-parameter VT-model (shown by **Eq. 3-9**) dedicated to the accurate determination of liquid densities for various substances [72]:

$$v^{VT} = v - c_1\left(\frac{RT_c}{P_c}\right) - \delta_c\left(\frac{1}{c_2 + c_3 d}\right) \tag{3-9}$$

We firstly optimized the substance-dependent parameters c_1, c_2 and c_3 in above 1-parameter VT-model (**Eq. 3-6**), 2-parameter VT-model (**Eq. 3-8**) and 3-parameter VT-model (**Eq. 3-9**) by reproducing the saturated-liquid molar volumes, respectively. The pseudo-experimental volumes and compound properties are retrieved from the NIST WTT with Version 2-2012-1-Pro [32]. The temperature range of regression is from the minimum integer above the value of triple point temperature (with the unit of K) to the maximum integer below the critical temperature; the temperature interval is 1 K. The parameter regression is done by the iterative reweighted least squares algorithm. Then we compare these three VT-SRK EOSs and the original SRK EOS in terms of the absolute percentage deviations (%AADs) in reproducing saturated and single-phase liquid molar volumes. The fitting and comparison results are summarized in **Table 3-1**. Moreover, **Fig. 3-1** visually compares the uncertainty of the pseudo-experimental data reported by NIST against relative percentage deviation (%RD) of different VT-SRK EOSs in reproducing saturated-liquid molar volumes at different temperatures for water. The %AAD and %RD are calculated to evaluate the performances of different VT-SRK EOSs:

$$\%AAD = \frac{100}{n}\sum_{i=1}^{n}\left|\frac{v^{VT} - v^{EXP}}{v^{EXP}}\right|_i \tag{3-10}$$

$$\%RD = 100 \times \left(\frac{v^{VT} - v^{EXP}}{v^{EXP}}\right) \tag{3-11}$$

where n is the number of data points used, v^{VT} and v^{EXP} are the molar volume obtained by VT-SRK EOS and the pseudo-experimental molar volume retrieved from NIST WTT, respectively. For the saturated-liquid molar volume, the data points used for %AAD calculation are consistent with those for VT-model parameter optimization. For the single-phase liquid molar volume, %AAD will be determined at different reduced pressures ($P_r = \frac{P}{P_c}$) and grouped into two categories, i.e., %AAD under subcritical pressures (P_r=0.1-1 with a step of 0.1) and %AAD under supercritical pressures (P_r=1.1, 1.2, 1.3, 1.4, 1.5, 2, 3 and 4).

Table 3-1. Fitted parameters in 1-parameter VT-SRK EOS (**Eq. 3-6**), 2-parameter VT-SRK EOS (**Eq. 3-8**) and 3-parameter VT-SRK EOS (**Eq. 3-9**) and the calculation errors for the saturated and single-phase liquid molar volumes of water yielded by these VT-SRK EOSs and the original SRK EOS.

VT-SRK EOS	c_1	c_2	c_3	$\%AAD^{sata}$	$\%AAD_{single}{}^{b}$	$\%AAD_{sub}{}^{c}$	$\%AAD_{sup}{}^{d}$
Original SRK EOS	-	-	-	39.9	38.40	37.86	38.96
1-parameter VT-SRK EOS	0.02495	-	-	2.44	2.59	2.26	2.93
2-parameter VT-SRK EOS	0.02549	0.32645	-	2.32	2.50	2.13	2.88
3-parameter VT-SRK EOS	0.02425	1.30564	2.17549	1.24	1.72	1.35	2.10

[a] %AAD for saturated-liquid volume.
[b] %AAD for single-phase liquid volume over the entire pressure range.
[c] %AAD for single-phase liquid volume under $P_r \leq 1$.
[d] %AAD for single-phase liquid volume under $P_r > 1$.

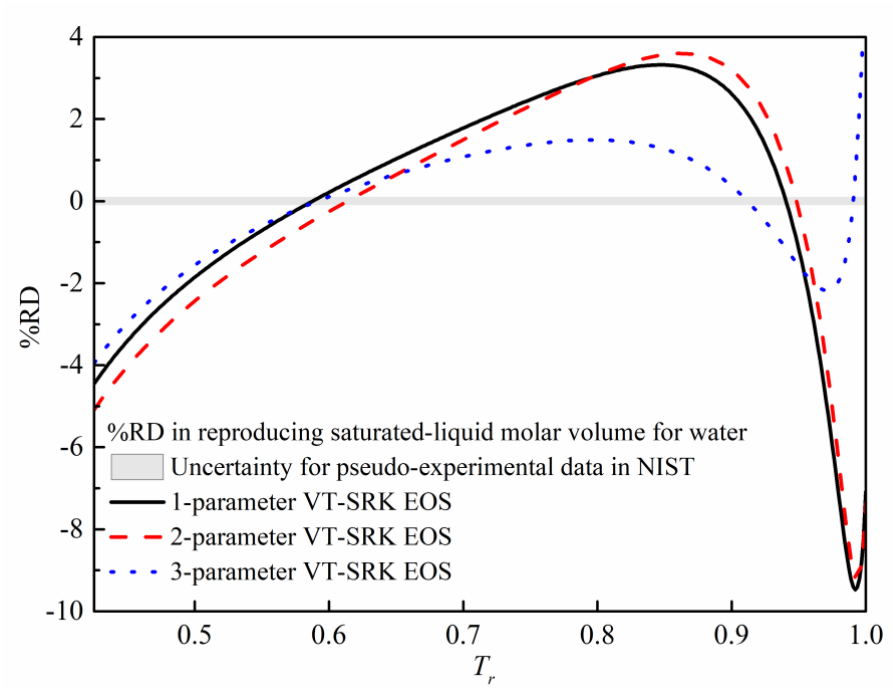

Fig. 3-1. Comparison of %RDs in reproducing the saturated-liquid molar volumes of water by the 1-parameter VT-SRK EOS (**Eq. 3-6**), the 2-parameter VT-SRK EOS (**Eq. 3-8**) and the 3-parameter VT-SRK EOS (**Eq. 3-9**) against the uncertainty of the pseudo-experimental data reported by NIST [32].

As shown in **Table 3-1**, all the %AADs yielded by the three VT-SRK EOSs are much lower than that yielded by the original SRK EOS, indicating remarkable improvements on density predictions. Compared to the 1-parameter VT-model (**Eq. 3-6**), the 2-parameter VT-model (**Eq. 3-8**) only slightly promotes the prediction accuracy while the 3-parameter VT-model (**Eq. 3-9**) can approximately halve the calculation errors. **Fig. 3-1** also proves that the 3-parameter VT-SRK EOS can produce more reliable and accurate density predictions for saturated water over the whole temperature range. However, the %RDs yielded by the 3-parameter VT-SRK EOS are still far away from the uncertainties of the pseudo-experimental data reported by NIST at most temperatures. These calculation results encourage us to adopt another substance-dependent parameter to further advance the VT-model. In addition, our previous study demonstrates that the overall %AADs of the saturated and single-phase liquid molar volumes yielded by the 3-parameter VT-SRK EOS (**Eq. 3-9**) for 56 compounds are

0.62 and 0.84, respectively, while the %AADs for water are much higher (i.e., 1.24 and 1.72) [72]. Due to the extensive use in industry, it is necessary to provide a more accurate and fast volumetric prediction for water through VT-EOS.

3.2.2 4-Parameter VT-SRK EOS

After many careful trials, we decide to adopt an additional fluid-dependent parameter c_4 as the power of the dimensionless distance d and propose a modified VT-model specially for water as follows:

$$v^{VT} = v - c_1\left(\frac{RT_c}{P_c}\right) - \delta_c\left(\frac{1}{c_2 + c_3 d^{c_4}}\right) \tag{3-12}$$

The VT-model parameters c_1, c_2, c_3 and c_4 in **Eq. 3-12** are optimized by reproducing *the saturated-liquid molar volumes* (**Type-1**) based on the above-mentioned fitting progress and the results are shown in **Table 2**. We compare the 4-parameter VT-SRK EOS (**Type 1**) against the previously developed 3-parameter VT-SRK EOS in terms of the accuracy in reproducing both saturated and single-phase liquid molar volumes and the results are summarized in **Table 3-2** and **Fig. 3-2**.

Table 3-2. Fitted parameters in previously developed 3-parameter VT-SRK EOS (**Eq. 3-9**), newly proposed 4-parameter VT-SRK EOSs (**Type-1** and **Type-2**, **Eq. 3-12**) and 5-parameter VT-SRK EOS (**Type-3**, **Eq. 3-14**) and the calculation errors for the saturated and single-phase liquid molar volumes of water yielded by these VT-SRK EOSs.

VT-SRK EOS	c_1	c_2	c_3	c_4	c_5	%AAD[sata]	%AAD$_{single}$[b]	%AAD$_{sub}$[c]	%AAD$_{sup}$[d]
3-parameter VT-SRK EOS	0.02425	1.30564	2.17549	-	-	1.24	1.72	1.35	2.10
4-parameter VT-SRK EOS (**Type-1**)[e]	0.01978	1.06368	1.98367	0.71207	-	0.26	1.15	0.60	1.72
4-parameter VT-SRK EOS (**Type-2**)[f]	0.02056	1.04894	1.89448	0.74355	-	1.06	0.68	0.46	0.90
5-parameter VT-SRK EOS (**Type-3**)	0.02056	1.04894	1.89448	0.74355	-0.29850	0.38	0.39	0.28	0.50

[a] %AAD for saturated-liquid volume.
[b] %AAD for single-phase liquid volume over the entire pressure range.
[c] %AAD for single-phase liquid volume under $P_r \leq 1$.
[d] %AAD for single-phase liquid volume under $P_r > 1$.
[e] Parameters optimized by reproducing saturated-liquid molar volume.
[f] Parameters optimized by reproducing single-phase liquid molar volume at $P_r = 1$.

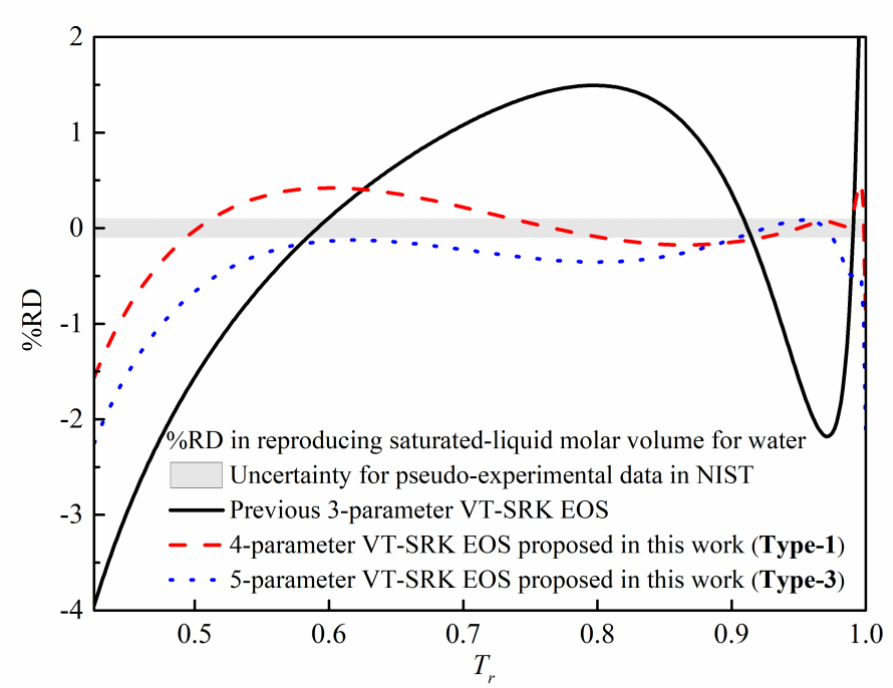

Fig. 3-2. Comparison of %RDs in reproducing the saturated-liquid molar volumes of water by the previously developed 3-parameter VT-SRK EOS (**Eq. 3-9**), the newly proposed 4-parameter VT-SRK EOS (**Type-1**, **Eq. 3-12**) and 5-parameter VT-SRK EOS (**Type-3**, **Eq. 3-14**) against the uncertainty of the pseudo-experimental data reported by NIST [32].

Table 3-2 shows that **Type-1** 4-parameter VT-SRK EOS (**Eq. 3-12**) yields dramatically lower %AADs in reproducing saturated and single-phase liquid volumes for water than the 3-parameter VT-SRK EOS (**Eq. 3-9**). Especially, the %AAD in reproducing saturated-liquid volume for water is only 0.26, which is slightly higher than the overall uncertainty yielded by the model recommended by IAPWS (0.1%) but lower than the counterparts yielded by APT (0.3%) as well as available CPA and PC-SAFT EOSs (1%) [31,32,46,47,56]. As can be seen from **Fig. 3-2**, in the most part of the covered temperature range, the saturated-liquid volume %RDs for water yielded by **Type-1** 4-parameter VT-SRK EOS (**Eq. 3-12**) are significantly lower than those yielded by the previously developed 3-parameter one (**Eq. 3-9**). Besides, except at the narrow regions of very high and very low temperatures, the %RDs yielded by **Type-1** VT-SRK EOS maintain low values (<0.4%) and are close to the uncertainties for pseudo-experimental data in NIST [32]. This indicates that the newly proposed 4-

parameter VT-SRK EOS reproduces well the saturated-liquid volume for water over the whole temperature range.

It is worthwhile of noting that the %AADs for single-phase liquid volume (including subcritical state, supercritical state and the entire pressure range) yielded by **Type-1** 4-parameter VT-SRK EOS are much higher than that for saturated-liquid volume. This is because, on the one hand, the properties of single-phase liquid tend to deviate from those of saturated liquid under high pressure/temperature conditions [5,89]. In other words, using the VT-model parameters optimized by reproducing the saturated-liquid volume may be not appropriate for predicting the single-phase liquid volume over the whole pressure/temperature range. On the other hand, the saturation pressures yielded by SRK EOS based on Maxwell' equal-area rule also slightly deviate from the experimental values, constituting another part of calculation error for predicting volume [90]. As such, the VT-model parameters optimized at saturation condition are more appropriate for correcting the saturated-liquid volume of water rather than the single-phase liquid volume.

In this study, we also fit the VT-model parameters c_1, c_2, c_3 and c_4 in **Eq. 3-12** by reproducing *the single-phase liquid molar volume of water* at P_r=1 (**Type-2**). **Table 3-2** presents the new VT-parameters and the performances of **Type-2** 4-parameter VT-SRK EOS in predicting the saturated and single-phase liquid volumes of water. **Type-2** 4-parameter VT-SRK EOS yields lower %AADs for single-phase liquid volumes than **Type-1** VT-SRK EOS but a higher %AAD for saturated-liquid volume. Hence, it is recommended that we adopt **Type-1** 4-parameter VT-SRK EOS to calculate the saturated-liquid volume of water while **Type-2** to calculate the single-phase liquid volume.

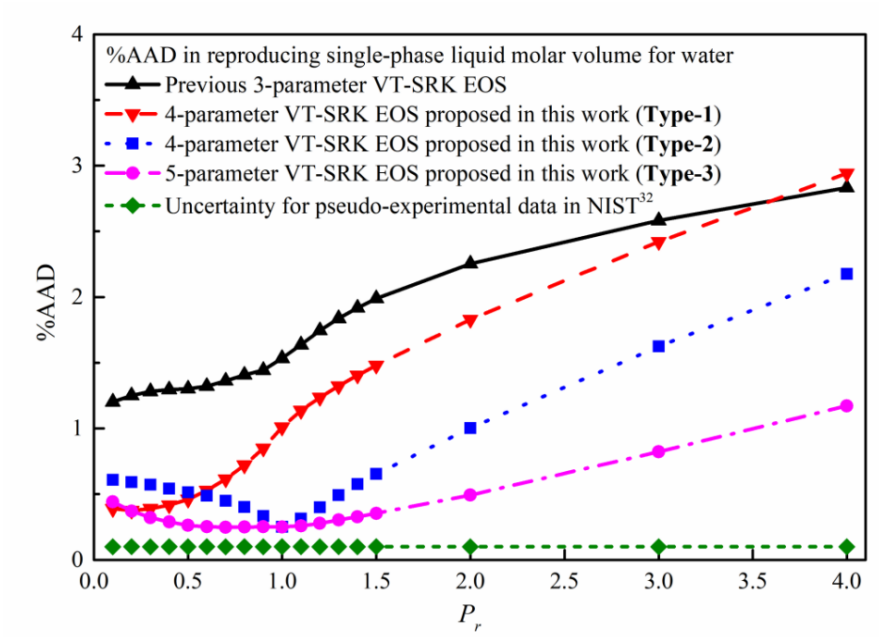

Fig. 3-3. Comparison of %AADs in reproducing the single-phase liquid molar volumes of water by the previously developed 3-parameter VT-SRK EOS (**Eq. 3-9**), the newly proposed 4-parameter VT-SRK EOSs (**Type-1** and **Type-2**, **Eq. 3-12**) and 5-parameter VT-SRK EOSs (**Type-3**, **Eq. 3-14**) against the uncertainty of the pseudo-experimental data reported by NIST [32].

To have a detailed comparison, **Fig. 3-3** shows the %AADs in single-phase liquid volumes for water yielded by different VT-SRK EOSs against the uncertainty of the pseudo-experimental liquid volume reported by NIST at different reduced pressures [32]. At $P_r \geq 0.6$, **Type-2** 4-parameter VT-SRK EOS yields more accurate calculations for single-phase liquid volumes of water than **Type-1**, while it does not exhibit good performances at low pressures. Moreover, we find that **Type-2** VT-model yields the lowest %AAD in single-phase liquid volumes at $P_r=1$ because its parameters are optimized at such condition, but the %AADs become increasingly higher when the reduced pressures are away from 1. Overall, although giving a lower overall %AAD, **Type-2** 4-parameter VT-SRK EOS still yields a compromised performance in reproducing the single-phase liquid volume of water over the entire pressure range.

3.2.3 5-Parameter VT-SRK EOS

We further plot the needed volume shifts (i.e., the differences between the single-phase liquid molar volumes predicted by SRK EOS and the experimental values) for water versus distance function at different reduced pressures as shown in **Fig. 3-4**. In **Fig. 3-4a**, although the changing trends of needed volume shifts versus distance function (d) at different reduced pressures are similar, those curves are almost parallel and do not coincide. Therefore, the VT-model, whose parameters are obtained by reproducing the single-phase liquid volume at P_r=1, is doomed to yield poor density predictions at pressures away from P_r=1. Aiming to address such problem, we set the curve of needed volume shifts versus distance function at P_r=1 as a benchmark curve and translate the distance functions at other pressures to make the curves close to the benchmark. After multiple trials and deliberation, we develop a liner translation for distance function (d') shown as,

$$d' = d + c_5\left(P_r - 1\right) \tag{3-13}$$

where c_5 is another fluid-dependent parameter and its value for water is -0.29850.

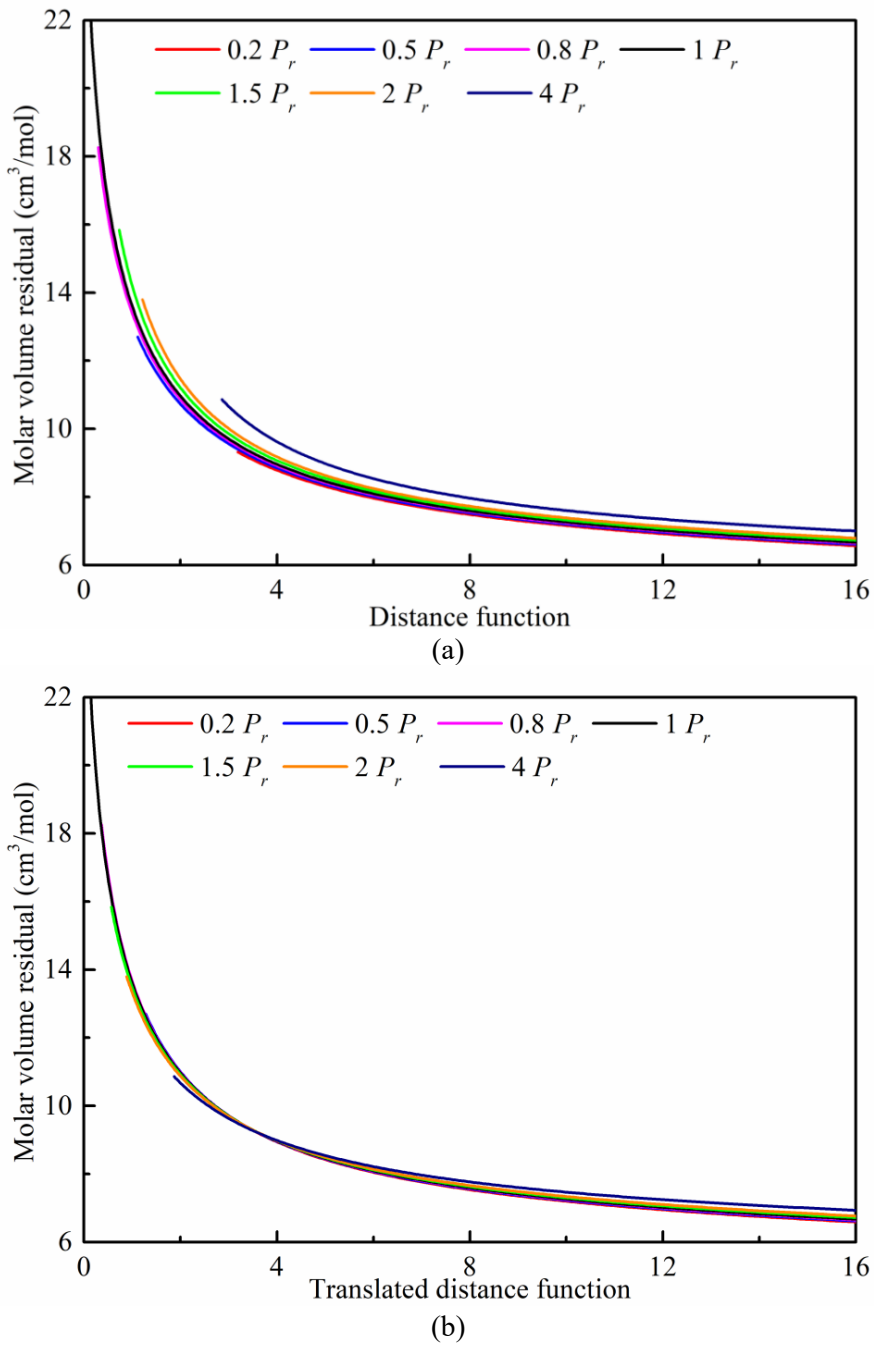

Fig. 3-4. The needed volume shifts in SRK EOS for water versus distance function d (a) and translated distance function d' (b) at different reduced pressures.

As shown in **Fig. 3-4b**, after replacing the original distance functions by the translated ones, the curves of needed volume shifts versus distance functions at different pressures are largely overlapped with each other. Then incorporating the translated distance function (d') into **Type-2** VT-model, a 5-parameter VT-model for SRK EOS (**Type-3**) can be given as,

$$v^{VT} = v - c_1\left(\frac{RT_c}{P_c}\right) - \delta_c\left(\frac{1}{c_2 + c_3 d'^{c_4}}\right) = v - c_1\left(\frac{RT_c}{P_c}\right) - \delta_c\left(\frac{1}{c_2 + c_3\left(d + c_5\left(P_r - 1\right)\right)^{c_4}}\right) \quad (3\text{-}14)$$

We also evaluate the performance of this 5-parameter VT-SRK EOS (**Type-3**) in reproducing the saturated and single-phase liquid volumes for water and the results are summarized in **Table 3-2**, **Figs. 3-2** and **3-3**, respectively. As shown in **Table 3-2**, after adopting the translated distance function, 5-parameter VT-SRK EOS can yield much lower %AADs for single-phase liquid volumes of water than the 4-parameter ones (including **Type-1** and **Type-2**). In particular, the %AADs yielded by **Type-3** VT-SRK EOS for the saturated-liquid volume and single-phase liquid volume under subcritical pressures are 0.38 and 0.28, respectively; those calculation errors are very close to the %AAD for saturated-liquid volume yielded by **Type-1** VT-SRK EOS (0.26%) and the uncertainty of the pseudo-experimental data reported by NIST (0.1%) [32]. **Fig. 3-3** shows that **Type-3** VT-SRK EOS gives a lower %AAD for single-phase liquid volume than **Type-2** VT-SRK EOS over the entire pressure range. Especially at P_r<2, the %AADs can keep low values (<0.5%). The above results indicate that the translation of distance function can effectively pull the prediction accuracy of single-phase liquid density at different pressures back to the similar level for reproducing the density at P_r=1. In addition, **Fig. 3-2** indicates that **Type-3** VT-SRK EOS provides low %RDs for saturated-liquid volume in most region of the covered temperatures like **Type-1** VT-SRK EOS. In general, **Type-3** 5-parameter VT-SRK EOS is well suited for calculating the saturated and single-phase liquid volumes of water over a wide temperature/pressure range, while **Type-1** 4-parameter VT-SRK EOS contributes to more accurate determination of the saturated-liquid volume of water.

3.3. Thermodynamic Consistency of the Newly Proposed VT-SRK EOS

The VT-model can improve the liquid density prediction yielded by CEOS, but the corrected volumes possibly become physically inconsistent [91]. To verify the reliability of our newly proposed VT-model (**Eq. 3-14**) for water, we present a diagram of calculated molar volume for liquid water over the entire subcritical region. As shown in **Fig. 3-5**, the surface of liquid water volume yielded by the proposed VT-SRK EOS is very smooth and complete. The volume increase of liquid water versus an increasing temperature is much more noticeable than that versus a decreasing pressure, which is in line with experimental observations. Thus, the 5-parameter VT-SRK EOS (**Eq. 3-14**) proposed in this work can provide a reliable volumetric calculation of water over the entire liquid-phase region.

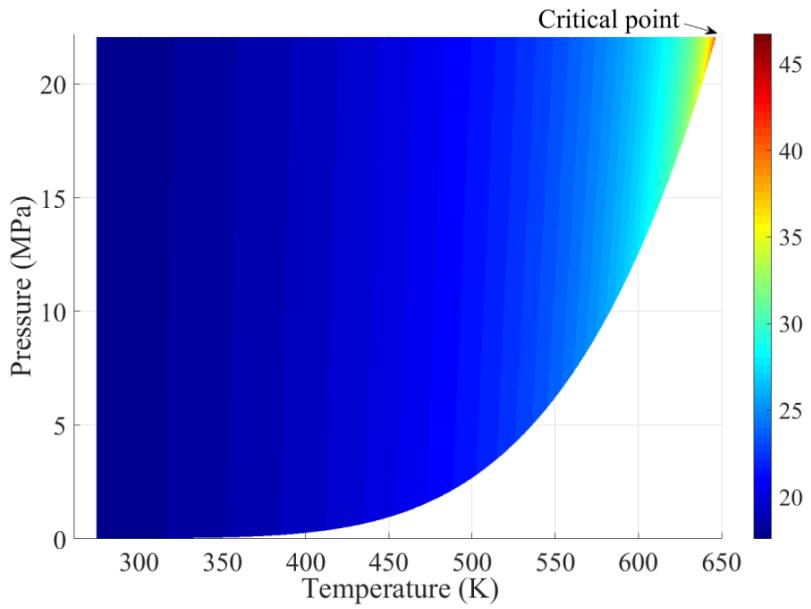

(a)

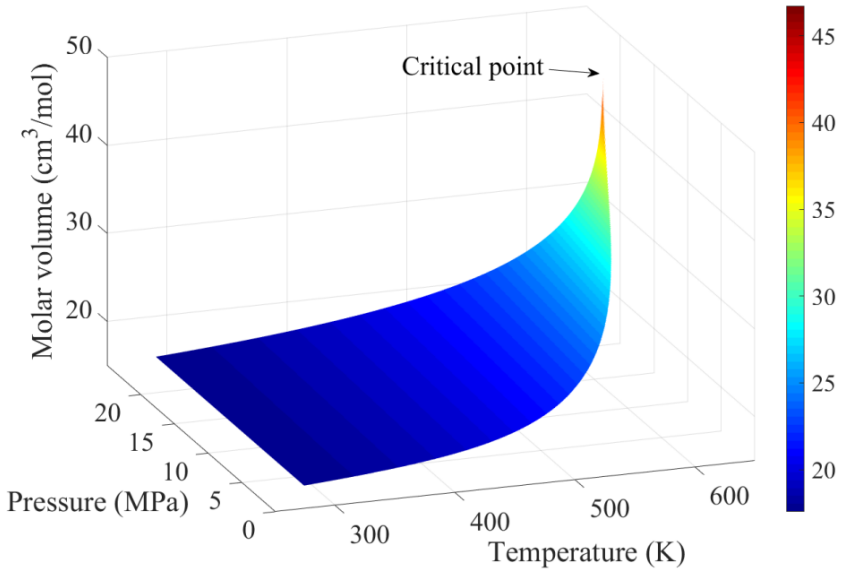

(b)

Fig. 3-5. Diagram of liquid water volume yielded by the 5-parameter VT-SRK EOS proposed in this work (**Eq. 3-14**) over the entire subcritical region: (a) top view; and (b) 3D diagram.

Besides, the temperature-dependent VT-EOS may lead to the crossing of pressure-volume (PV) isotherms at supercritical pressures [91]. Such thermodynamic inconsistency issue is assumed as one of major defects of temperature-dependent VT-EOS. In our previous study, we have investigated the crossover phenomenon generated by 3-parameter VT-model (**Eq. 3-9**) based on the criterion proposed by Shi and Li and found that this VT-model gives rise to the crossover issue only under extremely high pressures (after approaching P_r=10^{16}) [72,86]. Hence, in this part, we check whether the newly proposed 5-parameter VT-model (**Eq. 3-14**) for water leads to PV isotherm crossover over a wide pressure/temperature range. **Fig. 3-6** presents the PV isotherms generated by **Type-3** VT-SRK EOS (**Eq. 3-14**) at different reduced temperatures (T_r=0.5-3) under supercritical pressures (1-10^5 P_r).

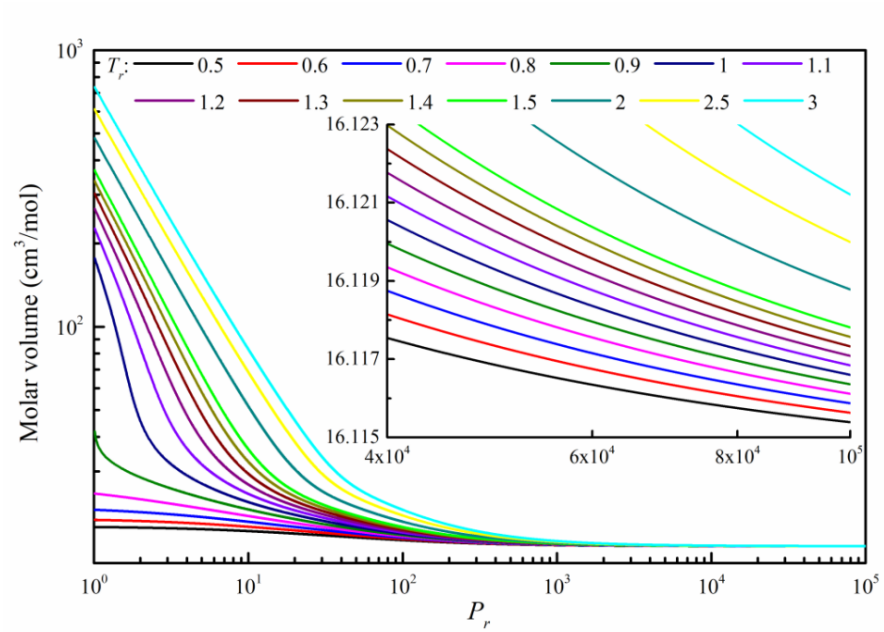

Fig. 3-6. PV diagrams for water generated by newly proposed 5-parameter VT-SRK EOS (**Type-3**, **Eq. 3-14**).

As seen in **Fig. 3-6**, the PV isotherms for water at different reduced temperatures do not intersect with each other, so the newly proposed 5-parameter VT-SRK EOS does not yield a crossover issue below 10^5 P_r. To be more compelling, we also determine the maximum pressure below which there is no PV-isotherm crossover according to the criterion developed by Shi and Li [86]:

$$D=\left(\frac{\partial v^{VT}}{\partial T}\right)_P=\frac{RT}{P}\left(\frac{\partial Z}{\partial T}\right)_P+\frac{ZR}{P}-\frac{\partial[C(T)]}{\partial T}>0 \tag{3-15}$$

where D is the first derivative of corrected molar volume with respect to T and greater than zero if there is no crossover phenomenon, Z is the compressibility factor, and $C(T)$ in the 5-parameter VT-SRK EOS is presented as:

$$C(T)=\Delta v=v-v^{VT}=c_1\left(\frac{RT_c}{P_c}\right)+\delta_c\left(\frac{1}{c_2+c_3(d+c_5(P_r-1))^{c_4}}\right) \tag{3-16}$$

Then we can get the first derivative of $C(T)$ with respect to T as:

$$\frac{\partial[C(T)]}{\partial T}=-\frac{\delta_c c_3 c_4(d+c_5(P_r-1))^{c_4-1}}{\left(c_2+c_3(d+c_5(P_r-1))^{c_4}\right)^2}\left(\frac{\partial d}{\partial T}\right)_P \tag{3-17}$$

The deduction process of D has been given by our previous papers [72,86] and the calculated values from triple point temperature to 10 T_r are shown in **Fig. 3-7**. As can be seen from **Fig. 3-7**, the values of D are distinctly greater than zero under P_r<10^{15}. After reaching P_r=10^{16}, the values of D start to become less than zero under relatively low temperatures, indicating a PV-isotherm crossover. Such crossover issue is very similar to that yielded by previously developed 3-parameter VT-model: only at extremely high pressures is there a PV-isotherm crossover [72]. Thus, **Type-3** 5-parameter VT-SRK EOS is capable of providing accurate volumetric calculations for water without causing PV-isotherm crossover issue over a wide pressure range.

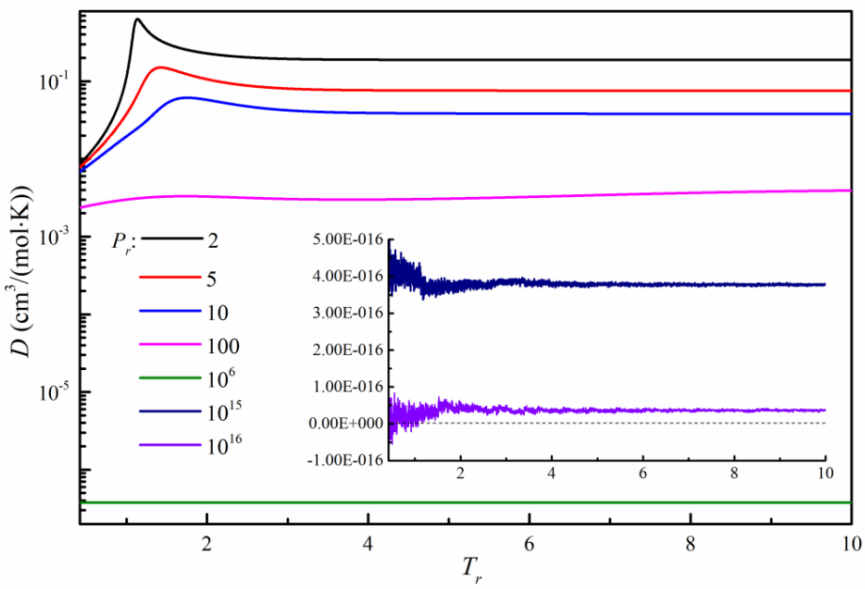

Fig. 3-7. Relationship between the first derivative of corrected molar volume by newly proposed 5-parameter VT-SRK EOS (**Type-3**, **Eq. 3-14**) with respect to temperature (D) and reduced temperature (T_r) at different pressures for water.

3.4. Extension of Proposed VT-SRK EOSs to Various Substances

Our previous study has shown that 3-parameter VT-SRK EOS (**Eq. 3-9**) possesses a good universality and can provide accurate determination of saturated and single-phase liquid densities for various substances [72]. Although the VT-models (**Type-1**,

Type-2 and **Type-3**) proposed in this study are specially designed for water, it is also necessary to check whether these VT-SRK EOSs may perform well for other substances. Hence, several distinct species (including carbon dioxide, hydrogen sulfide, propane, n-dodecane, ammonia, ethanol and difluoromethane) have been used to test the performances of these newly proposed VT-SRK EOSs on the volumetric predictions for these fluids. The fitted parameters in different VT-SRK EOSs and the testing results about %AADs for reproducing the saturated and single-phase liquid volumes of these substances can be found in **Table 3-3**.

Table 3-3. Fitted parameters in previously developed 3-parameter VT-SRK EOS (**Eq. 3-9**), the newly proposed 4-parameter VT-SRK EOSs (**Type-1** and **Type-2**, **Eq. 3-12**) and 5-parameter VT-SRK EOS (**Type-3**, **Eq. 3-14**) and the calculation errors for the saturated and single-phase liquid molar volumes for various substances yielded by these VT-SRK EOSs.

Substance	VT-SRK EOS	c_1	c_2	c_3	c_4	c_5	$\%AAD_{sat}$[a]	$\%AAD_{single}$[b]	$\%AAD_{sub}$[c]	$\%AAD_{sup}$[d]
Carbon dioxide	3-parameter VT-SRK EOS	0.00608	0.92912	2.65917	-	-	0.27	0.56	0.34	0.74
	4-parameter VT-SRK EOS (**Type-1**)[e]	0.00340	0.84640	2.15772	0.84532	-	0.10	0.36	0.19	0.50
	4-parameter VT-SRK EOS (**Type-2**)[f]	0.00372	0.85863	2.16825	0.91154	-	0.28	0.24	0.14	0.32
	5-parameter VT-SRK EOS (**Type-3**)	0.00372	0.85863	2.16825	0.91154	0.03337	0.32	0.23	0.14	0.31
Hydrogen sulfide	3-parameter VT-SRK EOS	0.00144	0.97009	2.45887	-	-	0.20	0.33	0.28	0.39
	4-parameter VT-SRK EOS (**Type-1**)[e]	0.00156	0.97805	2.48559	1.01585	-	0.20	0.33	0.27	0.38
	4-parameter VT-SRK EOS (**Type-2**)[f]	0.00182	0.99873	2.41206	1.10830	-	0.24	0.25	0.20	0.30
	5-parameter VT-SRK EOS (**Type-3**)	0.00182	0.99873	2.41206	1.10830	-0.05065	0.21	0.25	0.20	0.30
Propane	3-parameter VT-SRK EOS	0.00492	0.89221	2.75570	-	-	0.96	1.22	1.13	1.31
	4-parameter VT-SRK EOS (**Type-1**)[e]	0.00547	0.97840	2.83355	1.15765	-	0.84	1.05	0.96	1.14
	4-parameter VT-SRK EOS (**Type-2**)[f]	0.00564	1.13751	2.55916	1.39661	-	0.78	0.87	0.80	0.94
	5-parameter VT-SRK EOS (**Type-3**)	0.00564	1.13751	2.55916	1.39661	0.02744	0.79	0.87	0.80	0.94
Dodecane	3-parameter VT-SRK EOS	0.01795	1.06434	3.48078	-	-	0.80	1.10	0.93	1.27
	4-parameter VT-SRK EOS (**Type-1**)[e]	0.01776	1.04356	3.43917	0.96714	-	0.82	1.14	0.98	1.32
	4-parameter VT-SRK EOS (**Type-2**)[f]	0.01793	1.10087	3.34066	1.09478	-	0.78	0.91	0.78	1.05
	5-parameter VT-SRK EOS (**Type-3**)	0.01793	1.10087	3.34066	1.09478	0.02924	0.78	0.91	0.78	1.05
Ammonia	3-parameter VT-SRK EOS	0.02004	1.14567	2.55131	-	-	0.24	0.42	0.29	0.55
	4-parameter VT-SRK EOS (**Type-1**)[e]	0.01945	1.10419	2.48078	0.93801	-	0.23	0.43	0.31	0.55
	4-parameter VT-SRK EOS (**Type-2**)[f]	0.01977	1.13213	2.28261	1.02146	-	0.49	0.31	0.25	0.37
	5-parameter VT-SRK EOS (**Type-3**)	0.01977	1.13213	2.28261	1.02146	-0.17349	0.24	0.25	0.21	0.28
Ethanol	3-parameter VT-SRK EOS	0.01325	0.25264	0.45220	-	-	0.21	0.66	0.31	1.03

	4-parameter VT-SRK EOS (**Type-1**)[e]	0.01270	0.23973	0.45378	0.93123	-	0.19	0.67	0.32	1.04
	4-parameter VT-SRK EOS (**Type-2**)[f]	0.01374	0.29491	0.36479	1.11886	-	0.66	0.40	0.27	0.53
	5-parameter VT-SRK EOS (**Type-3**)	0.01374	0.29491	0.36479	1.11886	-0.27477	0.32	0.22	0.18	0.25
Difluoromethane	3-parameter VT-SRK EOS	0.02192	1.19333	3.07950	-	-	0.50	0.63	0.52	0.74
	4-parameter VT-SRK EOS (**Type-1**)[e]	0.02101	1.11432	2.95778	0.89107	-	0.55	0.73	0.64	0.82
	4-parameter VT-SRK EOS (**Type-2**)[f]	0.02158	1.19979	2.76625	1.01872	-	0.53	0.52	0.45	0.60
	5-parameter VT-SRK EOS (**Type-3**)	0.02158	1.19979	2.76625	1.01872	-0.11065	0.47	0.51	0.45	0.58

[a] %AAD for saturated-liquid volume.
[b] %AAD for single-phase liquid volume over the entire pressure range.
[c] %AAD for single-phase liquid volume under $P_r \leq 1$.
[d] %AAD for single-phase liquid volume under $P_r > 1$.
[e] Parameters optimized by reproducing saturated-liquid molar volume.
[f] Parameters optimized by reproducing single-phase liquid molar volume at $P_r = 1$.

One may observe that, compared to the benchmark model (i.e., the 3-parameter VT-SRK EOS, **Eq. 3-9**), **Type-1** 4-parameter VT-SRK EOS can significantly improve the prediction accuracy of saturated-liquid density only for carbon dioxide and water, while **Type-2** offers a moderate improvement on the single-phase liquid density prediction for carbon dioxide, hydrogen sulfide, ammonia, ethanol and difluoromethane (**Table 3-3**). It is worthwhile noting that in our previous study, we have compiled a database including the saturated and single-phase density data for 56 pure compounds, and 3-parameter VT-SRK EOS performs better than Abudour et al.'s VT-PR EOS for all compounds except water and carbon dioxide [71,72]. Hence, 4-parameter VT-SRK EOSs (including **Type-1** and **Type-2**) can serve as substitute EOS models to the previously developed 3-parameter VT-SRK EOS for water and carbon dioxide. **Figs. 3-8** and **3-9** compare the uncertainty of the pseudo-experimental data reported by NIST against calculation errors of different VT-SRK EOSs in reproducing saturated and single-phase liquid volumes for carbon dioxide [32].

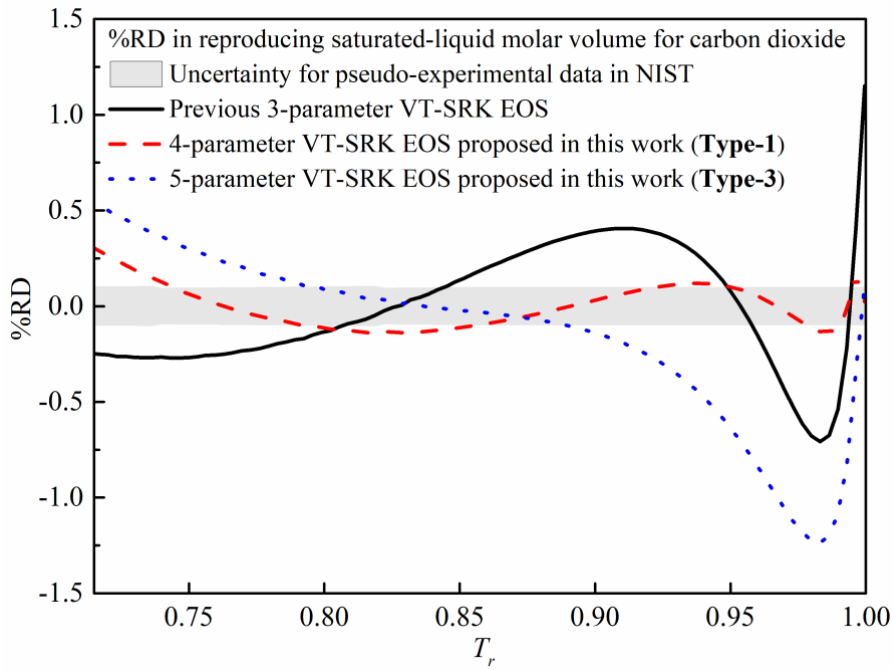

Fig. 3-8. Comparison of %RDs in reproducing the saturated-liquid molar volumes of carbon dioxide by the previously developed 3-parameter VT-SRK EOS (**Eq. 3-9**), the newly proposed 4-parameter VT-SRK EOS (**Type-1**, **Eq. 3-12**) and 5-parameter VT-SRK EOS (**Type-3**, **Eq. 3-14**) against the uncertainty of the pseudo-experimental data reported by NIST [32].

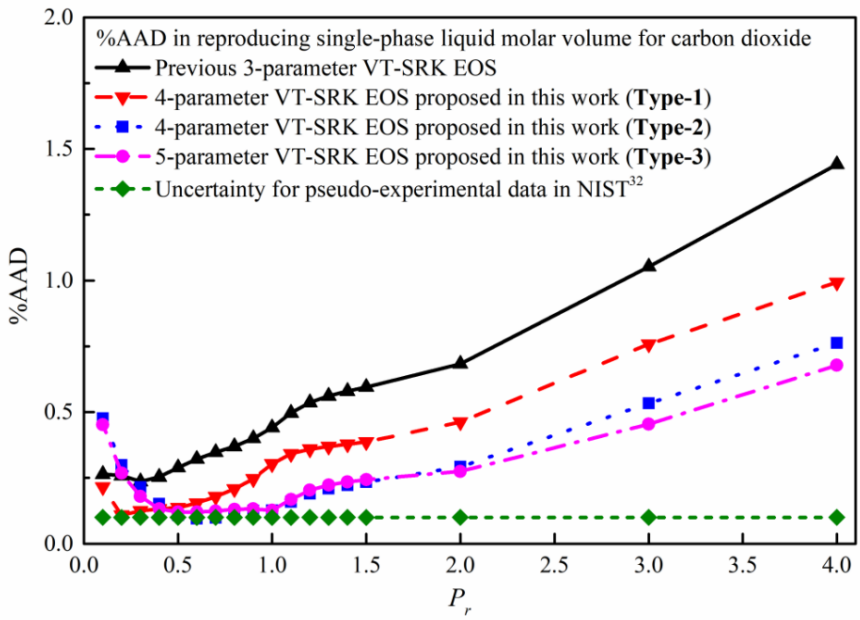

Fig. 3-9. Comparison of %AADs in reproducing the single-phase liquid molar volumes of carbon dioxide by the previously developed 3-parameter VT-SRK EOS (**Eq. 3-9**), the newly proposed 4-parameter VT-SRK EOSs (**Type-1** and **Type-2**, **Eq. 3-12**) and 5-parameter VT-SRK EOSs (**Type-3**, **Eq. 3-14**) against the uncertainty of the pseudo-experimental data reported by NIST [32].

As shown in **Fig. 3-8**, the %RDs in reproducing the saturated-liquid volume of carbon dioxide yielded by **Type-1** 4-parameter VT-SRK EOS are close to the uncertainties of the pseudo-experimental data given by NIST over the entire temperature range. Moreover, we can observe from **Fig. 3-9** that **Type-2** 4-parameter VT-SRK EOS produces much lower %AADs for the single-phase liquid volume than **Type-1** VT-SRK EOS at P_r>0.4. In particular, the %AADs yielded by **Type-2** 4-parameter VT-SRK EOS over the pressure range of P_r=0.4 to 1 approach the uncertainties of the pseudo-experimental data reported by NIST [32]. Note that the IAPWS pseudo-experimental equation adopted by NIST has been extended only to water and carbon dioxide because of its complicated function form [31,32]. However, for carbon dioxide, **Type-3** VT-SRK EOS does not seem to improve the calculation accuracy of the saturated-liquid volume compared to **Type-1** and the single-phase liquid volume compared to **Type-2**. On the contrary, for ethanol, **Type-3** VT-SRK EOS is capable of improving the accuracy in reproducing the single-phase liquid volume. Note that both ethanol and water are associating fluids and contain strong hydrogen bonds. Similarly, for the substances containing weak hydrogen bonds (i.e., ammonia), the translated distance function also helps to improve the volumetric calculation. Therefore, 5-parameter VT-SRK EOS (**Type-3**) can be utilized for improving the density prediction for associating fluids. More detailed explanations are presented in **Appendix A**.

3.5. Extension of Proposed VT-SRK EOS to Aqueous Solutions

Water is one of the most important and common solvents, so it is of significance to provide accurate volume calculations for aqueous solutions. In this section, we try to extend the newly proposed 5-parameter VT-SRK EOS (**Type-3**, **Eq. 3-14**) to mixtures

and demonstrate its performance in reproducing liquid density of aqueous solutions with given compositions. The tested binary mixtures include two water-carbon dioxide systems and two water-ethanol systems and the database of binary-mixture densities is presented in **Table 3-4**.

Table 3-4. Database of liquid densities of binary mixtures examined in this study.

System	No.	Temperature range (K)	Pressure range (MPa)	Density range of liquid phase (kg/m^3)	Mole-fraction range of Compound (1) in liquid phase	Number of data points	Data source
Carbon dioxide(1)-Water(2)	1	278-293	6.44-29.45	1013.68-1025.33	0.0250-0.0349	24	Teng et al. [92]
	2	288.15-298.15	6.08-24.42	1015-1027	0.02445-0.03070	27	King et al. [93]
Ethanol(1)-Water(2)	3	298.15-323.15	0.1-384.6	1031.247-786.658	0.2-0.8	184	Kubota et al. [94]
	4	293.15-303.15	0.101325	781.15-998.20	0.0501-0.9499	31	Gonzalez et al. [95]

At first, we determine the values of EOS parameters (a_m and b_m) for mixtures through traditional mixing rule as [38],

$$a_m = \sum_i \sum_j x_i x_j a_{ij} \tag{3-18}$$

$$a_{ij} = \sqrt{a_i a_j}\left(1 - C_{ij}\right) \tag{3-19}$$

$$b_m = \sum_i x_i b_i \tag{3-20}$$

where x is the mole fraction of a given compound in the mixture; the subscript i/j indicates the pure compound i/j in the mixture and the subscript m indicates the mixture. The C_{ij} in **Eq. 3-19** is the empirical "binary interaction parameter (BIP)". We have refitted the BIPs for water-carbon dioxide and water-ethanol systems based on the experimental composition fractions under vapor-liquid equilibria, respectively and the results are shown in **Table 3-5**. These VLE data were collected over wide temperature/pressure ranges and the experimental data used for reproducing the densities (**Table 3-4**) were also obtained under similar temperature/pressure conditions.

Please note that the mixing rules as well as BIPs adopted in this test are very classic and just employed to verify the performances of the VT-model.

Table 3-5. Database for refitting BIPs of binary mixtures examined in this study.

System	Temperature range (K)	Pressure range (MPa)	Number of data points	BIP	Data source
Carbon dioxide(1)-Water(2)	323.2-353.1	4.05-14.11	29	-0.14380	Bamberger et al. [96]
	278.22-318.23	0.465-7.963	23		Valtz [97]
Ethanol(1)-Water(2)	425.15-623.15	0.5586-18.9778	85	-0.03666	Barr-David and Dodge [98]
	325.15-333.15	0.0203-0.0470	107		Kurihara et al. [99]

The newly proposed 5-parameter VT-model for mixture is given as follows:

$$v_m^{VT} = v_m - c_{1m}\left(\frac{RT_{cm}}{P_{cm}}\right) - \delta_{cm}\left(\frac{1}{c_{2m} + c_{3m}\left(d_m + c_{5m}\left(P_{rm} - 1\right)\right)^{c_{4m}}}\right) \tag{3-21}$$

In this study, we determine the VT-parameters for mixture (c_{1m}, c_{2m}, c_{3m}, c_{4m} and c_{5m}) via the linear mixing rule proposed by Peneloux et al. [62] as:

$$c_{1m} = \sum_i x_i c_{1i} \quad c_{2m} = \sum_i x_i c_{2i} \quad c_{3m} = \sum_i x_i c_{3i} \quad c_{4m} = \sum_i x_i c_{4i} \quad c_{5m} = \sum_i x_i c_{5i} \tag{3-22}$$

The dimensionless distance function of mixture (d_m) and the volume shift of mixture at critical temperature (δ_{cm}) in SRK EOS are obtain as [70]:

$$d_m = -\frac{v_m^{\,2}}{RT_{cm}}\left(\frac{\partial P_m}{\partial v_m}\right)_T = \frac{v_m^{\,2}T}{T_{cm}\left(v_m - b_m\right)^2} - \frac{a_m\left(2v_m + b_m\right)}{RT_{cm}\left(v_m + b_m\right)^2} \tag{3-23}$$

$$\delta_{cm} = \frac{RT_{cm}Z_c^{\,EOS}}{P_{cm}} - v_{cm} \tag{3-24}$$

P_{cm} is the critical pressure of mixture and calculated through the correlation proposed by Aalto et al. [100]:

$$P_{cm} = \frac{\left(0.2905 - 0.085\omega_m\right)RT_{cm}}{v_{cm}} \tag{3-25}$$

where ω_m is the acentric factor of mixture and also determined via linear mixing rule:

$$\omega_m = \sum_i x_i \omega_i \tag{3-26}$$

Then we can get the reduced pressure of mixture:

$$P_{rm} = \frac{P}{P_{cm}} \tag{3-27}$$

T_{cm} and v_{cm} are the critical temperature and critical volume of mixture, respectively, and they can be calculated based on the method proposed by Chueh and Prausnitz [101]:

$$T_{cm} = \sum_i \theta_i T_{ci} \tag{3-28}$$

$$v_{cm} = \sum_i \theta_i v_{ci} \tag{3-29}$$

where θ_i is the surface fraction of compound i:

$$\theta_i = \frac{x_i v_{ci}^{\frac{2}{3}}}{\sum_i x_i v_{ci}^{\frac{2}{3}}} \tag{3-30}$$

Our previous study has proved that the above mixing rules for VT-model are reliable [72]. Here, we also extend the 3-parameter VT-model (**Eq. 3-9**) to mixtures according to the same process for comparison purpose. **Table 3-6** presents the calculation errors of liquid mixture density yielded by the 3-parameter VT-SRK EOS (**Eq. 3-9**), the 5-parameter VT-SRK EOS (**Eq. 3-14**) and the original SRK EOS, respectively; the effects of BIPs are also considered. One may see that both the 3-parameter VT-model and 5-parameter VT-model dramatically improve the density prediction yielded by SRK EOS. Besides, the BIPs have little impacts on the volumetric calculations, which are consistent with the previous observations from Abudour et al. [102] For the carbon dioxide-water system, the newly proposed 5-parameter VT-SRK EOS performs much better than the 3-parameter one. In contrast, for the ethanol-water system, although the %AADs in reproducing No. 3 density data yielded by the 5-parameter VT-model are lower than those yielded by 3-parameter VT-model, the 5-parameter VT-model produces slightly higher calculation errors for No. 4 data. This

may be because No. 4 experimental data were collected at the constant atmosphere pressure (**Table 3-4**). As illustrated by **Figs. 3-3** and **3-8**, the calculation accuracies for single-liquid phase volume yielded by 3-parameter and 5-parameter VT-models are on a par with each other under low pressures, while the 5-parameter VT-SRK EOS exhibits better performances with increasing pressures. In other words, the newly proposed 5-parameter VT-SRK EOS is more suitable for the mixture density predictions over wide pressure ranges rather than at low pressures.

Table 3-6. Comparison of the %AADs for molar volumes of mixtures (listed in **Table 3-4**) yielded by the original SRK EOS, the 3-parameter VT-SRK EOS (**Eq. 3-9**) and the 5-parameter VT-SRK EOS (**Eq. 3-14**) and the effects of BIPs.

System	No.	Original SRK EOS		5-parameter VT-SRK EOS		3-parameter VT-SRK EOS	
		No BIP	With BIP	No BIP	With BIP	No BIP	With BIP
Carbon dioxide(1)-Water(2)	1	30.43	30.33	0.52	0.46	2.27	2.34
	2	31.49	31.40	1.25	1.19	1.49	1.56
Ethanol(1)-Water(2)	3	27.83	27.48	2.64	2.58	3.33	3.19
	4	24.93	24.52	3.44	3.43	3.34	3.25

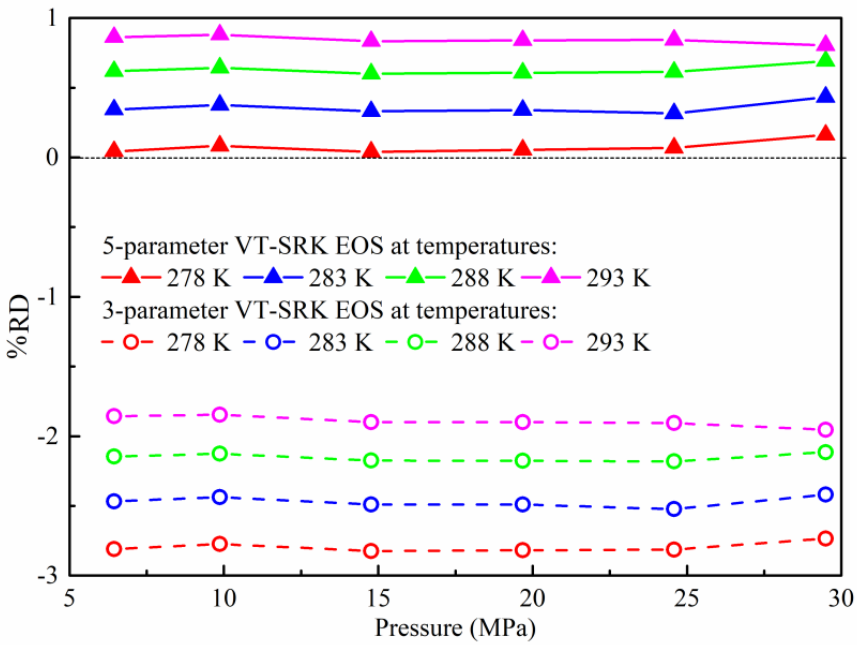

Fig. 3-10. Comparison of %RDs in reproducing molar volumes for No. 1 saturated carbon dioxide solution [92] by the 5-parameter VT-SRK EOS (**Eq. 3-14**) and the 3-parameter VT-SRK EOS (**Eq. 3-9**).

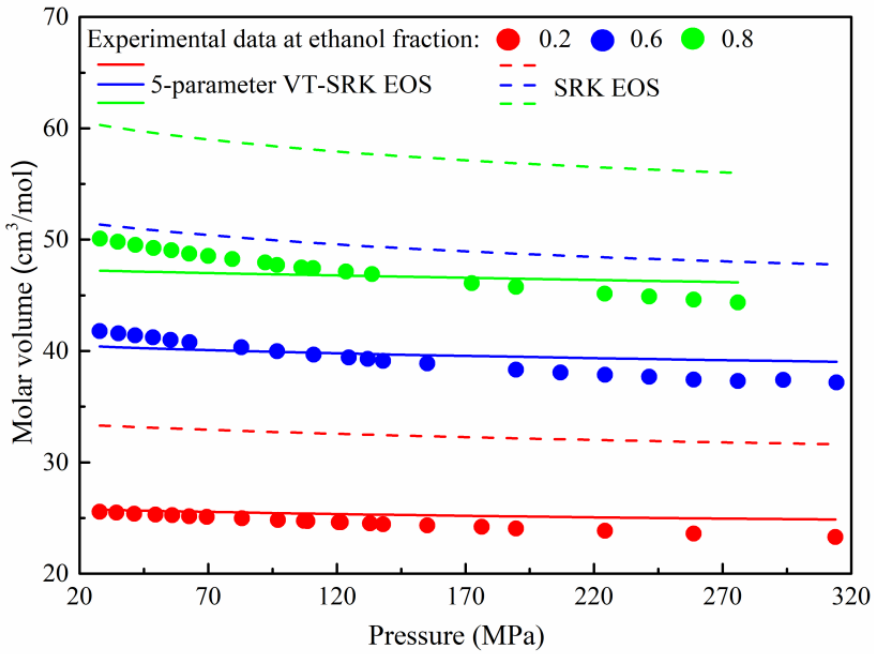

Fig. 3-11. Comparison of the molar volumes for No. 3 ethanol-water system yielded by the 5-parameter VT-SRK EOS (**Eq. 3-14**) and the original SRK EOS against experimental data [94].

To give a more vivid comparison, we plot the %RDs in reproducing No. 1 density data of saturated carbon dioxide solution yielded by the 3-parameter VT-SRK EOS (**Eq. 3-9**) and the 5-parameter VT-SRK EOS (**Eq. 3-14**) in **Fig. 3-10** as well as the molar volumes yielded by the proposed 5-parameter VT-SRK EOS (**Eq. 3-14**) and the original SRK EOS against the experimental data for No. 3 ethanol-water system with different fraction ratios at 323.15 K in **Fig. 3-11**. These calculations also take BIPs into account. As presented in **Fig. 3-10**, the 5-parameter VT-SRK EOS can yield lower calculation errors for saturated carbon dioxide volumes than the 3-parameter VT-SRK EOS under varying temperature/pressure conditions. Similarly, **Fig. 3-11** shows that the 5-parameter VT-SRK EOS can more acutely simulate the volume changes versus pressures and yield more accurate density calculations for the ethanol-water system with different compositions. In general, coupled with the traditional mixing rules, the 5-parameter VT-SRK EOS model developed in this work helps improve the volume

predictions for aqueous solutions. Certainly, the above mixing rule can be only applied to the mixtures where every every compound should be modeled by the 5-parameter VT-SRK EOS (**Eq. 3-14**). For the asymmetric mixtures, such as the water-hydrocarbon systems, we provide a novel hybrid VT-SRK EOS which combines the 5-parameter VT-model (for water) with the 3-parameter VT-model (for hydrocarbons) (See **Appendix B**).

3.6. Conclusions

Available models used for water density prediction cannot well balance computational accuracy and cost. For example, the formulation adopted by IAPWS produces a low calculation uncertainty in density (0.1%) but has limited applications in industrial simulators due to its complicated function form [31]. The commonly-used EOSs, such as CEOS, CPA EOS and PC-SAFT EOS may yield high calculation errors for water density (>1%) [14,46,47,56]. In this study, we propose a series of improved VT-SRK EOSs to provide more accurate volumetric prediction for water without inducing much computational cost. First, we develop two 4-parameter VT-SRK EOSs: the VT-parameters in **Type-1** and **Type 2** VT-model are determined by reproducing the saturated-liquid volume and the single-phase liquid volume at P_r=1 of water, respectively. The overall average absolute percentage deviation of the saturated-liquid molar volume for water yielded by **Type-1** 4-parameter VT-SRK EOS is 0.26; this calculation error is much lower than the counterpart yielded by our previously proposed 3-parameter VT-SRK EOS (1.24) and approaches a similar level of the uncertainty in the pseudo-experimental data reported by NIST (0.1%) [32]. Although giving a lower overall %AAD in the single-phase liquid volume, **Type-2** 4-parameter VT-SRK EOS gives a mediocre prediction for the single-phase liquid volume of water over the entire

pressure range of P_r=0.1 to 4. Through coupling **Type-2** 4-parameter VT with the translated distance function proposed in this study, **Type-3** 5-parameter VT-SRK EOS gives more accurate prediction for the single-phase liquid volume over a wide temperature/pressure range, and only leads to the crossover of pressure-volume isotherms at extremely high pressures. We have also evaluated the performances of these newly proposed VT-SRK EOSs on volumetric calculations for other substances, finding that **Type-1** and **Type-2** 4-parameter VT-SRK EOSs improve the liquid volume prediction for carbon dioxide, while **Type-3** 5-parameter VT-SRK EOS performs well in improving the density prediction for several associating fluids. Finally, we extend the **Type-3** 5-parameter VT-model to mixtures through conventional mixing rules, demonstrating that the VT-SRK EOS also performs well in the density predictions for aqueous solutions examined in this study.

Acknowledgments

The authors greatly acknowledge a Discovery Grant from the Natural Sciences and Engineering Research Council of Canada (NSERC) (Grant No.: NSERC RGPIN-2020-04571) to H. Li. X. Chen also greatly acknowledges the financial support provided by the China Scholarship Council (CSC) via a Ph.D. Scholarship (No.: 201806450029).

Appendix 3-A. Supplementary Explanations for the Translation of Distance Function

As shown in **Table 3-3**, **Type-3** VT-SRK EOS (**Eq. 3-14**) can improve the volume prediction of single-phase liquid for the associating fluids (including ethanol and ammonia) but has little effects on the non-associating fluids (such as carbon dioxide).

To explain the underlying reasons behind this observation, the needed volume shifts for carbon dioxide and ethanol versus distance function at different reduced pressures have been presented in **Figs. 3-A1** and **3-A2**, respectively.

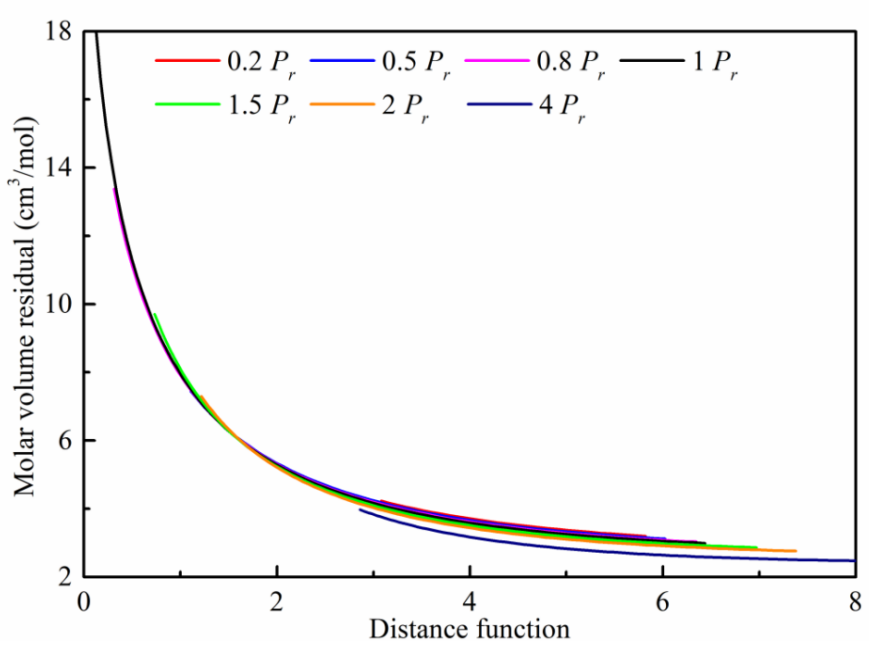

Fig. 3-A1. Needed volume shifts in SRK EOS for carbon dioxide versus distance function *d* at different reduced pressures.

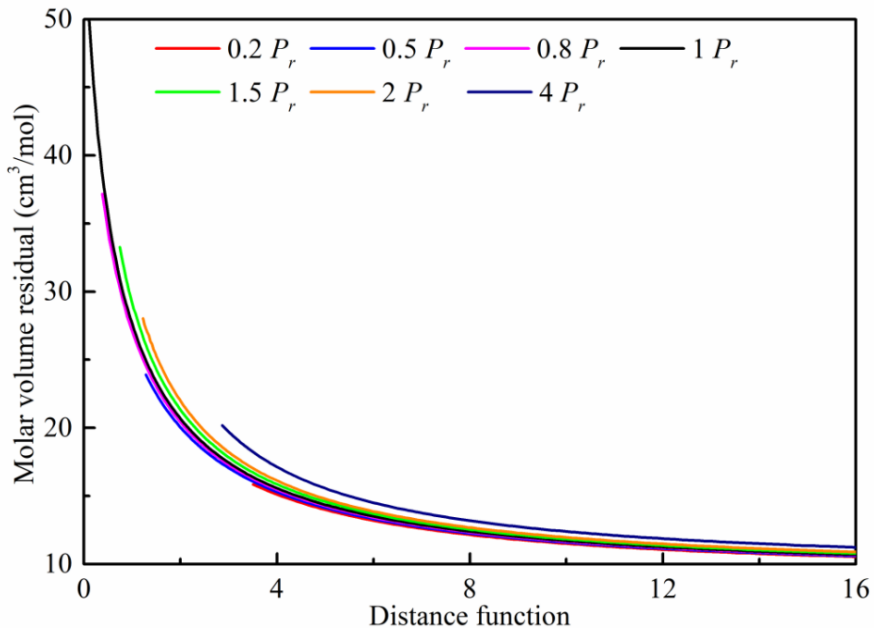

(a)

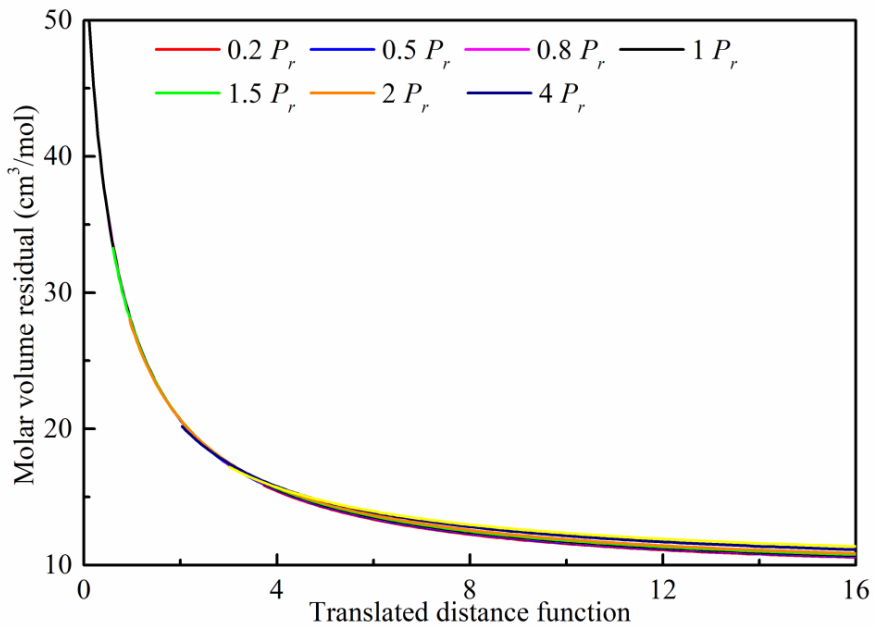

(b)

Fig. 3-A2. Needed volume shifts in SRK EOS for ethanol versus distance function d (a) and translated distance function d' (b) at different reduced pressures.

As shown in **Fig. 3-A1**, the curves of needed volume shifts for carbon dioxide versus distance function at most pressures (except P_r=4) have been largely overlapped with each other. Thus, the further translation of distance function will exert little effect on improving the density prediction. In contrast, the curves of needed volume shifts for ethanol versus distance function are quite scattered (**Fig. 3-A2a**). The translation of distance function is able to make these curves almost collapse into one curve (**Fig. 3-A2b**). As a result, the 5-parameter VT-SRK EOS (**Eq. 3-14**) gives a more accurate density prediction for the substance containing hydrogen bond and it is promising to extend the translation of distance function to the VT-models for other associating fluids.

Appendix 3-B. A Novel Hybrid VT-SRK EOS for Asymmetric Mixtures

To extend the application of the proposed VT-models, we provide a novel hybrid VT-SRK EOS for asymmetric mixtures which couples the 5-parameter VT-model with the 3-parameter VT-model based on the mole fraction of each compound,

$$v_m^{VT} = v_m - \sum_i x_{5i}\Delta v_{5i} - \sum_j x_{3j}\Delta v_{3j} \tag{3-B1}$$

where v_m^{VT} is the molar volume of mixture corrected by volume translations; v_m is the mixture volume yielded by original SRK EOS coupled with traditional mixing rules; x_{5i} and x_{3j} are the molar fractions of the compounds which are described by the 5-parameter VT-model and 3-parameter VT-model, respectively, and $\sum_i x_{5i} + \sum_j x_{3j} = 1$. Δv_{5i} and Δv_{3j} are the shifted molar volumes for the given compounds yielded by the 5-parameter VT-model (i) and the 3-parameter VT-model (j), respectively, and given as,

$$\Delta v_5 = c_1\left(\frac{RT_c}{P_c}\right) + \delta_c\left(\frac{1}{c_2 + c_3\left(d + c_5\left(P_r - 1\right)\right)^{c_4}}\right) \tag{3-B2}$$

$$\Delta v_3 = c_1\left(\frac{RT_c}{P_c}\right) + \delta_c\left(\frac{1}{c_2 + c_3 d}\right) \tag{3-B3}$$

Here, we adopt a hexane-water system [103] to verify the performance of the proposed hybrid VT-SRK EOS with regard to the molar volume predictions. The calculated results for the liquid volumes of water-rich phases (the molar fractions of hexane are 6.157×10^{-6}-1.883×10^{-4}) and hexane-rich phases (the molar fractions of hexane are 0.9866-0.9069) under equilibrium conditions are shown in **Table 3-B1** and **Fig. 3-B1**; the original SRK EOS and the previously proposed 3-parameter VT-SRK EOS (**Eq. 3-9**) extended to mixtures [72] have also been evaluated for comparison purpose.

Table 3-B1. Comparison of the average absolute percentage deviations (%AADs) for molar volumes of hexane-water system [103] yielded by the original SRK EOS, the 3-parameter VT-SRK EOS (**Eq. 3-9**) and the hybrid VT-SRK EOS proposed in this work (**Eq. 3-B1**).

EOS	%AAD for reproducing hexane-rich phase volume	%AAD for reproducing water-rich phase
Hybrid VT-SRK EOS	1.44	0.29
3-parameter VT-SRK EOS	3.21	2.75
SRK EOS	14.67	36.37

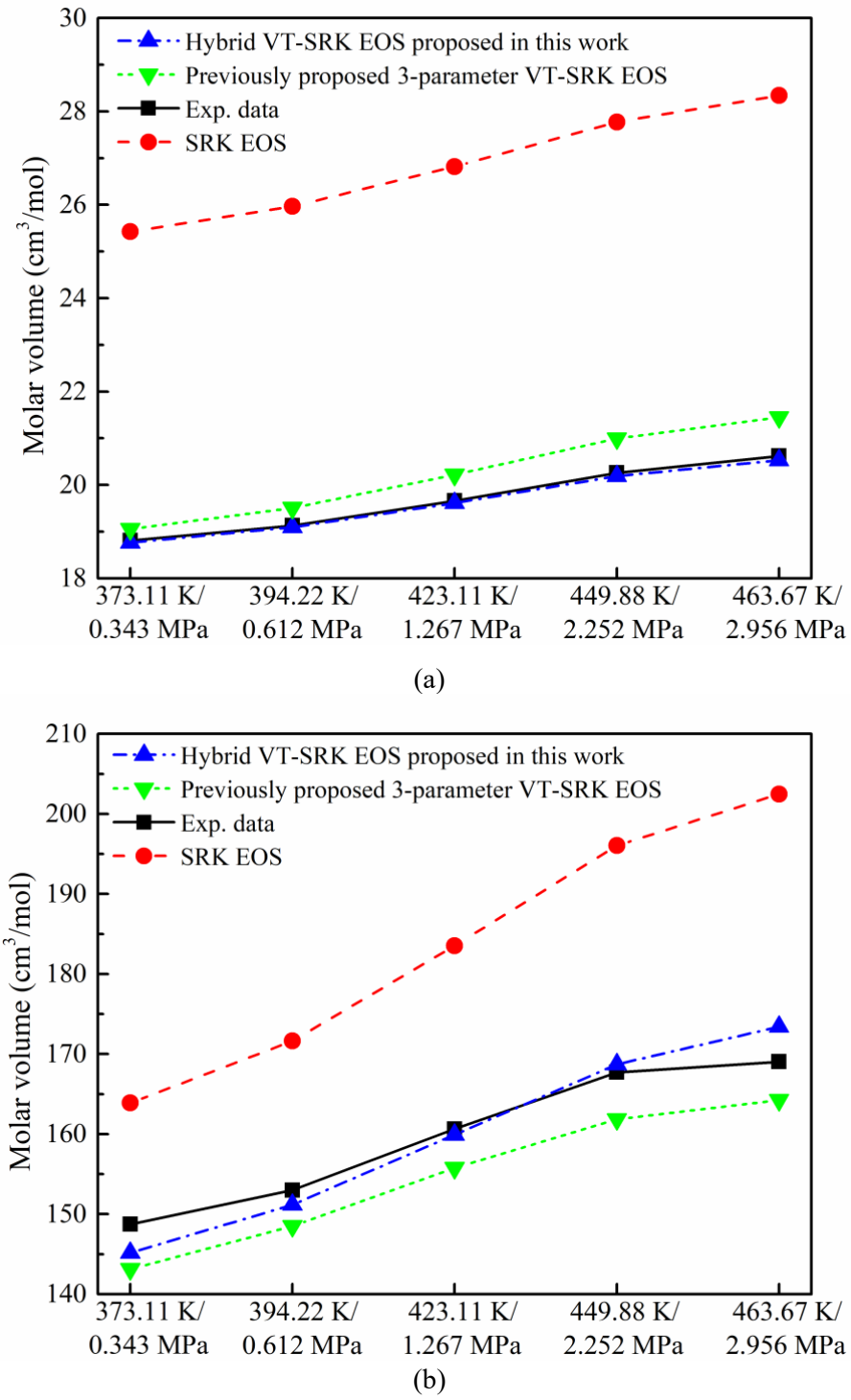

Fig. 3-B1. Comparison of the molar liquid volumes of hexane-water system under equilibrium condition yielded by the original SRK EOS, the previously proposed 3-parameter VT-SRK EOS (**Eq. 3-9**) and the hybrid VT-SRK EOS proposed in this work (**Eq. 3-B1**) against experimental data [103]: (a) water-rich liquid phase; and (b) hexane-rich liquid phase.

Compared to the original SRK EOS, the hybrid VT-SRK EOS proposed in this work (**Eq. 3-B1**) and the previously proposed 3-parameter VT-SRK EOS (**Eq. 3-9**) can significantly improve the volume predictions for both the water-rich and hexane-rich

liquid phases. More specifically, as shown in **Fig. 3-B1a**, the volumes of water-rich phase given by the hybrid VT-SRK EOS almost coincide with the experimental data while the 3-parameter VT-SRK EOS still yields noticeable calculation errors. Note that the molar fractions of hexane in the water-rich phase are negligible. The newly proposed 5-parameter VT-model performs much better for predicting the water volume than the 3-parameter VT-model, resulting in the accurate reproduction of water-rich phase volume. In addition, the presence of water in the hexane-rich phase cannot be overlooked and the 5-parameter VT-model for water embedded in the hybrid VT-SRK EOS helps to improve the volume calculation of hexane-rich phase by properly honoring the presence of water in the hexane-rich phase. Therefore, the hybrid VT-SRK EOS could be applied to the highly asymmetric mixtures and lead to more accurate density predictions for water-hydrocarbon systems.

References

[1] M. French, T.R. Mattsson, N. Nettelmann, R. Redmer, Equation of state and phase diagram of water at ultrahigh pressures as in planetary interiors, Phys. Rev. B 79 (2009) 054107, https://doi.org/10.1103/PhysRevB.79.054107.

[2] D. Bandyopadhyay, S. Mohan, S.K. Ghosh, N. Choudhury, Correlation of structural order, anomalous density, and hydrogen bonding network of liquid water, J. Phys. Chem. B 117 (2013) 8831-8843, https://doi.org/10.1021/jp404478y.

[3] S. Michel, H.H. Hooper, J.M. Prausnitz, Mutual solubilities of water and hydrocarbons from an equation of state. Need for an unconventional mixing rule, Fluid Phase Equilib. 45 (1989) 173-189, https://doi.org/10.1016/0378-3812(89)80256-0.

[4] Z. Wang, J. Zhang, B. Sun, L. Chen, Y. Zhao, W. Fu, A new hydrate deposition prediction model for gas-dominated systems with free water, Chem. Eng. Sci. 163 (2017) 145-154, https://doi.org/10.1016/j.ces.2017.01.030.

[5] D.A. Palmer, R. Fernandez-Prini, A.H. Harvey, Aqueous systems at elevated temperatures and pressures, Academic Press 2004, https://doi.org/10.1016/B978-0-12-544461-3.X5000-5.

[6] H.G. Rackett, Equation of state for saturated liquids, J. Chem. Eng. Data 15 (1970) 514-517, https://doi.org/10.1021/je60047a012.

[7] S. Wiryana, L.J. Slutsky, J.M. Brown, The equation of state of water to 200ºC and 3.5 GPa: Model potentials and the experimental pressure scale, Earth Planet. Sci. Lett. 163 (1970) 123-130, https://doi.org/10.1016/S0012-821X(98)00180-0.

[8] F. Civan, Critical modification to the Vogel-Tammann-Fulcher equation for temperature effect on the density of water, Ind. Eng. Chem. Res. 46 (2007) 5810-5814, https://doi.org/10.1021/ie070714j.

[9] R.B. Maximino, Surface tension and density of binary mixtures of monoalcohols, water and acetonitrile: Equation of correlation of the surface tension, Phys. Chem. Liq. 47 (1990) 475-486, https://doi.org/10.1080/00319100802241657.

[10] C.H. Cho, J. Urquidi, S. Singh, S.C. Park, G.W. Robinson, Pressure effect on the density of water, J. Phys. Chem. A 106 (2002) 7557-7561, https://doi.org/10.1021/jp0136260.

[11] Y. Shibue, A modified rackett equation applied to water and aqueous NaCl and KCl solutions, J. Chem. Eng. Data 45 (2000) 523-529, https://doi.org/10.1021/je0000017.

[12] E.H. Abramson, J.M. Brown, Equation of state of water based on speeds of sound measured in the diamond-anvil cell, Geochim. Cosmochim. Ac. 68 (2004) 1827-1835, https://doi.org/10.1016/j.gca.2003.10.020.

[13] J. Chandran, A. Salih, A modified equation of state for water for a wide range of pressure and the concept of water shock tube, Fluid Phase Equilib. 483 (2019) 182-188, https://doi.org/10.1016/j.fluid.2018.11.032.

[14] J.O. Valderrama, M. Alfaro, Liquid volumes from generalized cubic equations of state: Take it with care, Oil Gas Sci. Technol. 55 (2000) 523-531, https://doi.org/10.2516/ogst:2000039.

[15] M. Schottler, R. Redmer, M. French, Low-density equation of state for water from a chemical model, Contrib. Plasm. Phys. 53 (2013) 336-346, https://doi.org/10.1002/ctpp.201300020.

[16] S. Harrington, P.H. Poole, F. Sciortino, H.E. Stanley, Equation of state of supercooled water simulated using the extended simple point charge intermolecular potential, J. Chem. Phys. 107 (1997) 7443, https://doi.org/10.1063/1.474982.

[17] C.J. Roberts, P.G. Debenedetti, F.H. Stillinger, Equation of state of the energy landscape of SPC/E water, J. Phys. Chem. B 103 (1990) 10258-10265, https://doi.org/10.1021/jp991801v.

[18] G. Pallares, M.A. Gonzalez, J.L.F. Abascal, C. Valeriani, F. Caupin, Equation of state for water and its line of density maxima down to -120 MPa, Phys. Chem. Chem. Phys. 18 (2016) 5896, https://doi.org/10.1039/C5CP07580G.

[19] V. Holten, C. Qiu, E. Guillerm, M. Wilke, J. Ricka, M. Frenz, F. Caupin, Compressibility anomalies in stretched water and their interplay with density anomalies, J. Phys. Chem. Lett. 8 (2017) 5519-5522, https://doi.org/10.1021/acs.jpclett.7b02563.

[20] A. Ben-Naim, Application of an approximate Percus-Yevick equation for liquid water, J. Chem. Phys. 52 (1970) 5531, https://doi.org/10.1063/1.1672821.

[21] Y. Kataoka, Studies of liquid water by computer simulations. V. Equation of state of fluid water with Carravetta-Clementi potential, J. Chem. Phys. 87 (1987) 589, https://doi.org/10.1063/1.453607.

[22] A. Obeidat, M. Badarneh, New estimations of vapor density and surface tension of water at low temperatures using scaled model, J. Mol. Liq. 287 (2019) 110952, https://doi.org/10.1016/j.molliq.2019.110952.

[23] J. Habasaki, Heterogeneous-homogeneous transition and anomaly of density in SPC/E water examined by molecular dynamics simulations, Physica A 527 (2019) 121391, https://doi.org/10.1016/j.physa.2019.121391.

[24] D.A. Fuentevilla, M.A. Anisimov, Scaled equation of state for supercooled water near the liquid-liquid critical point, Phys. Rev. Lett. 97 (2006) 195702, https://doi.org/10.1103/PhysRevLett.97.195702.

[25] A. Saul, W. Wagner, A fundamental equation for water covering the range from the melting line to 1273 K at pressures up to 25000 MPa, J. Phys. Chem. Ref. Data 18 (1989) 1537-1564, https://doi.org/10.1063/1.555836.

[26] K.S. Pitzer, S.M. Sterner, Equations of state valid continuously from zero to extreme pressures for H_2O and CO_2, J. Chem. Phys. 101 (1994) 3111-3116, https://doi.org/10.1063/1.467624.

[27] C.-W. Lin, J.P.M. Trusler, The speed of sound and derived thermodynamic properties of pure water at temperatures between (253 and 473) K and at pressures up to 400 MPa, J. Chem. Phys. 136 (2012) 094511, https://doi.org/10.1063/1.3688054.

[28] C. Sanchez-Valle, D. Mantegazzi, J.D. Bass, E. Reusser, Equation of state, refractive index and polarizability of compressed water to 7 GPa and 673 K, J. Chem. Phys. 138 (2013) 054505, https://doi.org/10.1063/1.4789359.

[29] R. Span, W. Wagner, A new equation of state for carbon dioxide covering the fluid region from the triple-point temperature to 1100 K at pressures up to 800 MPa, J. Phys. Chem. Ref. Data 25 (1996) 1509-1596, https://doi.org/10.1063/1.555991.

[30] G. Du, J. Hu, An equation of state for accurate thermodynamic modeling of water and carbon dioxide from triple points to 647 K and 100-200 MPa, Int. J. Greenh. Gas Con. 49 (2016) 94-107, https://doi.org/10.1016/j.ijggc.2016.02.025.

[31] W. Wagner, A. Pruβ, The IAPWS formulation 1995 for the thermodynamic properties of ordinary water substance for general and scientific use, J. Phys. Chem. Ref. Data 31 (2002) 387-535, https://doi.org/10.1063/1.1461829.

[32] R.J. Linstrom, W.G. Mallard, NIST Chemistry WebBook, NIST standard reference subscription database 3n, National Institute of Standards and Technology, Gaithersburg, MD, 20899, http://webbook.nist.gov.

[33] E.A. Muller, K.E. Gubbins, An equation of state for water from a simplified intermolecular potential, Ind. Eng. Chem. Res. 34 (1995) 3662-3673, https://doi.org/10.1021/ie00037a055.

[34] C.A. Jeffery, P.H. Austin, A new analytic equation of state for liquid water, J. Chem. Phys. 110 (1999) 484-496, https://doi.org/10.1063/1.477977.

[35] L. Maftoon-Azad, S. Elyasi, An analytical equation of state for water and aliphatic alcohols, J. Mol. Liq. 211 (2015) 667-674, https://doi.org/10.1016/j.molliq.2015.07.047.

[36] H.M. Kim, A.J. Schultz, D.A. Kofke, Virial equation of state of water based on Wertheim's association theory, J. Phys. Chem. B 116 (2012) 14078-14088, https://doi.org/10.1021/jp3067475.

[37] E.B. Melo, E.T. Oliveira, T.D. Martins, A neural network correlation for molar density and specific heat of water: Predictions at pressures up to 100 MPa, Fluid Phase Equilib. 506 (2020) 112411, https://doi.org/10.1016/j.fluid.2019.112411.

[38] G. Soave, Equilibrium constants from a modified Redlich-Kwong equation of state, Chem. Eng. Sci. 27 (1972) 1197-1203, https://doi.org/10.1016/0009-2509(72)80096-4.

[39] D.Y. Peng, D.B. Robinson, A new two-constant equation of state, Ind. Eng. Chem. Fundam. 15 (1976) 59-64, https://doi.org/10.1021/i160057a011.

[40] G.M. Kontogeorgis, R. Privat, J. Jaubert, Taking another look at the van der Waals equation of state-almost 150 years later, J. Chem. Eng. Data 64 (2019) 4619-4637, https://doi.org/10.1021/acs.jced.9b00264.

[41] H.W. Curtis, R.B. Michael, Phase Behavior, SPE Monograph Series, 20 (2000).

[42] W.G. Chapman, G. Jackson, K.E. Gubbins, Phase equilibria of associating fluids: Chain molecules with multiple bonding sites, Mol. Phys. 65 (1988) 1067-1079, https://doi.org/10.1080/00268978800101601.

[43] W.G. Chapman, K.E. Gubbins, G. Jackson, M. Radosz, SAFT: Equation-of-state solution model for associating fluids, Fluid Phase Equilib. 52 (1989) 31-38, https://doi.org/10.1016/0378-3812(89)80308-5.

[44] W.G. Chapman, K.E. Gubbins, G. Jackson, M. Radosz, New reference equation of state for associating liquids, Ind. Eng. Chem. Res. 29 (1990) 1709-1721, https://doi.org/10.1021/ie00104a021.

[45] J. Gross, G. Sadowski, Perturbed-chain SAFT: An equation of state based on a perturbation theory for chain molecules, Ind. Eng. Chem. Res. 40 (2001) 1244-1260, https://doi.org/10.1021/ie0003887.

[46] B.D. Marshall, Mixture equation of state for water with an associating reference fluid, Ind. Eng. Chem. Res. 57 (2018) 4070-4080, https://doi.org/10.1021/acs.iecr.7b04712.

[47] B.D. Marshall, Perturbation theory for water with an associating reference fluid, Phys. Rev. E 96 (2017) 052602, https://doi.org/10.1103/PhysRevE.96.052602.

[48] S.H. Huang, M. Radosz, Equation of state for small, large, polydisperse, and associating molecules, Ind. Eng. Chem. Res. 29 (1990) 2284-2294, https://doi.org/10.1021/ie00107a014.

[49] I.G. Economou, M.D. Donohue, Equation of state with multiple associating sites for water and water-hydrocarbon mixtures, Ind. Eng. Chem. Res. 31 (1992) 2388-2394, https://doi.org/10.1021/ie00010a019.

[50] P.J. Smits, I.G. Economou, C.J. Peters, J.S. Arons, Equation of state description of thermodynamic properties of near-critical and supercritical water, J. Phys. Chem. 98 (1994) 12080-12085, https://doi.org/10.1021/j100097a038.

[51] T. Kraska, K.E. Gubbins, Phase equilibria calculations with a modified SAFT equation of state. 2. Binary mixtures of n-alkanes, 1-alkanols, and water, Ind. Eng. Chem. Res. 35 (1996) 4738-4746, https://doi.org/10.1021/ie960233s.

[52] F.P. Nascimento, M.L.L. Paredes, F.L.P. Pessoa, Evaluation of the polar contribution in the SAFT-VR Mie equation of state for simultaneous correlation of condensed-phase density, condensedphase speed of sound, saturated density and saturated pressure of pure polar fluids, J. Chem. Thermodyn. 134 (2019) 106-118, https://doi.org/10.1016/j.jct.2019.02.032.

[53] G.M. Kontogeorgis, E.C. Voutsas, I.V. Yakoumis, D.P. Tassios, An equation of state for associating fluids, Ind. Eng. Chem. Res. 35 (1996) 4310-4318, https://doi.org/10.1021/ie9600203.

[54] J. Wu, J.M. Prausnitz, Phase equilibria for systems containing hydrocarbons, water, and salt: An extended Peng-Robinson equation of state, Ind. Eng. Chem. Res. 37 (1998) 1634-1643, https://doi.org/10.1021/ie9706370.

[55] A.J. Queimada, C. Miqueu, I.M. Marrucho, G.M. Kontogeorgis, J.A.P. Coutinho, Modeling vapor-liquid interfaces with the gradient theory in combination with the CPA equation of state, Fluid Phase Equilib. 228-229 (2005) 479-485, https://doi.org/10.1016/j.fluid.2004.08.011.

[56] A.M. Palma, A.J. Queimada, J.A.P. Coutinho, Improved prediction of water properties and phase equilibria with a modified cubic plus association equation of state, Ind. Eng. Chem. Res. 56 (2017) 15163-15176, https://doi.org/10.1021/acs.iecr.7b03522.

[57] P. Guo, H. Tu, Z. Wang, Q. Wang, Calculation of thermodynamic properties of water by the CPA equation of state, Nat. Gas Ind. B 4 (2017) 305-310, https://doi.org/10.1016/j.ngib.2017.08.014.

[58] N.C. Patel, A.S. Teja, A new cubic equation of state for fluids and fluid mixtures, Chem. Eng. Sci. 37 (1982) 463-473, https://doi.org/10.1016/0009-2509(82)80099-7.

[59] J.O. Valoerrama, L.A. Cisternas, A cubic equation of state for polar and other complex mixtures, Fluid Phase Equilib. 29 (1986) 431-438, https://doi.org/10.1016/0378-3812(86)85041-5.

[60] M. Cismondi, J. Cruz, M.J. Gomez, G.F. Montoya, Modelling the phase behavior of alkane mixtures in wide ranges of conditions: New parameterization and predictive correlations of binary interactions for the RKPR EOS, Fluid Phase Equilib. 403 (2015) 49-59, https://doi.org/10.1016/j.fluid.2015.06.005.

[61] P.N.P. Ghoderao, V.H. Dalvi, M. Narayan, A four-parameter cubic equation of state for pure compounds and mixtures, Chem. Eng. Sci. 190 (2018) 173-189, https://doi.org/10.1016/j.ces.2018.06.010.

[62] A. Peneloux, E. Rauzy, R. Freze, A consistent correction for Redlich-Kwong-Soave volumes, Fluid Phase Equilib. 8 (1982) 7-23, https://doi.org/10.1016/0378-3812(82)80002-2.

[63] W.D. Monnery, W.Y. Svrcek, M.A. Satyro, Gaussian-like volume shifts for the Peng-Robinson equation of state, Ind. Eng. Chem. Res. 37 (1998) 1663-1672, https://doi.org/10.1021/ie970640j.

[64] H. Lin, Y.Y. Duan, T. Zhang, Z.M. Huang, Volumetric property improvement for the Soave-Redlich-Kwong equation of state, Ind. Eng. Chem. Res. 45 (2006) 1829-1839, https://doi.org/10.1021/ie051058v.

[65] M. Nazarzadeh, M. Moshfeghian, New volume translated PR equation of state for pure compounds and gas condensate systems, Fluid Phase Equilib. 337 (2013) 214-224, https://doi.org/10.1016/j.fluid.2012.10.003.

[66] J.C. Tsai, Y.P. Chen, Application of a volume-translated Peng-Robinson equation of state on vapor-liquid equilibrium calculations, Fluid Phase Equilib. 145 (1998) 193-215, https://doi.org/10.1016/S0378-3812(97)00342-7.

[67] W.R. Ji, D.A. Lempe, Density improvement of the SRK equation of state, Fluid Phase Equilib. 130 (1997) 49-63, https://doi.org/10.1016/S0378-3812(96)03190-1.

[68] J. Shi, H. Li, W. Pang, An improved volume translation strategy for PR EOS without crossover issue, Fluid Phase Equilib. 470 (2018) 164-175, https://doi.org/10.1016/j.fluid.2018.01.034.

[69] P.M. Mathias, T. Naheiri, E.M. Oh, A density correction for the Peng-Robinson equation of state, Fluid Phase Equilib. 47 (1989) 77-87, https://doi.org/10.1016/0378-3812(89)80051-2.

[70] G.F. Chou, J.M. Prausnitz, A phenomenological correction to an equation of state for the critical region, AIChE J. 35 (1989) 1487-1496, https://doi.org/10.1002/aic.690350909.

[71] A.M. Abudour, S.A. Mohammad, R.L. Robinson, K.A.M. Gasem, Volume-translated Peng-Robinson equation of state for saturated and single-phase liquid densities, Fluid Phase Equilib. 335 (2012) 74-87, https://doi.org/10.1016/j.fluid.2012.08.013.

[72] X. Chen, H. Li, An improved volume-translated SRK equation of state dedicated to accurate determination of saturated and single-phase liquid densities, Fluid Phase Equilib. 521 (2020) 112724, https://doi.org/10.1016/j.fluid.2020.112724.

[73] A.M. Palma, A.J. Queimada, J.A.P. Coutinho, Using a volume shift in perturbed-chain statistical associating fluid theory to improve the description of speed of sound and other derivative properties, Ind. Eng. Chem. Res. 57 (2018) 11804-11814, https://doi.org/10.1021/acs.iecr.8b02646.

[74] A.M. Palma, A.J. Queimada, J.A.P. Coutinho, Using volume shifts to improve the description of speed of sound and other derivative properties with cubic equations of state, Ind. Eng. Chem. Res. 58 (2019) 8856-8870, https://doi.org/10.1021/acs.iecr.9b00817.

[75] E. Moine, A. Pina-Martinez, J. Jaubert, B. Sirjean, R. Privat, I-PC-SAFT: An industrialized version of the volume-translated PC-SAFT equation of state for pure components, resulting from experience acquired all through the years on the parameterization of SAFT-type and cubic models, Ind. Eng. Chem. Res. 58 (2019) 20815-20827, https://doi.org/10.1021/acs.iecr.9b04660.

[76] M.J. Amani, L. Dehdari, A. Ghamartale, Modelling density and excess volume of hydrocarbon + water mixtures near the critical region, Fluid Phase Equilib. 492 (2019) 55-66, https://doi.org/10.1016/j.fluid.2019.03.020.

[77] F. Mangold, St. Pilz, S. Bjelic, F. Vogel, Equation of state and thermodynamic properties for mixtures of H_2O, O_2, N_2, and CO_2 from ambient up to 1000 K and 280 MPa, J. Supercrit. Fluid. 153 (2019) 104476, https://doi.org/10.1016/j.supflu.2019.02.016.

[78] B. Schmid, J. Gmehling, From van der Waals to VTPR: The systematic improvement of the van der Waals equation of state, J. Supercrit. Fluid. 55 (2010) 438-447, https://doi.org/10.1016/j.supflu.2010.10.018.

[79] D.S. Schechter, B. Guo, Parachors based on modern physics and their uses in IFT prediction of reservoir fluids, SPE Reserv. Eval. Eng. 1 (1998) 207-217, https://doi.org/10.2118/30785-PA.

[80] T. Sun, A. Takbiri-Borujeni, H. Nourozieh, M. Gu, Application of Peng-Robinson equation of state for modelling the multiphase equilibrium properties in Athabasca bitumen/ethane mixtures, Fuel 252 (2019) 439-447, https://doi.org/10.1016/j.fuel.2019.04.106.

[81] D.G. Archer, P. Wang, The dielectric constant of water and Debye-Hückel limiting law slopes, J. Phys. Chem. Ref. Data 19 (1990) 371-411, https://doi.org/10.1063/1.555853.

[82] D. Fu, X. Li, Investigation of vapor-liquid nucleation for water and heavy water by density functional theory, J. Phys. Chem. C 111 (2007) 13938-13944, https://doi.org/10.1021/jp073971a.

[83] A. Allal, C. Boned, Q. Baylaucq, Free volume viscosity model for fluids in the dense and gaseous states, Phys. Rev. E 64 (2001) 011203, https://doi.org/10.1103/PhysRevE.64.011203.

[84] W.A. Burgess, D. Tapriyal, I.K. Gamwo, B.D. Morreale, M.A. McHugh, R.M. Enick, Viscosity models based on the free volume and frictional theories for systems at pressures to 276 MPa and temperatures to 533 K, Ind. Eng. Chem. Res. 51 (2012) 16721-16733, https://doi.org/10.1021/ie301727k.

[85] W.A. Burgess, I.K. Gamwo, R.M. Enick, M.A. McHugh, Viscosity models for pure hydrocarbons at extreme conditions: A review and comparative study, Fuel 218 (2018) 89-111, https://doi.org/10.1016/j.fuel.2018.01.002.

[86] J. Shi, H. Li, Criterion for determining crossover phenomenon in volume-translated equation of states, Fluid Phase Equilib. 430 (2016) 1-12, https://doi.org/10.1016/j.fluid.2016.09.017.

[87] A. Pina-Martinez, Y. Le Guennec, R. Privat, J. Jaubert, P.M. Mathias, Analysis of the combinations of property data that are suitable for a safe estimation of consistent Twu α-function parameters: Updated parameter values for the translated-consistent tc-PR and tc-RK cubic equations of state, J. Chem. Eng. Data 63 (2018) 3980-3988, https://doi.org/10.1021/acs.jced.8b00640.

[88] C.H. Twu, D. Bluck, J.R. Cunningham, J.E. Coon, A cubic equation of state with a new alpha function and a new mixing rule, Fluid Phase Equilib. 69 (1991) 33-50, https://doi.org/10.1016/0378-3812(91)90024-2.

[89] S.G. Penoncello, Thermal energy systems: Design and analysis, CRC Press 2018.

[90] A. Firoozabadi, Thermodynamics and applications of hydrocarbons energy production, McGraw-Hill Education 2015.

[91] P.H. Salim, M.A. Trebble, A modified Trebble-Bishnoi equation of state: Thermodynamic consistency revisited, Fluid Phase Equilib. 65 (1991) 59-71, https://doi.org/10.1016/0378-3812(91)87017-4.

[92] H. Teng, A. Yamasaki, M.-K. Chun, H. Lee, Solubility of liquid CO_2 in water at temperatures from 278K to 293K and pressures from 6.44 MPa to 29.49 MPa and densities of the corresponding aqueous solutions, J. Chem. Thermodynamics 29 (1997) 1301-1310, https://doi.org/10.1006/jcht.1997.0249.

[93] M.B. King, A. Mubarak, J.D. Kim, T.R. Bott, The mutual solubilities of water with supercritical and liquid carbon dioxide? J. Supercrit. Fluid. 5 (1992) 296-302, https://doi.org/10.1016/0896-8446(92)90021-B.

[94] H. Kubota, Y. Tanaka, T. Makita, Volumetric behavior of pure alcohols and their water mixtures under high pressure, Int. J. Thermophysics 8 (1987) 47-70, https://doi.org/10.1007/BF00503224.

[95] B. Gonzalez, N. Calvar, E. Gomez, A. Dominguez, Density, dynamic viscosity, and derived properties of binary mixtures of methanol or ethanol with water, ethyl acetate, and methyl acetate at T=(293.15, 298.15, and 303.15) K, J. Chem. Thermodynamics 39 (2007) 1578-1588, https://doi.org/10.1016/j.jct.2007.05.004.

[96] A. Bamberger, G. Sieder, G. Maurer, High-pressure (vapor+liquid) equilibrium in binary mixtures of (carbon dioxide+water or acetic acid) at temperatures from 313 to 353 K, J. Supercrit. Fluid. 17 (2000) 97-110, https://doi.org/10.1016/S0896-8446(99)00054-6.

[97] A. Valtz, A. Chapoy, C. Coquelet, P. Paricaud, D. Richon, Vapour-liquid equilibria in the carbon dioxide-water system, measurement and modelling from 278.2 to 318.2 K, Fluid Phase Equilib. 226 (2004) 333-344, https://doi.org/10.1016/j.fluid.2004.10.013.

[98] F. Barr-David, B.F. Dodge, Vapor-liquid equilibrium at high pressures. The systems ethanol-water and 2-propanol-water, Chem. Eng. Data 4 (1959) 107-121, https://doi.org/10.1021/je60002a003.

[99] H. Kurihara, T. Minoura, K. Takeda, K. Kojima, Isothermal vapor-liquid equilibria for methanol+ethanol+water, methanol+water, and ethanol+water, J. Chem. Eng. Data 40 (1995) 679-684, https://doi.org/10.1021/je00019a033.

[100] M. Aalto, K.I. Keskinen, J. Aittamaa, S. Liukkonen, An improved correlation for compressed liquid densities of hydrocarbons. Part 2. Mixtures, Fluid Phase Equilib. 114 (1996) 21-35, https://doi.org/10.1016/0378-3812(95)02824-2.

[101] P.L. Chueh, J.M. Prausnitz, Vapor-liquid equilibria at high pressures: Calculation of critical temperatures, volumes, and pressures of nonpolar mixtures, AIChE J. 13 (1967) 1107-1113, https://doi.org/10.1002/aic.690130613.

[102] A.M. Abudour, S.A. Mohammad, R.L. Robinson, K.A.M. Gasem, Volume-translated Peng-Robinson equation of state for liquid densities of diverse binary mixtures, Fluid Phase Equilib. 349 (2013) 37-55, https://doi.org/10.1016/j.fluid.2013.04.002.

[103] M.A. Barrufet, H. Liu, S. Rahman, C. Wu, Simultaneous vapor-liquid-liquid equilibria and phase molar densities of a quaternary system of propane + pentane + octane + water, J. Chem. Eng. Data 41 (1996) 918-922, https://doi.org/10.1021/je9600616.

CHAPTER 4 NEW PRAGMATIC STRATEGIES FOR OPTIMIZING KIHARA POTENTIAL PARAMETERS USED IN VAN DER WAALS-PLATTEEUW HYDRATE MODEL

A version of this chapter has been published in *Chemical Engineering Science*

Abstract

The study aims to tune the Kihara potential parameters to construct a robust and accurate van der Waals-Platteeuw (vdW-P) model. A new procedure was developed for fitting the Kihara potential parameters in the vdW-P hydrate model using the experimental hydrate equilibrium data for both pure gases and binary-gas mixtures, considering the differences between hydrate structures I and II. To ensure reliability of the optimization results, a large database, with more than 3000 hydrate equilibrium data, was compiled for pure hydrate-forming gases and their binaries, measured over a wide temperature and pressure range. The Kihara potential parameters, optimized using the new fitting procedure, not only performed well in modeling pure-gas hydrates but also provided more accurate predictions on the hydrate equilibria of gas mixtures. Thus, the vdW-P hydrate model can be employed to detect the hydrate structure transition and cage occupancy behaviors when used in conjunction with the newly fitted Kihara potential parameters.

Keywords: van der Waals-Platteeuw model; Hydrate equilibrium calculation; Kihara potential parameters; Hydrate structure transition; Hydrate equilibrium database.

4.1. Introduction

Natural gas hydrates are solid crystalline mixtures of water and small gas molecules that typically form at relatively low temperatures and moderate pressures [1]. Gas molecules (guests) are encaged in the cavities (hosts) that comprise hydrogen-bonded water molecules [1,2]. Natural gases that typically form gas hydrates include methane (CH_4), ethane (C_2H_6), propane (C_3H_8), isobutane (i-C_4H_{10}), nitrogen (N_2), and carbon dioxide (CO_2) [2]. As illustrated in **Fig. 4-1**, hydrate crystal structures can be categorized under three distinct classes (I, II, and H), each of which comprises various combinations of polyhedra [2–4]. The geometric parameters of these three hydrate structures are listed in **Table 4-1**.

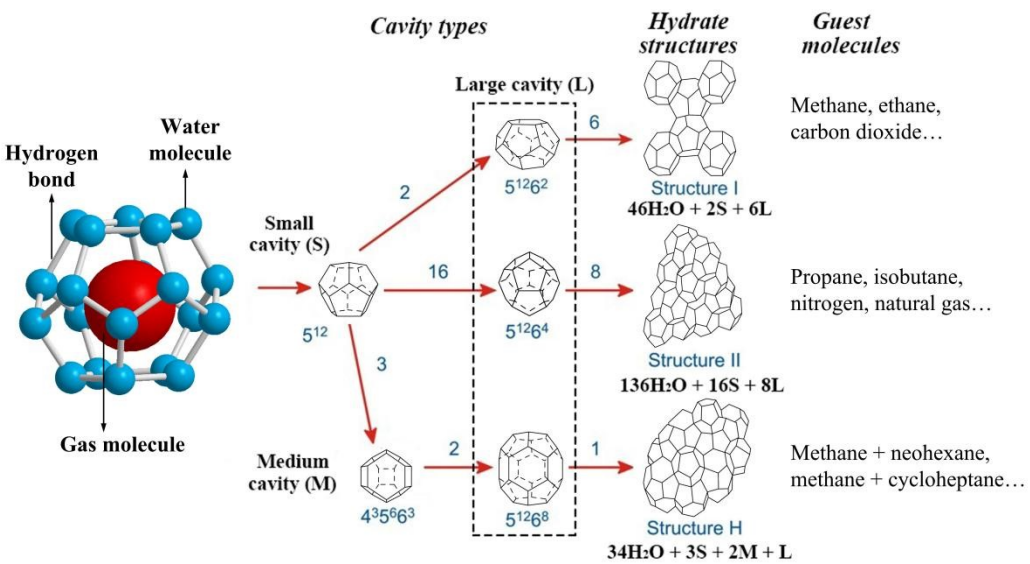

Fig. 4-1. Three structures of gas hydrates (I, II, and H) comprising five types of polyhedra (5^{12}, $5^{12}6^2$, $5^{12}6^4$, $5^{12}6^8$, and $4^35^66^3$). Specifications: $5^{12}6^2$ indicates a cavity comprising 12 pentagonal and 2 hexagonal faces; $46H_2O + 2S + 6L$ indicates a structure I unit crystal comprising two 5^{12} cavities, six $5^{12}6^2$ cavities, and 46 water molecules: Reprinted with permission of Springer Nature from Sloan (2003). Fundamental principles and applications of natural gas hydrates. Nature 426: 353-359; permission conveyed through Copyright Clearance Center, Inc. with modifications.

Table 4-1. Geometric parameters of the three gas hydrate crystal structures: Data from Sloan and Koh (2008) [4] and Parrish and Prausnitz (1972) [5].

Hydrate crystal structure	I		II		H		
Cavity	Small	Large	Small	Large	Small	Medium	Large

Description	5^{12}	$5^{12}6^{2}$	5^{12}	$5^{12}6^{4}$	5^{12}	$4^{3}5^{6}6^{3}$	$5^{12}6^{8}$
Number of cavities per unit cell	2	6	16	8	3	2	1
Average cavity radius (Å)	3.975	4.3	3.91	4.73	3.94	4.04	5.79
Number of water molecules per unit cell	20	24	20	28	20	20	36

Natural gas hydrates are a promising energy resource and have been discovered in many offshore and permafrost geological formations [6–9]. Natural gas hydrates have been observed to form within pipelines located in cold areas and in wellbores used in the offshore petroleum industry, and these cause flow assurance problems [10–12]. Decomposition of in-situ hydrates in reservoirs during the exploitation process as well as the formation of hydrates in pipelines or wellbores may alter the phase behavior in systems containing gas hydrates [13–16]. Thus, accurate modeling of gas hydrate equilibria is critical for describing multiphase flow involving gas hydrates, as it can provide insights for developing in-situ gas hydrates and preventing hydrate blockage in pipelines and wellbores [4,17–20].

Numerous frameworks for calculating gas hydrate equilibria have been proposed since the early 20th century [4,15]. These frameworks can be broadly classified into empirical methods and thermodynamic models [4,15]. In the 1940s, based on a large amount of experimental data, the gas gravity chart method and the vapor-hydrate distribution coefficient method were first proposed for determining the formation conditions of gas hydrates in pipelines [21–23]. While these empirical methods have been continuously updated and are simple to use, their application to gas-mixture hydrates over wide temperature and pressure ranges results in significant errors, thereby limiting their industrial applications [4,24–26]. Statistical thermodynamic methods can be used to quantitatively represent the properties of gas hydrates as they exhibit regular molecular structures (**Fig. 4-1**). Consequently, assuming the similarity between hydrate formation and Langmuir adsorption, van der Waals and Platteeuw (vdW-P) derived the

fundamental statistical thermodynamic equations for gas hydrates [27,28]. In addition, McKoy and Sinanoglu investigated the spherical approximations of various pairwise potential functions in the vdW-P hydrate model [29]. However, they stated that the Kihara potential was optimal for rod-like molecules because it considers the shapes of different molecules [29]. As a result, the Kihara potential model is widely used in vdW-P models for determining the Langmuir constants [25].

Compared with contemporary empirical methods, the thermodynamic models not only provide more precise calculations of hydrate equilibria but also aid in determining the gas adsorption in various types of cavities and the gas–water molar ratio in the hydrate phase [4,25]. Thus, researchers and engineers prefer the thermodynamic models, particularly the vdW-P hydrate model, to describe the multiphase equilibria of gas hydrate systems [25]. In addition, these models have been employed in commercial simulators, such as CSMGem developed by the Colorado School of Mines [30–33] and HWHYD developed by the Heriot-Watt University [34–36]. However, the vdW-P hydrate model has several limitations [25,37]. The functional forms of the vdW-P hydrate model, particularly the integral equations for calculating the Langmuir constants, are quite complex [5,38]. To reduce computational costs, several linear equations have been proposed to replace the integral equations for determining the Langmuir constants without affecting the accuracy [5,38–40]. Furthermore, the vdW-P model may occasionally exhibit non-convergence in calculations for hydrate equilibria [41–43]. However, contemporary research on hydrate-equilibrium calculations emphasizes accuracy over robustness [41–45]. Moreover, the vdW-P hydrate model produces large calculation errors for gas-hydrate equilibria at low as well as high temperatures. For instance, the calculation errors associated with reproducing the liquid-water/hydrate/liquid-CO_2 equilibria and ice/hydrate/vapor-CO_2 equilibria at

high and low temperatures, respectively, have always been >10% [43,46–59]. Finally, the hydrate equilibria of gas-mixture systems predicted by the vdW-P model are not as accurate as those predicted for pure-gas systems [41,50,51]. As illustrated in **Fig. 4-2**, the average absolute percentage deviations (%AADs) for reproducing the hydrate equilibria obtained using the vdW-P model increase with increasing number of constituting gas components [42].

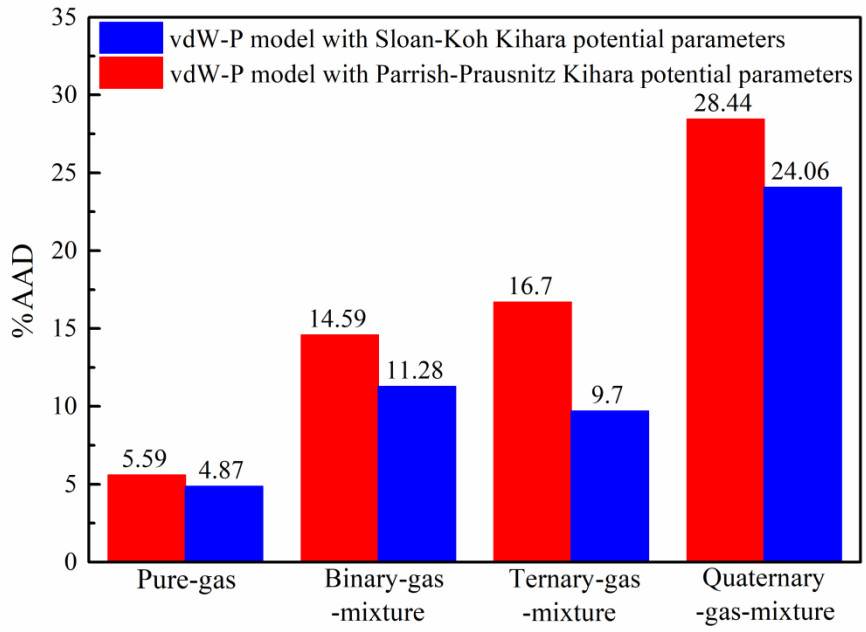

Fig. 4-2. Calculation errors (%AADs) in predicting hydrate equilibria for pure-gas and gas-mixture hydrates obtained using the vdW-P hydrate model with the Kihara potential parameters proposed by Sloan and Koh (2008) [4] and Parrish and Prausnitz (1972) [5]. The calculation errors were obtained from Meragawi et al. (2016) [42].

In practice, the Kihara potential parameters are critical to the performance of the vdW-P hydrate model [4,25]. As a result, the current study aims to develop a novel procedure for optimizing the Kihara potential parameters for enhancing the robustness and accuracy of the vdW-P model. To ensure the credibility of the optimization results, a large database comprising hydrate equilibrium values for common hydrate-forming gases (CH_4, C_2H_6, C_3H_8, iC_4H_{10}, CO_2, and N_2) was compiled. The database contained 1617 experimental data points for pure-gas hydrate equilibria derived from 126

publications and 1518 experimental data points for binary-gas-mixture hydrate equilibria derived from 75 publications. Subsequently, the hydrate structures, I and II, were considered for developing a novel fitting procedure for Kihara potential parameters in the vdW-P hydrate model using experimental data on the hydrate equilibrium for both pure gases and binary-gas mixtures. The ability of the vdW-P model to reproduce the hydrate equilibrium data for pure gases, binary-gas mixtures, and complex-gas mixtures was evaluated using the newly fitted Kihara potential parameters. In addition to the hydrate equilibrium calculations, the updated vdW-P model was used to predict hydrate structure transitions and cage occupancy behavior.

4.2. Methodology

4.2.1. Van der Waals-Platteeuw Hydrate Model

The classical vdW-P model is defined as [27]:

$$\frac{\mu_W^H - \mu_W^{I/L}}{RT} = \frac{\Delta\mu_W^0}{RT_0} + \int_{P_0}^{P} \frac{\Delta v_W^{\beta-I/L}}{R\overline{T}} dP - \int_{T_0}^{T} \frac{\Delta h_W^{\beta-I/L}}{RT^2} dT + \sum_k \lambda_k \ln\left(1 - \sum_i \theta_{ik}\right) \tag{4-1}$$

where T and P denote temperature and pressure, R denotes the universal gas constant, the superscript 0 refers to the triple point of water, and the superscripts H, β, and I/L refer to the hydrate with filled lattice, the assumed hydrate with empty lattice, and the ice/liquid water, respectively.

Fig. 4-3 depicts the physical meaning of the terms used in the vdW-P hydrate model. In **Eq. 4-1**, μ_W^H and $\mu_W^{I/L}$ are the chemical potentials of water in the hydrate and ice/liquid phases, respectively. When a gas hydrate is formed, the chemical potential of water in the hydrate should be less than the chemical potential of water in the ice/liquid phase (i.e. $\mu_W^H - \mu_W^{I/L} < 0$). However, at equilibrium, the chemical potentials of water in the hydrate and the ice/liquid phases are equal (i.e. $\mu_W^H - \mu_W^{I/L} = 0$). The right hand of

the **Eq. 4-1** can be divided into two groups, wherein the first three terms represent the energy change required to form the empty hydrate lattice, and the final term represents the energy change required to entrap the guest gas molecule in the hydrate lattice. In addition, $\Delta\mu_W^0$ denotes the difference between the chemical potential of water in the empty hydrate lattice and the chemical potential of water in the ice/liquid phase at the triple point, and $\Delta v_W^{\beta-I/L}$ denotes the change in the molar volume of water between the empty lattice and the ice/liquid phase. T_0 and P_0 were set to 273.16 K and 611.2 Pa, respectively, in this study. Moreover, $\overline{T}$ denotes the average temperature between T and T_0, whereas $\Delta h_W^{\beta-I/L}$ represents the difference in molar enthalpy of water between the empty lattice and the ice/liquid phase [5,27]. The value of $\Delta h_W^{\beta-I/L}$ is determined using the following equations:

$$\Delta h_W^{\beta-I/L} = \Delta h_W^0 + \int_{T_0}^{T} \Delta C_p dT \qquad T > T_0 \tag{4-2}$$

$$\Delta h_W^{\beta-I/L} = \Delta h_W^0 \qquad T < T_0 \tag{4-3}$$

where Δh_W^0 denotes the difference in molar enthalpy between pure liquid water (or ice) and the empty hydrate lattice at the triple point, and ΔC_p denotes the difference in heat capacity, which is typically a temperature-dependent function.

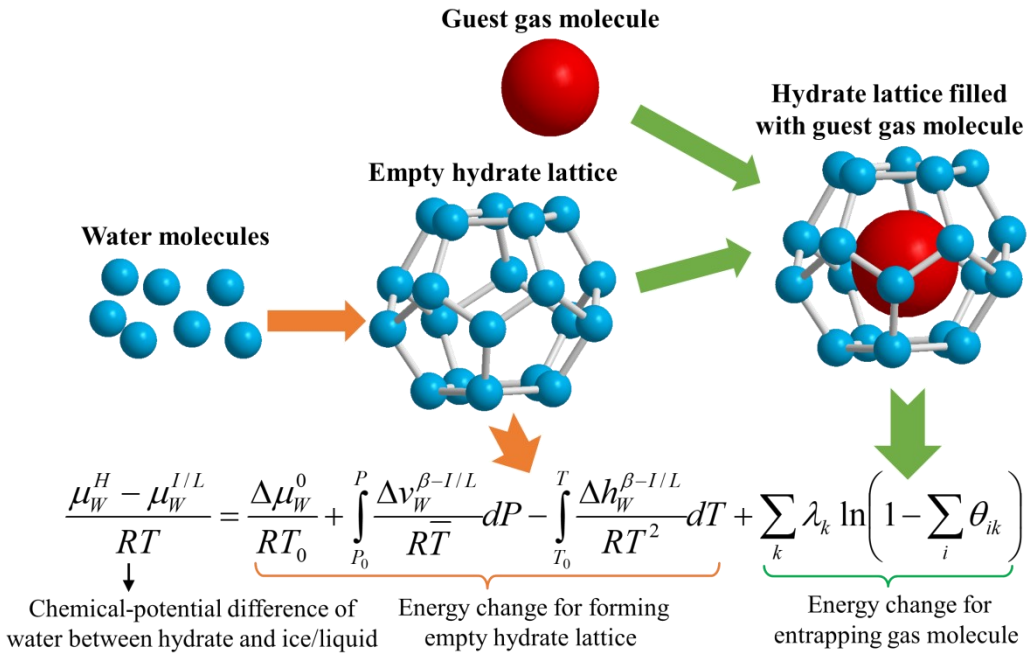

Fig. 4-3. Schematic representation for the physical meaning of the terms used in the vdW-P hydrate model.

In the final term of **Eq. 4-1**, λ_k denotes the number of k cavity per water molecule in the unit cell, that is, λ_k represents the ratio of water molecules over the type k cavity in the hydrate phase. For type I hydrate structures, λ_1=1/23 (small cavity) and λ_2=3/23 (large cavity). For type II hydrate structures, λ_1=2/17 (small cavity) and λ_2=1/17 (large cavity). In addition, θ_{ik} denotes the probability of a cage k being occupied by a guest molecule i and is determined using the following equation [27]:

$$\theta_{ik} = \frac{C_{ik} f_i}{1 + \sum_i C_{ik} f_i} \tag{4-4}$$

where f_i is the fugacity of the hydrate-forming gas i obtained using an equation of state (EOS), and C_{ik} is the Langmuir constant. The Lennard-Jones-Devonshire cell theory was used to calculate the Langmuir constant using the following equation [5,27,29]:

$$C_{ik} = \frac{4\pi}{k_B T} \int_0^{R_k - a} \exp\left(-\frac{w_{ik}(r)}{k_B T}\right) r^2 dr \tag{4-5}$$

where k_B denotes the Boltzmann constant, $w_{ik}(r)$ denotes the potential energy for the interaction between the guest molecule and the water molecule from the cavity, and r

is the radial distance of the guest molecule from the cavity center. Assuming a spherical core, the Kihara potential can aid in determining $w_{ik}(r)$ using the following equations [5,27,29]:

$$w_{ik}(r) = 2z\varepsilon\left[\frac{\sigma^{12}}{R_k^{11} r}\left(\delta^{10} + \frac{a}{R_k}\delta^{11}\right) - \frac{\sigma^{6}}{R_k^{5} r}\left(\delta^{4} + \frac{a}{R_k}\delta^{5}\right)\right] \tag{4-6}$$

$$\delta^n = \frac{1}{n}\left[\left(1 - \frac{r}{R_k} - \frac{a}{R_k}\right)^{-n} - \left(1 + \frac{r}{R_k} - \frac{a}{R_k}\right)^{-n}\right] \tag{4-7}$$

where z is the total quantity of water molecules in cavity k, and R_k and a are the radii of the cavity and the hydrate-forming molecule, respectively. The value of n can be 4, 5, 10, or 11. ε, σ, and a represent the Kihara potential parameters that must be tuned for each hydrate-forming gas. There are several other methods or modified functional forms for calculating the Langmuir constant; however, the Lennard-Jones-Devonshire theory coupled with Kihara potential (**Eqs. 4-5~4-7**) is one of most frequently used Langmuir coefficient expressions in academic and industrial applications [25].

4.2.2. Issues Related to the Application and Optimization of Kihara Potential Parameters in VdW-P Models

Numerous sets of Kihara potential parameters have been published previously [4,5,41–43,50–52]. However, certain Kihara potential parameters exhibit non-convergence and showcase significant errors in calculations for gas-mixture-hydrate equilibria [25,41,42]. As a result, the following statements have been hypothesized as the possible underlying causes of these issues:

(1) Insufficient experimental data were used to tune the Kihara potential parameters. One common limitation is that the experimental data do not span a broad temperature and pressure range. For example, if the Kihara potential parameters are

fitted to match the pure CH_4/CO_2 hydrate equilibria using experimental data from multiple research papers, the resulting values may be noticeably different (**Table 4-2**). In addition, the Kihara potential parameters optimized on the basis of a single set of experimental results can lead to substantial errors in reproducing the other sets of experimental data.

Table 4-2. Optimized Kihara potential parameters in the vdW-P hydrate model based on different sets of experimental data and their calculation errors (%AADs) in the reproduced hydrate equilibria.[a]

Guest gas	References	*T* range (K)	*P* rang (MPa)	Data number	*a* (Å)[b]	*σ* (Å)	*ε*/kB (K)	%AAD[c]	%AAD[d]
CH_4	Deaton and Frost (1946) [53]	273.7-285.9	2.77-9.78	13	0.3834	3.2501	156.2555	0.51	11.95
	Marshall et al. (1964) [54]	290.2-320.1	15.9-397	20		3.3097	157.6901	3.41	7.4
CO_2	Deaton and Frost (1946) [53]	273.7-282.9	1.324-4.323	19	0.6805	3.0592	170.3010	0.5	3.55
	Takenouchi and Kennedy (1965) [55]	283.2-292.7	4.5-186.2	15		3.0346	170.9588	4.29	29.6

[a] The optimization method for Kihara potential parameters and the calculation method of %AAD are presented in the subsequent text. The thermodynamic parameters used in the vdW-P hydrate model are listed in **Table 4-6**.
[b] This study directly takes the values of *a* from Sloan and Koh [4] and only optimizes *ε* and *σ*.
[c] The %AADs are yielded by the vdW-P hydrate model with the Kihara potential parameters optimized based on the same set of experimental data.
[b] The %AADs are yielded by the vdW-P hydrate model with the Kihara potential parameters optimized based on the other set of experimental data.

(2) The Kihara potential parameters do not match the EOS used to calculate the fugacity of the hydrate-forming gas and/or other thermodynamic parameters (such as $\Delta\mu_W^0$, $\Delta h_W^{\beta-I/L}$ and $\Delta v_W^{\beta-I/L}$) used in the vdW-P hydrate model [29,56–60]. When the Kihara potential parameters are coupled with different EOSs (such as PC-SAFT and PR EOSs), the calculated results may vary significantly [42, 59]. In addition, the optimization of $\Delta\mu_W^0$ and $\Delta v_W^{\beta-I/L}$ may contribute towards improving the hydrate equilibrium calculations [56–58]. Different combinations of $\Delta\mu_W^0$ and Δh_W^0 may also affect the optimized values of Kihara potential parameters, as illustrated in **Table 4-3**.

Table 4-3. Optimized Kihara potential parameters in vdW-P hydrate model based on different thermodynamic parameters and their calculation errors (%AADs) in reproducing hydrate equilibria.[a]

Guest gas	Experimental data source	$\Delta\mu_W^0$ (J/mol)[b]	Δh_W^0 (J/mol)[b]	Thermodynamic parameters sources	*a* (Å)[c]	*σ* (Å)	*ε*/*kB* (K)	%AAD[d]	%AAD[e]

CH_4	Deaton and Frost (1946) [53]	1297	-4620.5	Dharmawardhana et al. (1980) [60]	0.3834	3.2501	156.2555	0.51	2.81
		1287	-5080	Handa and Tse (1986) [61]		3.1231	159.8664	0.5	2.68

[a] The optimization method for Kihara potential parameters and the calculation method of %AAD are presented in the subsequent text. The other thermodynamic parameters used in the vdW-P hydrate model are listed in **Table 4-6**.
[b] These thermodynamic parameters are feasible for the structure I hydrate at the ice point.
[c] This study directly takes the values of a from Sloan and Koh [4] and only optimizes ε and σ.
[d] The %AADs are yielded by the vdW-P hydrate model with the Kihara potential parameters optimized based on the same thermodynamic parameters.
[e] The %AADs are yielded by the vdW-P hydrate model with the Kihara potential parameters optimized based on the other thermodynamic parameters.

(3) The Kihara potential parameters were optimized solely on the basis of pure-gas-hydrate equilibrium data, ignoring their ability to reproduce gas-mixture-hydrate equilibria and structure transitions. The crystal structures of several common pure-gas hydrates and binary-gas-mixture hydrates are listed in **Table 4-4** [4,51,62–64]. As observed, pure gases such as CH_4, C_2H_6, and CO_2 form the structure I hydrate, whereas C_3H_8, iC_4H_{10}, and N_2 form the structure II hydrate. In addition, binary-gas mixtures of CH_4-C_2H_6, C_2H_6-C_3H_8, CO_2-C_3H_8, CO_2-iC_4H_{10}, and CO_2-N_2 may form both structure I and II hydrates. Furthermore, the hydrate structure transitions are influenced by several factors including temperature, pressure, and gas composition.

Table 4-4. Crystal structures of common pure-gas hydrates and binary-gas-mixture hydrates [4,51,62–64].

Guest gas	CH_4	C_2H_6	C_3H_8	iC_4H_{10}	CO_2	N_2
CH_4	I	I, II	II	II	I	II
C_2H_6	I, II	I	I, II	N/A	I	N/A
C_3H_8	II	I, II	II	II	I, II	II
iC_4H_{10}	II	N/A	II	II	I, II	N/A
CO_2	I	I	I, II	I, II	I	I, II
N_2	II	N/A	II	N/A	I, II	II

* There are structure transitions for CH_4-C_3H_8 and CH_4-iC_4H_{10} hydrates only when the molar fraction of CH_4 is higher than 0.99 [62]; thus, we can consider that the gas mixtures of CH_4-C_3H_8 and CH_4-iC_4H_{10} only form structure II hydrates.
** The structure of CH_4-N_2 hydrate is controversial [63,64], and this study assumes that the gas mixture CH_4-N_2 only forms a structure II hydrate.

(4) Both structure I and II hydrates are composed of two types of cavities (polyhedra). These include small cavities (5^{12}) and large cavities ($5^{12}6^2$ for structure I and $5^{12}6^4$ for structure II). It is worth noting that while some guest gases can be trapped in both cavities, others can only be entrapped in the large cavities of a given hydrate structure, as illustrated in **Table 4-5**. The Langmuir constants of guest gases that

cannot enter certain cavities should be set as zero in the vdW-P hydrate model. However, several controversies about the cage occupancy have been reported. For example, several researchers have stated that the CO_2 molecule enters the small cages of structure I hydrates with significant constraints [64–66]. However, our preliminary tests indicate that trapping CO_2 in both small and large cages of structure I hydrates results in more reliable hydrate equilibrium calculations, which is also a widely recognized attribute in the application of the vdW-P hydrate model [4,5,25]. Moreover, the classical version of the vdW-P model adopted in this study is incapable of accommodating multiple molecules of small guest gases (such as H_2 and He) in a single hydrate cavity [58,67–69].

Table 4-5. Occupancy of guest gases in different cavities of hydrate crystal structures [4,5,70].

Guest gas	Structure I		Structure II	
	5^{12}	$5^{12}6^2$	5^{12}	$5^{12}6^4$
CH_4	+	+	+	+
C_2H_6	-	+	-	+
C_3H_8	-	-	-	+
iC_4H_{10}	-	-	-	+
CO_2	+	+	+	+
N_2	+	+	+	+

4.2.3. EOS for Fugacity Calculations

The current study employs the translated-consistent version of the Peng-Robinson (tc-PR) EOS recently updated by Pina-Martinez et al. to determine the fugacity of guest gases in the vdW-P hydrate model (**Eq. 4-4**) [71,72]. The improved EOS, when coupled with the consistent α-function, is capable of providing reliable calculations of various thermodynamic properties and is regarded as one of the most accurate EOSs over a wide temperature and pressure range [73]. The tc-PR EOS is represented using the following equation [71]:

$$P = \frac{RT}{v-b} - \frac{a}{(v+c)(v+b+2c)+(b+c)(v-b)} \tag{4-8}$$

where v is the molar volume in the PR EOS, c is the compound-dependent volume correction that accurately reproduces the experimental saturated liquid volume at a reduced temperature of 0.8, and a and b are the PR EOS parameters representing the attractive force and repulsive force between the molecules, respectively. In addition, the parameter a in the PR EOS is different from the Kihara potential parameter a in the vdW-P hydrate model (**Eqs. 4-5~4-7**). Consequently, the values of a and b in the PR EOS can be expressed using the following equations [71,72]:

$$a = 0.457535\frac{R^2T_c^2}{P_c}\alpha(T) \tag{4-9}$$

$$b = 0.077796\frac{RT_c}{P_c} - c \tag{4-10}$$

where T_c and P_c are the critical temperature and critical pressure, respectively; $\alpha(T)$ is the so-called α-function. The tc-PR EOS [71] adopts an α-function proposed by Twu [73,74]:

$$\alpha(T) = T_r^{N(M-1)}\exp[L(1-T_r^{MN})] \tag{4-11}$$

where T_r is the reduced temperature (i.e., $T_r = \frac{T}{T_c}$), and L, M, and N are compound-dependent parameters. The fugacity of the pure gas can be further calculated using tc-PR EOS based on the following equation [75,76]:

$$f = P\exp\left(Z - 1 - \ln(Z-B) - \frac{A}{2\sqrt{2}B}\ln\left[\frac{Z+(1+\sqrt{2})B}{Z+(1-\sqrt{2})B}\right] - \frac{cP}{RT}\right) \tag{4-12}$$

where $A = \frac{aP}{R^2T^2}$ and $B = \frac{(b+c)P}{RT}$, and Z is the compressibility factor calculated using the following equation [75,76]:

$$Z^3 - (1-B)Z^2 + (A - 3B^2 - 2B)Z - (AB - B^2 - B^3) = 0 \tag{4-13}$$

For mixtures, the fugacity of each compound is calculated using the following equation [75, 76]:

$$f_i = y_i P \exp\left(\frac{B_i}{B}(Z-1) - \ln(Z-B) + \frac{A}{2\sqrt{2}B}\left(\frac{B_i}{B} - \frac{2}{A}\sum_{j=1}^{N} y_i A_{ij} \right) \ln\left[\frac{Z+\left(1+\sqrt{2}\right)B}{Z+\left(1-\sqrt{2}\right)B} \right] - \frac{c_i P}{RT} \right)$$

(4-14)

where the subscript i denotes the pure compound i in the mixture and y_i is the mole fraction of the pure compound i in a given phase (usually vapor phase). The terms A and B are obtained using the following equations [75,76]:

$$A = \sum_{i=1}^{N}\sum_{j=1}^{N} y_i y_j A_{ij} \tag{4-15}$$

$$B = \sum_{i=1}^{N} y_i B_i \tag{4-16}$$

$$A_{ij} = \left(1 - k_{ij}\right)\sqrt{A_i A_j} \tag{4-17}$$

where k_{ij} denotes the empirical "binary interaction parameters (BIP)." The values of k_{ij} were set as a matrix containing zero elements in this study.

4.2.4. New Pragmatic Strategies for Optimizing Kihara Potential Parameters

It is critical to continue improving the robustness and accuracy of the vdW-P hydrate model. In contrast to the previous studies that focused on the modifications of functional forms, the current study aims to provide new pragmatic strategies for tuning the gas-dependent parameters in the vdW-P hydrate model. As a first step, a large database on experimental gas-hydrate equilibrium data was established, which includes 1617 experimental data points for pure-gas-hydrate equilibria retrieved from 126 publications, and 1518 experimental data points for binary-gas-mixture-hydrate equilibria retrieved from 75 publications. Detailed information on the hydrate

equilibrium database is provided in the **Supplementary Material**. The large database spans a broader temperature and pressure range, thereby mitigating the effects of experimental uncertainties on tuning the Kihara potential parameters [4,25].

The values of $\Delta\mu_W^0$ and Δh_W^0 were derived from Dharmawardhana et al. [60] because of their extensive use and accuracy, and were used to determine the energy change for forming an empty hydrate lattice in the vdW-P model [50,61,77–79]. In addition, the values of $\Delta v_W^{\beta-I/L}$ and the equation of ΔC_p were derived from the work of Parrish and Prausnitz [5]:

$$\Delta C_p = -38.13 + 0.141(T - T_0) \tag{4-18}$$

Table 4-6 shows the values of $\Delta\mu_W^0$, Δh_W^0, and $\Delta v_W^{\beta-I/L}$ for the hydrate structures I and II in the vdW-P hydrate model.

Table 4-6. Thermodynamic parameters used in vdW-P hydrate model [60].

Hydrate structure	Temperature range	$\Delta\mu_W^0$ (J/mol)	Δh_W^0 (J/mol)	$\Delta v_W^{\beta-I/L}$ (J/mol)
Structure I	$T>T_0$	1297	-4620.5	4.6
	$T<T_0$		1389	3
Structure II	$T>T_0$	937	-4984.5	5
	$T<T_0$		1025	3.4

Previous studies have indicated that the hydrate equilibrium data of both pure-gas systems and gas-mixture systems should be considered for fitting the gas-dependent parameters in the hydrate model [4,5,41,51,70,80]. Although recent studies emphasize on modifying the vdW-P model, there are no specific guidelines for optimizing the hydrate-model parameters [25]. In order to provide a more reliable calculation on hydrate equilibria for both pure-gas and gas-mixture systems, the current study proposes a new fitting procedure for tuning the Kihara potential parameters in the vdW-P hydrate model. **Fig. 4-4** illustrates the new fitting procedure using a flowchart. The procedure consists of the following steps:

Step 1: The hydrate equilibrium data that were used for optimizing Kihara potential parameters (ε, σ, and a) were entered as the primary input. These data can be classified into four categories: pure-gas hydrates with structure I (**P-SI**, including pure CH_4, C_2H_6 and CO_2), pure-gas hydrates with structure II (**P-SII**, including pure C_3H_8, iC_4H_{10} and N_2), binary-gas-mixture hydrates with structure I (**M-SI**, including partial data of CH_4-C_2H_6, C_2H_6-C_3H_8, CO_2-C_3H_8, CO_2-iC_4H_{10} and CO_2-N_2 systems), and binary-gas-mixture hydrates with structure II (**M-SII**, including partial data of CH_4-C_2H_6, C_2H_6-C_3H_8, CO_2-C_3H_8, CO_2-iC_4H_{10}, and CO_2-N_2 systems and all data of CH_4-C_3H_8 and CH_4-iC_4H_{10} and CH_4-N_2 systems).

Step 2: The original Kihara potential parameters for CH_4, C_2H_6, and CO_2, based on the pure-gas-hydrate equilibrium data corresponding to structure I (**P-SI**), were subjected to fitting to obtain $K^0_{\mathrm{CH_4}}$, $K^0_{\mathrm{C_2H_6}}$, and $K^0_{\mathrm{CO_4}}$. In addition, the original Kihara potential parameters for C_3H_8, iC_4H_{10}, and N_2 were fitted based on the pure-gas hydrate equilibrium data corresponding to structure II (**P-SII**) to obtain $K^0_{\mathrm{C_3H_8}}$, $K^0_{\mathrm{iC_4H_{10}}}$, and $K^0_{\mathrm{N_2}}$. The objective of the optimization is to minimize the summation of absolute deviations in reproducing the hydrate equilibrium pressures at the given temperatures. The objective function (OF) is given by the following equation:

$$OF = \min\left(\sum_{i=1}^{n}\left|\frac{P - P^{EXP}}{P^{EXP}}\right|_i\right) \tag{4-19}$$

where P^{EXP} is the experimental hydrate equilibrium pressure at a given temperature, P is the hydrate equilibrium pressure calculated by the vdW-P

model, and n is the number of data points used. In addition, the iterative reweighted least-squares algorithm was used as the optimization method.

Step 3: The Kihara potential parameters for CH_4, C_2H_6, and CO_2 were refitted, based on the pure-gas hydrate equilibrium data corresponding to structure I (**P-SI**) and the binary-gas-mixture hydrate equilibrium data corresponding to structure II (**M-SII**), to obtain $K^1_{CH_4}$, $K^1_{C_2H_6}$, and $K^1_{CO_4}$. The original Kihara potential parameters obtained from **Step 2** were used to presume the initial refitting of the Kihara potential parameters. For instance, pure CO_2 can only form a structure I hydrate. However, its binaries with C_3H_8, iC_4H_{10}, and N_2 may form structure II hydrates [4,51]. Hence, the hydrate equilibrium data of pure CO_2 with structure I (**P-SI**) and those of CO_2-C_3H_8, CO_2-iC_4H_{10}, and CO_2-N_2 systems with structure II (**M-SII**) were used to update the Kihara potential parameters for CO_2 ($K^1_{CO_4}$). To calculate the hydrate equilibria of the CO_2-C_3H_8, CO_2-iC_4H_{10}, and CO_2-N_2 systems, the Kihara potential parameters of C_3H_8, iC_4H_{10}, and N_2 are required in addition to those of CO_2. Hence, the original Kihara potential parameters of C_3H_8, iC_4H_{10}, and N_2 obtained from **Step 2** ($K^0_{C_3H_8}$, $K^0_{iC_4H_{10}}$ and $K^0_{N_2}$) were adopted to reproduce the equilibrium data of CO_2-C_3H_8, CO_2-iC_4H_{10}, and CO_2-N_2 binary-gas-mixture hydrates.

Concurrently, the Kihara potential parameters for C_3H_8, iC_4H_{10}, and N_2 were refitted, based on the pure-gas hydrate equilibrium data corresponding to structure II (**P-SII**) and the binary-gas-mixture hydrate equilibrium data corresponding to structure I (**M-SI**), to obtain $K^1_{C_3H_8}$, $K^1_{iC_4H_{10}}$, and $K^1_{N_2}$. For instance, the Kihara potential parameters of C_3H_8 ($K^1_{C_3H_8}$) were updated by reproducing the hydrate equilibrium data of pure C_3H_8 with structure II (**P-SII**)

and those of CO_2-C_3H_8 and C_2H_6-C_3H_8 systems with structure I (**M-SI**). Furthermore, the original Kihara potential parameters of CO_2 and C_2H_6 obtained from **Step 2** ($K^0_{C_2H_6}$ and $K^0_{CO_4}$) were adopted to reproduce the equilibrium data of CO_2-C_3H_8 and C_2H_6-C_3H_8 binary-gas-mixture hydrates.

Step 4: The refitted Kihara potential parameters ($K^1_{CH_4}$, $K^1_{C_2H_6}$, $K^1_{CO_4}$, $K^1_{C_3H_8}$, $K^1_{iC_4H_{10}}$, and $K^1_{N_2}$) of each of the hydrate-forming gases were compared with the original ones ($K^0_{CH_4}$, $K^0_{C_2H_6}$, $K^0_{CO_4}$, $K^0_{C_3H_8}$, $K^0_{iC_4H_{10}}$, and $K^0_{N_2}$). If the refitted Kihara potential parameters of each hydrate-forming gas were approximately equal to the original ones (i.e., meeting the tolerance level), the optimized Kihara potential parameters were obtained as the preferred output for all gases. If the refitted Kihara potential parameters were different from the original Kihara potential parameters, the original Kihara potential parameters ($K^0_{CH_4}$, $K^0_{C_2H_6}$, $K^0_{CO_4}$, $K^0_{C_3H_8}$, $K^0_{iC_4H_{10}}$ and $K^0_{N_2}$) were replaced by the refitted ones ($K^1_{CH_4}$, $K^1_{C_2H_6}$, $K^1_{CO_4}$, $K^1_{C_3H_8}$, $K^1_{iC_4H_{10}}$ and $K^1_{N_2}$). Then the **Steps 3** and **4** were repeated until the desired level of tolerance was met. The error tolerance exerted on the Kihara potential parameters was calculated as:

$$\frac{K^1 - K^0}{K^0} < 0.001 \tag{4-20}$$

where K can be ε, σ, or a. The purpose of this step was to ensure that a set of Kihara potential parameters that functioned well for both pure-gas hydrates and binary-gas-mixture hydrates was eventually obtained.

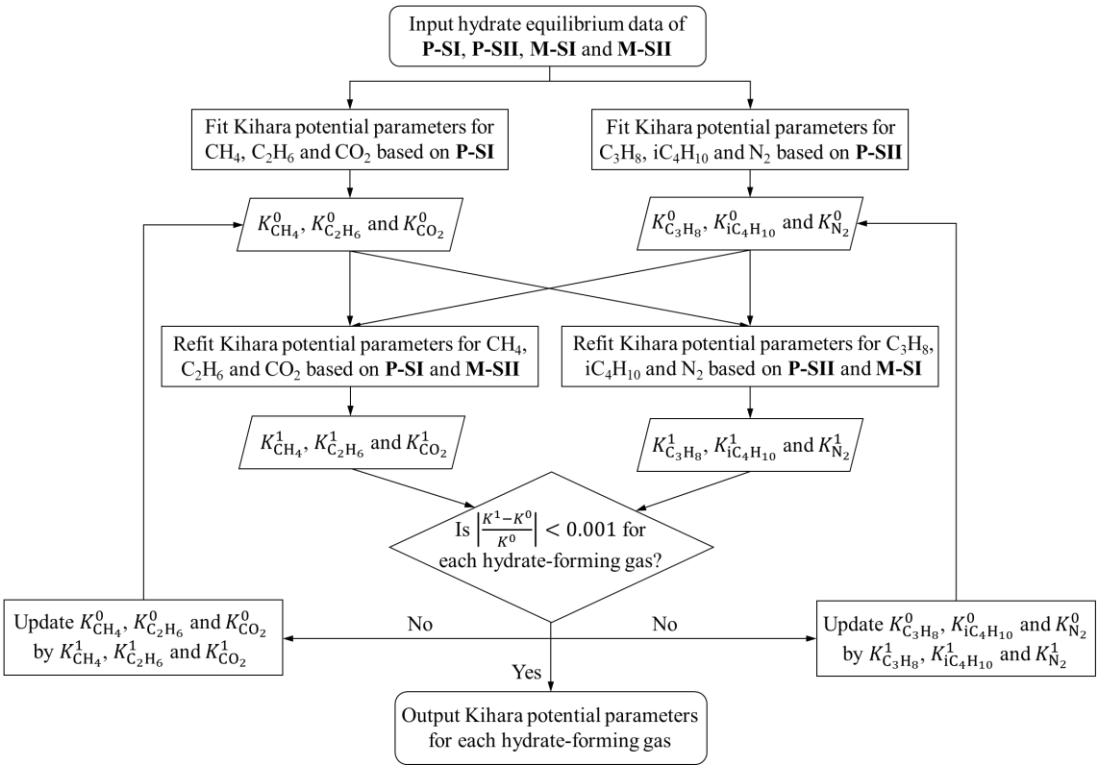

Fig. 4-4. Flowchart of new fitting procedure for optimizing Kihara potential parameters in vdW-P hydrate model with the consideration of both pure-gas and binary-gas-mixture hydrate equilibrium data. (**P-SI**: pure-gas hydrates with structure I; **P-SII**: pure-gas hydrates with structure II; **M-SI**: binary-gas-mixture hydrates with structure I; **M-SII**: binary-gas-mixture hydrates with structure II).

It is noted that several difficulties arise when optimizing the Kihara potential parameters:

- First, the Kihara potential parameters in the vdW-P hydrate model were fitted only for common hydrate-forming gases (CH_4, C_2H_6, C_3H_8, iC_4H_{10}, CO_2 and N_2) with hydrate structures I and II, owing to the abundant experimental data available. As a result, the Kihara potential parameters optimized in the current study may be incompatible with those of other gases (such as iC_5H_{12} and O_2) and may not be applicable to other hydrate structures (such as structure H).
- Additionally, the Kihara potential parameters were fitted using the free water assumption since the majority of available experiments on hydrate equilibria were conducted under free-water conditions where the amount of feed water was much

more than that of the feed gases. As a result, the mutual solubility and the binary interaction between water and gas were neglected.

- Moreover, the Kihara potential parameter a in the vdW-P hydrate model, indicative of the molecular radius of the hydrate-forming gas, may be deemed as a pseudo experimental value. As a result, the current study takes the values of a directly from Sloan and Koh [4] and only optimizes ε and σ.
- Finally, the vdW-P hydrate model is inefficient at predicting hydrate equilibrium pressures in the liquid C_3H_8/iC_4H_{10}–liquid water–hydrate equilibrium regions. As a result, the hydrate equilibrium data for liquid C_3H_8 and iC_4H_{10} were not used to optimize the Kihara potential parameters [33,43].

4.2.5. Performance Evaluation

To demonstrate the robustness and accuracy of the vdW-P hydrate model with the updated Kihara potential parameters, the absolute percentage deviations (%ADs, determined by **Eq. 4-21**), as well as the average absolute percentage deviations (%AADs, determined by **Eq. 4-22**) in reproducing the hydrate equilibrium pressures were estimated using the following equations:

$$\%AD = 100 \times \left| \frac{P - P^{EXP}}{P^{EXP}} \right| \tag{4-21}$$

$$\%AAD = \frac{100}{n} \sum_{i=1}^{n} \left| \frac{P - P^{EXP}}{P^{EXP}} \right|_i \tag{4-22}$$

where P^{EXP} is the experimental hydrate equilibrium pressure at a given temperature, P is the hydrate equilibrium pressure calculated by the vdW-P model, and n is the number of data points used.

The %AADs resulting from the reproduction of the hydrate equilibria data for pure gases, binary-gas mixtures, and complex-gas mixtures using the vdW-P model with the optimized Kihara potential parameters were estimated. The detailed hydrate equilibrium databases and the results of the calculation are listed in **Tables 4-S1~4-S13** of the **Supplementary Material**. In the previous frameworks that were employed for the calculation of hydrate equilibria, the hydrate structure had to be first assigned [4,5,70,80,81]. With the newly optimized Kihara potential parameters, the vdW-P model is capable of predicting the hydrate structure transition, as demonstrated in **Section 4.3.5**. **Fig. 4-5** shows a flowchart detailing the calculation of the equilibrium pressure of gas-mixture hydrates and how to determine structure transitions using the vdW-P hydrate model with the newly optimized Kihara potential parameters. To initialize the calculations, the initial value of hydrate equilibrium pressure ($P^{initial}$) can be estimated using the following equation:

$$P^{initial} = \sum_{i=1}^{n} y_i P_i^{pure} \tag{4-23}$$

where P_i^{pure} is the hydrate equilibrium pressure of pure gas i obtained by the vdW-P model at a given temperature, and y_i is the mole fraction of pure compound i in the vapor phase.

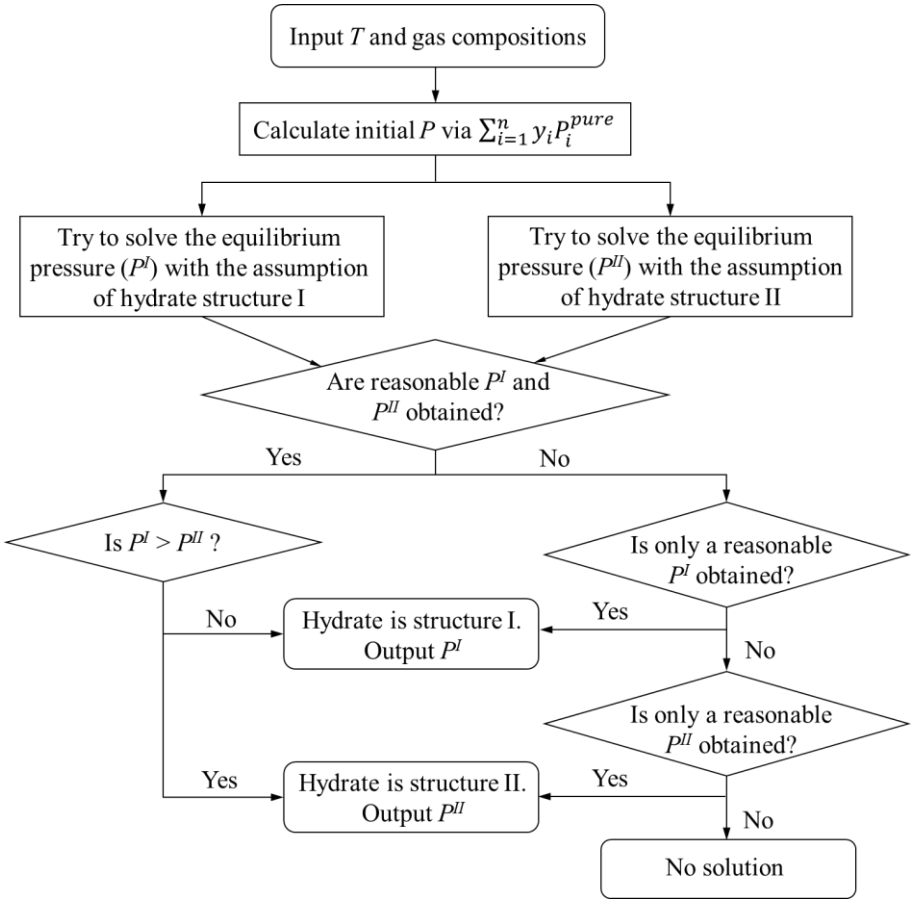

Fig. 4-5. Flowchart illustrating the calculation of the equilibrium pressure of gas-mixture hydrates and the determination of the structure transitions using the vdW-P hydrate model with the newly optimized Kihara potential parameters.

4.3. Results and Discussion

4.3.1. Newly Optimized Kihara Potential Parameters

Based on the gas hydrate equilibrium database and the new fitting procedure developed in this study, the Kihara potential parameters for CH_4, C_2H_6, C_3H_8, iC_4H_{10}, CO_2, and N_2 were optimized using the vdW-P hydrate model. In order to make an objective evaluation, the Kihara potential parameters were also optimized using the conventional method, wherein the equilibrium data of only pure-gas hydrates are considered. **Table 4-7** summarizes the fitted gas-dependent parameters in the vdW-P hydrate model.

Table 4-7 Thermodynamic parameters of hydrate-forming gases [60,82] and Kihara potential parameters in vdW-P hydrate model optimized in this study.

Guest gas	T_0 (K)[a]	T_L (K)[b]	a (Å)	Optimized with the conventional method				Optimized with the new fitting procedure			
				σ (Å) ± 95%CI		ε/k_B (K) ± 95%CI		σ (Å) ± 95%CI		ε/k_B (K) ± 95%CI	
CH_4	272.9	N/A	0.3834	3.2787	±0.0082	156.1904	±0.0012	3.1898	±0.0015	156.7348	±0.0010
C_2H_6	273.1	288	0.5651	3.3479	±0.0098	176.3696	±0.0037	3.3603	±0.0032	177.2618	±0.0026
C_3H_8	273.2	278.5	0.6502	3.7647	±0.0024	228.9913	±0.0005	3.7644	±0.0016	228.8093	±0.0008
iC_4H_{10}	273.2	275.1	0.8706	3.5591	±0.0011	236.8633	±0.0006	3.5599	±0.0012	237.3476	±0.0008
CO_2	271.8	282.8	0.6805	3.0531	±0.0025	170.7687	±0.0007	2.9826	±0.0032	172.1648	±0.0010
N_2	272	N/A	0.3526	2.7023	±0.0012	148.9535	±0.0017	2.9416	±0.0030	133.4185	±0.0007

[a] Quadruple point temperature at the hydrate-ice-liquid water-vapor (H-I-L_w-V) multiphase equilibrium.
[b] Quadruple point temperature at the hydrate-liquid water-vapor-liquid guest gas (H-L_w-V-L_g) multiphase equilibrium.

As evident from **Table 4-7**, although the Kihara potential parameters for C_3H_8 and iC_4H_{10} optimized by the two fitting procedures were observed to be similar, the Kihara potential parameters for CH_4, C_2H_6, CO_2, and N_2 optimized by the newly proposed fitting procedure were noticeably different from those optimized by the conventional method. This indicates that the various fitting procedures and experimental databases (whether or not they include data on gas-mixture-hydrate equilibrium) play an undeniable role in optimizing the gas-dependent parameters, particularly for the relatively light gases. For all the hydrate-forming gases adopted in this study, the 95% confidence intervals (95%CIs) yielded by the two fitting methods are relatively narrow, indicating that reliable optimizations of the Kihara potential parameters were achieved. In addition, to further reduce the computational costs, a linear equation was employed to approximate the Langmuir constants in this study (See **Appendix 4-A**).

4.3.2. Pure-Gas Hydrate Equilibrium Calculations

Fig. 4-6 shows the %AADs between the hydrate equilibrium pressures of pure-gas hydrates calculated by the vdW-P model coupled with the newly optimized Kihara potential parameters against those calculated by the vdW-P model coupled with the conventionally optimized Kihara potential parameters. For the six hydrate-forming

gases employed in this study, the %AADs in reproducing the pure-gas hydrate equilibria yielded by the vdW-P model with the newly fitted Kihara potential parameters were slightly higher than those yielded by the Kihara potential parameters fitted with the conventional method. This is because the new fitting procedure takes into account not only experimental equilibrium data for pure-gas hydrates, but also experimental equilibrium data for binary-gas-mixture hydrates with hydrate structure transitions. The overall %AAD yielded by newly fitted Kihara potential parameters was 6.39%, which is still acceptable for most industrial applications. Furthermore, if only the pure-gas hydrate equilibrium calculations are needed, especially for CH_4, CO_2, and N_2, the Kihara potential parameters optimized by only the pure-gas hydrate data can be directly adopted. In addition, due to the large database employed in this study, the overall calculation errors yielded by the vdW-P model with the newly optimized Kihara potential parameters were higher than those previously reported [4,5,43–46,50–52,83]. Experimental hydrate equilibrium data from various papers were determined using a variety of different methods and apparatuses over a wide range of temperatures and pressures, resulting in a wide range of experimental uncertainties and calculation errors. For example, the %AADs yielded by the vdW-P model with the newly fitted Kihara potential parameters for reproducing CH_4 hydrate equilibria vary from 0.54% to 36.76% (**Table 4-S1**), while those for reproducing C_2H_6 hydrate equilibria vary from 0.65% to 14.91% (**Table 4-S2**).

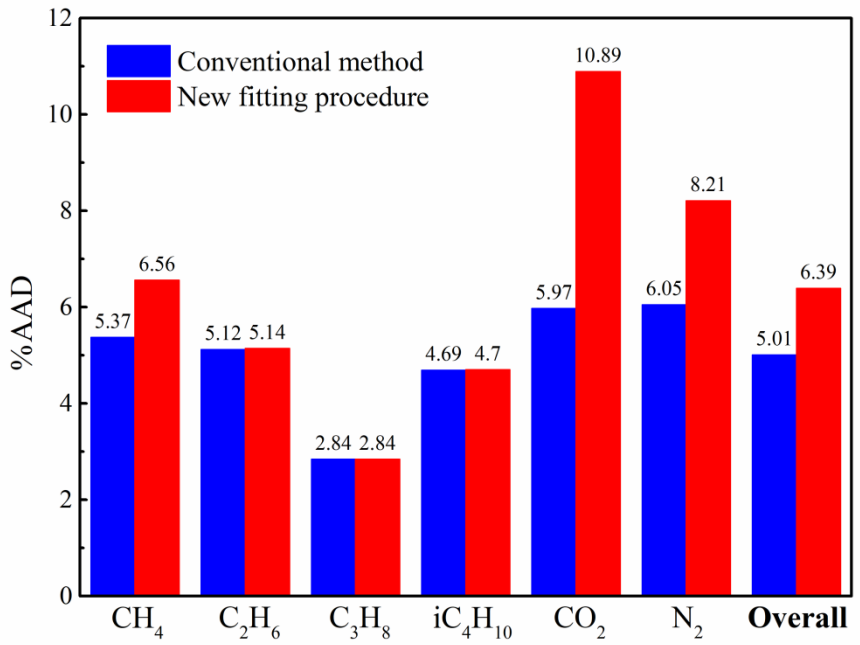

Fig. 4-6. Comparison of the calculation errors for pure-gas hydrate equilibria yielded by the vdW-P model with the Kihara potential parameters optimized by different methods.

Fig. 4-7 visually compares the %ADs yielded by vdW-P model with the newly fitted Kihara potential parameters and the conventionally fitted ones in reproducing the hydrate equilibrium pressure for CH_4 and CO_2. For CH_4 hydrate equilibrium calculations, the Kihara potential parameters optimized by the newly proposed method and those optimized by the conventional method yielded similar %ADs over the studied temperature range. Both of the two sets of Kihara potential parameters yielded low %ADs under relatively low temperatures. However, the two sets of Kihara potential parameters yielded significantly high %ADs over 310 K. This is consistent with the calculation results reported in previous papers [84, 85]. Conversely, the newly fitted Kihara potential parameters yielded higher %ADs in reproducing the CO_2 hydrate equilibrium pressures than the conventionally fitted ones over 284 K and below 272 K (**Fig. 4-7b**), resulting a higher %AAD as shown in **Fig. 4-6** (10.89%). Fortunately, the newly fitted Kihara potential parameters allow for precise calculations of liquid water-

vapor CO_2-hydrate equilibria (272-283 K), which are frequently encountered in petroleum engineering.

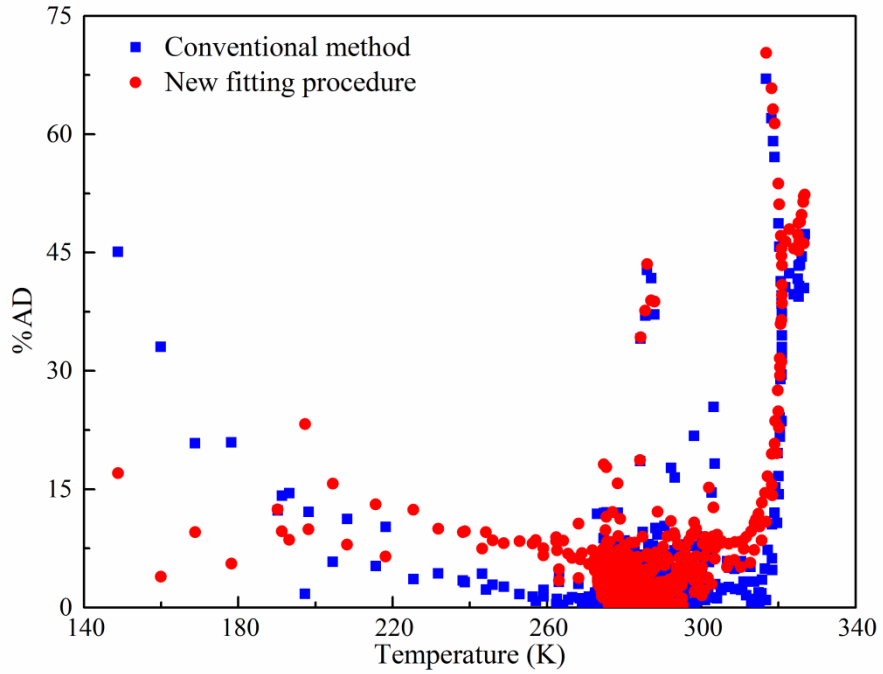

(a)

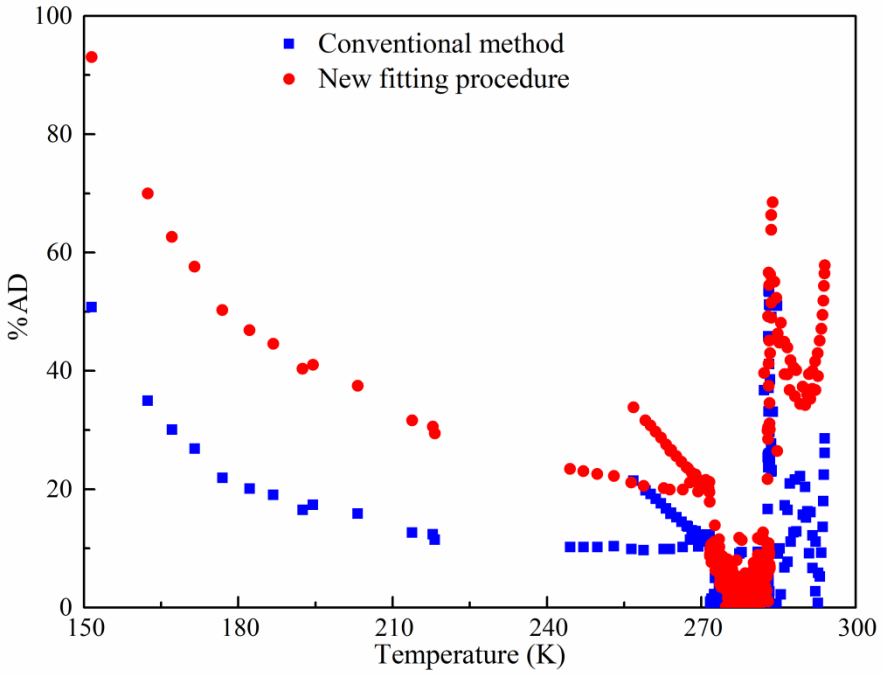

(b)

Fig. 4-7. Comparison of %ADs yielded by the vdW-P model with the Kihara potential parameters optimized by different methods in reproducing the hydrate equilibrium pressure versus temperature for CH_4 (a) and CO_2 (b).

4.3.3. Binary-Gas-Mixture Hydrate Equilibrium Calculations

Fig. 4-8 shows the %AADs between the hydrate equilibrium pressures of binary-gas-mixture hydrates calculated using the vdW-P model coupled with the newly optimized Kihara potential parameters against those calculated using the vdW-P model coupled with the conventionally optimized Kihara potential parameters. For most binary-gas-mixture hydrates, the Kihara potential parameters optimized using the new fitting procedure yielded much lower calculation errors than the conventionally fitted ones. For CH_4-C_3H_8, CH_4-iC_4H_{10}, CO_2-C_3H_8, and CO_2-iC_4H_{10} systems in particular, the %AADs yielded by the vdW-P model with the conventionally fitted Kihara potential parameters were even greater than 80%. It is worth noting that the CH_4-C_2H_6, CH_4-C_3H_8, CH_4-iC_4H_{10}, CO_2-C_3H_8, and CO_2-iC_4H_{10} systems can form both the structure I and II hydrates. Transitions in the hydrate structure can occur as a result of changes in the feed-gas composition. The conventional method optimizes the Kihara potential parameters solely on the basis of pure-gas-hydrate equilibrium data, ignoring structure transitions, resulting in large calculation errors when reproducing gas-mixture-hydrate equilibria. Conversely, the Kihara potential parameters optimized by the new fitting procedure have accounted for the experimental equilibrium data of both the pure-gas and binary-gas-mixture hydrates, leading to better performances in predicting gas-mixture-hydrate equilibria.

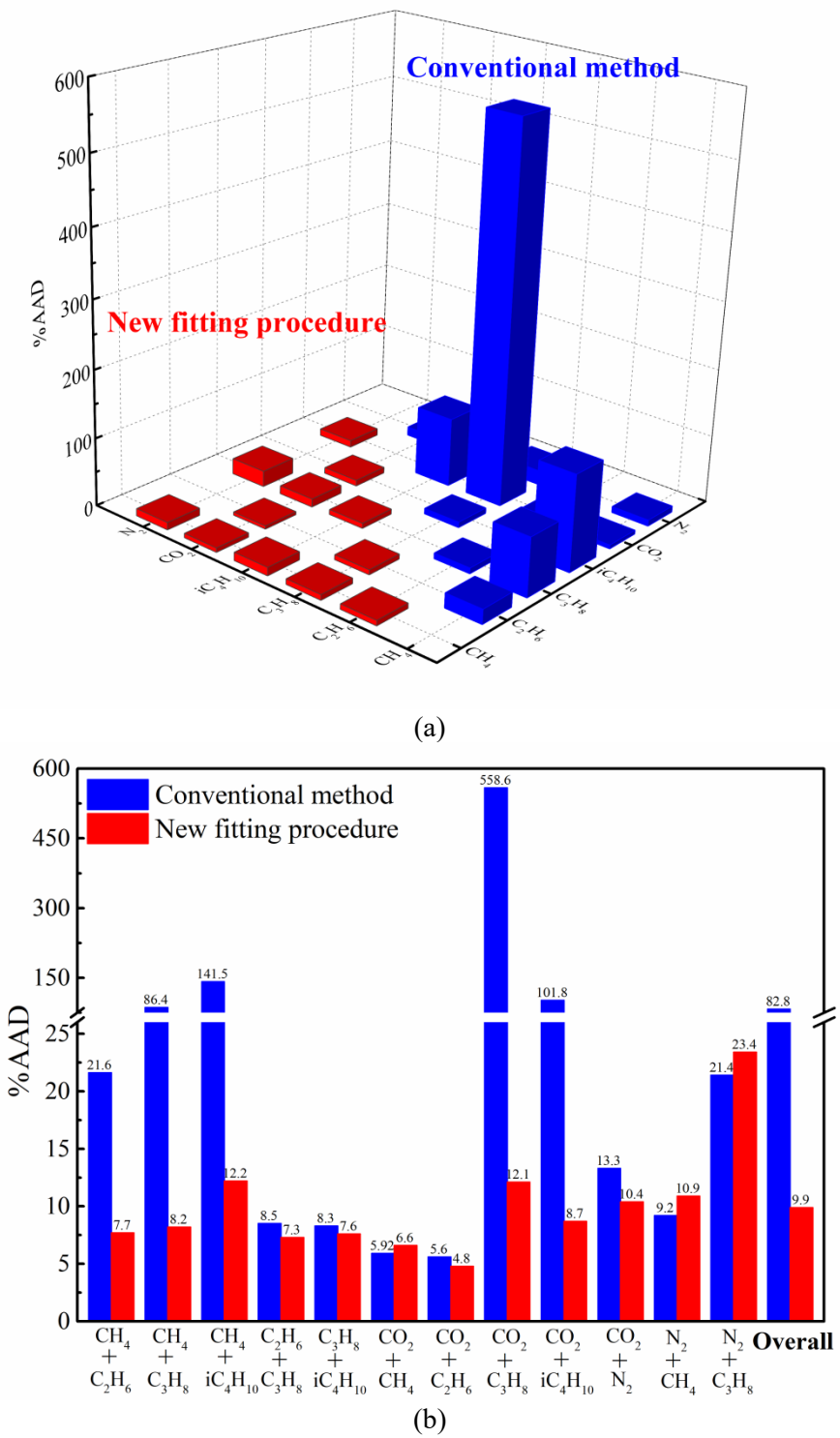

Fig. 4-8. Comparison of the calculation errors for binary-gas-mixture hydrate equilibria yielded by the vdW-P model with the Kihara potential parameters optimized by different methods: (a) 3D diagram; and (b) 2D diagram.

Fig. 4-9 visually compares the %ADs yielded by the vdW-P model with the newly fitted Kihara potential parameters and the conventionally fitted ones in reproducing the hydrate equilibrium pressures under different temperatures and mole fractions for CH_4-

C_2H_6 and CO_2-C_3H_8 binary-gas mixtures. As evident from the figure, under relatively high temperatures, the newly fitted Kihara potential parameters yielded significantly lower %ADs than the conventionally fitted ones for both the CH_4-C_2H_6 and CO_2-C_3H_8 hydrate equilibrium calculations. In addition, the newly fitted Kihara potential parameters perform significantly better than the conventionally fitted ones in the rich-CH_4 region and the rich-CO_2 region for the CH_4-C_2H_6 system (the mole fraction of CH_4 over 0.75) and the CO_2-C_3H_8 system (the mole fraction of CO_2 over 0.95), respectively. The available experimental data suggest that the structure of CH_4-C_2H_6 hydrate changes from SI to SII over the CH_4 vapor composition range of 0.72–0.75, and the structure of CO_2-C_3H_8 hydrate changes from SII to SI over the CO_2 vapor composition range of 0.94–0.99 [86, 87]. Thus, the hydrate structure transitions are the underlying reason for the high calculation errors yielded by the conventionally fitted Kihara potential parameters in reproducing the CH_4-C_2H_6 and CO_2-C_3H_8 hydrate equilibria. These calculation results provide further evidence of the effectiveness of the new pragmatic strategies proposed in the study: (1) the large hydrate equilibrium database used for parameter optimization that ensures the good performance of the vdW-P hydrate model over wide temperature and pressure ranges, and (2) the new fitting procedure accounting for hydrate structure transitions that contributes to more accurate predictions for gas-mixture-hydrate equilibria.

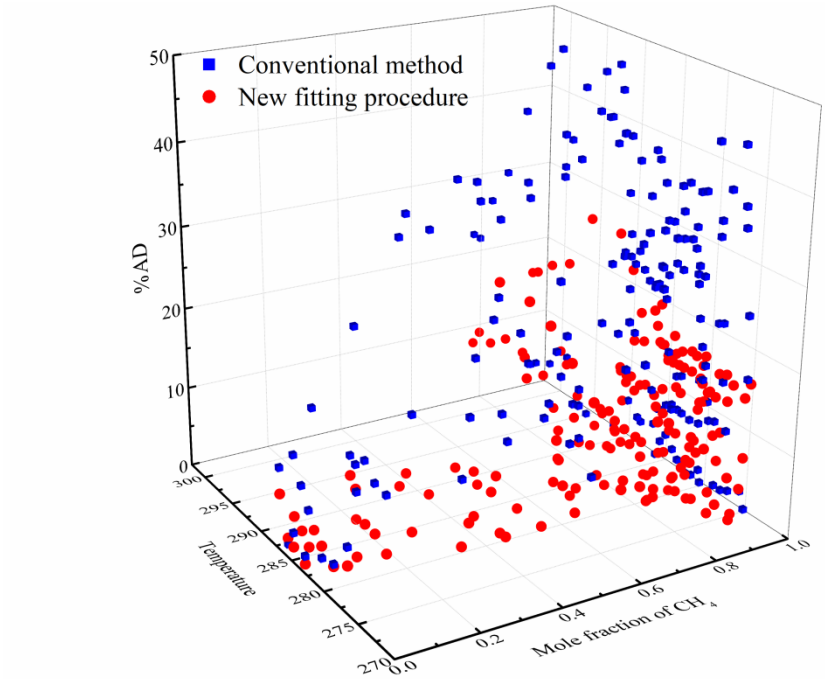

(a)

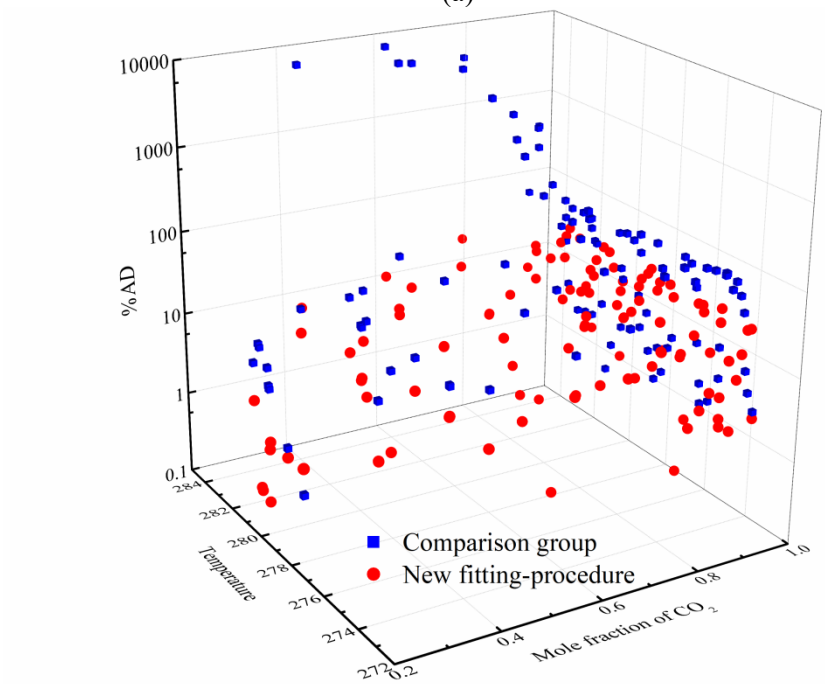

(b)

Fig. 4-9. Comparison of %ADs yielded by the vdW-P model with the Kihara potential parameters optimized by different methods in reproducing the hydrate equilibrium pressures under different temperatures and mole fractions for CH_4-C_2H_6 (a) and CO_2-C_3H_8 (b) binary-gas mixtures.

4.3.4. Complex-Gas-Mixture Hydrate Equilibrium Calculations

The performance of the Kihara potential parameters optimized using the new fitting procedure in reproducing complex-gas-mixture hydrate equilibria was further

compared to the Kihara potential parameters provided by Parrish and Prausnitz [5] and Sloan and Koh [4]. The database and detailed calculation results for complex-gas-mixture hydrate equilibria are listed in **Table 4-S13** of the **Supplementary Material**. In addition, the complex-gas-mixture hydrate equilibrium data were not included in the optimization of the Kihara potential parameters to ensure an objective performance evaluation. The calculation errors resulting from the three sets of Kihara potential parameters are summarized in **Fig. 4-10**. As evident from the figure, the %AADs yielded by the vdW-P model with the newly fitted Kihara potential parameters for reproducing the hydrate equilibria for ternary-, quaternary- and fix/six-membered-gas mixtures were 7.6%, 6.2%, and 11.6%, respectively. These numbers are much lower than those yielded by the Kihara potential parameters provided by Parrish and Prausnitz [5], as well as Sloan and Koh [4]. The findings, therefore, suggest that the Kihara potential parameters have a significant impact on the performances of the vdW-P model. Furthermore, the %AADs yielded by the newly fitted Kihara potential parameters for most gas-mixture systems were lower than 10.0% (**Tables 4-S13**). The overall calculation error was 7.9%, which was close to the calculation errors given by the state-of-art simulators, such as CSMGem (10.0%) [2,35]. However, the advanced vdW-P model employed in CSMGem has a more complicated functional form than the original vdW-P model employed in this study. These calculations, therefore, demonstrate that despite being proposed more than six decades ago, the vdW-P hydrate model, when coupled with appropriate Kihara potential parameters, remains a reliable tool for predicting gas hydrate equilibria.

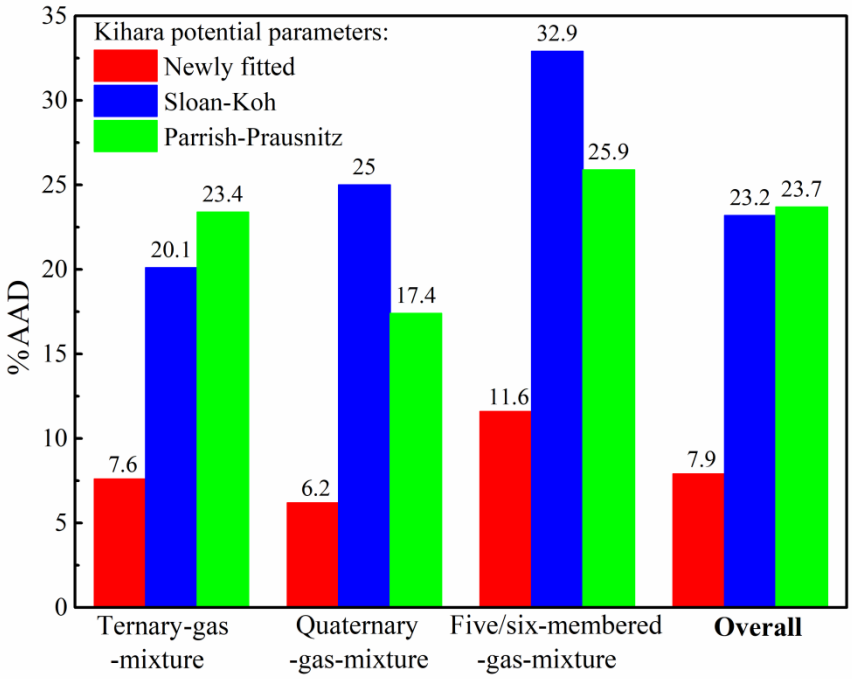

Fig. 4-10. Comparison of the calculation errors for complex-gas-mixture hydrate equilibria yielded by the vdW-P model with the newly fitted Kihara potential parameters against the vdW-P model with the Kihara potential parameters provided by Sloan and Koh [4] and Parrish and Prausnitz [5].

4.3.5. Prediction of Hydrate-Structure Transitions

In addition to performing accurate calculations of gas hydrate equilibria, an effective thermodynamic model should be able to predict the crystal structures of hydrates. As illustrated in **Fig. 4-1** and **Table 4-4**, gas hydrates can exhibit various crystal structures. Furthermore, the crystal structures of hydrates formed by gas-mixture systems may change at varied temperature and pressure conditions. Thus, the vdW-P hydrate model with the newly fitted Kihara potential parameters was examined with regards to its ability to correctly predict the hydrate structure transitions for gas mixtures, including CH_4-C_2H_6, C_2H_6-C_3H_8, CO_2-C_3H_8, CO_2-iC_4H_{10}, and CO_2-N_2 systems. **Fig. 4-11** presents temperature–composition diagrams corresponding to the hydrate structure transition regions, calculated using the vdW-P hydrate model with the newly fitted Kihara potential parameters.

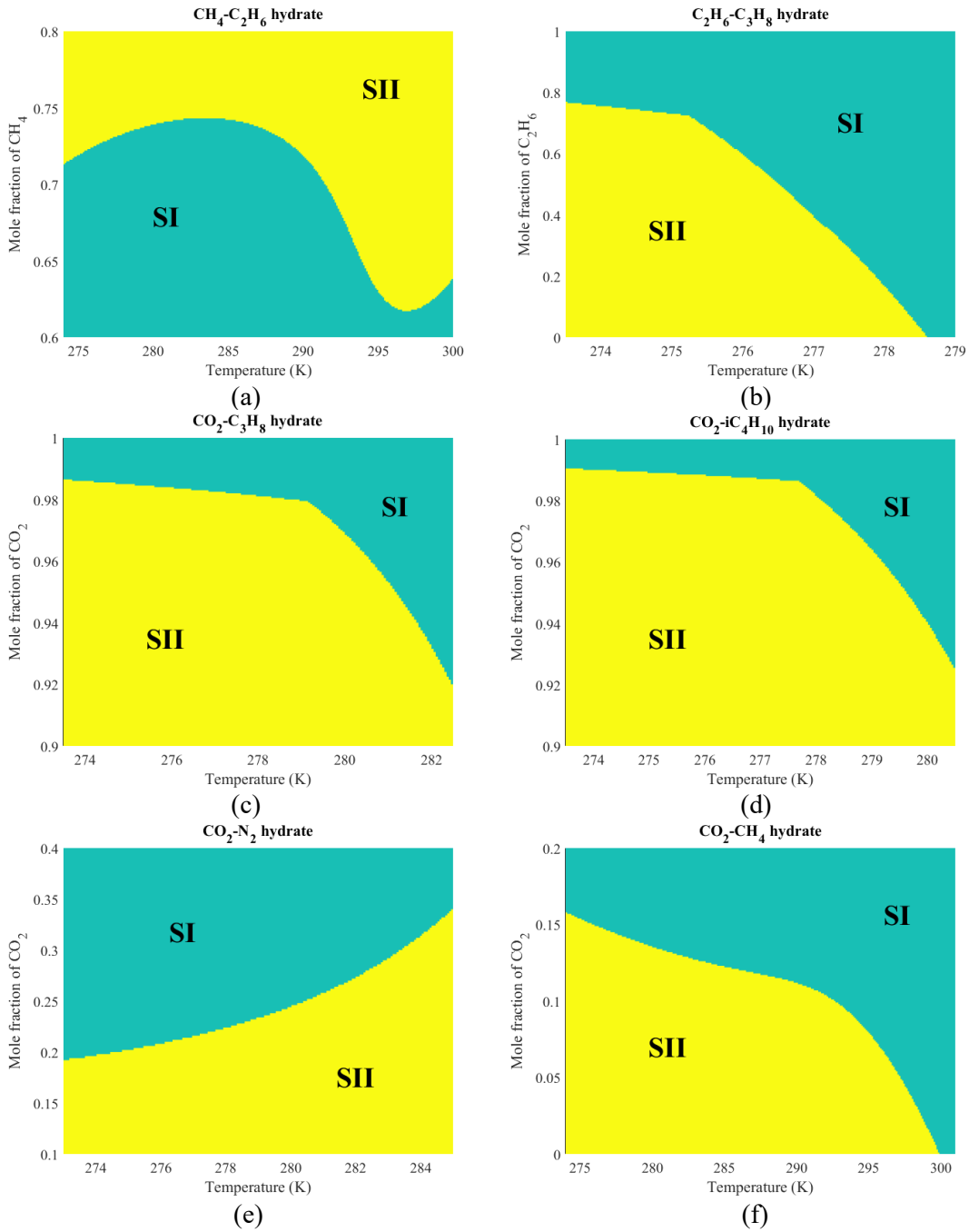

Fig. 4-11. Temperature–composition diagrams corresponding to hydrate structure transition regions at equilibrium conditions for CH_4-C_2H_6 system (a); C_2H_6-C_3H_8 system (b); CO_2-C_3H_8 system (c); CO_2-iC_4H_{10} system (d); CO_2-N_2 system (e); and CH_4-CO_2 system (f).

The temperature–composition diagrams, illustrated in **Fig. 4-11**, were plotted by conducting point-to-point calculations under hydrate equilibrium conditions. As evident from the figure, the dividing lines between hydrate structure I (SI) and structure II (SII) were distinct and smooth, confirming the robustness of the vdW-P hydrate model with the newly optimized Kihara potential parameters. However, under real-

world conditions, the transition between SI and SII hydrates may appear to correspond to a narrow region rather than a dividing line, over which both SI and SII hydrates can co-exist [51, 86-88]. As illustrated in **Fig. 4-11a**, the structure transition line for the CH_4-C_2H_6 system, predicted by the vdW-P hydrate model, fluctuates between 0.62 and 0.74 at 275–300 K over the molar composition range of CH_4. This is consistent with the findings reported by Subramanian et al. in 2000 [86], which reveal that the structure of CH_4-C_2H_6 hydrate changes from SI to SII over the CH_4 vapor composition range of 0.72–0.75 at 274.2 K. In addition, the structure transition lines descended slowly under low temperatures and rapidly under high temperatures for C_2H_6-C_3H_8, CO_2-C_3H_8, and CO_2-iC_4H_{10} hydrates, owing to which the temperature–composition diagrams were strikingly similar. The calculated structure transition behaviors for C_2H_6-C_3H_8, CO_2-C_3H_8, and CO_2-iC_4H_{10} hydrates are generally in line with the available experimental data [87, 88]. For the structure transition line of CO_2-N_2 hydrate, the molar composition of CO_2 increases continuously against temperature. Although there is a lack of experimental observations on the CO_2-N_2 hydrate structure, the previous modeling results suggest that the SI-SII boundary should lie over a CO_2 molar composition range of 0.1–0.2 at relatively low temperatures [89–92]. This finding is also consistent with the results of our calculations.

However, the newly optimized Kihara potential parameters presented in this study may have certain limitations. As illustrated in **Fig. 4-11f**, the CO_2-CH_4 hydrates may exhibit structure II under CH_4-rich conditions. However, previous studies have suggested that the CO_2-CH_4 system can only generate structure I hydrates. Although the structure II yielded by CO_2-CH_4 hydrates does not noticeably affect the calculation accuracy of hydrate equilibrium, such a predicted structure transition issue may be controversial and needs to be further verified experimentally. In addition, the hydrate

structures for the CH_4-C_2H_6, CH_4-C_3H_8, CH_4-iC_4H_{10}, and CH_4-N_2 systems should undergo a transition from SII to SI when the mole fraction of CH_4 is higher (> 0.99) [62]. However, the vdW-P hydrate model with our newly optimized Kihara potential parameters cannot predict such structure transitions.

Using the vdW-P hydrate model in conjunction with the Kihara potential parameters optimized by different methods, we can calculate the hydrate equilibrium pressures of pure CH_4 and CO_2 bearing structures I and II against temperature. **Fig. 4-12** compares the measured hydrate equilibrium pressures [93, 94] for pure CH_4 **(a)** and pure CO_2 **(b)** against those calculated using the vdW-P hydrate model with structures I and II. As evident from the figure, the newly fitted Kihara potential parameters, as well as the conventionally fitted ones, can provide accurate equilibrium calculations for CH_4 and CO_2 hydrates with the preset hydrate structure I. However, with the assumption of structure II, the CH_4 hydrate equilibrium pressures yielded by the newly fitted Kihara potential parameters were slightly lower than those calculated with the assumption of structure I. Consequently, the CH_4 hydrate should be classified as structure II hydrate since the assumption of structure II leads to lower equilibrium pressures. However, this conclusion violates physical reality. Nevertheless, this disadvantage of the newly fitted Kihara potential parameters can be readily circumvented by necessarily considering the pure CH_4 hydrate and CO_2-CH_4 hydrate as structure I hydrates during the equilibrium calculations. Moreover, with the preset hydrate structure II, the conventionally fitted Kihara potential parameters demonstrate extremely high equilibrium pressures for CH_4 and CO_2, leading to inaccurate equilibrium calculations for gas-mixture hydrates with structure II. These calculations further demonstrate the necessity for optimizing hydrate-model parameters while taking into account both pure-gas and gas-mixture

hydrate equilibria, as well as the effectiveness and practicability of the novel fitting procedure proposed in this study.

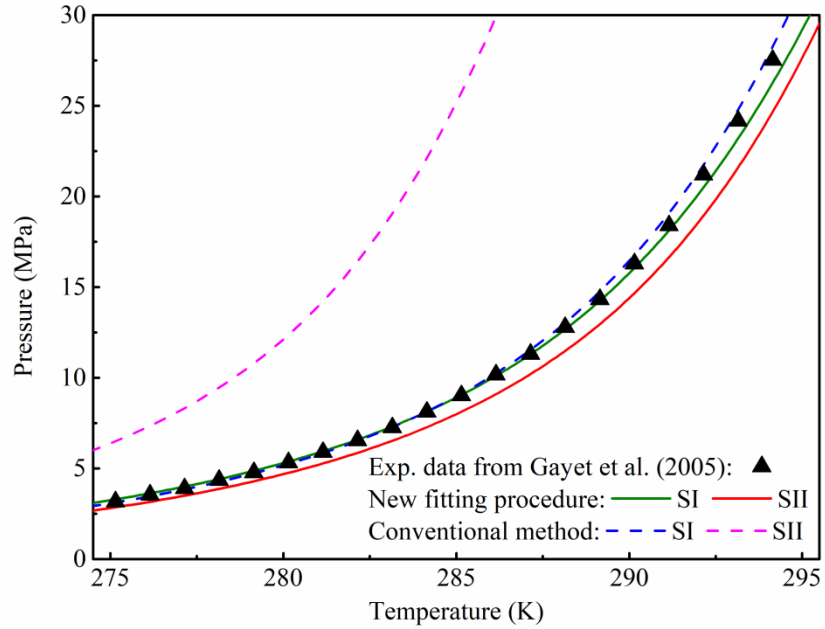

(a)

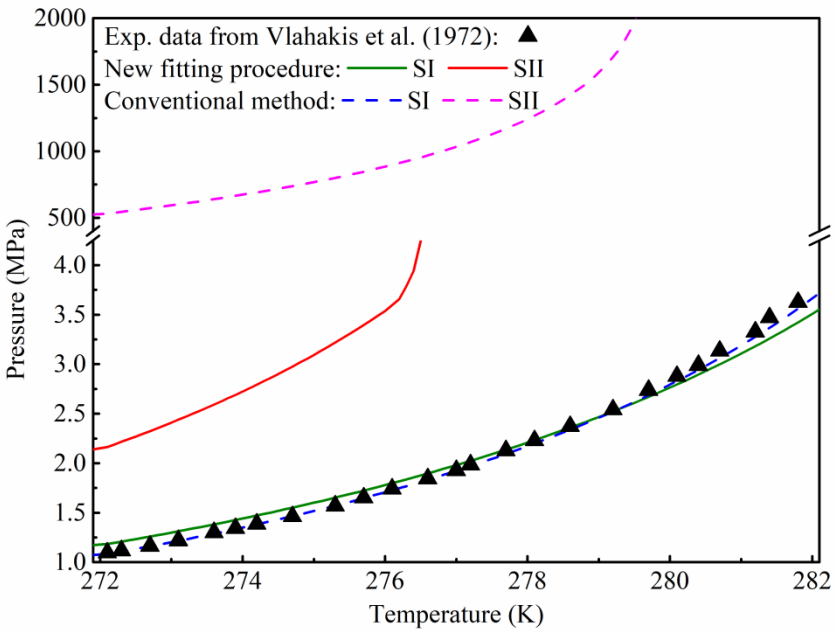

(b)

Fig. 4-12. Comparison of the measured hydrate equilibrium pressures [93,94] for pure CH_4 (a) and pure CO_2 (b) against those calculated with assigned structures I and II yielded by the vdW-P hydrate model with the optimized Kihara potential parameters.

4.3.6. Prediction of Cage Occupancy Behaviors

As illustrated in **Fig. 4-3**, the fundamental unit of a gas hydrate is composed of two components *viz.* the cage, composed of hydrogen-bonded water molecules, and the gas molecule, which is encaged in the cavity. Thus, in addition to determining the changes in hydrate structures, it is critical to determine the occupancy of gas molecules in different cages. Assuming a similarity between Langmuir adsorption and the entrapment of the gas molecules in the hydrate cavities, the vdW-P hydrate model can be used to characterize the probability of gas molecules becoming entrapped in the hydrate cavities. The cage occupancy values for CH_4 and CH_4-C_2H_6 hydrates calculated using the vdW-P hydrate model with the newly fitted Kihara potential parameters are shown in **Fig. 4-13**. As evident from the figure, the calculated occupations of the large and small cages were very close to the experimental data for pure CH_4 hydrates and CH_4-C_2H_6 hydrates. Thus, the vdW-P hydrate model with the newly fitted Kihara potential parameters not only provides accurate calculations of hydrate equilibria but also aids in determining the cage occupancy behaviors.

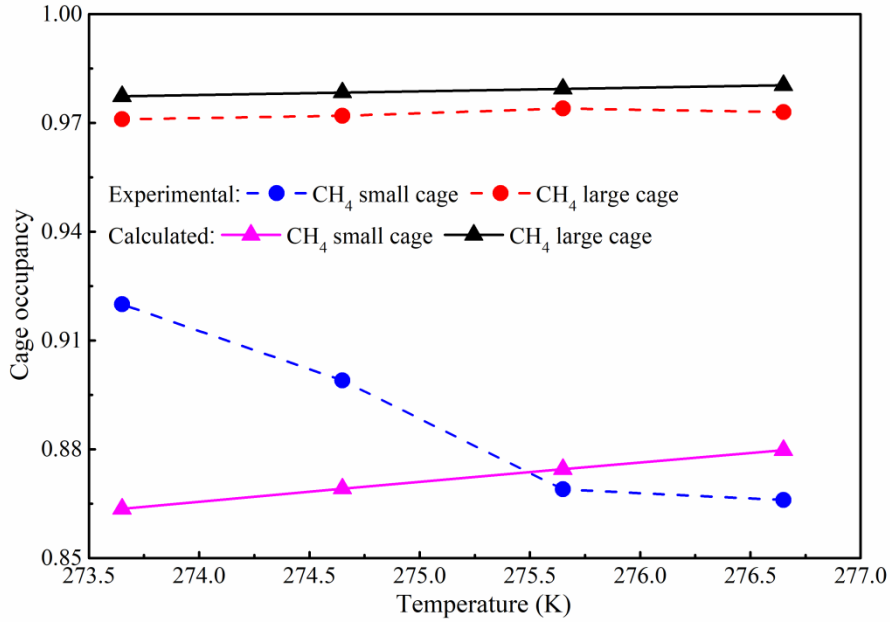

(a)

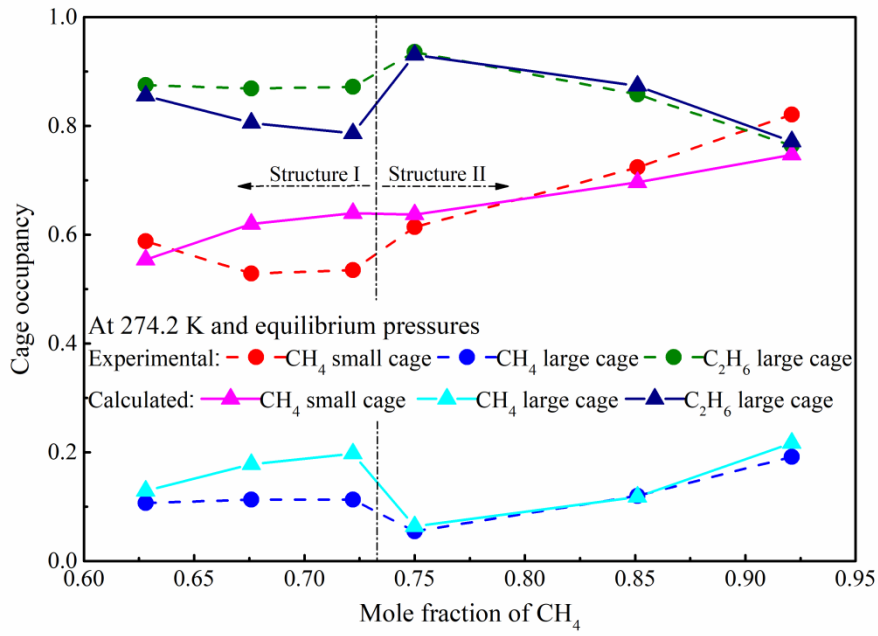

(b)

Fig. 4-13. Comparison of cage occupancy yielded by the vdW-P hydrate model with the newly fitted Kihara potential parameters against the experimental data [65,86] for CH_4 hydrate (a) and CH_4-C_2H_6 hydrate (b).

4.4. Conclusions and Directions for Future Works

With the goal of increasing the prediction accuracy of gas hydrate equilibria, the current study provides new pragmatic strategies for optimizing the Kihara potential parameters used in the vdW-P hydrate model. In contrast to the conventionally

optimized Kihara potential parameters that are based on pure-gas hydrate equilibrium data, a new procedure for fitting Kihara potential parameters in the vdW-P hydrate model was developed, based on the experimental hydrate equilibrium data of both pure gases and binary-gas mixtures. The new fitting procedure accounted for the differences between hydrate structures I and II. In addition, a large database, encompassing more than 3000 hydrate equilibrium data measured over wide temperature and pressure ranges, was compiled for pure hydrate-forming gases (CH_4, C_2H_6, C_3H_8, iC_4H_{10}, CO_2, and N_2) and their binaries, to ensure the reliability of the optimization results. The newly fitted Kihara potential parameters not only performed well in modeling pure-gas hydrates but also predicted binary-gas-mixture hydrate equilibria with relatively greater accuracy than the conventionally fitted ones. Moreover, the overall calculation error resulting from the newly fitted Kihara potential parameters in reproducing the hydrate equilibria of complex-gas mixtures amounted to 7.9%, which was comparable to the calculation error given by the state-of-the-art simulators, such as CSMGem (10.0%) [2,35], and significantly lower than the values yielded by the Kihara potential parameters provided by Parrish and Prausnitz (23.7%) [5], as well as Sloan and Koh (23.2%) [4]. Furthermore, the vdW-P hydrate model coupled with the newly fitted Kihara potential parameters was capable of accurately detecting the hydrate structure transitions and cage occupancy behaviors. However, the current study has primarily focused on optimizing the Kihara potential parameters in the classical vdW-P hydrate model for six gases (i.e., CH_4, C_2H_6, C_3H_8, iC_4H_{10}, CO_2, and N_2) by considering hydrate structures I and II. It is, therefore, critical to expand the database in future studies to include additional hydrate-forming gases (such as O_2, H_2S, and nC_4H_{10}) and upgrade the fitting procedure to include other hydrate structures (such as structure H).

Acknowledgments

The authors greatly acknowledge a Discovery Grant from the Natural Sciences and Engineering Research Council of Canada (NSERC) (Grant No.: NSERC RGPIN-2020-04571) to H. Li. X. Chen greatly acknowledges the financial support provided by the China Scholarship Council (CSC) via a Ph.D. Scholarship (No.: 201806450029).

Appendix 4-A. Simplified Method for Determining Langmuir Constants

Equations 5–7 corresponding to the vdW-P hydrate model have extremely complicated functional forms. To reduce the computational costs, some empirical relations have been proposed to replace these integral equations [5,38–40,70]. To facilitate industrial application, the current study updated the simplified equation proposed by Parrish and Prausnitz [5] to approximate the Langmuir constants (**Table 4-7**). **Table 4-A1** lists the optimized gas-dependent parameters in the simplified equation (**Eq. 4-A1**) and the recommended application temperature ranges.

$$C_{ik} = \left(\frac{AA_{ik}}{T}\right)\exp\left(\frac{BB_{ik}}{T}\right) \tag{4-A1}$$

Table 4-A1. Gas-dependent parameters in **Eq. 4-A1** to approximate the Langmuir constants in vdW-P hydrate model and the recommended application temperature ranges.

Guest gas	*T* range (K)	Structure I				Structure II			
		Small cage		Large cage		Small cage		Large cage	
		$AA\times10^3$ (K/MPa)	*BB* (K)	$AA\times10^3$ (K/MPa)	*BB* (K)	$AA\times10^3$ (K/MPa)	*BB* (K)	$AA\times10^3$ (K/MPa)	*BB* (K)
CH_4	250-300	217.484	2821.561	1807.201	2767.255	213.501	2809.951	5842.726	2411.266
C_2H_6	250-300	-	-	249.762	3957.513	-	-	1178.275	3885.603
C_3H_8	250-278.5	-	-	-	-	-	-	265.894	4938.664
iC_4H_{10}	250-275.1	-	-	-	-	-	-	224.621	5103.562
CO_2	250-290	142.474	2856.372	956.249	3215.154	140.938	2822.378	4431.083	2707.593
N_2	272-300	1284.230	2024.048	4970.319	1731.775	1235.830	2035.657	12492.860	1373.389

References

[1] E.D. Sloan, Fundamental principles and applications of natural gas hydrates, Nature 426 (2003) 353-359, https://doi.org/10.1038/nature02135.

[2] E.D. Sloan, Clathrate hydrates: The other common solid water phase, Ind. Eng. Chem. Res. 39 (2000) 3123-3129, https://doi.org/10.1021/ie000574c.

[3] P. Englezos, Clathrate hydrates, Ind. Eng. Chem. Res. 32 (1993) 1251-1274, https://doi.org/10.1021/ie00019a001.

[4] E.D. Sloan Jr., C.A. Koh, Clathrate Hydrates of Natural Gases, CRC Press/Taylor & Francis, 2008.

[5] W.R. Parrish, J.M. Prausnitz, Dissociation pressures of gas hydrates formed by gas mixtures, Ind. Eng. Chem. Process Des. Dev. 11 (1972) 26-35, https://doi.org/10.1021/i260041a006.

[6] Z.R. Chong, S.H.B. Yang, P. Babu, P. Linga, X.S. Li, Review of natural gas hydrates as an energy resource: Prospects and challenges, Appl. Energ. 162 (2016) 1633-1652, https://doi.org/10.1016/j.apenergy.2014.12.061.

[7] C.A. Koh, A.K. Sum, E.D. Sloan, State of the art: Natural gas hydrates as a natural resource, J. Nat. Gas Sci. Eng. 8 (2012) 132-138, https://doi.org/10.1016/j.jngse.2012.01.005.

[8] C.A. Koh, E.D. Sloan, Natural gas hydrates: Recent advances and challenges in energy and environmental applications, AIChE J. 53 (2007) 1636-1643, https://doi.org/10.1002/aic.11219.

[9] T.S. Collett, Energy resource potential of natural gas hydrates, AAPG Bull. 86 (2002) 1971-1992, https://doi.org/10.1306/61EEDDD2-173E-11D7-8645000102C1865D.

[10] Z. Wang, Y. Zhao, J. Zhang, X. Wang, J. Yu, B. Sun, Quantitatively assessing hydrate-blockage development during deepwater-gas-well testing, SPE J. 23 (2018)1166-1183, https://doi.org/10.2118/181402-PA.

[11] J. Zhang, Z. Wang, B. Sun, X. Sun, Y. Liao, An integrated prediction model of hydrate blockage formation in deep-water gas wells, Int. J. Heat Mass Tran. 140 (2019) 187-202, https://doi.org/10.1016/j.ijheatmasstransfer.2019.05.039.

[12] J. Zhang, Z. Wang, S. Liu, W. Zhang, J. Yi, B. Sun, Prediction of hydrate deposition in pipelines to improve gas transportation efficiency and safety, Appl. Energ. 253 (2019) 113521, https://doi.org/10.1016/j.apenergy.2019.113521.

[13] Y. Sun, S. Jiang, S. Li, X. Wang, S. Peng, Hydrate formation from clay bound water for CO_2 storage, Chem. Eng. J. 406 (2021) 126872, https://doi.org/10.1016/j.cej.2020.126872.

[14] Y. Sun, G. Zhang, S. Li, S. Jiang, CO_2/N_2 injection into $CH_4+C_3H_8$ hydrates for gas recovery and CO_2 sequestration, Chem. Eng. J. 375 (2019) 121973, https://doi.org/10.1016/j.cej.2019.121973.

[15] G.D. Holder, S.P. Zetts, N. Pradhan, Phase behavior in systems containing clathrate hydrates: A review, Rev. Chem. Eng. 5 (1988) 1-70, https://doi.org/10.1515/REVCE.1988.5.1-4.1.

[16] A.K. Sum, C.A. Koh, E.D. Sloan, Clathrate hydrates: From laboratory science to engineering practice, Ind. Eng. Chem. Res. 48 (2009) 7457-7465, https://doi.org/10.1021/ie900679m.

[17] I.S.V. Segtovich, A.G. Barreto Jr., F.W. Tavares, Simultaneous multiphase flash and stability analysis calculations including hydrates, Fluid Phase Equilib. 413 (2016) 196-208, https://doi.org/10.1016/j.fluid.2015.10.030.

[18] I.S.V. Segtovich, A.G. Barreto Jr., F.W. Tavares, Phase diagrams for hydrates beyond incipient condition - Complex behavior in methane/propane and carbon dioxide/iso-butane hydrates, Fluid Phase Equilib. 426 (2016) 75-82, https://doi.org/10.1016/j.fluid.2016.02.002.

[19] A.L. Ballard, E.D. Sloan Jr., The next generation of hydrate prediction: An overview, J. Supramol. Chem. 2 (2002) 385-392, https://doi.org/10.1016/S1472-7862(03)00063-7.

[20] S. Li, J. Wang, X. Lv, K. Ge, Z. Jiang, Y. Li, Experimental measurement and thermodynamic modeling of methane hydrate phase equilibria in the presence of chloride salt, Chem. Eng. J. 395 (2020) 125126, https://doi.org/10.1016/j.cej.2020.125126.

[21] D.L. Katz, Prediction of conditions for hydrate formation in natural gases, Trans. AIME 160 (1945) 140-149, https://doi.org/10.2118/945140-G.

[22] D.B. Carson, D.L. Katz, Natural gas hydrates, Trans. AIME 146 (1942) 150-158, https://doi.org/10.2118/942150-G.

[23] W.I. Wilcox, D.B. Carson, D.L. Katz, Natural gas hydrates, Ind. Eng. Chem. 33 (1941) 662-665, https://doi.org/10.1021/ie50377a027.

[24] N.B. Kummamuru, P. Perreault, S. Lenaerts, A new generalized empirical correlation for predicting methane hydrate equilibrium conditions in pure water, Ind. Eng. Chem. Res. 60 (2021) 3474-3483, https://doi.org/10.1021/acs.iecr.0c05833.

[25] F.A. Medeiros, I.S.V. Segtovich, F.W. Tavares, A.K. Sum, Sixty years of the van der Waals and Platteeuw model for clathrate hydrates-A critical review from its statistical thermodynamic basis to its extensions and applications, Chem. Rev. 120 (2020) 13349-13381, https://doi.org/10.1021/acs.chemrev.0c00494.

[26] A.A. Elgibaly, A.M. Elkamel, A new correlation for predicting hydrate formation conditions for various gas mixtures and inhibitors, Fluid Phase Equilib. 152 (1998) 23-42, https://doi.org/10.1016/S0378-3812(98)00368-9.

[27] J.H. van der Waals, J.C. Platteeuw, Clathrate solutions, Adv. Chem. Phys. 2 (1959) 1-57, https://doi.org/10.1002/9780470143483.ch1.

[28] J.C. Platteeuw, J.H. van der Waals, Thermodynamic properties of gas hydrates, Mol. Phys. 1 (1958) 91-96, https://doi.org/10.1080/00268975800100111.

[29] V. McKoy, O. Sinanoglu, Theory of dissociation pressures of some gas hydrates, J. Chem. Phys. 38 (1963) 2946-2956, https://doi.org/10.1063/1.1733625.

[30] A.L. Ballard, E.D. Sloan Jr., The next generation of hydrate prediction I. Hydrate standard states and incorporation of spectroscopy, Fluid Phase Equilib. 194-197 (2002) 371-383, https://doi.org/10.1016/S0378-3812(01)00697-5.

[31] M.D. Jager, A.L. Ballard, E.D. Sloan Jr., The next generation of hydrate prediction II. Dedicated aqueous phase fugacity model for hydrate prediction, Fluid Phase Equilib. 211 (2003) 85-107, https://doi.org/10.1016/S0378-3812(03)00155-9.

[32] A.L. Ballard, E.D. Sloan Jr., The next generation of hydrate prediction Part III. Gibbs energy minimization formalism, Fluid Phase Equilib. 218 (2004) 15-31, https://doi.org/10.1016/j.fluid.2003.08.005.

[33] A.L. Ballard, E.D. Sloan Jr., The next generation of hydrate prediction IV. A comparison of available hydrate prediction programs, Fluid Phase Equilib. 216 (2004) 257-270, https://doi.org/10.1016/j.fluid.2003.11.004.

[34] B. Tohidi, A. Danesh, A.C. Todd, Modeling single and mixed electrolyte-solutions and its applications to gas hydrates, Chem. Eng. Res. Des. 73 (1995) 464-472.

[35] B. Tohidi, A. Danesh, R.W. Burgass, A.C. Todd, Measurement and prediction of hydrate-phase equilibria for reservoir fluids, SPE Prod. Fac. 11 (1996) 69-76, https://doi.org/10.2118/28884-PA.

[36] B. Tohidi, A. Danesh, A.C. Todd, R.W. Burgass, K.K. Ostergaard, Equilibrium data and thermodynamic modelling of cyclopentane and neopentane hydrates, Fluid Phase Equilib. 138 (1997) 241-250, https://doi.org/10.1016/S0378-3812(97)00164-7.

[37] M.N. Khan, P. Warrier, C.J. Peters, C.A. Koh, Advancements in hydrate phase equilibria and modeling of gas hydrates systems, Fluid Phase Equilib. 463 (2018) 48-61, https://doi.org/10.1016/j.fluid.2018.01.014.

[38] G.J. Chen, T.M. Guo, A new approach to gas hydrate modelling, Chem. Eng. J. 71 (1998) 145-151, https://doi.org/10.1016/S1385-8947(98)00126-0.

[39] Y.H. Du, T.M. Guo, Prediction of hydrate formation for systems containing methanol, Chem. Eng. Sci. 45 (1990) 893-900, https://doi.org/10.1016/0009-2509(90)85011-2.

[40] M.Z. Bazant, B.L. Trout, A method to extract potentials from the temperature dependence of Langmuir constants for clathrate-hydrates, Phys. A 300 (2001) 139-173, https://doi.org/10.1016/S0378-4371(01)00339-9.

[41] J.B. Klauda, S.I. Sandler, Phase behavior of clathrate hydrates: A model for single and multiple gas component hydrates, Chem. Eng. Sci. 58 (2003) 27-41, https://doi.org/10.1016/S0009-2509(02)00435-9.

[42] S.E. Meragawi, N.I. Diamantonis, I.N. Tsimpanogiannis, I.G. Economou, Hydrate-fluid phase equilibria modeling using PC-SAFT and Peng-Robinson equations of state, Fluid Phase Equilib. 413 (2016) 209-219, https://doi.org/10.1016/j.fluid.2015.12.003.

[43] M.K. Hsieh, W.Y. Ting, Y.P. Chen, P.C. Chen, S.T. Lin, L.J. Chen, Explicit pressure dependence of the Langmuir adsorption constant in the van der Waals-Platteeuw model for the equilibrium conditions of clathrate hydrates, Fluid Phase Equilib. 325 (2012) 80-89, https://doi.org/10.1016/j.fluid.2012.04.012.

[44] A. Martin, C.J. Peters, New thermodynamic model of equilibrium states of gas hydrates considering lattice distortion, J. Phys. Chem. C 113 (2009) 422-430, https://doi.org/10.1021/jp8074546.

[45] J.H. Yoon, Y. Yamamoto, T. Komai, T. Kawamura, PSRK method for gas hydrate equilibria: I. Simple and mixed hydrates, AIChE J. 50 (2004) 203-214, https://doi.org/10.1002/aic.10019.

[46] S.K. Veesam, S.N. Punnathanam, VdWP-FL: An improved thermodynamic theory for gas hydrates with free-energy contributions due to hydrate lattice flexibility, J. Phys. Chem. C 123 (2019) 26406-26414, https://doi.org/10.1021/acs.jpcc.9b07608.

[47] G. Moradia, E. Khosravani, Modeling of hydrate formation conditions for CH_4, C_2H_6, C_3H_8, N_2, CO_2 and their mixtures using the PRSV2 equation of state and obtaining the Kihara potential parameters for these components, Fluid Phase Equilib. 338 (2013) 179-187, https://doi.org/10.1016/j.fluid.2012.11.010.

[48] E. Heidaryan, M.D.R. Fuentes, P.A.P. Filho, Equilibrium of methane and carbon dioxide hydrates below the freezing point of water: Literature review and modeling, J. Low Temp. Phys. 194 (2019) 27-45, https://doi.org/10.1007/s10909-018-2049-2.

[49] V.K. Michalis, I.N. Tsimpanogiannis, A.K. Stubos, I.G. Economou, Direct phase coexistence molecular dynamics study of the phase equilibria of the ternary methane-carbon dioxide-water hydrate system, Phys. Chem. Chem. Phys. 18 (2016) 23538-23548, https://doi.org/10.1039/C6CP04647A.

[50] T.H. Sirino, M.A.M. Neto, D. Bertoldi, R.E.M. Morales, A.K. Sum, Multiphase flash calculations for gas hydrates systems, Fluid Phase Equilib. 475 (2018) 45-63, https://doi.org/10.1016/j.fluid.2018.07.029.

[51] J.H. Yoon, M.K. Chun, H. Lee, Generalized model for predicting phase behavior of clathrate hydrate, AIChE J. 48 (2002) 1317-1330, https://doi.org/10.1002/aic.690480618.

[52] V.T. John, K.D. Papadopoulos, G.D. Holder, A generalized model for predicting equilibrium conditions for gas hydrates, AIChE J. 31 (1985) 252-259, https://doi.org/10.1002/aic.690310212.

[53] W.M. Deaton, E.M. Frost Jr., Gas hydrates and their relation to the operation of natural-gas pipe lines, U.S. Bureau of Mines Monograph 8 (1946).

[54] D.R. Marshall, S. Saito, R. Kobayashi, Hydrates at high pressures: Part I. Methane-water, argon-water, and nitrogen-water systems, AIChE J. 10 (1964) 202-205, https://doi.org/10.1002/aic.690100214.

[55] S. Takenouchi, G.C. Kennedy, Dissociation pressures of the phase $CO_2 \cdot 5\ 3/4\ H_2O$, J. Geol. 73 (1965) 383-390, https://doi.org/10.1086/627068.

[56] F.A. Medeiros, I.S.V. Segtovich, A.G. Barreto Jr., F.W. Tavares, Heat of dissociation from statistical thermodynamics: Using calorimetric data to estimate gas hydrate parameters, J. Chem. Thermodyn. 117 (2018) 164-179, https://doi.org/10.1016/j.jct.2017.08.005.

[57] J.B. Klauda, S.I. Sandler, A fugacity model for gas hydrate phase equilibria, Ind. Eng. Chem. Res. 39 (2000) 3377-3386, https://doi.org/10.1021/ie000322b.

[58] V. Vins, A. Jager, R. Span, J. Hruby, Model for gas hydrates applied to CCS systems part I. Parameter study of the van der Waals and Platteeuw model, Fluid Phase Equilib. 427 (2016) 268-281, http://dx.doi.org/10.1016/j.fluid.2016.07.014.

[59] D.R. Bhawangirkar, J. Adhikari, J.S. Sangwai, Thermodynamic modeling of phase equilibria of clathrate hydrates formed from CH_4, CO_2, C_2H_6, N_2 and C_3H_8, with

different equations of state, J. Chem. Thermodyn. 117 (2018) 180-192, https://doi.org/10.1016/j.jct.2017.09.024.

[60] P.B. Dharmawardhana, W.R. Parrish, E.D. Sloan, Experimental thermodynamic parameters for the prediction of natural gas hydrate dissociation conditions, Ind. Eng. Chem. Fundam. 19 (1980) 410-414, https://doi.org/10.1021/i160076a015.

[61] Y.P. Handa, J.S. Tse, Thermodynamic properties of empty lattices of structure I and structure II clathrate hydrates, J. Phys. Chem. 90 (1986) 5917-5921, https://doi.org/10.1021/j100280a092.

[62] C. Smith, D. Pack, A. Barifcani, Propane, n-butane and i-butane stabilization effects on methane gas hydrates, J. Chem. Thermodyn. 115 (2017) 293-301, https://doi.org/10.1016/j.jct.2017.08.013.

[63] J. Jhaveri, D.B. Robinson, Hydrates in the methane-nitrogen system, Can. J. Chem. Eng. 43 (1965) 75-78, https://doi.org/10.1002/cjce.5450430207.

[64] D. Sadeq, S. Iglauer, M. Lebedev, C. Smith, A. Barifcani, Experimental determination of hydrate phase equilibrium for different gas mixtures containing methane, carbon dioxide and nitrogen with motor current measurements, J. Nat. Gas. Sci. Eng. 38 (2017) 59-73, https://doi.org/10.1016/j.jngse.2016.12.025.

[65] A.K. Sum, R.C. Burruss, E.D. Sloan Jr., Measurement of clathrate hydrates via raman spectroscopy, J. Phys. Chem. B 101 (1997) 7371-7377, https://doi.org/10.1021/jp970768e.

[66] J.A. Ripmeester, C.I. Ratcliffe, The diverse nature of dodecahedral cages in clathrate hydrates as revealed by ^{129}Xe and ^{13}C NMR spectroscopy: CO_2 as a small-cage guest, Energy Fuels 12 (1998) 197-200, https://doi.org/10.1021/ef970171y.

[67] L.J. Florusse, C.J. Peters, J. Schoonman, K.C. Hester, C.A. Koh, S.F. Dec, K.M. Marsch, E.D. Sloan, Stable low-pressure hydrogen clusters stored in a binary clathrate hydrate, Science 306 (2004) 469-471, https://doi.org/10.1126/science.1102076.

[68] W.L. Mao, H.K. Mao, A.F. Goncharov, V.V. Struzhkin, Q.Z. Guo, J.Z. Hu, J.F. Shu, R.J. Hemley, M. Somayazulu, Y.S. Zhao, Hydrogen clusters in clathrate hydrate, Science 297 (2002) 2247-2249, https://doi.org/10.1126/science.1075394.

[69] I.N. Tsimpanogiannis, N.I. Papadimitriou, A.K. Stubos, On the limitation of the van der Waals-Platteeuw-based thermodynamic models for hydrates with multiple occupancy of cavities, Mol. Phy. 110 (2012) 1213-1221, https://doi.org/10.1080/00268976.2012.666278.

[70] J. Munck, S. Skjold-Jorgensen, P. Rasmussen, Computations of the formation of gas hydrates, Chem. Eng. Sci. 43 (1988) 2661-2672, https://doi.org/10.1016/0009-2509(88)80010-1.

[71] A. Pina-Martinez, Y. Le Guennec, R. Privat, J. Jaubert, P.M. Mathias, Analysis of the combinations of property data that are suitable for a safe estimation of consistent Twu α-function parameters: updated parameter values for the translated-consistent tc-PR and tc-RK cubic equations of state, J. Chem. Eng. Data 63 (2018) 3980-3988, https://doi.org/10.1021/acs.jced.8b00640.

[72] D.Y. Peng, D.B. Robinson, A new two-constant equation of state, Ind. Eng. Chem. Fundam. 15 (1976) 59-64, https://doi.org/10.1021/i160057a011.

[73] C.H. Twu, D. Bluck, J.R. Cunningham, J.E. Coon, A cubic equation of state with a new alpha function and a new mixing rule, Fluid Phase Equil. 69 (1991) 33-50, https://doi.org/10.1016/0378-3812(91)90024-2.

[74] G. Soave, Equilibrium constants from a modified Redlich-Kwong equation of state, Chem. Eng. Sci. 27 (1972) 1197-1203, https://doi.org/10.1016/0009-2509(72)80096-4.

[75] J.D. van der Waals, Continuity of the gaseous and liquid state of matter, Ph.D. thesis, Leiden, 1873.

[76] H.W. Curtis, R.B. Michael, Phase behavior, SPE Monograph Series 20, 2000.

[77] G.D. Holder, G. Corbin, K.D. Papadopoulos, Thermodynamic and molecular properties of gas hydrates from mixtures containing methane, argon, and krypton, Ind. Eng. Chem. Fundam. 19 (1980) 282-286, https://doi.org/10.1021/i160075a008.

[78] B.J. Anderson, J.W. Tester, B.L. Trout, Accurate potentials for argon-water and methane-water interactions via ab initio methods and their application to clathrate hydrates, J. Phys. Chem. B 108 (2004) 18705-18715, https://doi.org/10.1021/jp047448x.

[79] A. Chapoy, H. Haghighi, R. Burgass, B. Tohidi, On the phase behaviour of the (carbon dioxide + water) systems at low temperatures: Experimental and modelling, J. Chem. Thermodyn. 47 (2012) 6-12, https://doi.org/10.1016/j.jct.2011.10.026.

[80] E.S. Barkan, D.A. Sheinin, A general technique for the calculation of formation conditions of natural gas hydrates, Fluid Phase Equilib. 86 (1993) 111-136, https://doi.org/10.1016/0378-3812(93)87171-V.

[81] Y.H. Sun, S.L. Li, G.B. Zhang, W. Guo, Y.H. Zhu, Hydrate phase equilibrium of CH_4+N_2+CO_2 gas mixtures and cage occupancy behaviors, Ind. Eng. Chem. Res. 56 (2017) 8133-8142, https://doi.org/10.1021/acs.iecr.7b01093.

[82] K. Yasuda, R. Ohmura, Phase equilibrium for clathrate hydrates formed with methane, ethane, propane, or carbon dioxide at temperatures below the freezing point of water, J. Chem. Eng. Data, 53 (2008) 2182-2188, https://doi.org/10.1021/je800396v.

[83] R. Zheng, Z. Fan, X. Li, S. Negahban, Phase boundary of CH_4, CO_2, and binary CH_4-CO_2 hydrates formed in NaCl solutions, J. Chem. Thermodyn. 154 (2021) 106333, https://doi.org/10.1016/j.jct.2020.106333.

[84] D.E.S. de Menezes, P.A.P. Filho, M.D.R. Fuentes, Phase equilibrium for methane, ethane and carbon dioxide hydrates at pressures up to 100 MPa through high-pressure microcalorimetry: Experimental data, analysis and modeling, Fluid Phase Equilib. 518 (2020) 112590, https://doi.org/10.1016/j.fluid.2020.112590.

[85] M.D. Jager, E.D. Sloan, The effect of pressure on methane hydration in pure water and sodium chloride solutions, Fluid Phase Equilib. 185 (2001) 89-99, https://doi.org/10.1016/S0378-3812(01)00459-9.

[86] S. Subramanian, R.A. Kini, S.F. Dec, E.D. Sloan Jr., Evidence of structure II hydrate formation from methane-ethane mixtures, Chem. Eng. Sci. 55 (2000) 1981-1999, https://doi.org/10.1016/S0009-2509(99)00389-9.

[87] S. Adisasmito, E.D. Sloan Jr., Hydrates of hydrocarbon gases containing carbon dioxide, J. Chem. Eng. Data 37 (1992) 343-349, https://doi.org/10.1021/je00007a020.

[88] G.D. Holder, J.H. Hand, Multiple-phase equilibria in hydrates from methane, ethane, propane and water mixtures, AIChE J. 28 (1982) 440-447, https://doi.org/10.1002/aic.690280312.

[89] S.M. Babakhani, B. Bouillot, J. Douzet, S. Ho-Van, J.M. Herri, PVTx measurements of mixed clathrate hydrates in batch conditions under different crystallization rates: Influence on equilibrium, J. Chem. Thermodyn. 122 (2018) 73-84, https://doi.org/10.1016/j.jct.2018.03.006.

[90] P. Linga, R. Kumar, P. Englezos, Gas hydrate formation from hydrogen/carbon dioxide and nitrogen/carbon dioxide gas mixtures, Chem. Eng. Sci. 62 (2007) 4268-4276, https://doi.org/10.1016/j.ces.2007.04.033.

[91] B. Chazallon, C. Pirim, Selectivity and CO_2 capture efficiency in CO_2-N_2 clathrate hydrates investigated by in-situ Raman spectroscopy, Chem. Eng. J. 342 (2018) 171-183, https://doi.org/10.1016/j.cej.2018.01.116.

[92] L.W. Diamond, Salinity of multivolatile fluid inclusions determined from clathrate hydrate stability, Geochim. Cosmochim. Acta 58 (1994) 19-41, https://doi.org/10.1016/0016-7037(94)90443-X.

[93] P. Gayet, C. Dicharry, G. Marion, A. Graciaa, J. Lachaise, A. Nesterov, Experimental determination of methane hydrate dissociation curve up to 55 MPa by using a small amount of surfactant as hydrate promoter, Chem. Eng. Sci. 60 (2005) 5751-5758, https://doi.org/10.1016/j.ces.2005.04.069.

[94] J.G. Vlahakis, H.S. Chen, M.S. Suwandi, A.J. Barduhn, The growth rate of ice crystals: Properties of carbon dioxide hydrate, a review of properties of 51 gas hydrates, Syracuse U, Research and Development Report, No. 830, 1972.

Supplementary Material

Table 4-S1. Database of CH_4 hydrate equilibria and comparison of the calculation accuracy yielded by the vdW-P model with the Kihara potential parameters optimized by different methods.

Phases	References	%AAD		*T* range (k)	*P* rang (MPa)	Data number
		Conventional method	New fitting procedure			
H-L_w-V	Roberts et al. (1940) [1]	1.73	1.53	273.2-286.7	2.641-10.8	4
	Deaton and Frost (1946) [2]	1.09	3.02	273.7-285.9	2.77-9.78	13
	Kobayashi and Katz (1949) [3]	2.20	9.56	295.7-302	33.99-77.5	4
	McLeod and Campbell (1961) [4]	2.18	3.15	285.7-301.6	9.62-62.4	10
	Marshall et al. (1964) [5]	6.03	7.27	290.2-320.1	15.9-397	20
	Jhaveri and Robinson (1965) [6]	1.89	2.25	273.2-294.3	2.65-28.57	8

Galloway et al. (1970) [7]	4.74	3.26	283.2-288.7	7.1-13.11	4
Verma (1974) [8]	3.30	3.46	275.2-291.2	3.02-18.55	7
de Roo et al. (1983) [9]	1.73	1.63	273.3-286	2.69-10.04	9
Thakore and Holder (1987) [10]	4.57	5.45	275.4-281.2	2.87-6.1	6
Song and Kobayashi (1989) [11]	7.48	10.66	284.45-274.75	8.099-2.688	6
Adisasmito et al. (1991) [12]	1.67	2.11	273.4-286.4	2.68-10.57	11
Svartas and Fadnes (1992) [13]	3.43	3.00	274.85-299.15	3.081-49.96	10
Ross and Toczylkint (1992) [14]	2.93	3.49	273.6-294	2.77-28.02	13
Dickens and Quinby-Hun (1994) [15]	1.70	3.16	276.1-285.4	3.45-9.58	7
Mei et al. (1996) [16]	2.16	2.70	274.2-285.2	2.96-8.96	12
Dyadin and Aladko (1996) [17]	31.62	36.76	287-326.8	8-1000	43
Nixdorf and Oellrich (1997) [18]	2.09	1.83	274.36-293.57	2.961-24.959	29
Nakano et al. (1999) [19]	8.03	16.04	305.08-320.54	98-493	16
Maekawa (2001) [20]	2.26	2.30	274.2-288.2	2.9-12.6	30
Jager and Sloan (2001) [21]	6.21	4.50	291.86-303.48	20.19-72.26	12
Freer et al. (2001) [22]	1.07	1.60	276.15-285.25	3.55-9.06	6
Yang et al. (2001) [23]	2.69	2.97	276.5-286.3	3.68-9.66	10
Clarke and Bishnoi (2001) [24]	7.77	4.41	274.65-281.15	3.266-6.361	5
Kharrat Dalmazzone (2003) [25]	3.82	4.43	281.2-284	5.73-7.68	3
Nakamura et al. (2003) [26]	1.29	2.25	274.25-285.78	2.92-9.54	17
Mohammadi et al. (2005) [27]	1.77	3.51	280.5-298.3	5.426-47.863	11
Gayet et al. (2005) [28]	2.57	2.15	275.15-300.15	3.17-54.53	26
Circone et al. (2005) [29]	1.00	1.19	275.15-285.15	3.2-9	8
Gupta et al. (2008) [30]	5.28	2.95	280.6-291.65	5.5-19.3	7
Yasuda and Ohmura (2008) [31]	0.82	5.38	273.6-274.7	2.673-3.016	12
Kim et at. (2010) [32]	2.72	4.39	274.55-285.1	2.9-8.98	10
Herri et al. (2011) [33]	5.59	3.94	273-275.8	2.86-3.4	3
Javanmardi et al. (2012) [34]	1.96	4.30	274.7-282	3.05-6.29	7
Fan et al. (2013) [35]	0.80	1.50	276.3-283.3	3.58-7.39	4
Sami et al. (2013) [36]	3.61	2.26	279.9-283.56	5.25-7.98	4
Sabil et al. (2014) [37]	5.35	5.94	280.15-288.65	5.55-15.29	9
Sangwaia and Oellrich (2014) [38]	3.08	2.01	279.72-292.41	5.02-21.09	7
Sabil et al. (2015) [39]	4.06	3.24	276.21-287.45	3.6-11.1	6
Long et al. (2015) [40]	1.56	2.16	275.8-288.5	3.4-13.27	5
Mech et al. (2015) [41]	3.59	2.06	279.36-282.73	4.97-7.09	5
Ward et al. (2015) [42]	1.04	1.65	276.29-285.57	3.53-9.38	8
Long et al. (2015) [43]	4.28	3.04	278.8-289.7	4.53-14.99	6
Le Quang et al. (2016) [44]	2.74	0.54	276.15-282.85	3.7-7.05	6
Kastanidis et al. (2016) [45]	3.01	1.74	280-282.7	5.36-7.07	3
Pahlavanzadeh et al. (2016) [46]	1.57	3.85	277.4-282.7	3.85-6.79	3

	Long et al. (2016) [47]	1.26	1.84	281.5-284.4	6-8.28	2
	Smith et al. (2017) [48]	2.86	4.33	274.95-290.05	3.13-17.19	6
	Mannar et al. (2017) [49]	1.94	2.78	279-286	4.58-9.7	4
	Kamari et al. (2017) [50]	1.36	2.23	274.3-285.8	2.92-9.54	17
	Khan et al. (2017) [51]	6.50	8.32	277-284.8	3.52-8	4
	Sadeq et al. (2017) [52]	2.76	4.95	279.45-292.95	5-25	6
	Bavoh et al. (2017) [53]	1.92	2.66	277-286	3.86-9.7	5
	Lim et al. (2017) [54]	4.74	3.07	281.5-291.6	5.7-19.61	6
	Nashed et al. (2018) [55]	3.97	3.30	279.77-287.45	5.1-11.1	4
	Bavoh et al. (2018) [56]	1.93	3.36	277.3-286.1	3.9-9.7	5
	Sun et al. (2018) [57]	1.34	0.87	280.9-289	5.7-14	9
	Mu and Solms (2018) [58]	1.84	3.33	275.54-286.35	3.163-10.143	10
	Xiao et al. (2019) [59]	11.74	7.44	273.15-303.15	2.64-65.81	7
	de Menezes et al. (2020) [60]	1.55	7.38	281.01-305.26	5.5-100	11
	Aghajanloo et al. (2020) [61]	1.86	1.23	283.1-288.4	7.13-13.16	7
	Pahlavanzadeh et al. (2020) [62]	1.26	3.13	275.3-279.26	3.2-4.74	5
H-I-V	Roberts et al. (1940) [1]	2.43	5.18	259.1-273.2	1.648-2.641	2
	Deaton and Frost (1946) [2]	0.92	7.05	262.4-270.9	1.79-2.39	5
	Falabella (1975) [63]	24.76	9.04	148.8-193.2	0.0053-0.1013	6
	Svartas and Fadnes (1992) [13]	1.24	5.70	271.75-272.45	2.41-2.52	3
	Makogon and Sloan (1994) [64]	8.37	8.78	190.2-262.4	0.0825-1.798	6
	Circone et al. (2005) [29]	3.12	7.74	263.09-268.15	1.9-2.1	2
	Yasuda and Ohmura (2008) [31]	1.36	7.08	244.2-272.8	0.971-2.523	16
	Nagashima and Ohmura (2016) [65]	3.90	13.38	197.3-238.7	0.1117-0.7941	7
	Xiao et al. (2019) [59]	3.99	3.56	263.15-268.15	1.93-2.24	2
	Overall	**5.37**	**6.56**	**148.8-326.8**	**0.0053-1000**	**622**

Table 4-S2. Database of C_2H_6 hydrate equilibria and comparison of the calculation accuracy yielded by the vdW-P model with the Kihara potential parameters optimized by different methods.

Phases	References	%AAD		*T* range (k)	*P* rang (MPa)	Data number
		Conventional method	New fitting procedure			
H-L_w-V	Roberts et al. (1940) [1]	7.18	7.26	273.4-287	0.545-3.054	11
	Deaton and Frost (1946) [2]	2.25	2.34	273.7-286.5	0.51-2.73	20
	Reamer et al. (1952) [66]	6.89	6.89	279.9-287.4	0.972-3.298	4
	Galloway et al. (1970) [7]	2.17	2.27	277.6-282.5	0.814-1.551	3
	Holder and Grigoriou (1980) [67]	2.66	2.62	277.5-286.5	0.78-2.62	7
	Holder and Hand (1982) [68]	8.42	8.49	278.8-288.2	0.95-3.36	7
	Avlonitis (1988) [69]	4.09	4.16	277.8-287.2	0.848-3.082	10
	Englezos and Bishnoi (1991) [70]	2.44	2.55	274.3-282.98	0.548-1.637	6

	Ross and Toczylkint (1992) [14]	11.42	11.52	273.9-283	0.6-1.74	3
	Nixdorf and Oellrich (1997) [18]	1.49	1.57	273.68-287.61	0.499-3.244	15
	Mohammadi et al. (2008) [71]	1.24	1.23	275.2-282.1	0.6-1.4	3
	Yasuda and Ohmura (2008) [31]	0.54	0.65	273.9-275.9	0.508-0.658	13
	Long et al. (2010) [72]	0.65	0.67	280.1-285.6	1.11-2.32	5
	Mottahedin et al. (2011) [73]	2.01	2.16	274-276	0.5261-0.6725	3
H-L_w-L_g	Ng and Robinson (1985) [74]	8.84	8.77	288-290.6	3.33-20.34	8
	Nakano et al. (1998) [75]	5.33	5.32	290.42-298.36	19.48-83.75	26
	Morita et al. (2000) [76]	10.95	11.14	298.01-323.93	89-479	21
	de Menezes et al. (2020) [60]	15.05	14.91	287.96-296	5-70	8
H-I-V	Roberts et al. (1940) [1]	7.16	7.43	260.8-269.3	0.294-0.441	3
	Deaton and Frost (1946) [2]	1.85	2.09	263.6-272	0.313-0.457	4
	Falabella and Vanpee (1974) [77]	10.29	9.44	200.8-240.8	0.0083-0.1013	5
	Yasuda and Ohmura (2008) [31]	1.89	1.77	244.9-272.8	0.122-0.459	19
	Overall	**5.12**	**5.14**	**200.8-323.93**	**0.0083-479**	**204**

Table 4-S3. Database of C_3H_8 hydrate equilibria and comparison of the calculation accuracy yielded by the vdW-P model with the Kihara potential parameters optimized by different methods.

Phases	References	%AAD		*T* range (k)	*P* rang (MPa)	Data number
		Conventional method	New fitting procedure			
H-L_w-V	Miller and Strong (1946) [78]	2.41	2.41	273.2-278	0.165-0.472	10
	Deaton and Frost (1946) [2]	2.24	2.24	273.7-277.1	0.183-0.386	6
	Reamer et al. (1952) [66]	5.83	5.83	274.3-277.2	0.241-0.414	3
	Robinson and Mehta (1971) [79]	2.39	2.38	274.3-277.8	0.207-0.455	4
	Verma (1974) [8]	2.28	2.28	273.9-278	0.188-0.512	8
	Kubota et al. (1984) [80]	1.12	1.12	274.2-278.4	0.207-0.542	9
	Thakore and Holder (1987) [10]	4.66	4.66	274.2-278.2	0.217-0.51	5
	Patil (1987) [81]	5.88	5.88	273.6-278	0.207-0.51	5
	Bishnoi and Dholabhai (1993) [82]	9.30	9.30	273.63-277.73	0.208-0.503	4
	Englezos and Ngan (1993) [83]	2.35	2.35	274.2-278.3	0.208-0.545	6
	Nixdorf and Oellrich (1997) [18]	3.99	3.99	273.55-278.52	0.186-0.567	10
	Mooijer-van den Heuvel et al. (2002) [84]	2.37	2.37	276.77-278.55	0.368-0.547	9
	Mohammadi et al. (2008) [71]	3.09	3.09	274.6-278.3	0.22-0.5	3
	Yasuda and Ohmura (2008) [31]	0.73	0.73	273.9-276	0.194-0.309	12
H-I-V	Deaton and Frost (1946) [2]	3.03	3.03	261.2-272.9	0.1-0.172	7
	Holder and Godbole (1982) [85]	4.83	4.83	247.9-262.1	0.0482-0.0994	8
	Yasuda and Ohmura (2008) [31]	1.92	1.92	245-273.1	0.041-0.167	25
	Mohammadi and Richon (2013) [86]	2.78	2.78	259.4-268.7	0.085-0.137	4
	Overall	**2.84**	**2.84**	**245-278.55**	**0.041-0.567**	**138**

Table 4-S4. Database of iC_4H_{10} hydrate equilibria and comparison of the calculation accuracy yielded by the vdW-P model with the Kihara potential parameters optimized by different methods.

Phases	References	%AAD		*T* range (k)	*P* rang (MPa)	Data number
		Conventional method	New fitting procedure			
H-L_w-V	Schneider and Farrar (1968) [87]	1.76	1.76	273.2-275.1	0.11-0.167	10
	Rouher and Barduhn (1969) [88]	3.67	3.67	273.2-275	0.115-0.169	24
	Buleiko (2018) [89]	6.02	6.02	273.23-274.88	0.121-0.161	7
H-I-V	Schneider and Farrar (1968) [87]	2.09	2.09	271.2-273.1	0.095-0.109	7
	Holder and Godbole (1982) [85]	10.98	10.99	241.4-269.5	0.0176-0.0913	10
Overall		**4.69**	**4.70**	**241.4-275.1**	**0.0176-0.169**	**58**

Table 4-S5. Database of CO_2 hydrate equilibria and comparison of the calculation accuracy yielded by the vdW-P model with the Kihara potential parameters optimized by different methods.

Phases	References	%AAD		*T* range (k)	*P* rang (MPa)	Data number
		Conventional method	New fitting procedure			
H-L_w-V	Deaton and Frost (1946) [2]	1.82	4.15	273.7-282.9	1.324-4.323	19
	Unruh and Katz (1949) [90]	2.89	4.86	277.2-283.1	2.041-4.502	5
	Larson (1955) [91]	1.30	5.59	271.8-283.2	1.048-4.502	36
	Robinson and Mehta (1971) [79]	1.78	4.46	273.9-283.3	1.379-4.468	7
	Vlahakis et al. (1972) [92]	1.43	5.38	271.6-283.2	1.04-4.509	44
	Ng and Robinson (1985) [74]	5.27	8.62	279.6-282.8	2.74-4.36	3
	Adisasmito et al. (1991) [12]	2.30	4.47	274.3-282.9	1.42-4.37	9
	Ohgaki et al. (1993) [93]	4.21	3.40	275.97-280.33	1.74-3.076	7
	Dholabhai et al. (1993) [94]	1.95	2.58	273.75-279.04	1.34-2.52	4
	Englezos and Hall (1994) [95]	1.91	3.72	275.05-282.65	1.542-4.155	6
	Dholabhai et al. (1996) [96]	0.82	2.14	275.11-279.49	1.56-2.62	2
	Breland and Englezos (1996) [97]	3.56	2.90	275.5-280.2	1.651-3.021	3
	Dholabhai et al. (1997) [98]	1.44	1.49	275.72-278.7	1.682-2.393	2
	Fan and Guo (1999) [99]	2.75	5.30	273.6-282	1.31-4.02	9
	Wendland (1999) [100]	2.31	4.56	273.93-282.16	1.365-3.85	7
	Fan et al. (2000) [101]	2.12	3.45	274.7-279.7	1.5-2.78	3
	Mooijer-van den Heuvel et al. (2001) [102]	2.39	4.38	276.52-282.5	1.82-4.01	10
	Anderson (2003) [103]	1.62	3.58	274.15-282.15	1.377-3.858	9
	Mohammadi et al. (2005) [27]	1.30	5.12	277.5-282.5	2.048-4.02	3
	Yasuda and Ohmura (2008) [31]	0.81	8.50	273.8-275	1.312-1.501	14
	Chen et al. (2009) [104]	2.61	2.25	275.25-279.85	1.56-2.86	7
	Sabil et al. (2010) [105]	2.24	3.89	275.12-282.9	1.51-4.3	10
	Ruffine and Trusler (2010) [106]	2.62	3.53	275.03-282.76	1.502-4.079	10
	Maekawa (2010) [107]	2.43	4.20	273.6-283.1	1.33-4.54	13
	Herri et al. (2011) [33]	3.34	2.11	275.6-274.8	1.45-1.7	3
	Melnikov et al. (2011) [108]	1.60	5.10	273.3-280.2	1.25-2.95	6
	Sami et al. (2013) [36]	2.61	4.81	276.7-281.57	1.82-3.76	5

	Sabil et al. (2014) [37]	1.42	4.38	272.65-281.45	1.1-3.38	11
	Xu et al. (2014) [109]	2.10	3.17	278.7-281.3	2.39-3.42	5
	Maekawa (2014) [110]	1.16	5.71	272.4-282.9	1.12-4.34	8
	Le Quang et al. (2016) [44]	1.75	1.75	275.35-278.15	1.62-2.26	4
	Kastanidis et al. (2016) [45]	6.00	8.20	278.6-282	2.33-3.97	5
	Ilani-Kashkouli et al. (2016) [111]	0.97	4.14	279.3-283.3	2.57-4.45	4
	Yu et al. (2016) [112]	2.00	2.37	275.7-279.7	1.641-2.761	5
	Sun et al. (2016) [113]	1.85	1.61	276.15-278.15	1.76-2.258	9
	Ferrari et al. (2016) [114]	0.50	2.86	275.65-281.65	1.65-3.48	5
	Mannar et al. (2017) [49]	3.16	1.21	276.65-282.7	1.87-3.78	5
	Kamari et al. (2017) [50]	2.70	3.60	277.2-281.9	2.04-3.69	4
	Khan et al. (2017) [51]	5.49	3.92	277.4-283	1.85-3.95	5
	Bavoh et al. (2017) [53]	1.46	2.70	276.65-282.7	1.81-3.95	5
	Nema et al. (2017) [115]	3.01	6.32	271.65-275.75	1.056-1.708	7
	Mu and Solms (2018) [58]	2.07	2.94	273.54-277.57	1.29-2.144	6
	Jarrahian and Nakhaee (2019) [116]	1.08	2.93	274.15-280.15	280.15-280.15	7
	Ilani-Kashkouli et al. (2019) [117]	4.65	5.06	276.1-282.4	1.79-4.06	4
	Chima-Maceda et al. (2019) [118]	1.24	3.92	276.22-282.54	1.74-4.09	5
	Dai et al. (2020) [119]	1.20	4.80	275.65-283.25	1.616-4.452	11
H-I-V	Larson (1955) [91]	10.95	20.73	256.8-271.8	0.545-1.048	9
	Miller and Smythe (1970) [120]	27.52	58.19	151.5-192.5	0.000535-0.0219	8
	Falabella (1975) [63]	13.95	34.03	194.5-217.8	0.0248-0.1013	5
	Anderson (2003) [103]	15.35	25.76	259.15-271.15	0.605-1.018	13
	Yasuda and Ohmura (2008) [31]	10.99	21.25	244.5-271.6	0.364-1.025	19
H-L_w-L_g	Takenouchi and Kennedy (1965) [121]	13.33	38.29	283.2-292.7	4.5-186.2	15
	Ng and Robinson (1985) [74]	34.14	45.97	282.9-283.9	5.03-14.36	6
	Ohgaki et al. (1993) [93]	20.04	31.79	283.23-283.59	4.541-4.541	3
	Nakano et al. (1998) [122]	13.35	46.18	289.73-294	104-328	13
	Fan and Guo (1999) [99]	52.02	59.80	283.1-283.6	9.32-12.87	3
	Mooijer-van den Heuvel et al. (2001) [102]	31.66	36.52	283.33-283.36	5.97-7.35	2
	Ruffine and Trusler (2010) [106]	31.20	32.28	283.25-286.76	5.993-46.575	3
	Kastanidis et al. (2016) [45]	37.33	41.48	283-283.4	5.58-9.65	7
	de Menezes et al. (2020) [60]	10.72	45.10	283.7-288.45	9.8-80	8
	Overall	**5.97**	**10.89**	**151.5-294**	**0.000535-328**	**485**

Table 4-S6. Database of N_2 hydrate equilibria and comparison of the calculation accuracy yielded by the vdW-P model with the Kihara potential parameters optimized by different methods.

Phases	References	%AAD		*T* range (k)	*P* rang (MPa)	Data number
		Conventional method	New fitting procedure			
H-L_w-V	van Cleeff and Diepen (1960) [123]	5.77	8.28	272-291	14.48-95.86	38
	Marshall et al. (1964) [5]	7.99	8.77	277.6-305.5	24.93-328.89	14
	Jhaveri and Robinson (1965) [6]	2.80	6.30	273.2-281.1	16.27-35.16	8

Sugahara et al. (2002) [124]	7.50	9.70	285.63-309.43	55-439	33
Mohammadi (2003) [125]	3.54	8.61	274.55-283.05	19.093-45.355	3
Lee et al. (2014) [126]	5.55	3.46	273-277.5	16.13-23.9	7
Jarrahian and Nakhaee (2019) [116]	2.18	6.43	274.15-280.15	17.95-32.91	7
Overall	**6.05**	**7.81**	**272-309.43**	**14.48-439**	**110**

Table 4-S7. Database of CH_4-C_2H_6, CH_4-C_3H_8 and CH_4-iC_4H_{10} gas-mixture hydrate equilibria and comparison of the calculation accuracy yielded by the vdW-P model with the Kihara potential parameters optimized by different methods.

Mixtures	References	%AAD		*T* range (k)	*P* rang (MPa)	Molar fraction of component (1)	Data number
		Conventional method	New fitting procedure				
CH_4(1)-C_2H_6(2)	Deaton and Frost (1946) [2]	21.51	8.64	274.8-283.2	0.945-6.088	0.564-0.988	24
	McLeod and Campbell (1961) [4]	19.67	14.28	284.9-304.1	6.93-68.57	0.809-0.946	16
	Holder and Grigoriou (1980) [67]	5.90	2.54	279.4-287.8	0.99-3.08	0.016-0.177	15
	Nixdorf and Oellrich (1997) [18]	40.28	3.20	278.21-295.52	2.254-23.196	0.9047	8
	Subramanian et al. (2000) [127]	33.39	10.16	274.2	0.88-1.45	0.63-0.92	6
	Maekawa (2001) [20]	19.41	9.67	275.4-289.6	1.7-11.1	0.902-0.989	52
	Kumar et al. (2008) [128]	38.06	0.83	273.7	1.43	0.918	1
	Hashimoto et al. (2008) [129]	23.94	5.77	279.1-288.1	1.12-12.3	0.102-0.991	62
	Overall	**21.60**	**7.73**	**273.7-304.1**	**0.88-68.57**	**0.016-0.991**	**184**
CH_4(1)-C_3H_8(2)	Deaton and Frost (1946) [2]	109.59	6.60	274.8-283.2	0.272-4.358	0.362-0.99	25
	McLeod and Campbell (1961) [4]	120.37	10.13	290.5-304.9	6.93-68.98	0.945-0.965	17
	Verma et al. (1974) [8]	33.60	6.99	274.4-282.3	0.263-0.945	0.2375-0.371	12
	Thakore and Holder (1987) [10]	52.63	3.18	275.15-278.15	0.245-1.306	0.021-0.956	28
	Nixdorf and Oellrich (1997) [18]	151.26	3.44	278.09-297.53	1.418-24.363	0.9707	7
	Kumar et al. (2008) [128]	97.59	3.90	273.7	0.52	0.904	1
	Smith et al. (2017) [48]	82.71	15.91	278.45-295.35	2.36-16.75	0.95967-0.99484	20
	Sun et al. (2018) [57]	41.52	15.42	275.2-279.2	2.77-2.82	0.992-0.997	3
	de Menezes et al. (2019) [130]	114.54	11.33	295.75-310.45	13.6-100.5	0.92	6
	Overall	**86.43**	**8.16**	**273.7-310.45**	**0.245-100.5**	**0.021-0.997**	**119**
CH_4(1)-iC_4H_{10}	Deaton and Frost (1946) [62]	126.57	8.50	274.8-277.6	1.324-1.841	0.989	2
	McLeod and Campbell (1961) [4]	135.32	13.92	288.6-305	6.72-63.33	0.954-0.986	20
	Wu et al. (1976) [131]	157.33	13.09	273.5-293.6	0.159-10.07	0.364-0.9977	46
	Ng and Robinson (1976) [132]	178.48	14.38	273.928-293.594	0.205-10.068	0.364-0.996	19
	Thakore and Holder (1987) [10]	34.18	11.02	274.35	0.127-0.841	0.036-0.949	19
	Smith et al. (2017) [48]	192.16	6.36	281.25-297.45	2.745-15.524	0.93187-0.99405	15
	Overall	**141.49**	**12.19**	**273.5-305**	**0.127-63.33**	**0.364-0.9977**	**121**

Table 4-S8. Database of C_2H_6-C_3H_8 and C_3H_8-iC_4H_{10} gas-mixture hydrate equilibria and comparison of the calculation accuracy yielded by the vdW-P model with the Kihara potential parameters optimized by different methods.

Mixtures	References	%AAD		*T* range (k)	*P* rang (MPa)	Molar fraction of component (1)	Data number
		Conventional method	New fitting procedure				
C_2H_6(1) - C_3H_8(2)	Holder and Hand (1982) [68]	9.03	7.72	273.1-283.3	0.44-2.03	0.28-0.857	60
	Nixdorf and Oellrich (1997) [18]	4.62	4.52	276.66-283.32	0.825-1.936	0.8515	6
	Mooijer-van den Heuvel (2004) [133]	6.79	5.87	277.03-278.17	0.54-0.67	0.299	5
	Overall	**8.50**	**7.32**	**273.1-283.32**	**0.44-2.03**	**0.28-0.857**	**71**
C_3H_8(1) - iC_4H_{10}(2)	Kamath and Holder (1984) [134]	2.07	2.09	272.1-272.2	0.1082-0.1537	0.125-0.959	11
	Paranjpe et al. (1989) [135]	19.84	17.58	275.25-277.85	0.213-0.49	0.112-0.794	6
	Overall	**8.34**	**7.56**	**272.1-277.85**	**0.1082-0.49**	**0.112-0.959**	**17**

Table 4-S9. Database of CO_2-CH_4 gas-mixture hydrate equilibria and comparison of the calculation accuracy yielded by the vdW-P model with the Kihara potential parameters optimized by different methods.

References	%AAD		*T* range (k)	*P* rang (MPa)	Molar fraction of component CO_2	Data number
	Conventional method	New fitting procedure				
Adisasmito et al. (1991) [12]	2.21	2.86	273.7-287.6	1.45-10.95	0.08-0.85	42
Dholabhai and Bishnoi (1994) [136]	2.59	4.46	274.1-284.84	2.36-7.53	0.153-0.179	4
Ohgaki et al. (1996) [137]	3.65	4.42	280.3	3.24-4.99	0.065-0.683	29
Dholabhai et al. (1997) [98]	1.54	4.30	274.41-281.51	2.419-5.112	0.183	2
Servio et al. (1999) [138]	4.85	5.80	273.5-283.1	1.78-5.07	0.1244-0.5347	17
Fan and Guo (1999) [99]	9.23	13.69	273.5-282.3	1.1-4.8	0.9652	9
Seo et al. (2000) [139]	3.28	5.84	272.66-283.56	1.5-5	0.1854-0.9041	19
Beltran and Servio (2008) [140]	16.75	17.86	275.14-285.34	1.92-7.47	0.131-0.455	23
Bruusgaard et al. (2010) [141]	1.38	4.52	274.02-280.12	1.66-4.03	0.203-0.668	12
Belandria et al. (2010) [142]	16.44	10.40	279.1-289.9	2.96-13.06	0.264-0.73	11
Bouchafaa and Dalmazzone (2011) [143]	17.41	18.38	278.22-280.77	2.1-3.79	0.5	4
Belandria et al. (2011) [144]	4.29	7.01	273.6-284.2	1.51-7.19	0.081-0.694	40
Herri et al. (2011) [33]	1.18	2.54	277.15	2.36-3.55	0.11-0.64	4
Lee et al. (2012) [145]	1.39	3.94	274-278	1.53-3.65	0.109-0.808	12
Fan et al. (2013) [35]	3.32	3.41	276-286.6	2.85-9.22	0.33	5
Mohammadi et al. (2013) [146]	12.25	13.16	275.5-283.4	2.03-5.17	0.4029	4
Lee et al. (2013) [147]	2.90	3.17	273.4-285	1.46-6.69	0.4-0.8	18
Sabil et al. (2014) [37]	17.29	10.79	280.35-287.95	2.76-11.28	0.7249	5
Chapoy et al. (2014) [148]	10.86	15.62	276-286.95	1.82-19.97	0.941	7

Shi et al. (2014) [149]	4.11	1.56	280.9-286.8	4.07-8.55	0.5	6
Partoon et al. (2016) [150]	13.16	8.68	281.35-284.65	3.25-5.32	0.701	3
Zhang et al. (2016) [151]	1.15	4.23	273.7-276.4	1.45-3.1	0.09-0.79	6
Long et al. (2016) [47]	9.22	7.74	273.6-285.1	2.16-7.77	0.33	5
Sun et al. (2016) [113]	4.15	5.76	280.5-280.6	3.2	0.95	3
Le Quang et al. (2016) [44]	1.59	2.35	275.35-282.65	2.91-5.63	0.12-0.225	14
Kastanidis et al. (2017) [152]	5.36	3.21	274.3-289.2	2.63-12.55	0.0979-0.2492	15
Zang and Liang (2017) [153]	6.29	5.40	278.2-284.1	2.76-5.61	0.5	5
Sadeq et al. (2017) [52]	9.74	6.03	280.55-293.95	5.0-25	0.1-0.2	18
Belosludov et al. (2018) [154]	15.69	18.96	273-277	1.06-3.09	0.3-0.7	6
Mu and Solms (2018) [58]	5.33	1.61	279.9-286.37	3.381-7.935	0.503	6
Legoix et al. (2018) [155]	2.82	8.18	280.92-284.97	3.41-6.206	0.8996	3
Fan et al. (2019) [156]	2.47	3.47	278.68-286.46	4.33-10.06	0.08	5
Khan et al. (2019) [157]	3.75	3.09	275.2-285	1.98-6.52	0.5	4
Overall	**5.92**	**6.56**	**272.66-293.95**	**1.06-25**	**0.065-0.9652**	**366**

Table 4-S10. Database of CO_2-C_2H_6, CO_2-C_3H_8 and CO_2-iC_4H_{10} gas-mixture hydrate equilibria and comparison of the calculation accuracy yielded by the vdW-P model with the Kihara potential parameters optimized by different methods.

Mixtures	References	%AAD		*T* range (k)	*P* rang (MPa)	Molar fraction of component (1)	Data number
		Conventional method	New fitting procedure				
CO_2(1)-C_2H_6(2)	Adisasmito and Sloan (1992) [158]	8.78	3.45	273.5-287.8	0.5654-4.0817	0.189-0.967	40
	Fan and Guo (1999) [99]	2.47	6.74	276-282.7	1.58-3.9	0.9469	5
	Matsui et al. (2010) [159]	3.23	5.70	274.15-284.15	0.545-4.602	0.044-0.95	48
	Overall	**5.58**	**4.79**	**273.5-287.8**	**0.545-4.602**	**0.044-0.967**	**93**
CO_2(1)-C_3H_8(2)	Robinson and Mehta (1971) [79]	925.22	8.62	273.8-286.2	0.303-4.268	0.14-0.945	37
	Ng and Robinson (1976) [132]	265.53	7.66	273.9277-281.8167	0.303424-1.303344	0.16-0.94	13
	Adisasmito and Sloan (1992) [158]	489.81	14.02	273.7-282	0.2206-3.8207	0.099-0.99	55
	Babakhani et al. (2018) [160]	15.99	19.89	274.95-282.15	1.43-2.67	0.924-0.965	11
	Overall	**558.63**	**12.14**	**273.7-286.2**	**0.2206-4.268**	**0.099-0.99**	**116**
CO_2(1)-iC_4H_{10}(2)	Adisasmito and Sloan (1992) [158]	101.78	8.70	273.7-280.9	0.1448-3.1785	0.207-0.996	52

Table 4-S11. Database of CO_2-N_2 gas-mixture hydrate equilibria and comparison of the calculation accuracy yielded by the vdW-P model with the Kihara potential parameters optimized by different methods.

References	%AAD	*T* range (k)	*P* rang (MPa)

	Conventional method	New fitting procedure			Molar fraction of component CO_2	Data number
Olsen et al. (1999) [161]	6.82	9.11	273.4-281.9	1.986-9.55	0.162-0.7189	15
Fan and Guo (1999) [99]	4.58	6.66	273.1-280.2	1.22-3.09	0.9099-0.9652	9
Kang et al. (2001) [162]	17.84	12.60	272.85-284.25	1.565-24.12	0.0663-0.9659	28
Linga et al. (2007) [163]	11.45	3.77	273.7	1.6-7.7	0.169-0.83	3
Linga et al. (2007) [164]	0.31	3.81	273.7	7.7	0.139	1
Bruusgaard et al. (2008) [165]	7.31	9.51	275.3-283.1	2-22.4	0.162-0.787	24
Lu et al. (2009) [166]	12.02	8.10	275.35-278.15	10.48-13.68	0.159	5
Herri et al. (2011) [33]	9.38	22.60	273.4-281.1	5.3-6.6	0.16-0.59	16
Belandria et al. (2011) [144]	10.78	9.00	273.6-281.2	2.032-17.628	0.127-0.734	29
Sfaxi et al. (2012) [167]	19.86	12.48	278.1-285.3	3.24-29.92	0.271-0.812	9
Chapoy et al. (2014) [148]	6.74	6.99	276.91-283.64	2.05-5.72	0.954	4
Lee et al. (2014) [126]	14.97	7.05	275-281.1	8.23-24.51	0.1-0.2	17
Sun et al. (2015) [168]	24.73	12.47	273.4-278.4	5.28-17.53	0.101-0.251	17
Le Quang et al. (2016) [44]	14.31	9.24	275.61-279.9	2.46-3.38	0.667-0.768	6
Sun et al. (2016) [113]	5.04	1.29	276.15-278.15	2.08-2.675	0.85	9
Sadeq et al. (2017) [52]	10.07	20.78	275.75-284.45	5.0-20	0.26-0.36	10
Chazallon and Pirim (2018) [169]	8.85	6.75	273.25-278.25	3.6-16.4	0.009-0.449	30
Legoix et al. (2018) [155]	38.45	22.70	276.06-280.97	9.762-20.583	0.2317	4
Zang et al. (2019) [170]	13.08	4.37	273-277	2.5-4.2	0.5	9
Jarrahian and Nakhaee (2019) [116]	19.63	10.34	274.15-280.15	5.87-29.01	0.05-0.25	35
Overall	**13.26**	**10.35**	**272.85-285.3**	**1.22-29.92**	**0.009-0.9659**	**280**

Table 4-S12. Database of N_2-CH_4 and N_2-C_3H_8 gas-mixture hydrate equilibria and comparison of the calculation accuracy yielded by the vdW-P model with the Kihara potential parameters optimized by different methods.

Mixtures	References	%AAD		*T* range (k)	*P* rang (MPa)	Molar fraction of component (1)	Data number
		Conventional method	New fitting procedure				
N_2(1)-CH_4(2)	Jhaveri and Robinson (1965) [6]	11.91	11.39	273.2-295.2	3.62-35.96	0.127-0.94	63
	Mei et al. (1996) [16]	1.34	10.23	273.7-285.3	2.99-10.1	0.1074	8
	Lee at al. (2006) [171]	10.52	14.47	273.3-285.05	7.1-20.7	0.5961-0.7476	20
	Zhong and Englezos (2012) [172]	2.51	15.30	273.65-274.15	6.9-7.3	0.7	2
	Sadeq et al. (2017) [52]	6.37	7.10	277.8-292.75	5.0-25	0.1-0.36	23
	Nixdorf and Oellrich (1997) [18]	2.06	9.17	278.7-292.44	4.938-24.428	0.1074	6
	Overall	**9.24**	**10.94**	**273.2-295.2**	**2.99-35.96**	**0.1-0.94**	**122**

N_2(1)-C_3H_8(2)	Ng et al. (1977) [173]	21.44	23.44	274.2-289.2	0.256-18.09	0.25-0.9906	29

Table 4-S13. Database of complex gas-mixture hydrate equilibria adopted in this study and the calculation accuracy yielded by the vdW-P model with the Kihara potential parameters optimized by new fitting procedure against the vdW-P model with the Kihara potential parameters provided by Sloan and Koh [174] and Parrish and Prausnitz [175].

Guest gases	Structures	References	%AAD			T range (k)	P rang (MPa)	Data number
			New fitting procedure	Sloan and Koh	Parrish and Prausnitz			
CH_4-C_2H_6-C_3H_8	II	Sun et al. (2001) [176]	4.84	23.82	3.20	273.58-288.96	0.91-5.37	7
		Lee et al. (2013) [177]	12.12	12.28	20.85	276.1-289.3	0.84-5.28	7
CH_4-C_3H_8-iC_4H_{10}	II	Nixdorf and Oellrich (1997) [18]	3.33	24.04	22.72	277.1-298.14	1.198-24.474	13
		Paranjpe et al. (1989) [135]	8.21	24.72	82.42	276.2-281.2	0.2206-0.832	17
CH_4-CO_2-N_2	I,II	Kakati et al. (2015) [178]	10.39	9.33	11.32	284.5-289.34	8.75-11.23	6
		Sun et al. (2017) [179]	2.91	10.04	6.30	274.9-283.9	2.29-14.97	45
		Lim et al. (2017) [54]	3.02	7.14	3.84	279.6	4.81	30
		Zang and Liang (2018) [180]	3.58	8.17	5.27	276.2-286.3	2.59-8.84	34
CH_4-C_2H_6-CO_2	II	Le Quang et al. (2016) [44]	13.39	20.11	9.34	274.15-285.2	2.71-6.57	17
CH_4-C_3H_8-CO_2	II	Bishnoi and Dholabhai (1999) [181]	5.80	28.12	27.52	277.18-288.62	1.66-7.241	4
CH_4-C_3H_8-N_2	II	Smith et al. (2017) [48]	20.74	40.50	19.15	284.15-294.75	2.89-16.027	5
CH_4-iC_4H_{10}-N_2	II		3.31	35.72	63.22	286.35-295.85	3.191-14.963	4
CH_4-C_2H_6-N_2	II		7.00	17.70	29.26	277.36-294.23	2.575-23.833	7
CH_4-C_2H_6-CO_2-N_2	II	Nixdorf and Oellrich (1997) [18]	7.15	28.54	13.09	279.01-294.21	2.964-24.326	6
CH_4-C_3H_8-CO_2-N_2	II		5.17	21.37	21.61	279.19-296.07	1.693-23.565	6
CH_4-C_2H_6-C_3H_8-CO_2-N_2	II	Wilcox et al. (1941) [182]	7.37	29.60	5.49	277.7-296.7	1.6-27.5	16
CH_4-C_2H_6-C_3H_8-iC_4H_{10}-CO_2-N_2	II	Deaton and Frost (1946) [2]	15.82	36.25	41.35	273.7-294	0.6-10.439	95
	Overall		**7.89**	**23.21**	**23.70**	273.58-298.14	0.6-27.5	319

References

[1] O.L. Roberts, E.R. Brownscombe, L.S. Howe, Constitution diagrams and composition of methane and ethane hydrates, Oil Gas J. 39 (1940) 37-40.

[2] W.M. Deaton, E.M. Frost Jr., Gas hydrates and their relation to the operation of natural-gas pipe lines, U.S. Bureau of Mines Monograph 8 (1946).

[3] R. Kobayashi, D.L. Katz, Methane hydrate at high pressure, J. Pet. Technol. 1 (1949) 66-70, https://doi.org/10.2118/949066-G.

[4] H.O. McLeod, J.M. Campbell, Natural gas hydrates at pressures to 10,000 psia, J. Pet. Technol. 13 (1961) 590-594, https://doi.org/10.2118/1566-G-PA.

[5] D.R. Marshall, S. Saito, R. Kobayashi, Hydrates at high pressures: Part I. Methane-water, argon-water, and nitrogen-water systems, AIChE J. 10 (1964) 202-205, https://doi.org/10.1002/aic.690100214.

[6] J. Jhaveri, D.B. Robinson, Hydrates in the methane-nitrogen system, Can. J. Chem. Eng. 43 (1965) 75-78, https://doi.org/10.1002/cjce.5450430207.

[7] T.J. Galloway, W. Ruska, P.S. Chappelear, R. Kobayashi, Experimental measurement of hydrate numbers for methane and ethane and comparison with theoretical values, Ind. Eng. Chem. Fundam. 9 (1970) 237-243, https://doi.org/10.1021/i160034a008.

[8] V.K. Verma, Gas hydrates from liquid hydrocarbon-water systems, Ph.D. Thesis, Department of Chemical Engineering, University of Michigan, USA, 1974.

[9] J.L. De Roo, C.J. Peters, R.N. Lichtenthaler, G.A.M. Diepen, Occurrence of methane hydrate in saturated and unsaturated solutions of sodium chloride and water in dependence of temperature and pressure, AIChE J. 29 (1983) 651-657, https://doi.org/10.1002/aic.690290420.

[10] J.L. Thakore, G.D. Holder, Solid vapor azeotropes in hydrate-forming systems, Ind. Eng. Chem. Res. 26 (1987) 462-469, https://doi.org/10.1021/ie00063a011.

[11] K.Y. Song, R. Kobayashi, Measurement and interpretation of the water content of a methane-propane mixture in the gaseous state in equilibrium with hydrate, Ind. Eng. Chem. Fundam. 21 (1982) 391-395, https://doi.org/10.1021/i100008a013.

[12] S. Adisasmito, R.J. Frank, E.D. Sloan Jr., Hydrates of carbon dioxide and methane mixtures, Chem. Eng. Data, 36 (1991) 68-71, https://doi.org/10.1021/je00001a020.

[13] T. Svartas, F. Fadnes, Methane hydrate equilibrium data for the methane-water-methanol system up to 500 bara, in: The Second International Offshore and Polar Engineering Conference, San Francisco, California, USA, June 1992.

[14] M.J. Ross, L.S. Toczylkin, Hydrate dissociation pressures for methane or ethane in the presence of aqueous solutions of triethylene glycol, J. Chem. Eng. Data 37 (1992) 488-491, https://doi.org/10.1021/je00008a026.

[15] G.R. Dickens, M.S. Quinby-Hunt, Methane hydrate stability in seawater, Geophys. Res. Lett. 21 (1994) 2115-2118, https://doi.org/10.1029/94GL01858.

[16] D.H. Mei, J. Liao, J.T. Yang, T.M. Guo, Experimental and modeling studies on the hydrate formation of a methane + nitrogen gas mixture in the presence of aqueous electrolyte solutions, Ind. Eng. Chem. Res. 35 (1996) 4342-4347, https://doi.org/10.1021/ie9601662.

[17] Y. Dyadin, E. Aladko, Decomposition of the methane hydrate up to 10 Kbar, in: Second International Conference on Natural Gas Hydrates, Toulouse, France, June 1996.

[18] J. Nixdorf, L.R. Oellrich, Experimental determination of hydrate equilibrium conditions for pure gases, binary and ternary mixtures and natural gases, Fluid

Phase Equilib. 139 (1997) 325-333, https://doi.org/10.1016/S0378-3812(97)00141-6.

[19] S. Nakano, M. Moritoki, K. Ohgaki, High-pressure phase equilibrium and Raman microprobe spectroscopic studies on the methane hydrate system, J. Chem. Eng. Data 44 (1999) 254-257, https://doi.org/10.1021/je980152y.

[20] T. Maekawa, Equilibrium conditions for gas hydrates of methane and ethane mixtures in pure water and sodium chloride solution, Geochem. J. 35 (2001) 59-66, https://doi.org/10.2343/geochemj.35.59.

[21] M.D. Jager, E.D. Sloan, The effect of pressure on methane hydration in pure water and sodium chloride solutions, Fluid Phase Equilib. 185 (2001) 89-99, https://doi.org/10.1016/S0378-3812(01)00459-9.

[22] E.M. Freer, M.S. Selim, E.D. Sloan Jr., Methane hydrate film growth kinetics, Fluid Phase Equilib. 185 (2001) 65-75, https://doi.org/10.1016/S0378-3812(01)00457-5.

[23] S.O. Yang, S.H. Cho, H. Lee, C.S. Lee, Measurement and prediction of phase equilibria for water + methane in hydrate forming conditions, Fluid Phase Equilib. 185 (2001) 53-63, https://doi.org/10.1016/S0378-3812(01)00456-3.

[24] M. Clarke, P.R. Bishnoi, Determination of the activation energy and intrinsic rate constant of methane gas hydrate decomposition, Can. J. Chem. Eng. 79 (2001) 143-147, https://doi.org/10.1002/cjce.5450790122.

[25] M. Kharrat, D. Dalmazzone, Experimental determination of stability conditions of methane hydrate in aqueous calcium chloride solutions using high pressure differential scanning calorimetry, J. Chem. Thermodyn. 35 (2003) 1489-1505, https://doi.org/10.1016/S0021-9614(03)00121-6.

[26] T. Nakamura, T. Makino, T. Sugahara, K. Ohgaki, Stability boundaries of gas hydrates helped by methane—structure-H hydrates of methylcyclohexane and cis-1,2-dimethylcyclohexane, Chem. Eng. Sci. 58 (2003) 269-273, https://doi.org/10.1016/S0009-2509(02)00518-3.

[27] A.H. Mohammadi, R. Anderson, B. Tohidi, Carbon monoxide clathrate hydrates: Equilibrium data and thermodynamic modeling, AIChE J. 51 (2005) 2825-2833, https://doi.org/10.1002/aic.10526.

[28] P. Gayet, C. Dicharry, G. Marion, A. Graciaa, J. Lachaise, A. Nesterov, Experimental determination of methane hydrate dissociation curve up to 55 MPa by using a small amount of surfactant as hydrate promoter, Chem. Eng. Sci. 60 (2005) 5751-5758, https://doi.org/10.1016/j.ces.2005.04.069.

[29] S. Circone, S.H. Kirby, L.A. Stern, Direct measurement of methane hydrate composition along the hydrate equilibrium boundary, J. Phys. Chem. B 109 (2005) 9468-9475, https://doi.org/10.1021/jp0504874.

[30] A. Gupta, J. Lachance, E.D. Sloan Jr., C.A. Koh, Measurements of methane hydrate heat of dissociation using high pressure differential scanning calorimetry, Chem. Eng. Sci. 63 (2008) 5848-5853, https://doi.org/10.1016/j.ces.2008.09.002.

[31] K. Yasuda, R. Ohmura, Phase equilibrium for clathrate hydrates formed with methane, ethane, propane, or carbon dioxide at temperatures below the freezing

point of water, J. Chem. Eng. Data, 53 (2008) 2182-2188, https://doi.org/10.1021/je800396v.

[32] N.J. Kim, J.H. Lee, Y.S. Cho, W. Chun, Formation enhancement of methane hydrate for natural gas transport and storage, Energy 35 (2010) 2717-2722, https://doi.org/10.1016/j.energy.2009.07.020.

[33] J.M. Herri, A. Bouchemoua, M. Kwaterski, A. Fezoua, Y. Ouabbas, A. Cameirao, Gas hydrate equilibria for CO_2-N_2 and CO_2-CH_4 gas mixtures—Experimental studies and thermodynamic modelling, Fluid Phase Equilib. 301 (2011) 171-190, https://doi.org/10.1016/j.fluid.2010.09.041.

[34] J. Javanmardi, S. Babaee, A. Eslamimanesh, A.H. Mohammadi, Experimental measurements and predictions of gas hydrate dissociation conditions in the presence of methanol and ethane-1,2-diol aqueous solutions, J. Chem. Eng. Data 57 (2012) 1474-1479, https://doi.org/10.1021/je2013846.

[35] S. Fan, Q. Li, J. Nie, X. Lang, Y. Wen, Y. Wang, Semiclathrate hydrate phase equilibrium for CO_2/CH_4 gas mixtures in the presence of tetrabutylammonium halide (bromide, chloride, or fluoride), J. Chem. Eng. Data 58 (2013) 3137-3141, https://doi.org/10.1021/je4005933.

[36] N.A. Sami, K. Das, J.S. Sangwai, N. Balasubramanian, Phase equilibria of methane and carbon dioxide clathrate hydrates in the presence of (methanol + $MgCl_2$) and (ethylene glycol + $MgCl_2$) aqueous solutions, J. Chem. Thermodyn. 65 (2013) 198-203, https://doi.org/10.1016/j.jct.2013.05.050.

[37] K.M. Sabil, Q. Nasir, B. Partoon, A.A. Seman, Measurement of H-L_W-V and dissociation enthalpy of carbon dioxide rich synthetic natural gas mixtures, J. Chem. Eng. Data 59 (2014) 3502-3509, https://doi.org/10.1021/je500453j.

[38] E.O. Obanijesu, A. Barifcani, V.K. Pareek, M.O. Tade, Experimental study on feasibility of H_2 and N_2 as hydrate inhibitors in natural gas pipelines, J. Chem. Eng. Data 59 (2014) 3756-3766, https://doi.org/10.1021/je500633u.

[39] K.M. Sabil, O. Nashed, B. Lal, L. Ismail, A. Japper-Jaafar, Experimental investigation on the dissociation conditions of methane hydrate in the presence of imidazolium-based ionic liquids, J. Chem. Thermodyn. 84 (2015) 7-13, https://doi.org/10.1016/j.jct.2014.12.017.

[40] Z. Long, X. Zhou, X. Shen, D. Li, D. Liang, Phase equilibria and dissociation enthalpies of methane hydrate in imidazolium ionic liquid aqueous solutions, Ind. Eng. Chem. Res. 54 (2015) 11701-11708, https://doi.org/10.1021/acs.iecr.5b03480.

[41] D. Mech, G. Pandey, J.S. Sangwai, Effect of molecular weight of polyethylene glycol on the equilibrium dissociation pressures of methane hydrate system, J. Chem. Eng. Data 60 (2015) 1878-1885, https://doi.org/10.1021/acs.jced.5b00088.

[42] Z.T. Ward, C.E. Deering, R.A. Marriott, A.K. Sum, E.D. Sloan, C.A. Koh, Phase equilibrium data and model comparisons for H_2S hydrates, J. Chem. Eng. Data 60 (2015) 403-408, https://doi.org/doi.org/10.1021/je500657f.

[43] Z. Long, X. Zhou, D. Liang, D. Li, Experimental study of methane hydrate equilibria in [EMIM]-NO_3 aqueous solutions, J. Chem. Eng. Data 60 (2015) 2728-2732, https://doi.org/10.1021/acs.jced.5b00435.

[44] D. Le Quang, B. Bouillot, J.M. Herri, P. Glenat, P. Duchet-Suchaux, Experimental procedure and results to measure the composition of gas hydrate, during crystallization and at equilibrium, from N_2-CO_2-CH_4-C_2H_6-C_3H_8-C_4H_{10} gas mixtures, Fluid Phase Equilib. 413 (2016) 10-21, https://doi.org/10.1016/j.fluid.2015.10.022.

[45] P. Kastanidis, G.E. Romanos, V.K. Michalis, I.G. Economou, A.K. Stubos, I.N. Tsimpanogiannis, Development of a novel experimental apparatus for hydrate equilibrium measurements, Fluid Phase Equilib. 424 (2016) 152-161, https://doi.org/10.1016/j.fluid.2015.12.036.

[46] H. Pahlavanzadeh, M. Khanlarkhani, A.H. Mohammadi, Clathrate hydrate formation in (methane, carbon dioxide or nitrogen + tetrahydropyran or furan + water) system: Thermodynamic and kinetic study, J. Chem. Thermodyn. 92 (2016) 168-174, https://doi.org/10.1016/j.jct.2015.08.034.

[47] X. Long, Y. Wang, X. Lang, S. Fan, J. Chen, Hydrate equilibrium measurements for CH_4, CO_2, and CH_4 + CO_2 in the presence of tetra-n-butyl ammonium bromide, J. Chem. Eng. Data 61 (2016) 3897-3901, https://doi.org/10.1021/acs.jced.6b00641.

[48] C. Smith, D. Pack, A. Barifcani, Propane, n-butane and i-butane stabilization effects on methane gas hydrates, J. Chem. Thermodyn. 115 (2017) 293-301, https://doi.org/10.1016/j.jct.2017.08.013.

[49] N. Mannar, C.B. Bavoh, A.H. Baharudin, B. Lal, N.B. Mellon, Thermophysical properties of aqueous lysine and its inhibition influence on methane and carbon dioxide hydrate phase boundary condition, Fluid Phase Equilib. 454 (2017) 57-63, https://doi.org/10.1016/j.fluid.2017.09.012.

[50] A. Kamari, H. Hashemi, S. Babaee, A.H. Mohammadi, D. Ramjugernath, Phase stability conditions of carbon dioxide and methane clathrate hydrates in the presence of KBr, $CaBr_2$, $MgCl_2$, HCOONa, and HCOOK aqueous solutions: Experimental measurements and thermodynamic modelling, J. Chem. Thermodyn. 115 (2017) 30-317, https://doi.org/10.1016/j.jct.2017.07.030.

[51] M.S. Khan, B. Partoon, C.B. Bavoh, B. Lal, N.B. Mellon, Influence of tetramethylammonium hydroxide on methane and carbon dioxide gas hydrate phase equilibrium conditions, Fluid Phase Equilib. 440 (2017) 1-8, https://doi.org/10.1016/j.fluid.2017.02.011.

[52] D. Sadeq, S. Iglauer, M. Lebedev, C. Smith, A. Barifcani, Experimental determination of hydrate phase equilibrium for different gas mixtures containing methane, carbon dioxide and nitrogen with motor current measurements, J. Nat. Gas. Sci. Eng. 38 (2017) 59-73, https://doi.org/10.1016/j.jngse.2016.12.025.

[53] C.B. Bavoh, B. Partoon, B. Lal, L.K. Keong, Methane hydrate-liquid-vapour-equilibrium phase condition measurements in the presence of natural amino acids, J. Nat. Gas Sci. Eng. 37 (2017) 425-434, https://doi.org/10.1016/j.jngse.2016.11.061.

[54] D. Lim, H. Ro, Y. Seo, Y. Seo, J.Y. Lee, S.J. Kim, J. Lee, H. Lee, Thermodynamic stability and guest distribution of CH_4/N_2/CO_2 mixed hydrates for methane hydrate production using N_2/CO_2 injection, J. Chem. Thermodyn. 106 (2017) 16-21, https://doi.org/10.1016/j.jct.2016.11.012.

[55] O. Nashed, D. Dadebayev, M.S. Khan, C.B. Bavoh, B. Lal, A.M. Shariff, Experimental and modelling studies on thermodynamic methane hydrate inhibition in the presence of ionic liquids, J. Mol. Liq. 249 (2018) 886-891, https://doi.org/10.1016/j.molliq.2017.11.115.

[56] C.B. Bavoh, M.S. Khan, B. Lal, N.I.B.A. Ghaniri, K.M. Sabil, New methane hydrate phase boundary data in the presence of aqueous amino acids, Fluid Phase Equilib. 478 (2018) 129-133, https://doi.org/10.1016/j.fluid.2018.09.011.

[57] S. Sun, J. Zhao, D. Yu, Dissociation enthalpy of methane hydrate in salt solution, Fluid Phase Equilib. 456 (2018) 92-97, https://doi.org/10.1016/j.fluid.2017.10.013.

[58] L. Mu, N. von Solms, Hydrate thermal dissociation behavior and dissociation enthalpies in methane-carbon dioxide swapping process, J. Chem. Thermodyn. 117 (2018) 33-42, https://doi.org/10.1016/j.jct.2017.08.018.

[59] K. Xiao, C. Zou, Y. Yang, H. Zhang, H. Li, Z. Qin, A preliminary study of the gas hydrate stability zone in a gas hydrate potential region of China, Energy Sci. Eng. 8 (2020) 1080-1091, https://doi.org/10.1002/ese3.569.

[60] D.E.S. de Menezes, P.A.P. Filho, M.D.R. Fuentes, Phase equilibrium for methane, ethane and carbon dioxide hydrates at pressures up to 100 MPa through high-pressure microcalorimetry: Experimental data, analysis and modeling, Fluid Phase Equilib. 518 (2020) 112590, https://doi.org/10.1016/j.fluid.2020.112590.

[61] M. Aghajanloo, Z. Taheri, T.J. Behbahani, A.H. Mohammadi, M.R. Ehsani, H. Heydarian, Experimental determination and thermodynamic modeling of clathrate hydrate stability conditions in methane + hydrogen sulfide + water system, J. Nat. Gas Sci. Eng. 83 (2020) 103549, https://doi.org/10.1016/j.jngse.2020.103549.

[62] H. Pahlavanzadeh, H. Hassan, M. Pourranjbar, Hydrate dissociation conditions of CH_4 in the presence of $TBANO_3$ and cyclopentane promoter mixture: Thermodynamic modeling and experimental measurement, J. Chem. Eng. Data 65 (2020) 1927-1935, https://doi.org/10.1021/acs.jced.9b01108.

[63] B.J. Falabella, A study of natural gas hydrates, Ph.D. Thesis, University of Massachusetts, USA, 1975.

[64] T.Y. Makogon, E.D. Sloan Jr., Phase equilibrium for methane hydrate from 190 to 262 K, J. Chem. Eng. Data 39 (1994) 351-353, https://doi.org/10.1021/je00014a035.

[65] H.D. Nagashima, R. Ohmura, Phase equilibrium condition measurements in methane clathrate hydrate forming system from 197.3 K to 238.7 K, J. Chem. Thermodyn. 102 (2016) 252-256, https://doi.org/10.1016/j.jct.2016.07.018.

[66] H.H. Reamer, F.T. Selleck, B.H. Sage, Some properties of mixed paraffinic and olefinic hydrates, J. Pet. Technol. 4 (1952) 197-202, https://doi.org/10.2118/952197-G.

[67] G.D. Holder, G.C. Grigoriou, Hydrate dissociation pressures of (methane + ethane + water) existence of a locus of minimum pressures, J. Chem. Thermodyn. 12 (1980) 1093-1104, https://doi.org/10.1016/0021-9614(80)90166-4.

[68] G.D. Holder, J.H. Hand, Multiple-phase equilibria in hydrates from methane, ethane, propane and water mixtures, AIChE J. 28 (1982) 440-447, https://doi.org/10.1002/aic.690280312.

[69] D. Avlonitis, Multiphase equilibria in oil-water hydrate forming systems, M.Sc. Thesis, Heriot-Watt University, Edinburgh, Scotland, 1988.

[70] P. Englezos, P.R. Bishnoi, Experimental study on the equilibrium ethane hydrate formation conditions in aqueous electrolyte solutions, Ind. Eng. Chem. Res. 30 (1991) 1655-1659, https://doi.org/10.1021/ie00055a038.

[71] A.H. Mohammadi, W. Afzal, D. Richon, Experimental data and predictions of dissociation conditions for ethane and propane simple hydrates in the presence of distilled water and methane, ethane, propane, and carbon dioxide simple hydrates in the presence of ethanol aqueous solutions, J. Chem. Eng. Data 53 (2008) 73-76, https://doi.org/10.1021/je700383p.

[72] Z. Long, J.W. Du, D.L. Li, D.Q. Liang, Phase equilibria of ethane hydrate in $MgCl_2$ aqueous solutions, J. Chem. Eng. Data 55 (2010) 2938-2941, https://doi.org/10.1021/je901039m.

[73] M. Mottahedin, F. Varaminian, K. Mafakheri, Modeling of methane and ethane hydrate formation kinetics based on non-equilibrium thermodynamics, J. Non-Equilib. Thermodyn. 36 (2011) 3-22, https://doi.org/10.1515/jnetdy.2011.002.

[74] H.J. Ng, D.B. Robinson, Hydrate formation in systems containing methane, ethane, propane, carbon dioxide or hydrogen sulfide in the presence of methanol, Fluid Phase Equilib. 21 (1985) 145-155, https://doi.org/10.1016/0378-3812(85)90065-2.

[75] S. Nakano, K. Yamamoto, K. Ohgaki, Natural gas exploitation by carbon dioxide from gas hydrate fields—high-pressure phase equilibrium for an ethane hydrate system, Proc. Inst. Mech. Eng. A-J. Pow. 212 (1998) 159-163, https://doi.org/10.1243/0957650981536826.

[76] K. Morita, S. Nakano, K. Ohgaki, Structure and stability of ethane hydrate crystal, Fluid Phase Equilib. 169 (2000) 167-175, https://doi.org/10.1016/S0378-3812(00)00320-4.

[77] B.J. Falabella, M. Vanpee, Experimental determination of gas hydrate equilibrium below the ice point, Ind. Eng. Chem. Fundamen. 13 (1974) 228-231, https://doi.org/10.1021/i160051a012.

[78] B. Miller, E.R. Strong, Hydrate storage of natural gas, Am. Gas Assoc. Mon. 28 (1946) 63-67.

[79] D.B. Robinson, B.R. Metha, Hydrates in the propane-carbon dioxide-water system, J. Can. Pet. Technol. 10 (1971) 33-35, https://doi.org/10.2118/71-01-04.

[80] H. Kubota, K. Shimizu, Y. Tanaka, T. Makita, Thermodynamic properties of R13 ($CCIF_3$), R23 (CHF_3), R152A ($C_2H_4F_2$), and propane hydrates for desalination of sea water, J. Chem. Eng. Japan 17 (1984) 423-429, https://doi.org/10.1252/jcej.17.423.

[81] S.L. Patil, Measurements of multiphase gas hydrates phase equilibria: Effect of inhibitors and heavier hydrocarbon components, M.Sc. Thesis, University of Alaska, Anchorage, Alaska, USA, 1987.

[82] P.R. Bishnoi, P.D. Dholabhai, Experimental study on propane hydrate equilibrium conditions in aqueous electrolyte solutions, Fluid Phase Equilib. 83 (1993) 455-462, https://doi.org/10.1016/0378-3812(93)87050-B.

[83] P. Englezos, Y.T. Ngan, Incipient equilibrium data for propane hydrate formation in aqueous solutions of sodium chloride, potassium chloride and calcium chloride, J. Chem. Eng. Data 38 (1993) 250-253, https://doi.org/10.1021/je00010a017.

[84] M.M. Mooijer-van den Heuvel, C.J. Peters, J. de Swaan Arons, Gas hydrate phase equilibria for propane in the presence of additive components, Fluid Phase Equilib. 193 (2002) 245-259, https://doi.org/10.1016/S0378-3812(01)00757-9.

[85] G.D. Holder, S.P. Godbole, Measurement and prediction of dissociation pressures of isobutane and propane hydrates below the ice point, AIChE J. 28 (1982) 930-934, https://doi.org/10.1002/aic.690280607.

[86] A.H. Mohammadi, D. Richon, Clathrate hydrate phase equilibria for carbonyl sulfide, hydrogen sulfide, ethylene, or propane + water system below water freezing point, Chem. Eng. Commun. 200 (2013) 1635-1644, https://doi.org/10.1080/00986445.2012.757550.

[87] G.R. Schneider, J. Farrar, Nucleation and growth of ice crystals, U.S. Dept. of Interior, Office of Saline Water, Research Development Report, No. 292, 1968.

[88] O.S. Rouher, A.J. Barduhn, Hydrates of iso- and normal butane and their mixtures, Desalination 6 (1969) 57-73, https://doi.org/10.1016/S0011-9164(00)80011-9.

[89] V.M. Buleiko, B.A. Grigoriev, J. Mendoza, Calorimetric investigation of hydrates of pure isobutane and iso- and normal butane mixtures, Fluid Phase Equilib. 462 (2018) 14-24, https://doi.org/10.1016/j.fluid.2018.01.012.

[90] C.H. Unruh, D.L. Katz, Gas hydrates of carbon dioxide-methane mixtures, J. Pet. Technol. 1 (1949) 83-86, https://doi.org/10.2118/949983-G.

[91] S.D. Larson, Phase studies of the two-component carbon dioxide-water system involving the carbon dioxide hydrate, Ph.D. Thesis, University of Illinois, USA, 1955.

[92] J.G. Vlahakis, H.S. Chen, M.S. Suwandi, A.J. Barduhn, The growth rate of ice crystals: Properties of carbon dioxide hydrate, a review of properties of 51 gas hydrates, Syracuse U, Research and Development Report, No. 830, 1972.

[93] K. Ohgaki, Y. Makihara, K. Takano, Formation of CO_2 hydrate in pure and sea waters, J. Chem. Eng. Japan 26 (1993) 558-564, https://doi.org/10.1252/jcej.26.558.

[94] P.D. Dholabhai, N. Kalogerakis, P.R. Bishnoi, Equilibrium conditions for carbon dioxide hydrate formation in aqueous electrolyte solutions, J. Chem. Eng. Data 38 (1993) 650-654, https://doi.org/10.1021/je00012a045.

[95] P. Englezos, S. Hall, Phase equilibrium data on carbon dioxide hydrate in the presence of electrolytes, water soluble polymers and montmorillonite, Can. J. Chem. Eng. 72 (1994) 887-893, https://doi.org/10.1002/cjce.5450720516.

[96] P.D. Dholabhai, J.S. Parent, P.R. Bishnoi, Carbon dioxide hydrate equilibrium conditions in aqueous solutions containing electrolytes and methanol using a new apparatus, Ind. Eng. Chem. Res. 35 (1996) 819-823, https://doi.org/10.1021/ie950136j.

[97] E. Breland, P. Englezos, Equilibrium hydrate formation data for carbon dioxide in aqueous glycerol solutions, J. Chem. Eng. Data 41 (1996) 11-13, https://doi.org/10.1021/je950181y.

[98] P.D. Dholabhai, J.S. Parent, P.R. Bishnoi, Equilibrium conditions for hydrate formation from binary mixtures of methane and carbon dioxide in the presence of electrolytes, methanol and ethylene glycol, Fluid Phase Equilib. 141 (1997) 235-246, https://doi.org/10.1016/S0378-3812(97)00214-8.

[99] S.S. Fan, T.M. Guo, Hydrate formation of CO_2-rich binary and quaternary gas mixtures in aqueous sodium chloride solutions, J. Chem. Eng. Data 44 (1999) 829-832, https://doi.org/10.1021/je990011b.

[100] M. Wendland, H. Hasse, G. Maurer, Experimental pressure−temperature data on three- and four-phase equilibria of fluid, hydrate, and ice phases in the system carbon dioxide−water, J. Chem. Eng. Data 44 (1999) 901-906, https://doi.org/10.1021/je980208o.

[101] S.S. Fan, G.J. Chen, Q.L. Ma, T.M. Guo, Experimental and modeling studies on the hydrate formation of CO_2 and CO_2-rich gas mixtures, Chem. Eng. J. 78 (2000) 173-178, https://doi.org/10.1016/S1385-8947(00)00157-1.

[102] M.M. Mooijer-van den Heuvel, R. Witteman, C.J. Peters, Phase behaviour of gas hydrates of carbon dioxide in the presence of tetrahydropyran, cyclobutanone, cyclohexane and methylcyclohexane, Fluid Phase Equilib. 182 (2001) 97-110, https://doi.org/10.1016/S0378-3812(01)00384-3.

[103] G.K. Anderson, Enthalpy of dissociation and hydration number of carbon dioxide hydrate from the Clapeyron equation, J. Chem. Thermodyn. 35 (2003) 1171-1183, https://doi.org/10.1016/S0021-9614(03)00093-4.

[104] L. Chen, C. Sun, G. Chen, Y. Nie, Z. Sun, Y. Liu, Measurements of hydrate equilibrium conditions for CH_4, CO_2, and $CH_4 + C_2H_6 + C_3H_8$ in various systems by step-heating method, Chinese J. Chem. Eng. 17 (2009) 635-641, https://doi.org/10.1016/S1004-9541(08)60256-6.

[105] K.M. Sabil, G.J. Witkamp, C.J. Peters, Estimations of enthalpies of dissociation of simple and mixed carbon dioxide hydrates from phase equilibrium data, Fluid Phase Equilib. 290 (2010) 109-114, https://doi.org/10.1016/j.fluid.2009.07.006.

[106] L. Ruffine, J.P.M. Trusler, Phase behaviour of mixed-gas hydrate systems containing carbon dioxide, J. Chem. Thermodyn. 42 (2010) 605-611, https://doi.org/10.1016/j.jct.2009.11.019.

[107] T. Maekawa, Equilibrium conditions for carbon dioxide hydrates in the presence of aqueous solutions of alcohols, glycols, and glycerol, J. Chem. Eng. Data 55 (2010) 1280-1284, https://doi.org/10.1021/je900626y.

[108] V.P. Melnikov, A.N. Nesterov, A.M. Reshetnikov, V.A. Istomin, Metastable states during dissociation of carbon dioxide hydrates below 273 K, Chem. Eng. Sci. 66 (2011) 73-77, https://doi.org/10.1016/j.ces.2010.10.007.

[109] Z.C. Xu, D.Q. Liang, Equilibrium data of (tert-butylamine + CO_2) and (tert-butylamine + N_2) clathrate hydrates, J. Chem. Eng. Data 59 (2014) 476-480, https://doi.org/10.1021/je400922j.

[110] T. Maekawa, Equilibrium conditions for clathrate hydrates formed from carbon dioxide or ethane in the presence of aqueous solutions of 1,4-dioxane and 1,3-dioxolane, Fluid Phase Equilib. 384 (2014) 95-99, https://doi.org/10.1016/j.fluid.2014.10.032.

[111] P. Ilani-Kashkouli, A.H. Mohammadi, P. Naidoo, D. Ramjugernath, Thermodynamic stability conditions for semi-clathrate hydrates of CO_2, CH_4, or N_2 with tetrabutyl ammonium nitrate ($TBANO_3$) aqueous solution, J. Chem. Thermodyn. 96 (2016) 52-56, https://doi.org/10.1016/j.jct.2015.11.030.

[112] Y. Yu, S. Zhou, X. Li, S. Wang, Effect of graphite nanoparticles on CO_2 hydrate phase equilibrium, Fluid Phase Equilib. 414 (2016) 23-28, https://doi.org/10.1016/j.fluid.2015.12.054.

[113] D. Sun, J. Ripmeester, P. Englezos, Phase equilibria for the $CO_2/CH_4/N_2/H_2O$ system in the hydrate region under conditions relevant to storage of CO_2 in depleted natural gas reservoirs, J. Chem. Eng. Data 61 (2016) 4061-4067, https://doi.org/10.1021/acs.jced.6b00547.

[114] P.F. Ferrari, A.Z. Guembaroski, M.A.M. Neto, R.E.M. Morales, A.K. Sum, Experimental measurements and modelling of carbon dioxide hydrate phase equilibrium with and without ethanol, Fluid Phase Equilib. 413 (2016) 176-183, https://doi.org/10.1016/j.fluid.2015.10.008.

[115] Y. Nema, R. Ohmura, I. Senaha, K. Yasuda, Quadruple point determination in carbon dioxide hydrate forming system, Fluid Phase Equilib. 441 (2017) 49-53, https://doi.org/10.1016/j.fluid.2016.12.014.

[116] A. Jarrahian, A. Nakhaee, Hydrate-liquid-vapor equilibrium condition of N_2+CO_2+H_2O system: Measurement and modeling, Fuel 237 (2019) 769-774, https://doi.org/10.1016/j.fuel.2018.10.017.

[117] P. Ilani-Kashkouli, H. Hashemi, A. Basdeo, P. Naidoo, D. Ramjugernath, Hydrate dissociation data for the systems (CO_2/CH_4/Ar) + water with (TBAF/TBAA/TBPB/$TBANO_3$ and cyclopentane), J. Chem. Eng. Data 64 (2019) 2542-2549, https://doi.org/10.1021/acs.jced.8b01195.

[118] J.M. Chima-Maceda, P. Esquivel-Mora, A. Pimentel-Rodas, L.A. Galicia-Luna, J.J. Castro-Arellano, Effect of 1-propanol and TBAB on gas hydrates dissociation conditions for CO_2 + hexane + water systems, J. Chem. Eng. Data 64 (2019) 4775-4780, https://doi.org/10.1021/acs.jced.9b00158.

[119] M.L. Dai, Z.G. Sun, J. Li, C.M. Li, H.F. Huang, Effect of n-dodecane on equilibrium dissociation conditions of carbon dioxide hydrate, J. Chem. Thermodyn. 148 (2020) 106144, https://doi.org/10.1016/j.jct.2020.106144.

[120] S.L. Miller, W.D. Smythe, Carbon dioxide clathrate in the martian ice cap, Science 170 (1970) 531-533, https://doi.org/10.1126/science.170.3957.531.

[121] S. Takenouchi, G.C. Kennedy, Dissociation pressures of the phase $CO_2 \cdot 5\ 3/4\ H_2O$, J. Geol. 73 (1965) 383-390, https://doi.org/10.1086/627068.

[122] S. Nakano, M. Moritoki, K. Ohgaki, High-pressure phase equilibrium and Raman microprobe spectroscopic studies on the CO_2 hydrate system, J. Chem. Eng. Data 43 (1998) 807-810, https://doi.org/10.1021/je9800555.

[123] A. van Cleeff, G.A.M. Diepen, Gas hydrates of nitrogen and oxygen, Rec. Trav. Chim. 79 (1960) 582-586, https://doi.org/10.1002/recl.19600790606.

[124] K. Sugahara, Y. Tanaka, T. Sugahara, K. Ohgaki, Thermodynamic stability and structure of nitrogen hydrate crystal, J. Supramol. Chem. 2 (2002) 365-368, https://doi.org/10.1016/S1472-7862(03)00060-1.

[125] A.H. Mohammadi, B. Tohidi, R.W. Burgass, Equilibrium data and thermodynamic modeling of nitrogen, oxygen, and air clathrate hydrates, J. Chem. Eng. Data 48 (2003) 612-616, https://doi.org/10.1021/je025608x.

[126] Y. Lee, S. Lee, J. Lee, Y. Seo, Structure identification and dissociation enthalpy measurements of the CO_2 + N_2 hydrates for their application to CO_2 capture and storage, Chem. Eng. J. 246 (2014) 20-26, https://doi.org/10.1016/j.cej.2014.02.045.

[127] S. Subramanian, R.A. Kini, S.F. Dec, E.D. Sloan Jr., Evidence of structure II hydrate formation from methane-ethane mixtures, Chem. Eng. Sci. 55 (2000) 1981-1999, https://doi.org/10.1016/S0009-2509(99)00389-9.

[128] R. Kumar, P. Linga, I. Moudrakovski, J.A. Ripmeester, P. Englezos, Structure and kinetics of gas hydrates from methane/ethane/propane mixtures relevant to the design of natural gas hydrate storage and transport facilities, AIChE J. 54 (2008) 2132-2144, https://doi.org/10.1002/aic.11527.

[129] S. Hashimoto, A. Sasatani, Y. Matsui, T. Sugahara, K. Ohgaki, Isothermal phase equilibria for methane + ethane + water ternary system containing gas hydrates, Open Thermodyn. J. 2 (2008) 100-105, https://doi.org/10.2174/1874396X00802010100.

[130] D.E.S. de Menezes, A.K. Sum, A. Desmedt, P.A.P. Filho, M.D.R. Fuentes, Coexistence of sI and sII in methane-propane hydrate former systems at high pressures, Chem. Eng. Sci. 208 (2019) 115149, https://doi.org/10.1016/j.ces.2019.08.007.

[131] B.J. Wu, D.B. Robinson, H.J. Ng, Three- and four-phase hydrate forming conditions in methane + isobutane + water, J. Chem. Thermodyn. 8 (1976) 461-469, https://doi.org/10.1016/0021-9614(76)90067-7.

[132] H.J. Ng, D.B. Robinson, The measurement and prediction of hydrate formation in liquid hydrocarbon-water systems, Ind. Eng. Chem. Fundamen. 15 (1976) 293-298, https://doi.org/10.1021/i160060a012.

[133] M.M. Mooijer-van den Heuvel, Phase behaviour and structural aspects of ternary clathrate hydrate systems. The role of additives, Ph.D. Thesis, Chemical Engineering, Delft University of Technology, Netherlands, 2004.

[134] G.D. Holder, V.A. Kamath, Hydrates of (methane + cis-2-butene) and (methane + trans-2-butene), J. Chem. Thermodyn. 16 (1984) 399-400, https://doi.org/10.1016/0021-9614(84)90179-4.

[135] S.G. Paranjpe, S.L. Patil, V.A. Kamath, S.P. Godbole, Hydrate equilibria for binary and ternary mixtures of methane, propanes isobutane, and n-butane: Effect of salinity, SPE Res. Eng. 4 (1989) 446-454, https://doi.org/10.2118/16871-PA.

[136] P.D. Dholabhai, P.R. Bishnoi, Hydrate equilibrium conditions in aqueous electrolyte solutions: Mixtures of methane and carbon dioxide, J. Chem. Eng. Data 39 (1994) 191-194, https://doi.org/10.1021/je00013a054.

[137] K. Ohgaki, K. Takano, H. Sangawa, T. Matsubara, S. Nakano, Methane exploitation by carbon dioxide from gas hydrates—Phase equilibria for CO_2-CH_4 mixed hydrate system, J. Chem. Eng. Japan 29 (1996) 478-483, https://doi.org/10.1252/jcej.29.478.

[138] P. Servio, F. Lagers, C. Peters, P. Englezos, Gas hydrate phase equilibrium in the system methane-carbon dioxide-neohexane and water, Fluid Phase Equilib. 158-160 (1999) 795-800, https://doi.org/10.1016/S0378-3812(99)00084-9.

[139] Y.T. Seo, S.P. Kang, H. Lee, C.S. Lee, W.M. Sung, Hydrate phase equilibria for gas mixtures containing carbon dioxide: A proof-of-concept to carbon dioxide recovery from multicomponent gas stream, Korean J. Chem. Eng. 17 (2000) 659-667, https://doi.org/10.1007/BF02699114.

[140] J.G. Beltran, P. Servio, Equilibrium studies for the system methane + carbon dioxide + neohexane + Water, J. Chem. Eng. Data 53 (2008) 1745-1749, https://doi.org/10.1021/je800066q.

[141] H. Bruusgaard, J.G. Beltran, P. Servio, Solubility measurements for the CH_4 + CO_2 + H_2O system under hydrate-liquid-vapor equilibrium, Fluid Phase Equilib. 296 (2010) 106-109, https://doi.org/10.1016/j.fluid.2010.02.042.

[142] V. Belandria, A.H. Mohammadi, D. Richon, Phase equilibria of clathrate hydrates of methane + carbon dioxide: New experimental data and predictions, Fluid Phase Equilib. 296 (2010) 60-65, https://doi.org/10.1016/j.fluid.2010.03.038.

[143] W. Bouchafaa, D. Dalmazzone, Thermodynamic equilibrium data for mixed hydrates of CO_2-N_2, CO_2-CH_4 and CO_2-H_2 in pure water and TBAB solutions, in: 7th International Conference on Gas Hydrates, Edinburgh, United Kingdom, July 2011.

[144] V. Belandria, A. Eslamimanesh, A.H. Mohammadi, P. Theveneau, H. Legendre, D. Richon, Compositional analysis and hydrate dissociation conditions measurements for carbon dioxide + methane + water system, Ind. Eng. Chem. Res. 50 (2011) 5783-5794, https://doi.org/10.1021/ie101959t.

[145] Y.J. Lee, T. Kawamura, Y. Yamamoto, J.H. Yoon, Phase equilibrium studies of tetrahydrofuran (THF) + CH_4, THF + CO_2, CH_4 + CO_2, and THF + CO_2 + CH_4 hydrates, J. Chem. Eng. Data 57 (2012) 3543-3548, https://doi.org/10.1021/je300850q.

[146] A.H. Mohammadi, A. Eslamimanesh, D. Richon, Semi-clathrate hydrate phase equilibrium measurements for the CO_2 + H_2/CH_4 + tetra-n-butylammonium bromide aqueous solution system, Chem. Eng. Sci. 94 (2013) 284-290, https://doi.org/10.1016/j.ces.2013.01.063.

[147] S. Lee, Y. Lee, J. Lee, H. Lee, Y. Seo, Experimental verification of methane-carbon dioxide replacement in natural gas hydrates using a differential scanning calorimeter, Environ. Sci. Technol. 47 (2013) 13184-13190, https://doi.org/10.1021/es403542z.

[148] A. Chapoy, R. Burgass, B. Tohidi, I. Alsiyabi, Hydrate and phase behavior modeling in CO_2-rich pipelines, J. Chem. Eng. Data 60 (2015) 447-453, https://doi.org/10.1021/je500834t.

[149] L.L. Shi, D.Q. Liang, D.L. Li, Phase equilibrium conditions for simulated landfill gas hydrate formation in aqueous solutions of tetrabutylammonium nitrate, J. Chem. Thermodyn. 68 (2014) 322-326, https://doi.org/10.1016/j.jct.2013.09.029.

[150] B. Partoon, K.M. Sabil, H. Roslan, B. Lal, L.K. Keong, Impact of acetone on phase boundary of methane and carbon dioxide mixed hydrates, Fluid Phase Equilib. 412 (2016) 51-56, https://doi.org/10.1016/j.fluid.2015.12.027.

[151] Y.D. Zhang, D. Wang, J.P. Yang, L. Tian, L. Wu, Research on the hydrate formation in the process of gas phase CO_2 pipeline transportation, Int. J. Heat Technol. 34 (2016) 339-344, https://doi.org/10.18280/ijht.340226.

[152] X. Zang, D. Liang, Phase equilibrium data for semiclathrate hydrate of synthesized binary CO_2/CH_4 gas mixture in tetra-n-butylammonium bromide aqueous solution, J. Chem. Eng. Data 62 (2017) 851-856, https://doi.org/10.1021/acs.jced.6b00876.

[153] P. Kastanidis, G.E. Romanos, A.K. Stubos, I.G. Economou, I.N. Tsimpanogiannis, Two- and three-phase equilibrium experimental measurements for the ternary CH_4 + CO_2 + H_2O mixture, Fluid Phase Equilib. 451 (2017) 96-105, https://doi.org/10.1016/j.fluid.2017.08.002.

[154] V.R. Belosludov, Y.Y. Bozhko, O.S. Subbotin, R.V. Belosludov, R.K. Zhdanov, K.V. Gets, Y. Kawazoe, Influence of N_2 on formation conditions and guest distribution of mixed CO_2 + CH_4 gas hydrates, Molecules 23 (2018) 3336, https://doi.org/10.3390/molecules23123336.

[155] L.N. Legoix, L. Ruffine, C. Deusner, M. Haeckel, Experimental study of mixed gas hydrates from gas feed containing CH_4, CO_2 and N_2: Phase equilibrium in the presence of excess water and gas exchange, Energies 11 (2018) 1984, https://doi.org/10.3390/en11081984.

[156] S. Fan, S. You, Y. Wang, X. Lang, C. Yu, S. Wang, Z. Li, W. Li, Y. Liu, Z. Zhou, Hydrate phase equilibrium of CH_4-rich binary and ternary gas mixtures in the presence of tetra-n-butyl ammonium bromide, J. Chem. Eng. Data 64 (2019) 5929-5934, https://doi.org/10.1021/acs.jced.9b00804.

[157] M.S. Khan, B. Lal, A.M. Shariff, H. Mukhtar, Ammonium hydroxide ILs as dual-functional gas hydrate inhibitors for binary mixed gas (carbon dioxide and methane) hydrates, J. Mol. Liq. 274 (2019) 33-44, https://doi.org/10.1016/j.molliq.2018.10.076.

[158] S. Adisasmito, E.D. Sloan Jr., Hydrates of hydrocarbon gases containing carbon dioxide, J. Chem. Eng. Data 37 (1992) 343-349, https://doi.org/10.1021/je00007a020.

[159] Y. Matsui, Y. Ogura, H. Miyauchi, T. Makino, T. Sugahara, K. Ohgaki, Isothermal phase equilibria for binary hydrate systems of carbon dioxide + ethane and carbon dioxide + tetrafluoromethane, J. Chem. Eng. Data 55 (2010) 3297-3301, https://doi.org/10.1021/je100097x.

[160] S.M. Babakhani, B. Bouillot, J. Douzet, S. Ho-Van, J.M. Herri, PVTx measurements of mixed clathrate hydrates in batch conditions under different

crystallization rates: Influence on equilibrium, J. Chem. Thermodyn. 122 (2018) 73-84, https://doi.org/10.1016/j.jct.2018.03.006.

[161] M.B. Olseni, A. Majumdar, P.R. Bishnoi, Experimental studies on hydrate equilibrium-carbon dioxide and its systems, Int. J. Soc. of Mat. Eng. Resour. 7 (1999) 17-23, https://doi.org/10.5188/ijsmer.7.17.

[162] S.P. Kang, H. Lee, C.S. Lee, W.M. Sung, Hydrate phase equilibria of the guest mixtures containing CO_2, N_2 and tetrahydrofuran, Fluid Phase Equilib. 185 (2001) 101-109, https://doi.org/10.1016/S0378-3812(01)00460-5.

[163] P. Linga, R. Kumar, P. Englezos, The clathrate hydrate process for post and pre-combustion capture of carbon dioxide, J. Hazard. Mater. 149 (2007) 625-629, https://doi.org/10.1016/j.jhazmat.2007.06.086.

[164] P. Linga, R. Kumar, P. Englezos, Gas hydrate formation from hydrogen/carbon dioxide and nitrogen/carbon dioxide gas mixtures, Chem. Eng. Sci. 62 (2007) 4268-4276, https://doi.org/10.1016/j.ces.2007.04.033.

[165] H. Bruusgaard, J.G. Beltran, P. Servio, Vapor-liquid water-hydrate equilibrium data for the system $N_2 + CO_2 + H_2O$, J. Chem. Eng. Data 53 (2008) 2594-2597, https://doi.org/10.1021/je800445x.

[166] T. Lu, Y. Zhang, X.S. Li, Z.Y. Chen, K.F. Yan, Equilibrium conditions of hydrate formation in the systems of CO_2-N_2-TBAB and CO_2-N_2-THF, Chinese J. Process Eng. 9 (2009) 541-544.

[167] I.B.A. Sfaxi, V. Belandria, A.H. Mohammadi, R. Lugo, D. Richon, Phase equilibria of $CO_2 + N_2$ and $CO_2 + CH_4$ clathrate hydrates: Experimental measurements and thermodynamic modelling, Chem. Eng. Sci. 84 (2012) 602-611, https://doi.org/10.1016/j.ces.2012.08.041.

[168] S.C. Sun, C.L. Liu, Q.G. Meng, Hydrate phase equilibrium of binary guest-mixtures containing CO_2 and N_2 in various systems, J. Chem. Thermodyn. 84 (2015) 1-6, https://doi.org/10.1016/j.jct.2014.12.018.

[169] B. Chazallon, C. Pirim, Selectivity and CO_2 capture efficiency in CO_2-N_2 clathrate hydrates investigated by in-situ Raman spectroscopy, Chem. Eng. J. 342 (2018) 171-183, https://doi.org/10.1016/j.cej.2018.01.116.

[170] X. Zang, L. Wan, D. Liang, Investigation of the hydrate formation process in fine sediments by a binary CO_2/N_2 gas mixture, Chinese J. Chem. Eng. 27 (2019) 2157-2163, https://doi.org/10.1016/j.cjche.2019.02.032.

[171] J.W. Lee, D.Y. Kim, H. Lee, Phase behavior and structure transition of the mixed methane and nitrogen hydrates, Korean J. Chem. Eng. 23 (2006) 299-302, https://doi.org/10.1007/BF02705731.

[172] D. Zhong, P. Englezos, Methane separation from coal mine methane gas by tetra-n-butyl ammonium bromide semiclathrate hydrate formation, Energy Fuels 26 (2012) 2098-2106, https://doi.org/10.1021/ef202007x.

[173] H.J. Ng, J.P. Petrunia, D.B. Robinson, Experimental measurement and prediction of hydrate forming conditions in the nitrogen-propane-water system, Fluid Phase Equilib. 1 (1977-1978) 283-291, https://doi.org/10.1016/0378-3812(77)80011-3.

[174] E.D. Sloan Jr., C.A. Koh, Clathrate Hydrates of Natural Gases, CRC Press/Taylor & Francis, 2008.

[175] W.R. Parrish, J.M. Prausnitz, Dissociation pressures of gas hydrates formed by gas mixtures, Ind. Eng. Chem. Process Des. Dev. 11 (1972) 26-35, https://doi.org/10.1021/i260041a006.

[176] Z.G. Sun, S.S. Fan, L. Shi, Y.K. Guo, K.H. Guo, Equilibrium conditions hydrate dissociation for a ternary mixture of methane, ethane, and propane in aqueous solutions of ethylene glycol and electrolytes, J. Chem. Eng. Data 46 (2001) 927-929, https://doi.org/10.1021/je000365z.

[177] S. Lee, Y. Lee, S. Park, Y. Kim, I. Cha, Y. Seo, Stability conditions and guest distribution of the methane + ethane + propane hydrates or semiclathrates in the presence of tetrahydrofuran or quaternary ammonium salts, J. Chem. Thermodyn. 65 (2013) 113-119, https://doi.org/10.1016/j.jct.2013.05.042.

[178] H. Kakati, A. Mandal, S. Laik, Phase stability and kinetics of CH_4 + CO_2 + N_2 hydrates in synthetic seawater and aqueous electrolyte solutions of NaCl and $CaCl_2$, J. Chem. Eng. Data 60 (2015) 1835-1843, https://doi.org/10.1021/acs.jced.5b00042.

[179] Y.H. Sun, S.L. Li, G.B. Zhang, W. Guo, Y.H. Zhu, Hydrate phase equilibrium of CH_4+N_2+CO_2 gas mixtures and cage occupancy behaviors, Ind. Eng. Chem. Res. 56 (2017) 8133-8142, https://doi.org/10.1021/acs.iecr.7b01093.

[180] X. Zang, D. Liang, Phase equilibrium data for the hydrates of synthesized ternary CH_4/CO_2/N_2 biogas mixtures, J. Chem. Eng. Data 63 (2018) 197-201, https://doi.org/10.1021/acs.jced.7b00823.

[181] P.R. Bishnoi, P.D. Dholabhai, Equilibrium conditions for hydrate formation for a ternary mixture of methane, propane and carbon dioxide, and a natural gas mixture in the presence of electrolytes and methanol, Fluid Phase Equilib. 158-160 (1999) 821-827, https://doi.org/10.1016/S0378-3812(99)00103-X.

[182] W.I. Wilcox, D.B. Carson, D.L. Katz, Natural gas hydrates, Ind. Eng. Chem. 33 (1941) 662-665, https://doi.org/10.1021/ie50377a027.

CHAPTER 5 A NEW FOUR-PHASE EQUILIBRIUM CALCULATION ALGORITHM FOR WATER/HYDROCARBONS SYSTEMS IN THE PRESENCE OF GAS HYDRATES

A version of this chapter was submitted to *Chemical Engineering Science*

Abstract

Gas hydrates may form in the water/hydrocarbons mixtures at relatively low temperatures and high pressures. It is critical to detect the formation and dissociation of hydrates as well as capture its effects on multiphase equilibria at different temperature/pressure conditions. This study develops an algorithm for multiphase equilibrium calculations in the presence of gas hydrates. The number of equilibrium phases that can be detected by this algorithm is up to four phases, i.e., a vapor phase, a hydrocarbon-rich liquid phase, an aqueous phase, and a gas hydrate phase. The new four-phase equilibrium calculation algorithm is formulated in a stage-wise manner, i.e., a stability test is first conducted and followed by flash calculations if an instability is invoked. Besides using the van der Waals-Platteeuw model to predict the appearance of hydrate phase, we propose a new criterion for determining the onset of hydrate dissociation. To calculate the phase fractions and phase compositions, this new algorithm provides a series of material-balance equations involving hydrates. Example calculations are conducted on a number of example fluids. For these example fluids, the pressure-temperature phase diagrams and pressure-composition phase diagrams in the presence of a hydrate phase have been plotted by using the developed algorithm to conduct point-to-point calculations. The calculation results demonstrate the robustness and accuracy of the newly developed four-phase equilibrium calculation algorithm.

Keywords: Multiphase equilibrium calculation; Gas hydrates; Phase diagram; Algorithm development.

Graphic Abstract

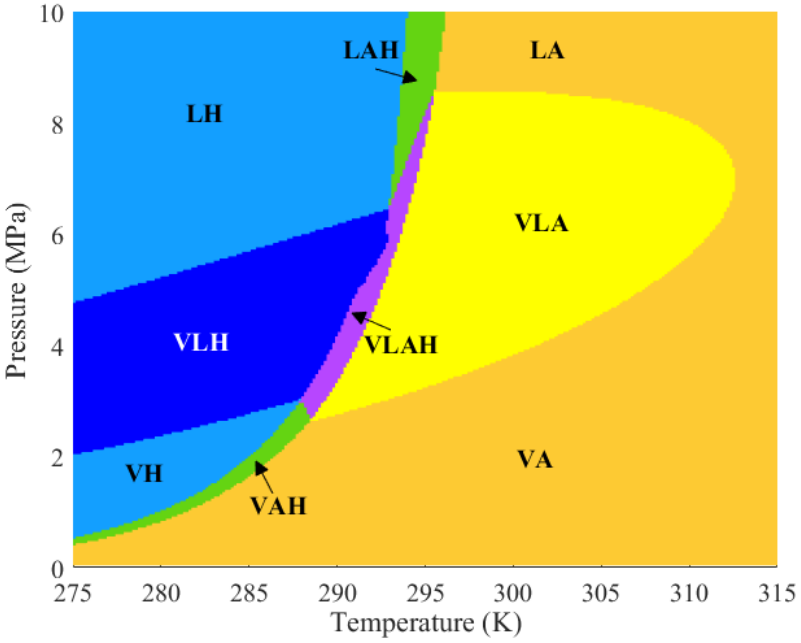

Pressure-temperature phase diagram calculated by the new VLAH four-phase equilibrium calculation algorithm for a $H_2O/CH_4/C_2H_6/C_3H_8$ mixture with a molar fraction ratio of 40:5:2:3. Specifications: V-vapor phase; L-hydrocarbon-rich liquid phase; A-aqueous phase; H-gas hydrate phase.

5.1. Introduction

Gas hydrates are solid crystalline mixtures of water and small gas molecules that typically form at relatively low temperatures and high pressures [1,2]. As a promising energy resource, the natural gas hydrates are discovered in many offshore and permafrost geological formations [3-6]. Besides, the natural gas hydrates are also found to form in the pipelines located in cold areas and in the wellbores used in offshore petroleum industry, causing flow assurance problems [7-9]. Decomposition of in-situ hydrates in reservoirs during the exploitation process as well as the formation of hydrates in pipelines or wellbores may lead to a series of changes on the number of equilibrium phases and the phase compositions [10-13]. How to accurately describe the phase behavior of natural gas hydrates plays a fundamentally important role in the accurate modeling of multiphase flow involving gas hydrates in both reservoirs, wellbore, and pipelines [14-16].

The appearance of a hydrate phase will significantly raise the computational difficulty of the multiphase equilibrium calculations [15-18]. **Fig. 5-1** shows the possible phase equilibria that could be encountered by water/hydrocarbon mixtures. The feed water can exist as a water-rich liquid phase (i.e., an aqueous phase), while the feed hydrocarbons may split into a vapor phase and a hydrocarbon-rich liquid phase. As indicated by the left panel of **Fig. 5-1**, without the presence of hydrate phase, the following phase equilibria can possibly appear: vapor-liquid (VL), vapor-aqueous (VA) and liquid-aqueous (LA) two-phase equilibria, plus vapor-liquid-aqueous (VLA) three-phase equilibria. After the appearance of hydrate phase, the possible phase equilibria become much more complicated, as illustrated by the right panel of **Fig. 5-1**. Besides the above-mentioned four types of multiphase equilibria, the following phase equilibria are possible: vapor-hydrate (VH), liquid-hydrate (LH) and aqueous-hydrate (AH) two-

phase equilibria; vapor-aqueous-hydrate (VAH), liquid-aqueous-hydrate (LAH) and vapor-liquid-hydrate (VLH) three-phase equilibria; vapor-liquid-aqueous-hydrate (VLAH) four-phase equilibria. Undoubtedly, it is quite challenging to correctly characterize the multiphase equilibria of water/hydrocarbons mixtures with the consideration of hydrate formations.

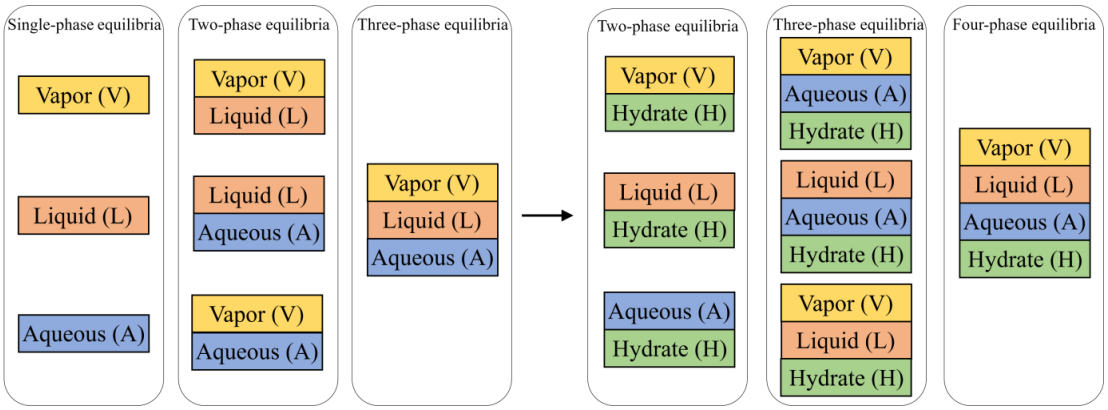

Fig. 5-1. Possible phase equilibria for water/hydrocarbons mixtures without (left) and with (right) the appearance of hydrate phase.

Since the proposal of van der Waals equation, cubic equation of state (CEOS) has been widely used to describe the pressure-volume-temperature (PVT) relationships of pure compounds and mixtures [19,20]. Various robust CEOS models have been developed in the past, of which Soave-Redlich-Kwong (SRK) EOS and Peng-Robinson (PR) EOS are the most commonly used ones [21,22]. Meanwhile, numerous frameworks for multiphase equilibrium calculations have been proposed along with the development of CEOS [23-26]. For a given feed, the isothermal-isobaric multiphase equilibrium calculations can be formulated as a Gibbs energy minimization problem [27-29]. In a stage-wise manner, Michelsen et al. (1982) developed a classical multiphase equilibrium calculation framework consisting of stability test and flash calculation [30-32]. Stability test is conducted to test if a given phase is stable or not, while flash calculation is conducted to work out the molar fractions and compositions

of the equilibrium phases. Over the past four decades, this framework has been adopted by many commercial simulators [33-38]. Although this classical multiphase equilibrium calculation framework performs well in describing the phase behavior of fluid mixtures, it may not work well in describing the phase behavior of hydrate-inclusive systems [19-22].

The van der Waals and Platteeuw (vdW-P) model is the most widely used method to predict gas hydrate equilibria [39-41]. This model can quantitatively reproduce the energy changes required to form the empty hydrate lattices composed of hydrogen-bonded water molecules and the probabilities of gas molecules encaged in the hydrate lattices [40-42]. The calculation errors resulting from the vdW-P model in reproducing the hydrate equilibrium pressures at given temperatures may be lower than 10% [16,43-48]. The vdW-P hydrate model has been incorporated into multiphase equilibrium calculation programs [49-54]. In 1989, Bishnoi et al. first proposed a multiphase equilibrium calculation algorithm for gas hydrate systems based on the concept of Gibbs free energy minimization [53,54]. This algorithm combined the vdW-P hydrate model with the simultaneous stability analysis and flash calculation [53-55]. Later, Ballard and Sloan implemented this methodology in developing CSMGem, which is deemed as a start-of-the-art software for modeling the equilibria of gas hydrate systems [56-59]. Recent researchers have tried to further improve the efficiency and robustness of this framework through improving fugacity calculations for gases and water [60-63]. However, the simultaneous stability and multiphase computations adopted in these frameworks may cause non-convergence issues in the composition simulations [16,54,63]. Even the credible software CSMGem cannot yield reliable multiphase equilibrium calculation results occasionally [48,63,64]. In addition, these available algorithms are mainly focused on determining the phase boundaries in phase diagrams

[16,39,61-63]. A better way to test the robustness of a multiphase equilibrium calculation algorithm should be using it to perform point-to-point calculations to lay out the entire phase diagrams.

In this work, we develop a new vapor-liquid-aqueous-hydrate four-phase equilibrium calculation algorithm for water/hydrocarbons mixtures. Different from previous works relying on the approach of simultaneous stability analysis and flash calculation [53,54], we employ the stage-wise approach as suggested by Michelsen [30,31]. The classical vdW-P hydrate model is applied to determine the formation of hydrate phase [40]. We propose a new criterion for determining the dissociation of hydrate phase. To calculate the phase fractions and the compositions of the equilibrium phases, we present a series of material-balance equations used for the multiphase equilibrium calculations with the consideration of hydrate phase. We test this algorithm by using it to perform point-to-point calculations to plot the entire phase diagrams for a number of water/hydrocarbons mixtures.

5.2. Methodology

5.2.1. Thermodynamic Models

In a simple form, CEOS serves as a fast and reliable tool for describing the PVT relationships of fluids [20]. PR EOS is one of the most commonly used CEOSs in the chemical and petroleum engineering [20]. This study employs the volume translated PR (vt-PR) EOS for solving multiphase equilibrium for fluids [21,65]. The vt-PR EOS can be described by the following equation [21,65],

$$P = \frac{RT}{v-b} - \frac{a}{(v+t)(v+b+2t)+(b+t)(v-b)} \tag{5-1}$$

where P and T are pressure and temperature, respectively; R denotes the universal gas constant; v is molar volume; t is the volume translation term to improve the density calculations over a wide temperature and pressure range; a and b are PR EOS parameters representing the attractive force and repulsive force between the molecules, respectively. The values of a and b in the vt-PR EOS can be expressed using the following equations [21,65],

$$a = 0.457535\frac{R^2T_c^2}{P_c}\alpha(T) \tag{5-2}$$

$$b = 0.077796\frac{RT_c}{P_c} - t \tag{5-3}$$

where T_c and P_c are critical temperature and critical pressure, respectively; $\alpha(T)$ is the so-called α-function. This study adopts the Twu α-function updated by Pina-Martinez et al. [65,66] and the volume-temperature-dependent volume translation model [67,68] in view of their good performances in reproducing thermodynamic properties.

In the multiphase equilibrium calculations, the fugacity is frequently used as a measure of the chemical potential. The fugacity and fugacity coefficient of the component i (f_i and ϕ_i) can be given as [21,24],

$$\ln\phi_i = \ln\frac{f_i}{y_iP} = \frac{1}{RT}\int_V^\infty\left(\frac{\partial P}{\partial n_i} - \frac{RT}{V}\right)dV - \ln Z \tag{5-4}$$

where y_i and n_i are the molar fraction and molar number of component i, respectively; V is volume; Z is compressibility factor. The detailed derivation of fugacity based on vt-PR EOS is presented in **Supplementary Material**.

The vdW-P model is widely used for the assessment of gas hydrate thermodynamic properties [39,40]. The classical vdW-P model is expressed as [40],

$$\frac{\mu_w^H - \mu_w^W}{RT} = \frac{\Delta\mu_w^0}{RT_0} + \int_{P_0}^{P}\frac{\Delta v_w^{\beta-W}}{R\overline{T}}dP - \int_{T_0}^{T}\frac{\Delta h_w^{\beta-W}}{RT^2}dT + \sum_k \lambda_k \ln\left(1 - \sum_i \theta_{ik}\right) - \ln a_w \tag{5-5}$$

where μ_w^H and μ_w^W are the chemical potentials of water in the hydrate phase and aqueous phase, respectively. When a hydrate phase is formed, the chemical potential of water in the hydrate phase should be less than the chemical potential of water in the aqueous phase (i.e. $\mu_w^H - \mu_w^W < 0$). At equilibrium, the chemical potentials of water in the hydrate phase and the aqueous phase are equal (i.e. $\mu_w^H - \mu_w^W = 0$). In addition, the superscript 0 refers to the triple point of water; the superscripts *H*, *β*, and *W* refer to the hydrate with filled lattice, the assumed hydrate with empty lattice, and the aqueous phase, respectively. $\Delta\mu_w^0$ denotes the difference between the chemical potential of water in the empty hydrate lattice and the chemical potential of water in the aqueous phase at the triple point. $\Delta v_w^{\beta-W}$ denotes the difference in the molar volume of water between the empty lattice and the aqueous phase. T_0 and P_0 are set to 273.16 K and 611.2 Pa, respectively, in this study. Moreover, $\overline{T}$ denotes the average temperature between *T* and T_0. $\Delta h_w^{\beta-W}$ represents the difference in the molar enthalpy of water between the empty lattice and the aqueous phase. Besides, λ_k denotes the number of *k* cavity per water molecule in the unit cell. θ_{ik} denotes the probability of a cage *k* being occupied by a guest molecule *i*. It is determined using the following equation [40],

$$\theta_{ik} = \frac{C_{ik} f_i}{1 + \sum_i C_{ik} f_i} \tag{5-6}$$

where f_i is the fugacity of the hydrate-forming gas *i* obtained using vt-PR EOS; C_{ik} is the Langmuir constant which can be obtained by the Lennard-Jones-Devonshire cell theory [39,40]. In the final term of **Eq. 5-5**, a_w is the water activity in the aqueous phase. Since the solubilities of gases in water are very small, a_w is assumed to be equal to the molar fraction of water in aqueous phase, which is close to unity [44]. **Supplementary Material** gives more details about the vdW-P model.

5.2.2. Conventional Three-Phase Equilibrium Calculation Algorithm

Two pivotal aspects should be addressed by multiphase equilibrium calculations: whether a mixture will actually split into two (or more) phases (i.e., stability test) and what the amounts and compositions of equilibrium phases are (i.e., flash calculation) [30,31]. The tangent plane distance (TPD) function and Rachford-Rice equation are the mainstream tools used to conduct stability test and flash calculation, respectively [29-33,69]. Based on the criterion of Gibbs energy minimization, the expression of the TPD function for a fluid system is shown as [30],

$$TPD = \sum_{i=1}^{c} x_i \left[\ln x_i + \ln \phi_i(x) - \ln z_i - \ln \phi_i(z) \right] \tag{5-7}$$

where x_i and z_i are the molar fractions of component i in the trial phase and test phase, respectively; $\phi_i(x)$ and $\phi_i(z)$ are the fugacity coefficients of component i in the trial phase and test phase, respectively; c is the total number of components in the mixture. If all the calculated values of the TPD function with any given compositions in the trial phase (x_i) are non-negative, the fluid would be considered to be stable. Otherwise, the fluid is unstable and tends to split into two phases.

If two or more phases appear in a given fluid system, the amounts and compositions of equilibrium phases can be determined by flash calculation. There are two constraints addressed in flash calculation: one is the fugacity-equality constraint; the other is the material-balance constraint. For a vapor-liquid-aqueous three-phase equilibrium, the fugacity-equality constraint can be written as,

$$f_i^V = f_i^L = f_i^W \qquad i = 1,\ldots,c \tag{5-8}$$

where f_i^V, f_i^L and f_i^W are the fugacity of component i in vapor phase, liquid phase and aqueous phase, respectively. The fugacity of each composition in different phases should be equal at equilibrium.

For a vapor-liquid-aqueous three-phase system, the material-balance constraint can be described as:

$$1 = V + L + W \tag{5-9}$$

$$z_{0i} = V \cdot v_i + L \cdot l_i + W \cdot w_i \qquad i = 1,...,c \tag{5-10}$$

where V, L, and W denote the molar fractions of vapor phase, liquid phase, and aqueous phase, respectively; z_{0i}, y_i, x_i, and w_i stand for the molar fractions of component i in feed, vapor phase, liquid phase, aqueous phase, and hydrate phase, respectively.

To reduce the number of variables in material-balance constraint equations, we can introduce the equilibrium ratios of component i in vapor phase and aqueous phase with respect to liquid phase (K_i^V and K_i^W) as,

$$K_i^V = \frac{v_i}{l_i} \qquad i = 1,...,c \tag{5-11}$$

$$K_i^W = \frac{w_i}{l_i} \qquad i = 1,...,c \tag{5-12}$$

Then we can obtain the following equations,

$$\sum_{i=1}^{c}(v_i - l_i) = \sum_{i=1}^{c}\left[\frac{z_{0i}\left(K_i^V - 1\right)}{1 + V\left(K_i^V - 1\right) + W\left(K_i^W - 1\right)}\right] = 0 \tag{5-13}$$

$$\sum_{i=1}^{c}(w_i - l_i) = \sum_{i=1}^{c}\left[\frac{z_{0i}\left(K_i^W - 1\right)}{1 + V\left(K_i^V - 1\right) + W\left(K_i^W - 1\right)}\right] = 0 \tag{5-14}$$

Eqs. 5-13 and **5-14** refer to Rachford-Rice equations [69]. The number of the governing equations is $2c$+2 (**Eqs. 5-8**, **5-13** and **5-14**), while the number of unknows in these equations is also $2c$+2 (K_i^V, K_i^W, V and W). The amounts and compositions of

vapor phase, liquid phase and aqueous phase can be determined through solving this group of equations.

On the basis of the stage-wise approach combining stability test and flash calculation, our previous study has provided an improved VLA three-phase equilibrium calculation algorithm for water/hydrocarbons mixtures [29]. The robustness and efficiency of this algorithm have been demonstrated by several example calculations [29]. This algorithm lays a cornerstone for the VLAH four-phase equilibrium calculation algorithm developed in this work.

5.2.3. Four-Phase Equilibrium Calculation in the Presence of Hydrates

Previous multiphase equilibrium calculations in the presence of hydrate phase usually employ the approach where stability test and flash calculation are simultaneously solved [53,54]. This framework can reduce the computational cost but easily leads to non-convergence problems in compositional simulations [55]. To improve the robustness and accuracy, this study will develop a new VLAH four-phase equilibrium calculation algorithm based on a stage-wise approach. For this purpose, a new criterion for determining the onset of hydrate dissociation and some new constraints in flash calculation would be introduced.

This study employs the vdW-P model to predict the appearance of hydrate phase. If the calculated chemical potential of water in hydrate phase is equal or less than that in aqueous phase (i.e. $\mu_w^H - \mu_w^W \leq 0$), a hydrate phase is found to be present in this system. Please note that when we calculate the chemical potential difference of water through the vdW-P model, the fugacity of guest gas in hydrate phase is considered equal to that in liquid phase or vapor phase as,

$$f_i^H = f_i^V = f_i^L \qquad i = 1,...,c-1 \tag{5-15}$$

where f_i^H is the fugacity of composition i in hydrate phase. The values of f_i^V and f_i^L can be determined by the VLA three-phase equilibrium calculations. Here, the largest value of component index i is equal to c-1, because water has been excluded. The chemical potential of water in the hydrate phase and that in the aqueous phase should be equal,

$$\mu_w^H - \mu_w^W = 0 \tag{5-16}$$

As for a vapor-liquid-aqueous-hydrate four-phase equilibrium, the material-balance constraint equations are given as [49,70],

$$1 = V + L + W + H \tag{5-17}$$

$$z_{0i} = V \cdot v_i + L \cdot l_i + W \cdot w_i + H \cdot h_i \qquad i = 1,...,c \tag{5-18}$$

where H and h_i denote the molar fraction of hydrate phase and the molar fraction of component i in hydrate phase. The conventional VLA three-phase equilibrium calculation algorithm [29] can help determine the relationships between V, L, W, v_i, l_i and w_i. As such, we need to develop a framework to determine H and h_i in the multiphase equilibria.

Based on the vdW-P model, the amount of gas component i in the hydrate phase per water molecule (n_i^H) should be,

$$n_i^H = \sum_k^2 \lambda_k \theta_{ik} \qquad i = 1,...,c-1 \tag{5-19}$$

As shown in **Eq. 5-6**, the value of θ_{ik} depends on the fugacity of guest gas. The fugacity can be determined based on the assumed gas fractions in vapor phase (v_i'') or/and liquid phase (l_i''). We can first conduct the VLA equilibrium calculation based

on the feed compositions. Then the obtained compositions in the equilibrium phases would be set as initial guesses for calculating θ_{ik} by the vdW-P model.

Next, the molar fractions of gas component i (excluding water) and water w in hydrate phase (h_i and h_w) can be expressed as,

$$h_i = \frac{n_i^H}{1+\sum_i^{c-1} n_i^H} \qquad i = 1,...,c-1 \tag{5-20}$$

$$h_w = \frac{1}{1+\sum_i^{c-1} n_i^H} \tag{5-21}$$

Using m to represent the molar fraction of water that is converted to solid hydrate, the total amount of water converted to hydrate (M) and the molar fraction of hydrate phase (H) can be calculated as [49,70],

$$M = m \cdot z_{0w} \tag{5-22}$$

$$H = M + M \cdot \sum_i^{c-1} n_i^H \tag{5-23}$$

where z_{0w} is the molar fraction of feed water. The initial value of m can be set as 0.1.

Due to the formation of gas hydrate, the original feed composition z_{0i} should be corrected. The corrected feed compositions (z'_{0i} , i.e., the overall compositions excluding those in hydrate phase) can be determined as,

$$z'_{0i} = \frac{z_{0i} - H \cdot h_i}{1-H} \qquad i = 1,...,c \tag{5-24}$$

Then we can conduct the VLA three-phase equilibrium calculation again based on z'_{0i} and obtain the compositions in vapor phase (v'_i) and/or liquids phase (l'_i).

Theoretically, the newly obtained compositions in vapor phase (v_i') or/and liquid phase (l_i') based on z_{0i}' should be equal to the assumed compositions of vapor phase (v_i'') or/and liquid phase (l_i'') used for determining θ_{ik} as,

$$v_i' = v_i'' \quad \text{or} \quad l_i' = l_i'' \qquad\qquad i = 1,...,c-1 \tag{5-25}$$

In addition, at equilibrium, the chemical potential of water in hydrate phase and that in aqueous phase should be equal (i.e., $\mu_w^H - \mu_w^W = 0$). As a result, an extra set of equations have been established; the number of both the governing equations (**Eqs. 5-16** and 5-**25**) and the unknows (including *m* and $v_i' / v_i'' / l_i' / l_i''$) is equal to *c*. By solving this group of equations, we can determine the phase fractions and compositions at VAH, LAH, or VLAH multiphase equilibria.

In general, the vdW-P model can help predict the hydrate phase equilibrium with the existence of an aqueous phase and hydrocarbon phases (vapor phase or liquid phase) [39,40]. With the increase of pressure or the decrease of temperature, either the hydrocarbons (water excess) or water (hydrocarbon excess) may be completely consumed and converted into hydrate phase. Consequently, there may be VH, LH, AH or VLH multiphase equilibria; the chemical potential difference of water between hydrate phase and aqueous phase calculated by vdW-P model cannot reach zero. Therefore, we can try to minimize the absolute value of the chemical potential difference of water under the constraints of material balance as,

$$\min\left|\mu_w^H - \mu_w^W\right| \quad \text{subjects to } (v_i' = v_i'' \quad \text{or} \quad l_i' = l_i'',\ i=1,...,c\text{-}1) \tag{5-26}$$

If the minimum of $\left|\mu_w^H - \mu_w^W\right|$ can reach zero (i.e., less than the threshold of 10^{-12} in this study), the equation $\mu_w^H - \mu_w^W = 0$ is solvable under the material-balance constraints. The hydrate phase would be in equilibrium with both a hydrocarbon-rich

phase and an aqueous phase. Otherwise, $\mu_w^H - \mu_w^W = 0$ is unsolvable; either hydrocarbon-rich phase (vapor phase or/and liquid phase) or aqueous phase would disappear. **Eq. 5-26** can also be interpreted as a criterion for the onset of hydrate dissociation.

Next, we can determine whether hydrocarbons or water in the feed is excessive for hydrate formation through calculating the total hydrate number (N^H) as [18],

$$N^H = \frac{1}{\sum_{i=1}^{c-1}\sum_{k=1}^{2} z'_{0i}\lambda_k\theta'_{ik}} \tag{5-27}$$

where θ'_{ik} is the calculated probability of a cage occupancy with the assumption of pure gas i and z'_{0i} is the molar fraction of feed gas after excluding feed water. The hydrate number indicates the molar ratio between water and gases in hydrate phase.

The molar ratio between water and hydrocarbons in the feed is given as [18],

$$N_0 = \frac{z_{0w}}{\sum_{i=1}^{c-1} z_{0i}} \tag{5-28}$$

If the calculated hydrate number (N^H) is less than the molar ratio between the feed water and feed hydrocarbons (N_0), the feed water is considered to be excessive for hydrate formation. Otherwise, the feed hydrocarbons are excessive.

If water is excessive for hydrate formation, there may be only an AH two-phase equilibrium. All the hydrocarbons would be encaged in hydrates except a small amount of gases dissolved in water. Then the total amount of water converted into hydrate phase (z'_{0w}) and the molar fraction of hydrate phase (H') can be determined as,

$$M' = \frac{\sum_{i=1}^{c-1} z_{0i}}{\sum_{k=1}^{2} \lambda_k\theta'_{ik}} \tag{5-29}$$

$$H' = \frac{M'}{z_{0w}} \tag{5-30}$$

If hydrocarbons are excessive for hydrate formation, there may be VH, LH or VLH multiphase equilibria. All water would be consumed to form hydrates except a trivial amount of water dissolved in hydrocarbon-rich phase. Hence, the molar fraction of the remaining water (z'_{0w}) should be equal to zero,

$$z'_{0w} = \frac{z_{0w} - H \cdot h_w}{1 - H} = 0 \tag{5-31}$$

Combining **Eq. 5-31** and material-balance constraints (**Eq. 5-25**), we can calculate the molar fractions of the remaining hydrocarbons. We can then conduct the VLA three-phase equilibrium calculation again based on the remaining hydrocarbons and obtain the phase fractions and the phase compositions of vapor phase and/or liquid phase.

5.2.4. Flowchart of the New Four-Phase Equilibrium Calculation Algorithm in the Presence of Hydrates

Based on the above-mentioned theoretical models, a framework for VLAH four-phase equilibrium calculations can be formulated. **Fig. 5-2** depicts the flowchart of the new multiphase equilibrium calculation algorithm developed in this research. The detailed procedures are listed below:

(1) Conduct the VLA three-phase equilibrium calculation with given temperature, pressure, and feed compositions. Then check if aqueous phase appears. If aqueous phase appears, continue to **Step (2)**. Otherwise, hydrates cannot form without enough water [16] and the algorithm outputs a one-phase equilibrium or a VL two-phase equilibrium.

(2) Calculate the chemical potential difference of water between hydrate phase and aqueous phase (i.e. $\mu_w^H - \mu_w^W$) through the vdW-P model and check if the hydrate phase appears. If the hydrate phase appears (i.e. $\mu_w^H - \mu_w^W < 0$), continue to **Step (3)**. If the hydrate phase would not form, output a VA/LA two-phase equilibrium or a VLA three-phase equilibrium.

(3) Calculate the minimum of $\left|\mu_w^H - \mu_w^W\right|$ under the material-balance constraints (**Eq. 5-25**). If the minimum of $\left|\mu_w^H - \mu_w^W\right|$ is equal to 0 (i.e., less than the convergence tolerance of 10^{-12}), both feed gases and feed water have not been completely converted to hydrate phase. In this case, go to **Step (4)**. Otherwise, either feed water or feed gases have been completely consumed and go to **Step (5)**.

(4) Solve $\mu_w^H - \mu_w^W = 0$ under the material-balance constraints and obtain the remaining compositions excluding hydrate phase. Then conduct VLA three-phase equilibrium calculation for the remaining compositions and output a VAH/LAH three-phase equilibrium or a VLAH four-phase equilibrium.

(5) Calculate the total hydrate number to detect whether feed gases or feed water are excessive. If the feed water is excessive, calculate the molar fractions of hydrate phase and aqueous phase (remaining water) and output an AH two-phase equilibrium. If the feed gases are excessive, calculate the molar fractions of the remaining gases. Then conduct VL two-phase equilibrium calculation for the remaining gases and output a VH/LH two-phase equilibrium or a VLH three-phase equilibrium.

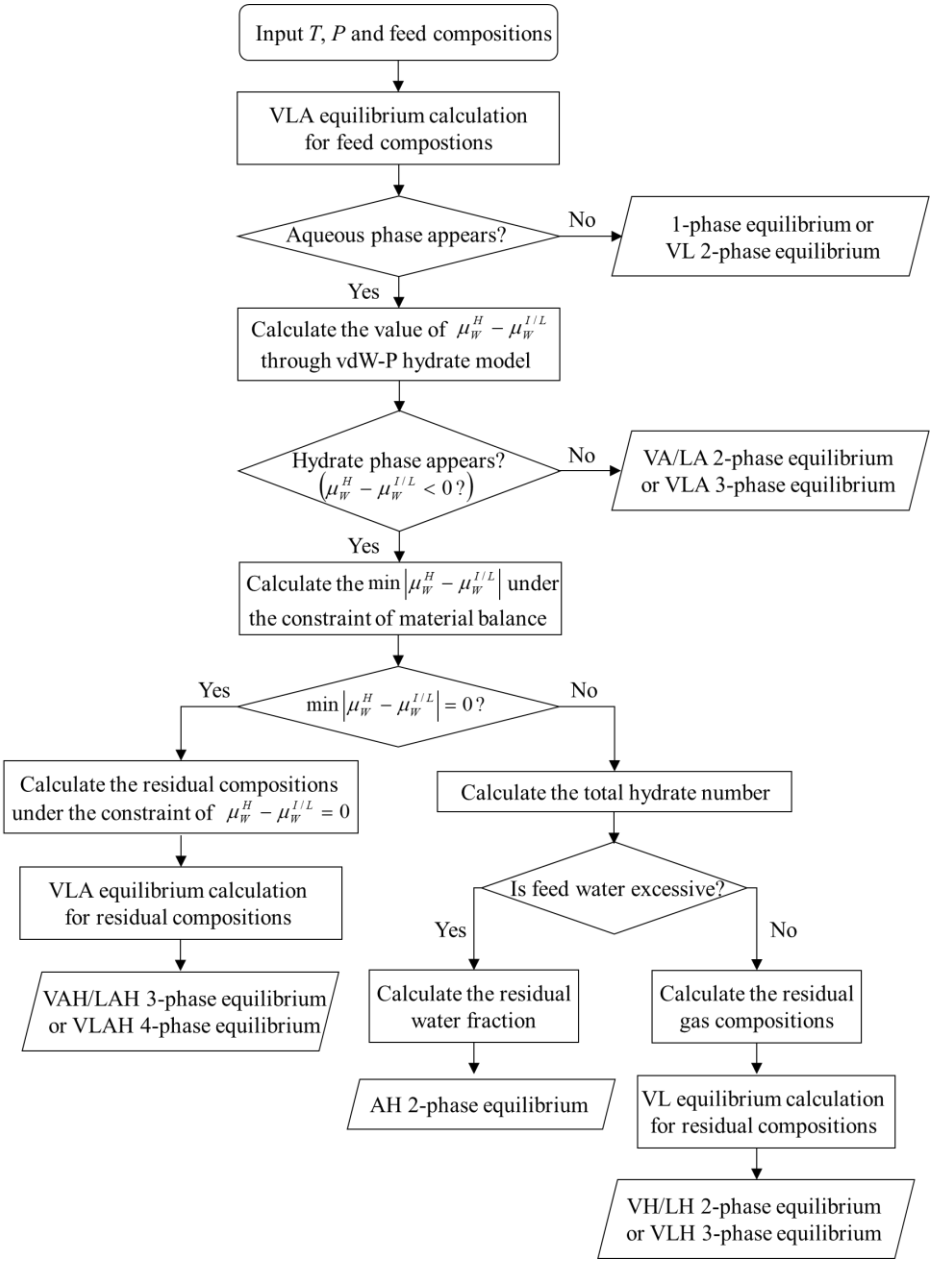

Fig. 5-2. Flowchart of the VLAH four-phase equilibrium calculation algorithm developed in this study.

We would like to make the following remarks regarding the practical implementation of the above algorithm:

(1) VLA three-phase equilibrium calculations would be conducted using the algorithm recently developed in our research group [29]. Although this algorithm performs well in most cases, it may occasionally exhibit non-convergence problems [29]. The mixing rules and binary interaction parameters (BIPs) used in the algorithm

pose a significant effect on VLA three-phase equilibrium calculations [29,71-73]. However, most of the available BIPs are obtained under temperatures higher than hydrate-forming temperatures, which may not be suitable for the multiphase equilibrium calculations in the presence of hydrate. In this study, the BIPs adopted for the tested fluids are summarized in **Supplementary Material**.

(2) The minimization problems in VLAH four-phase equilibrium calculations should be solved using a nonlinear least-squares algorithm. The performance of this algorithm depends on initial guesses. **Section 5.2.3** and our previous study give detailed introductions on the initialization methods used in this newly developed algorithm [29]. Moreover, when plotting the point-to-point phase diagrams for hydrate systems, we can directly use the calculation results of the neighboring points as the initial guesses for a new point to improve the robustness and effectiveness of the multiphase equilibrium calculations.

(3) The equation $\mu_w^H - \mu_w^W = 0$ would also be solved based on the nonlinear least-squares algorithm, which is similar to the process of minimizing $\left|\mu_w^H - \mu_w^W\right|$. Hence, to reduce the computational cost, we can directly check whether $\mu_w^H - \mu_w^W = 0$ is solvable. If we can obtain a real solution, the minimum $\left|\mu_w^H - \mu_w^W\right|$ must approach zero and the feed gases and water are in equilibrium with hydrates. Otherwise, the minimum of $\left|\mu_w^H - \mu_w^W\right|$ cannot reach zero and either feed water or feed gases have been completely consumed.

(4) The molar fractions of hydrocarbons in aqueous phase as well as those of water in hydrocarbon-rich phases (vapor phase and liquid phase) are very small (usually less than 0.01). As such, we can assume that the effects of the mutual solubilities of gases and water on the multiphase equilibrium calculations in the presence of hydrates are

negligible. In addition, most of the available experiments on hydrate equilibria were conducted under free-water conditions where the mutual solubilities of gases and water were neglected [16]. Hence, the example calculations (**Section 5.3**) in this study were also conducted based on the free-water assumption. **Appendix 5-A** provides an algorithm with the full consideration of the mutual solubilities of gases and water.

(5) The vdW-P model may occasionally exhibit non-convergence problems during multiphase equilibrium calculations. To address this issue, our previous study has provided a new set of Kihara potential parameters [43]. By applying the vdW-P model with the newly fitted Kihara potential parameters, the algorithm developed in this work can be used to robustly conduct VLAH four-phase equilibrium calculations in the presence of gas hydrates over the following pressure and temperature ranges: 0-20 MPa and 273.15-300 K.

(6) All the feed gases in the mixtures adopted in the example calculations (**Section 5.3**) tend to form gas hydrates. In addition, we do not detect the transitions of hydrate structures over the tested temperature and pressure ranges in the example calculations. The gas hydrates presented in **Cases 1**, **3** and **4** are of structure II, while those in **Case 2** are of structure I (**Section 5.3**).

5.3. Results and Discussion

The newly developed VLAH four-phase equilibrium calculation algorithm has been conducted on four water/hydrocarbons mixtures to examine its performance. For each mixture, the pressure-temperature (P-T) and pressure-composition (P-X) phase diagrams as well as the phase fractions and phase compositions are calculated using the newly developed algorithm. **Table 5-1** summarizes the basic information about the example calculations.

Table 5-1. Basic information about the example calculations.

Case No.	Gas compositions	*T* range (K)	*P* rang (MPa)	Verification items
1	C_2H_6, C_3H_8	274-280	0.008-2	P-T phase diagrams
2	CH_4, CO_2	277, 285, 287	0.04-10	P-X phase diagrams, phase compositions
3	CH_4, C_2H_6, C_3H_8	275-315	0.04-10	P-T phase diagrams, phase fractions and phase compositions
4	Natural gas	275-295	0.04-10	P-T phase diagrams, phase compositions

5.3.1. Case 1 ($H_2O/C_2H_6/C_3H_8$ Mixture)

Fig. 5-3 graphically shows the number of equilibrium phases in P-T diagrams for $H_2O/C_2H_6/C_3H_8$ mixtures with different feed water/gas molar ratios (19:1, 9:1 and 2:1). The feed molar ratio between C_2H_6 and C_3H_8 is 3:7. The tested pressure ranges from 0.008 MPa to 2 MPa with a step size of 0.008 MPa, while the tested temperature ranges from 274 K to 280 K with a step size of 0.025 K. We can see that all the points presented in **Fig. 5-3** are solvable, confirming the robustness of the new algorithm.

Water is excessive for hydrate formation with the feed water/gas molar ratio of 19:1. Hence, at the low-temperature and high-pressure area (the top left corner) of **Fig. 5-3**a, there is an AH two-phase equilibrium region. With a decrease in pressure, hydrates would dissociate and lead to a VAH three-phase equilibrium region. Then hydrates would completely dissociate, while the vapor phase and aqueous phase remain in the system. In addition, at the high-pressure region, there is an LAH there-phase equilibrium region in between the AH and LA two-phase equilibrium regions. Besides, we can notice a steep transformation from the VAH to VLA three-phase equilibrium areas near the center of **Fig. 5-3**a. The dividing line indicates a VLAH four-phase equilibrium. The thermodynamic equilibria of a given mixture are governed by Gibbs' phase rule [74],

$$F=c-p+2 \tag{29}$$

where F is the number of degrees of freedom, c is the number of components and p is the number of phases. For a $H_2O/C_2H_6/C_3H_8$ mixture (p=3), when the number of phases is four (p=4), the degree of freedom is one (F=1). As a result, either temperature or pressure must be specified, and the four-phase equilibrium exhibits a line in P-T phase diagram, as seen from **Fig. 5-3**a. As seen above, a VLAH four-phase equilibrium area may form in complicated mixtures. We will evaluate the performance of the newly developed algorithm in detecting four-phase equilibria in **Case 3**.

With a lower feed water/gas molar ratio (9:1), the feed hydrocarbons are excessive for hydrate formation. Consequently, the low-temperature and high-pressure area (the top left corner of **Fig. 5-3**b) becomes an LH two-phase equilibrium region. With a decrease in pressure, the hydrocarbons tend to evaporate, leading to a VLH three-phase equilibrium region. Until all the hydrocarbons have evaporated, a VH two-phase equilibrium area would emerge. As pressure further decreases, hydrates start to dissociate and a VAH three-phase equilibrium region appears. Once hydrates completely dissociate, only the vapor phase and aqueous phase remain in the system at low pressures. Most notably, the VLH three-phase equilibrium area is situated above the VLA three-phase equilibrium area. This is because heavier hydrocarbons (i.e., C_3H_8 in this case) are more prone to be encaged in hydrates than lighter ones [12,16]. As such, there is a larger amount of lighter hydrocarbons remaining in the vapor phase after hydrate formation, which impedes the appearance of liquid phase. Besides, similar to **Fig. 5-3**a, at the high-pressure region, there is an LAH there-phase equilibrium region between the LH and LA two-phase equilibrium regions in **Fig. 5-3**b.

Fig. 5-3c is similar to **Fig. 5-3**b. Because of the less feed water (a feed water/gas molar ratio of 2:1), a smaller amount of hydrates may form, leading to the shrinkage of three-phase equilibrium areas (VAH, VLH and LAH). If we further reduce the feed

water/gas molar ratio, the three-phase equilibrium regions of VAH and LAH may become too narrow to detect. Segtovich et al. [61] have presented a P-T phase diagram for a $H_2O/C_2H_6/C_3H_8$ mixture with a molar fraction ratio of 10:3:7 as shown in **Fig. 5-4**. Obviously, our newly plotted P-T diagram (**Fig. 5-3**c) bears a striking resemblance to **Fig. 5-4** and matches the experimental data in the literature [75].

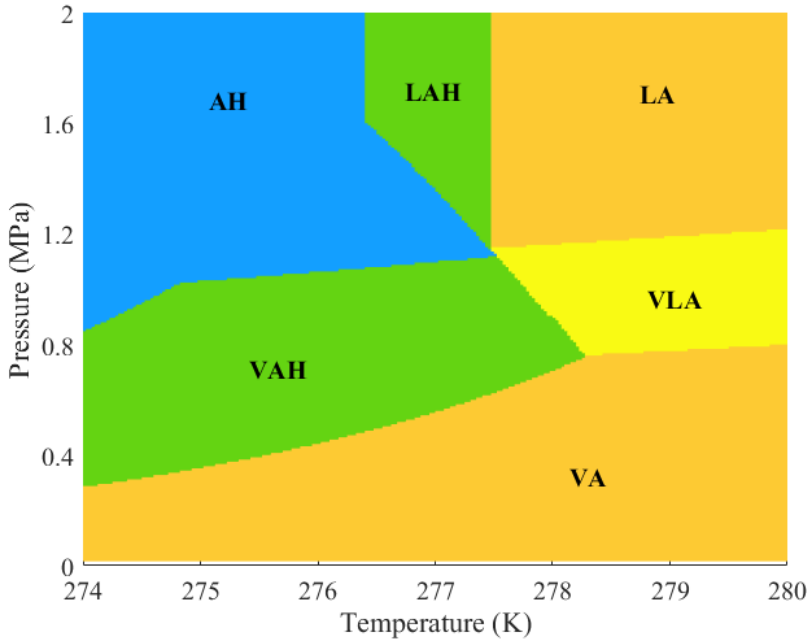

(a)

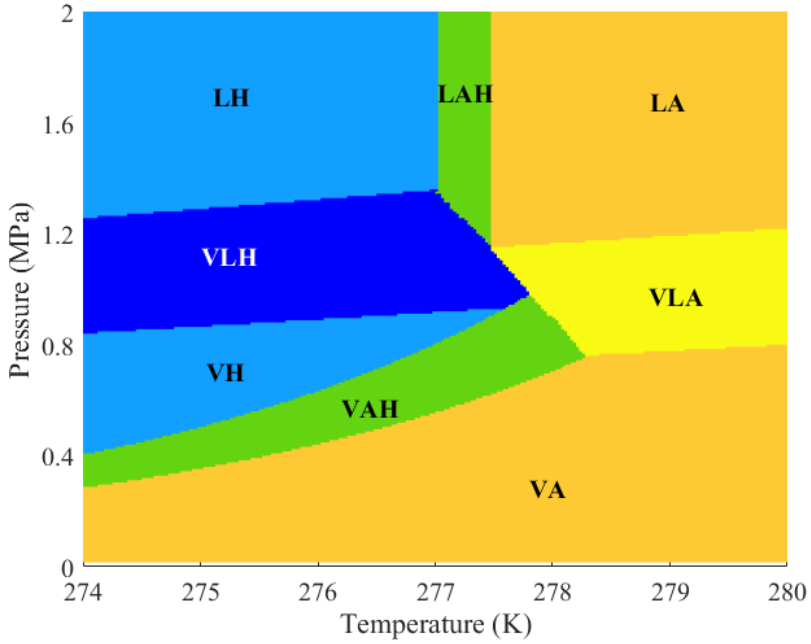

(b)

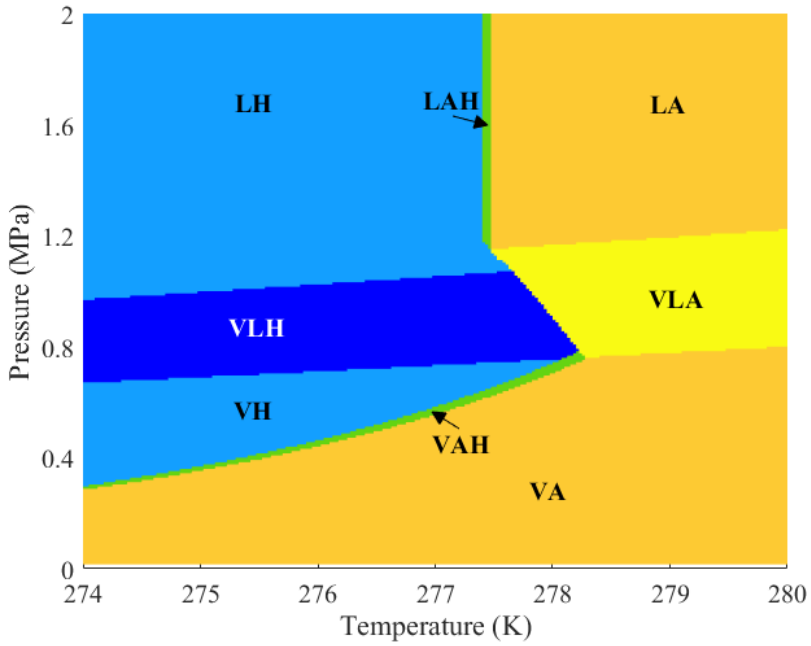

(c)

Fig. 5-3. P-T phase diagram calculated by the new VLAH four-phase equilibrium calculation algorithm for $H_2O/C_2H_6/C_3H_8$ mixtures with different feed water/gas molar ratios: (a) 19:1, (b) 9:1, and (c) 2:1. The feed molar ratio of C_2H_6 and C_3H_8 is 3:7. Specifications: V-vapor phase; L-liquid phase; A-aqueous phase; H-hydrate phase.

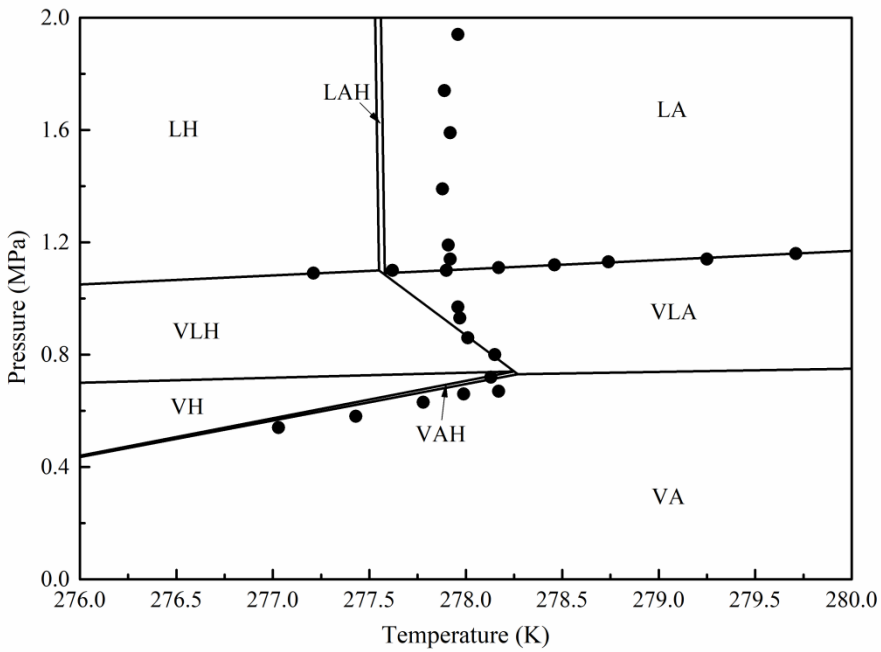

Fig. 5-4. P-T phase diagram for a $H_2O/C_2H_6/C_3H_8$ system with a molar fraction ratio of 10:3:7 provided by Segtovich et al. [61] and the experimental data (dots) from Mooijer-van den Heuvel [75]. Specifications: V-vapor phase; L-liquid phase; A-aqueous phase; H-hydrate phase. Reprinted with permission of Elsevier from Segtovich et al. (2016). Simultaneous multiphase flash and stability analysis calculations including hydrates. Fluid Phase Equilib. 413: 196-208; permission conveyed through Copyright Clearance Center, Inc. with modifications.

5.3.2. Case 2 ($H_2O/CH_4/CO_2$ Mixture)

Instead of the P-T phase diagrams presented in **Fig. 5-3**, we would test the performance of the newly developed algorithm by generating P-X phase diagrams for $H_2O/CH_4/CO_2$ mixtures as shown in **Fig. 5-5**. The feed water/gas molar ratio is 4:1 and the tested temperatures are 277 K, 285 K and 287 K, respectively. The tested pressure ranges from 0.05 MPa to 12 MPa with a step size of 0.05 MPa, while the tested CO_2 mole fraction in the feed gases ranges from 0.004 to 0.996 with a step size of 0.004. Similar to the P-T phase diagrams in **Fig. 5-3**, all the points presented in the P-X phase diagrams of **Fig. 5-5** have converged to proper solutions.

At a low temperature of 277 K, gas hydrates form at relatively low pressures (**Fig. 5-5**a). Since CO_2 is easier to form hydrates than CH_4 [12,16,47], the hydrate-forming pressure would decrease with an increasing concentration of CO_2. In addition, we can see a narrow VAH three-phase equilibrium area between the VA and VH two-phase equilibrium areas. What is more interesting, a VLH three-phase equilibrium area appears in the CO_2-rich region and an LH two-phase equilibrium area is located above the VLH three-phase equilibrium area. Moreover, there should be a supercritical phase in the top left corner of **Fig. 5-5**a. Although we can further distinguish the pseudo-liquid phase and pseudo-vapor phase through Widom lines [76,77], this study emphasizes on the multiphase calculations for gas hydrate systems rather than supercritical fluids. In the following figures (**Figs. 5-5**b&c), such supercritical fluids would be marked as V/L for convenience.

At a higher temperature of 285 K (**Fig. 5-5**b), the hydrate-forming pressures would be higher than those at 277 K (**Fig. 5-5**a). Thus, the hydrate-forming line would intersect the original VLH three-phase equilibrium area. At the same time, an LA two-phase equilibrium area as well as LAH and VLA three-phase equilibrium areas appear

in the CO_2-rich region. Another thing to note is that the area of VLH three-phase equilibrium is narrower than that of VLA three-phase equilibrium. This is because CO_2 is easier to be encaged in hydrates than CH_4 [12,16]. The CO_2/CH_4 molar ratio becomes lower due to hydrate formation, leading to a smaller VLH three-phase equilibrium area.

If we further increase temperature to 288 K (**Fig. 5-5**c), the hydrate-forming pressure increases accordingly. Meanwhile, the hydrate-involving area would locate at the supercritical region of CO_2-CH_4 mixture. Hence, we can only detect a V/LH two-phase equilibrium in the top left corner of **Fig. 5-5**a. The two original three-phase LAH and VAH equilibrium areas would merge into a continuous area, i.e., V/LAH, as shown in **Fig. 5-5**c.

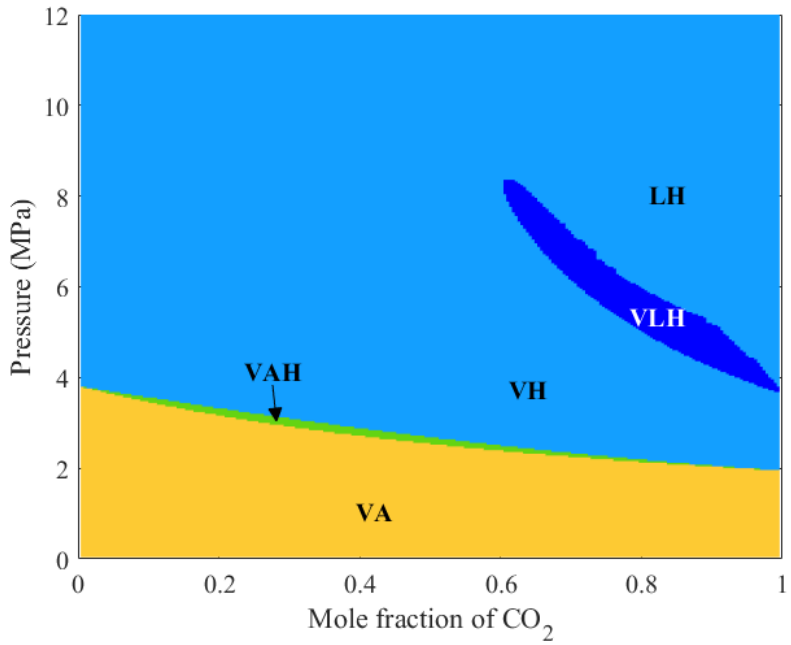

(a)

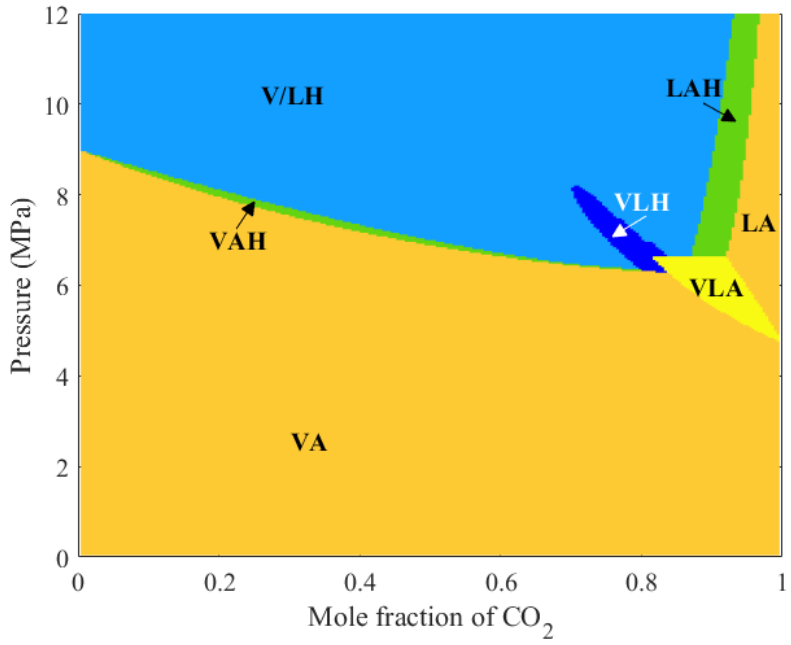

(b)

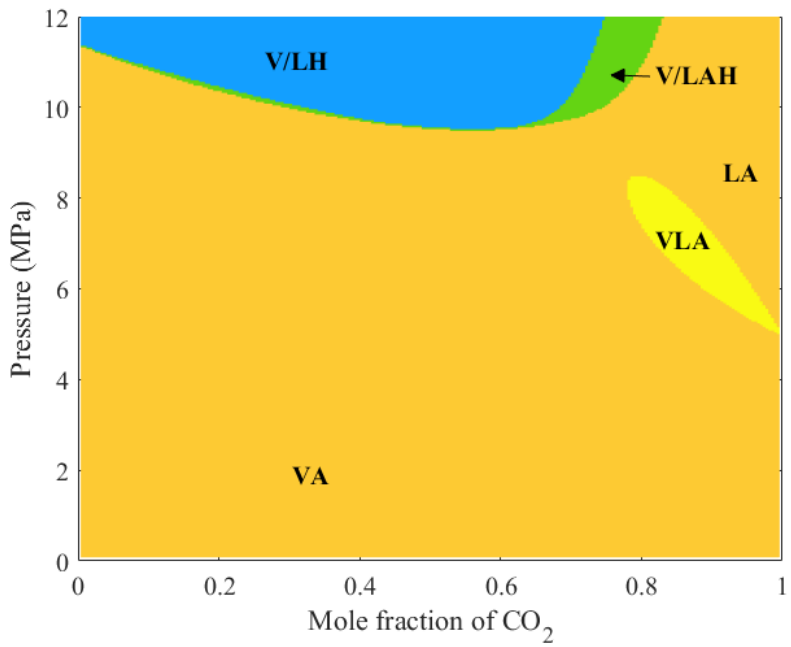

(c)

Fig. 5-5. P-X phase diagram calculated by the new VLAH four-phase equilibrium calculation algorithm for $H_2O/CH_4/CO_2$ mixtures at different temperatures: (a) 277 K, (b) 285 K, and (c) 287 K. Specifications: V-vapor phase; L-liquid phase; A-aqueous phase; H-hydrate phase; V/L-supercritical phase.

Besides the above P-X phase diagrams for $H_2O/CH_4/CO_2$ mixtures, we have compared the calculated CO_2 and CH_4 fractions in vapor phase and hydrate phase

against the available experimental results. The average absolute percentage deviations (%AADs) in reproducing the gas fractions are calculated as,

$$\%AAD = \frac{100}{d}\sum_{i=1}^{d}\left|\frac{\varphi-\varphi^{EXP}}{\varphi^{EXP}}\right|_i \tag{32}$$

where φ^{EXP} represents the experimental data of gas fractions in hydrate phase or vapor phase under equilibrium conditions; φ represents the gas fractions calculated by the new VLAH four-phase equilibrium calculation algorithm; d is the number of data points. The evaluation results are summarized in **Table 5-2** and more detailed calculation results are presented in **Supplementary Materials**. We can see from **Table 5-2** that the overall %AADs yielded by the new algorithm in reproducing the gas fractions in vapor phase and hydrate phase are about 15%. Such calculation accuracy is close to that yielded by the software CSMGem and previous multiphase equilibrium algorithms for gas hydrate systems [16,78-80].

Table 5-2. Calculation errors in reproducing gas fractions in hydrate phase and vapor phase yielded by the new VLAH four-phase equilibrium algorithm for $H_2O/CH_4/CO_2$ mixtures.

References	%AAD				*T* range (k)	*P* rang (MPa)	Data number
	CO_2 fraction in vapor	CH_4 fraction in vapor	CO_2 fraction in hydrate	CH_4 fraction in hydrate			
Belandria et al. [64]	34.92	14.85	20.78	14.71	273.6-282.2	1.51-5.767	30
Le Quang et al. [78]	11.97	1.99	14.17	6.13	276.55-278.35	3.33-4.93	11
Overall	**15.93**		**13.95**		**273.6-282.2**	**1.51-5.767**	**41**

5.3.3. Case 3 ($H_2O/CH_4/C_2H_6/C_3H_8$ Mixture)

In theory, a VLAH four-phase equilibrium may appear in a ternary-gas-mixture hydrate system. Hence, in this example application, we plot the P-T phase diagram for a $H_2O/CH_4/C_2H_6/C_3H_8$ mixture using the newly developed algorithm (**Fig. 5-6**) and check its performance in conducting four-phase VLAH equilibrium calculations. The feed water/gas molar ratio is 4:1 and the molar ratio of $CH_4/C_2H_6/C_3H_8$ is 5:2:3. The

tested pressure ranges from 0.04 MPa to 10 MPa with a step size of 0.04 MPa, while the tested temperature ranges from 275 K to 315 K with a step size of 0.16 K. Besides the P-T phase diagram, we also calculate the phase fractions and phase compositions for this mixture. **Fig. 5-7** shows the calculated phase fractions as a function of pressure at 290 K, while **Figs. 5-8** shows the calculated gas-fraction variations in hydrate phase as a function of pressure at 285 K.

In **Fig. 5-6**, there is a VLAH four-phase equilibrium area surrounded by four three-phase VLH, LAH, VAH and VLA equilibrium areas. In addition, the size of the VLH three-phase equilibrium area is reduced as compared to that of the VLA three-phase equilibrium area. As shown in **Fig. 5-7**, at a constant temperature of 290 K, the $H_2O/CH_4/C_2H_6/C_3H_8$ mixture adopted in this study presents a VA two-phase equilibrium under low pressures. Starting with 2.5 MPa, a liquid phase appears and the fraction of vapor phase decreases. Then hydrates would form under about 3.4 MPa. Note that the initial fraction of hydrate phase is 0.24 rather than 0, leading to a sudden decrease of other phase fractions accordingly. Based on the state-of-the-art hydrate nucleation hypotheses, the nucleation and growth of hydrate lattices may proceed only with enough gas molecules being encaged in hydrate cavities [83,84]. Hence, such proliferation of the hydrate phase is reasonable. Then all water would be consumed at 4.3 MPa and the vapor phase disappears at 6.2 MPa. Finally, the phase fractions keep stable under LH two-phase equilibria.

Besides the phase fractions, **Fig. 5-8** presents the compositional variations (free-water) in hydrate phase calculated by the newly developed algorithm at 285 K. One can see that gas hydrates would form at about 1.8 MPa. The initial fraction of C_3H_8 in hydrate phase is 0.44, which is obviously larger than its feed gas fraction (0.3). This is because heavier hydrocarbons are more easily to form hydrates than lighter ones at low

temperatures [12,16]. The initial fraction of CH_4 is also slightly larger than the feed one (0.5). It is worthwhile noting that CH_4 can enter into both the small and large cavities of structure II hydrates while C_2H_6 and C_3H_8 can only be encaged in large cavities [1,16]. Theoretically, the amount of small cavities in structure II hydrate is twice as that of large cavities [1,16]. As such, lots of CH_4 molecules have been encaged in hydrate phase. Meanwhile, the initial fraction of C_2H_6 in hydrate phase is relatively small. With an increase of pressure, the fractions of CH_4 and C_2H_6 increase, while that of C_3H_8 decreases. This indicates that smaller molecules (CH_4 and C_2H_6) seem to be able to replace larger ones (C_3H_8) in the large cavities of hydrates. Although some researchers have proved that CO_2 can replace CH_4 in hydrate cavities [11,81,82], there is lack of direct proof of the molecule replacement between CH_4/C_2H_6 and C_3H_8, which requires further experimental verification. Of course, such molecule replacement is gradual and the C_3H_8 fraction remaining in vapor phase is still lower than that of the feed at early ages. Consequently, as shown in **Fig. 5-6**, the lower boundary of VLH three-phase equilibrium area (liquid-phase forming line) has shifted up compared to that of VLA three-phase equilibrium area. At a higher pressure, more CH_4 would be encaged in hydrates. As such, the less CH_4 remaining in the non-hydrate phases leads to the upper boundary of VLH three-phase equilibrium area being lower than that of the VLA three-phase equilibrium area. Besides, there is an abrupt change of gas fractions at about 5.5 MPa, where the VLH three-phase equilibrium transforms to LH two-phase equilibria. Afterwards, the gas-fraction curves level off.

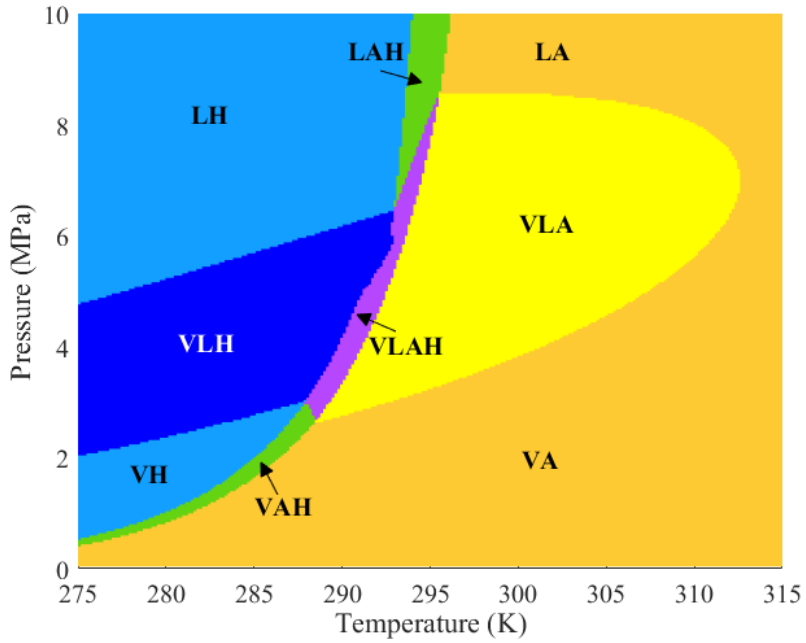

Fig. 5-6. P-T phase diagram calculated by the new VLAH four-phase equilibrium calculation algorithm for a $H_2O/CH_4/C_2H_6/C_3H_8$ mixture with a molar fraction ratio of 40:5:2:3. Specifications: V-vapor phase; L-liquid phase; A-aqueous phase; H-hydrate phase.

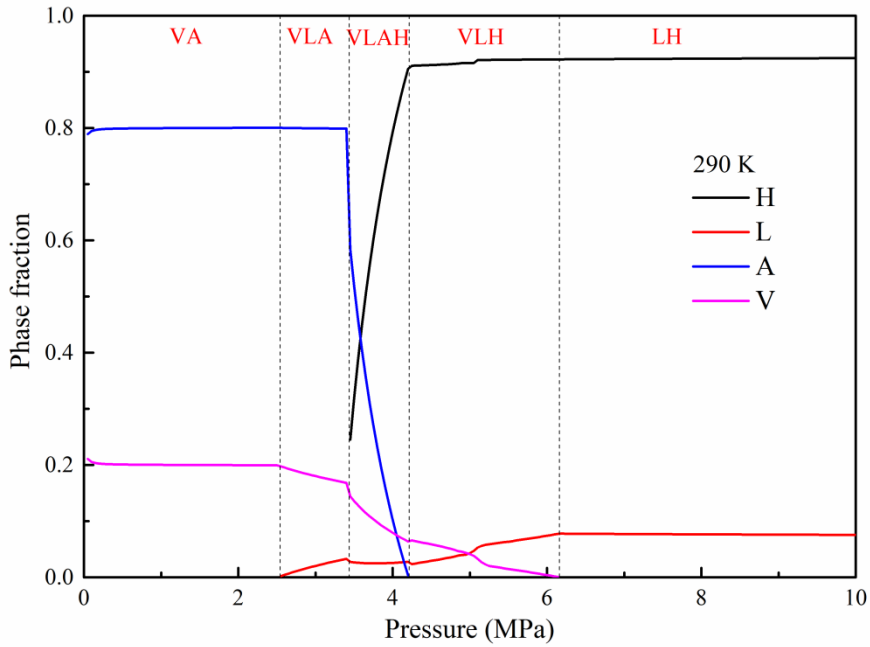

Fig. 5-7. Phase fractions calculated by the new VLAH four-phase equilibrium calculation algorithm for a $H_2O/CH_4/C_2H_6/C_3H_8$ mixture with a molar fraction ratio of 40:5:2:3 at 290 K. Specifications: V-vapor phase; L-liquid phase; A-aqueous phase; H-hydrate phase.

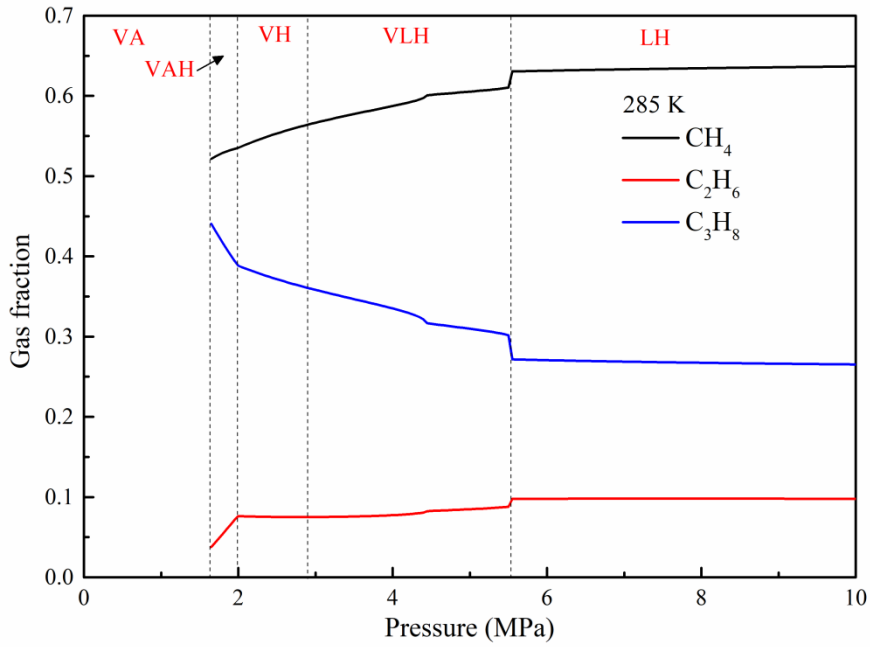

Fig. 5-8. Gas-fraction variations in hydrate phase calculated by the new VLAH four-phase equilibrium calculation algorithm for a $H_2O/CH_4/C_2H_6/C_3H_8$ mixture with a molar fraction ratio of 40:5:2:3 at 285 K. Specifications: V-vapor phase; L-liquid phase; A-aqueous phase; H-hydrate phase.

5.3.4. Case 4 (Water/Natural Gas Mixtures)

In this last example, we evaluate the performance of the newly developed algorithm in predicting the multiphase equilibria of water/natural gas mixtures. **Fig. 5-9** graphically shows the P-T phase diagrams calculated for two water/natural gas mixtures. **Table 5-3** lists the feed compositions of the two water/natural gas mixtures. In **Fig. 5-9**, the tested pressure ranges from 0.04 MPa to 10 MPa with a step size of 0.04 MPa, while the tested temperature ranges from 275 K to 295 K with a step size of 0.08 K. Since CH_4 is the dominating composition in natural gas systems, the P-T phase diagrams presented in **Fig. 5-9** are relatively simple. From the top left corner to the bottom right corner, the following phase equilibria appear in a sequential manner: AH (**Fig. 5-9a**) or VH (**Fig. 5-9b**) two-phase equilibria, VAH three-phase equilibria, and VA two-phase equilibria, respectively. Moreover, **Table 5-4** presents the errors yielded by the newly developed algorithm in reproducing the measured gas fractions in

different phases for the two water/natural gas mixtures. We can see that the overall %AADs yielded by the new algorithm in reproducing the gas fractions in vapor phase and hydrate phase are 15.68% and 11.65%, respectively. Such calculation errors are close to the uncertainty associated with the experimental measurements [78-80].

Table 5-3 Feed compositions of two water/natural gas mixtures used in this study.

Samples	CH_4	C_2H_6	C_3H_8	iC_4H_{10}	nC_4H_{10}	CO_2	N_2	Water/gas molar ratios	References
1	0.8744	0.06	0.0243	0.002	0.003	0.0213	0.015	13.76:1	Mahabadian et al. [63]
2	0.865	0.06	0.04	0.005	0.01	0.02	-	2:1*	Ng [85]

*The feed water/gas molar ratio was approximately calculated based on the volume ratio in the literature [85].

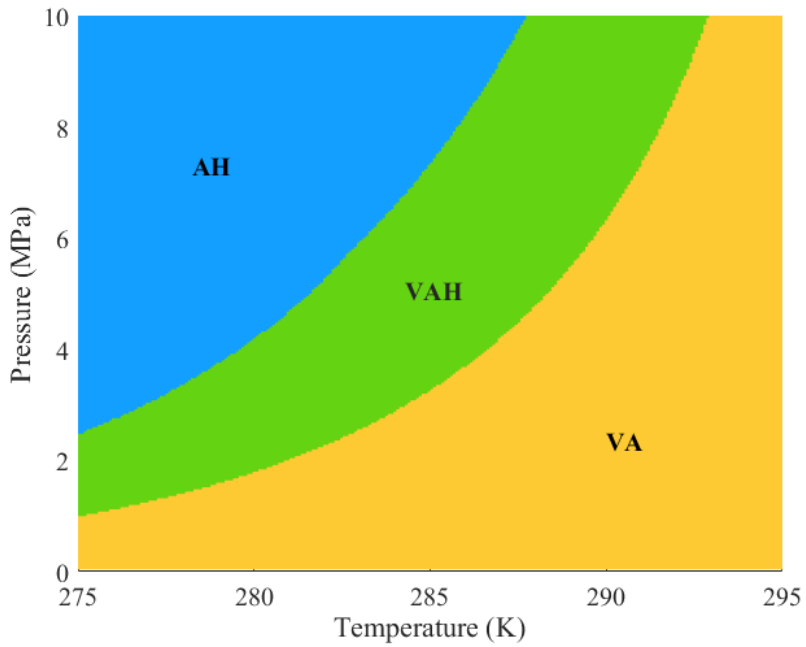

(a)

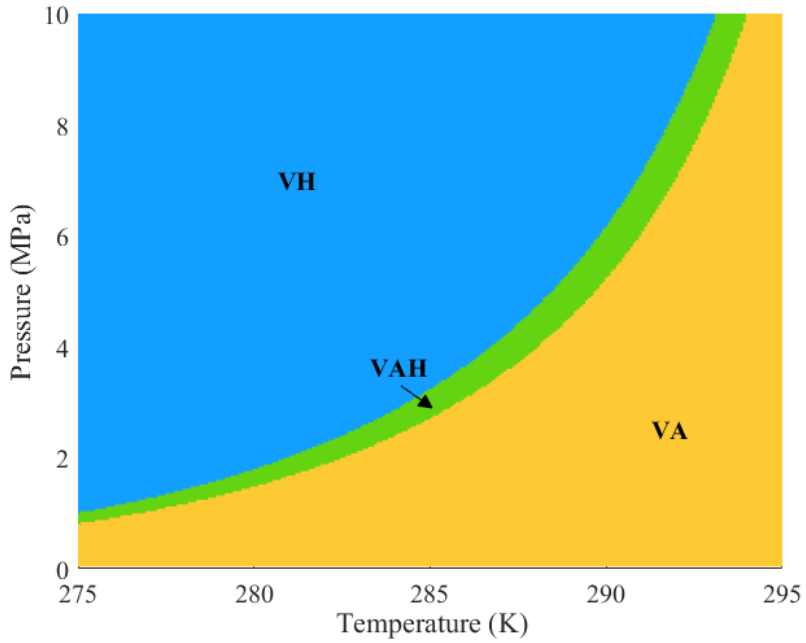

(b)

Fig. 5-9. P-T phase diagrams calculated by the new VLAH four-phase equilibrium calculation algorithm for water/natural gas mixtures: (a) Sample 1 and (b) Sample 2 shown in **Table 5-3**. Specifications: V-vapor phase; L-liquid phase; A-aqueous phase; H-hydrate phase.

Table 5-4. Errors yielded by the newly developed algorithm in reproducing the measured gas fractions in hydrate phase and vapor phase for water/natural gas mixtures.

References	%AAD		*T* range (K)	*P* rang (MPa)	Data number
	Gas fractions in vapor phase	Gas fractions in hydrate phase			
Ng [85]	-	11.65	284.3-292.6	2.07-6.89	4
Mahabadian et al [63]	15.68	-	277.45-289.25	2.785-6.601	8

5.4. Conclusions

In this work, we develop a multiphase equilibrium calculation algorithm for water/hydrocarbons systems in the presence of gas hydrates. This algorithm is designed to determine the multiphase equilibria involving vapor phase, hydrocarbon-rich liquid phase, aqueous phase, and gas hydrate phase in a stage-wise manner. In the developed algorithm, we propose a new criterion for determining the onset of hydrate dissociation and derive a series of material-balance equations involving hydrate phase. The performance of the new algorithm has been examined by four example calculations. These example calculations demonstrate that this algorithm is capable of robustly conducting hydrate-inclusive multiphase equilibrium calculations for a given fluid at

specified temperature and pressure. In addition, the overall deviations yielded by the new algorithm in reproducing the measured gas fractions in vapor phase and hydrate phase are about 15%, which are acceptable for industrial applications.

Acknowledgments

The authors greatly acknowledge a Discovery Grant from the Natural Sciences and Engineering Research Council of Canada (NSERC) (Grant No.: NSERC RGPIN-2020-04571) to H. Li. X. Chen greatly acknowledges the financial support provided by the China Scholarship Council (CSC) via a Ph.D. Scholarship (No.: 201806450029).

Appendix 5-A. Effects of the Mutual Solubilities of Gases and Water on the Multiphase Equilibrium Calculation

The solubilities of gases in water may affect the water activity in vdW-P model (**Eq. 5-5**). Likewise, the molar fractions of water in hydrocarbon-rich phases (vapor phase and liquid phase) may also affect the calculations of gas fugacities. To consider the effects of the mutual solubilities of gases and water on multiphase equilibrium calculations, another loop of material-balance calculations should be conducted. **Fig. 5-A** presents the flowchart of this loop. First, we conduct the VLA three-phase equilibrium calculations based on the feed compositions (z_{0i}). Then the molar fractions (solubilities) of gases in aqueous phase (s_i^W) and those of water in vapor phase and liquid phase (s_w^V and s_w^L) are obtained. Based on the calculated mutual solubilities of gases and water, the water activity and gas fugacities used in the vdW-P model would be determined. Next, we conduct the VLAH four-phase equilibrium calculations with the consideration of the mutual solubilities of gases and water. In the presence of hydrate phase, the solubilities of gases in aqueous phase (s_i^W') and those of water in

vapor phase and liquid phase (s_w^V' and s_w^L') are determined. If all the newly obtained solubilities are approximately equal to the old ones (i.e., meeting the tolerance level), we can output the calculation results. Otherwise, the old solubilities would be replaced by the newly obtained ones and the loop would be repeated until the desired level of tolerance is met. The error tolerance exerted on the solubilities is calculated as,

$$\left|\frac{s_i^W{}'-s_i^W}{s_i^W}\right|<10^{-6} \qquad i=1,\ldots,c-1 \tag{5-A}$$

where s_i^W and s_i^W' can be replace by s_w^V and s_w^V' as well as s_w^L and s_w^L', respectively. Since the mutual solubilities of hydrocarbons and water are very small, their effects on multiphase equilibrium calculations are reasonably small [59,86].

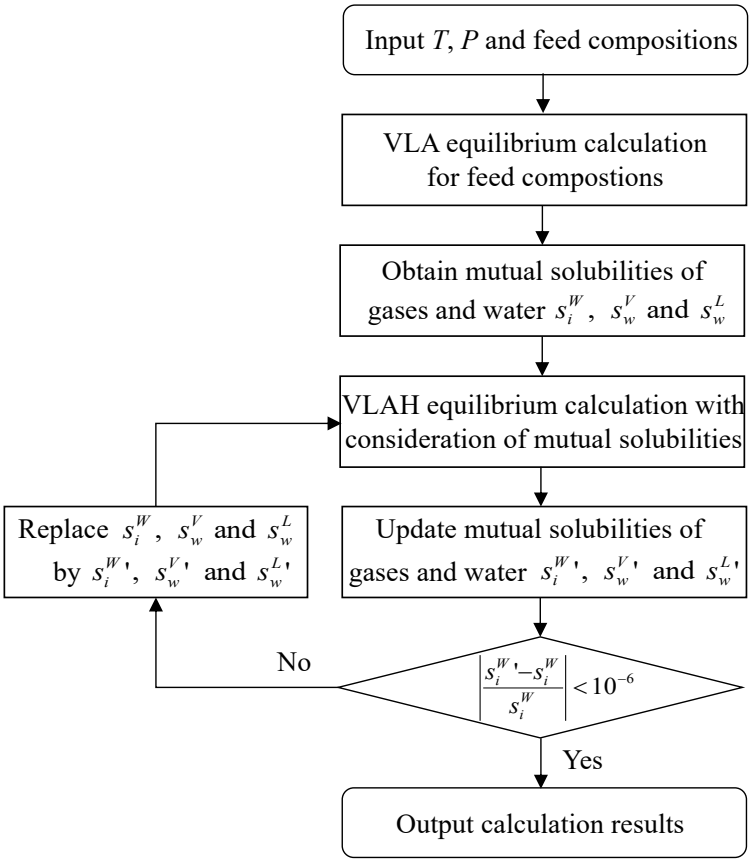

Fig. 5-A. Flowchart of the VLAH four-phase equilibrium calculation algorithm with the consideration of the mutual solubilities of gases and water.

References

[1] E.D. Sloan, Fundamental principles and applications of natural gas hydrates, Nature 426 (2003) 353-359, https://doi.org/10.1038/nature02135.

[2] P. Englezos, Clathrate hydrates, Ind. Eng. Chem. Res. 32 (1993) 1251-1274, https://doi.org/10.1021/ie00019a001.

[3] Z.R. Chong, S.H.B. Yang, P. Babu, P. Linga, X.S. Li, Review of natural gas hydrates as an energy resource: Prospects and challenges, Appl. Energ. 162 (2016) 1633-1652, https://doi.org/10.1016/j.apenergy.2014.12.061.

[4] C.A. Koh, A.K. Sum, E.D. Sloan, State of the art: Natural gas hydrates as a natural resource, J. Nat. Gas Sci. Eng. 8 (2012) 132-138, https://doi.org/10.1016/j.jngse.2012.01.005.

[5] C.A. Koh, E.D. Sloan, Natural gas hydrates: Recent advances and challenges in energy and environmental applications, AIChE J. 53 (2007) 1636-1643, https://doi.org/10.1002/aic.11219.

[6] T.S. Collett, Energy resource potential of natural gas hydrates, AAPG Bull. 86 (2002) 1971-1992, https://doi.org/10.1306/61EEDDD2-173E-11D7-8645000102C1865D.

[7] Z. Wang, Y. Zhao, J. Zhang, X. Wang, J. Yu, B. Sun, Quantitatively assessing hydrate-blockage development during deepwater-gas-well testing, SPE J. 23 (2018)1166-1183, https://doi.org/10.2118/181402-PA.

[8] J. Zhang, Z. Wang, B. Sun, X. Sun, Y. Liao, An integrated prediction model of hydrate blockage formation in deep-water gas wells, Int. J. Heat Mass Tran. 140 (2019) 187-202, https://doi.org/10.1016/j.ijheatmasstransfer.2019.05.039.

[9] J. Zhang, Z. Wang, S. Liu, W. Zhang, J. Yi, B. Sun, Prediction of hydrate deposition in pipelines to improve gas transportation efficiency and safety, Appl. Energ. 253 (2019) 113521, https://doi.org/10.1016/j.apenergy.2019.113521.

[10] Y. Sun, S. Jiang, S. Li, X. Wang, S. Peng, Hydrate formation from clay bound water for CO_2 storage, Chem. Eng. J. 406 (2021) 126872, https://doi.org/10.1016/j.cej.2020.126872.

[11] Y. Sun, G. Zhang, S. Li, S. Jiang, CO_2/N_2 injection into $CH_4+C_3H_8$ hydrates for gas recovery and CO_2 sequestration, Chem. Eng. J. 375 (2019) 121973, https://doi.org/10.1016/j.cej.2019.121973.

[12] G.D. Holder, S.P. Zetts, N. Pradhan, Phase behavior in systems containing clathrate hydrates: A review, Rev. Chem. Eng. 5 (1988) 1-70, https://doi.org/10.1515/REVCE.1988.5.1-4.1.

[13] A.K. Sum, C.A. Koh, E.D. Sloan, Clathrate hydrates: From laboratory science to engineering practice, Ind. Eng. Chem. Res. 48 (2009) 7457-7465, https://doi.org/10.1021/ie900679m.

[14] S. Li, J. Wang, X. Lv, K. Ge, Z. Jiang, Y. Li, Experimental measurement and thermodynamic modeling of methane hydrate phase equilibria in the presence of chloride salt, Chem. Eng. J. 395 (2020) 125126, https://doi.org/10.1016/j.cej.2020.125126.

[15] A.L. Ballard, E.D. Sloan Jr., The next generation of hydrate prediction: An overview, J. Supramol. Chem. 2 (2002) 385-392, https://doi.org/10.1016/S1472-7862(03)00063-7.

[16] E.D. Sloan Jr., C.A. Koh, Clathrate Hydrates of Natural Gases, CRC Press/Taylor & Francis, 2008.

[17] W.A. Cole, P. Stephen, Flash calculations for gas hydrates: A rigorous approach, Chem. Eng. Sci. 45 (1990) 569-573, http://dx.doi.org/10.1016/0009-2509(90)87001-9.

[18] M.L. Michelsen, Calculation of hydrate fugacities, Chem. Eng. Sci. 46 (1991) 1192-1193, http://dx.doi.org/10.1016/0009-2509(91)85113-C.

[19] J.D. van der Waals, Continuity of the Gaseous and Liquid State of Matter, Ph.D. thesis, Leiden, 1873.

[20] H.W. Curtis, R.B. Michael, Phase Behavior, SPE Monograph Series 20, 2000.

[21] D.Y. Peng, D.B. Robinson, A new two-constant equation of state, Ind. Eng. Chem. Fundam. 15 (1976) 59-64, https://doi.org/10.1021/i160057a011.

[22] G. Soave, Equilibrium constants from a modified Redlich-Kwong equation of state, Chem. Eng. Sci. 27 (1972) 1197-1203, https://doi.org/10.1016/0009-2509(72)80096-4.

[23] M.L. Michelsen, J. Mollerup, Thermodynamic modelling: Fundamentals and computational aspects, Tie-Line Publications, 2004.

[24] A. Firoozabadi, Thermodynamics and applications of hydrocarbons energy production, McGraw-Hill Education, 2015.

[25] H. Li, Multiphase equilibria of complex reservoir fluids, Springer, 2022, https://doi.org/10.1007/978-3-030-87440-7.

[26] M.L. Michelsen, Calculation of multiphase equilibrium, Comput. Chem. Eng. 18 (1994) 545-550, https://doi.org/10.1016/0098-1354(93)E0017-4.

[27] Y. Sofyan, A.J. Ghajar, K.A.M. Gasem, Multiphase equilibrium calculations using Gibbs minimization techniques, Ind. Eng. Chem. Res. 42 (2003) 3786-3801, https://doi.org/10.1021/ie020844m.

[28] W.D. Seider, S. Widagdo, Multiphase equilibria of reactive systems, Fluid Phase Equilib. 123 (1996) 283-303, https://doi.org/10.1016/S0378-3812(96)90039-4.

[29] R. Li, H. Li, Improved three-phase equilibrium calculation algorithm for water/hydrocarbon mixtures, Fuel 244 (2019) 517-527, https://doi.org/10.1016/j.fuel.2019.02.026.

[30] M.L. Michelsen, The isothermal flash problem. Part I Stability, Fluid Phase Equilib. 9 (1982) 1-19, https://doi.org/10.1016/0378-3812(82)85001-2.

[31] M.L. Michelsen, The isothermal flash problem. Part II. Phase-split calculation, Fluid Phase Equilib. 9 (1982) 21-40, https://doi.org/10.1016/0378-3812(82)85002-4.

[32] C.H. Whitson, M.L. Michelsen, The negative flash, Fluid Phase Equilib. 53 (1989) 51-71, https://doi.org/10.1016/0378-3812(89)80072-X.

[33] Z. Li, A. Firoozabadi, General strategy for stability testing and phase-split calculation in two and three phases, SPE J. 17 (2012) 1096-1107, https://doi.org/10.2118/129844-PA.

[34] D.V. Nichita, D. Broseta, F. Montel, Calculation of convergence pressure/temperature and stability test limit loci of mixtures with cubic equations of state, Fluid Phase Equilib. 261 (2007) 176-184, https://doi.org/10.1016/j.fluid.2007.07.041.

[35] S.E. Gorucu, R.T. Johns, Robustness of three-phase equilibrium calculations, J. Petrol. Sci. Eng. 143 (2016) 72-85, https://doi.org/10.1016/j.petrol.2016.02.025.

[36] K.B. Haugen, A. Firoozabadi, L. Sun, Efficient and robust three-phase split computations, AIChE J. 57 (2011) 2555-2565, https://doi.org/10.1002/aic.12452.

[37] R. Okuno, R.T. Johns, K. Sepehrnoori, Three-phase flash in compositional simulation using a reduced method, SPE J. 15 (2010) 689-703, https://doi.org/10.2118/125226-PA.

[38] H. Pan, M. Connolly, H. Tchelepi, Multiphase equilibrium calculation framework for compositional simulation of CO_2 injection in low-temperature reservoirs, Ind. Eng. Chem. Res. 58 (2019) 2052-2070, https://doi.org/10.1021/acs.iecr.8b05229.

[39] F.A. Medeiros, I.S.V. Segtovich, F.W. Tavares, A.K. Sum, Sixty years of the van der Waals and Platteeuw model for clathrate hydrates-A critical review from its statistical thermodynamic basis to its extensions and applications, Chem. Rev. 120 (2020) 13349-13381, https://doi.org/10.1021/acs.chemrev.0c00494.

[40] J.H. van der Waals, J.C. Platteeuw, Clathrate solutions, Adv. Chem. Phys. 2 (1959) 1-57, https://doi.org/10.1002/9780470143483.ch1.

[41] J.C. Platteeuw, J.H. van der Waals, Thermodynamic properties of gas hydrates, Mol. Phys. 1 (1958) 91-96, https://doi.org/10.1080/00268975800100111.

[42] V. McKoy, O. Sinanoglu, Theory of dissociation pressures of some gas hydrates, J. Chem. Phys. 38 (1963) 2946-2956, https://doi.org/10.1063/1.1733625.

[43] X. Chen, H. Li, New pragmatic strategies for optimizing Kihara potential parameters used in van der Waals-Platteeuw hydrate model, Chem. Eng. Sci. 248 (2022) 117213, https://doi.org/10.1016/j.jngse.2015.04.003.

[44] W.R. Parrish, J.M. Prausnitz, Dissociation pressures of gas hydrates formed by gas mixtures, Ind. Eng. Chem. Process Des. Dev. 11 (1972) 26-35, https://doi.org/10.1021/i260041a006.

[45] J. Munck, S. Skjold-Jorgensen, P. Rasmussen, Computations of the formation of gas hydrates, Chem. Eng. Sci. 43 (1988) 2661-2672, https://doi.org/10.1016/0009-2509(88)80010-1.

[46] J.H. Yoon, M.K. Chun, H. Lee, Generalized model for predicting phase behavior of clathrate hydrate, AIChE J. 48 (2002) 1317-1330, https://doi.org/10.1002/aic.690480618.

[47] R. Zheng, Z. Fan, X. Li, S. Negahban, Phase boundary of CH_4, CO_2, and binary CH_4-CO_2 hydrates formed in NaCl solutions, J. Chem. Thermodyn. 154 (2021) 106333, https://doi.org/10.1016/j.jct.2020.106333.

[48] S.E. Meragawi, N.I. Diamantonis, I.N. Tsimpanogiannis, I.G. Economou, Hydrate-fluid phase equilibria modeling using PC-SAFT and Peng-Robinson equations of state, Fluid Phase Equilib. 413 (2016) 209-219, https://doi.org/10.1016/j.fluid.2015.12.003.

[49] H. Tavasoli, F. Feyzi, Compositional data calculation of vapor-aqueous-hydrate systems in batch operations by a new algorithm, J. Nat. Gas. Sci. Eng. 24 (2015) 473-488, http://dx.doi.org/10.1016/j.jngse.2015.04.003.

[50] B. Tohidi, A. Danesh, A.C. Todd, Modeling single and mixed electrolyte-solutions and its applications to gas hydrates, Chem. Eng. Res. Des. 73 (1995) 464-472.

[51] B. Tohidi, A. Danesh, R.W. Burgass, A.C. Todd, Measurement and prediction of hydrate-phase equilibria for reservoir fluids, SPE Prod. Fac. 11 (1996) 69-76, https://doi.org/10.2118/28884-PA.

[52] B. Tohidi, A. Danesh, A.C. Todd, R.W. Burgass, K.K. Ostergaard, Equilibrium data and thermodynamic modelling of cyclopentane and neopentane hydrates, Fluid Phase Equilib. 138 (1997) 241-250, https://doi.org/10.1016/S0378-3812(97)00164-7.

[53] P.R. Bishnoi, A.K. Gupta, P. Englezos, N. Kalogerakis, Multiphase equilibrium flash calculations for systems containing gas hydrates, Fluid Phase Equilib. 53 (1989) 97-104, http://dx.doi.org/10.1016/0378-3812(89)80076-7.

[54] A.K. Gupta, P. Raj Bishnoi, N. Kalogerakis, A method for the simultaneous phase equilibria and stability calculations for multiphase reacting and non-reacting systems, Fluid Phase Equilib. 63 (1991) 65-89, http://dx.doi.org/10.1016/0378-3812(91)80021-M.

[55] A.K. Gupta, Steady state simulation of chemical processes. Ph.D. Thesis, University of Calgary, Calgary, Canada, 1988.

[56] A.L. Ballard, E.D. Sloan Jr., The next generation of hydrate prediction I. Hydrate standard states and incorporation of spectroscopy, Fluid Phase Equilib. 194-197 (2002) 371-383, https://doi.org/10.1016/S0378-3812(01)00697-5.

[57] M.D. Jager, A.L. Ballard, E.D. Sloan Jr., The next generation of hydrate prediction II. Dedicated aqueous phase fugacity model for hydrate prediction, Fluid Phase Equilib. 211 (2003) 85-107, https://doi.org/10.1016/S0378-3812(03)00155-9.

[58] A.L. Ballard, E.D. Sloan Jr., The next generation of hydrate prediction Part III. Gibbs energy minimization formalism, Fluid Phase Equilib. 218 (2004) 15-31, https://doi.org/10.1016/j.fluid.2003.08.005.

[59] A.L. Ballard, E.D. Sloan Jr., The next generation of hydrate prediction IV. A comparison of available hydrate prediction programs, Fluid Phase Equilib. 216 (2004) 257-270, https://doi.org/10.1016/j.fluid.2003.11.004.

[60] T.H. Sirino, M.A.M. Neto, D. Bertoldi, R.E.M. Morales, A.K. Sum, Multiphase flash calculations for gas hydrates systems, Fluid Phase Equilib. 475 (2018) 45-63, https://doi.org/10.1016/j.fluid.2018.07.029.

[61] I.S.V. Segtovich, A.G. Barreto Jr., F.W. Tavares, Simultaneous multiphase flash and stability analysis calculations including hydrates, Fluid Phase Equilib. 413 (2016) 196-208, https://doi.org/10.1016/j.fluid.2015.10.030.

[62] I.S.V. Segtovich, A.G. Barreto Jr., F.W. Tavares, Phase diagrams for hydrates beyond incipient condition - Complex behavior in methane/propane and carbon dioxide/iso-butane hydrates, Fluid Phase Equilib. 426 (2016) 75-82, https://doi.org/10.1016/j.fluid.2016.02.002.

[63] M.A. Mahabadian, A. Chapoy, B. Burgass, B. Tohidi, Development of a multiphase flash in presence of hydrates: Experimental measurements and validation with the CPA equation of state, Fluid Phase Equilib. 414 (2016) 117-132, http://dx.doi.org/10.1016/j.fluid.2016.01.009.

[64] V. Belandria, A. Eslamimanesh, A.H. Mohammadi, P. Theveneau, H. Legendre, D. Richon, Compositional analysis and hydrate dissociation conditions measurements for carbon dioxide + methane + water system, Ind. Eng. Chem. Res. 50 (2011) 5783-5794, https://doi.org/10.1021/ie101959t.

[65] A. Pina-Martinez, Y. Le Guennec, R. Privat, J. Jaubert, P.M. Mathias, Analysis of the combinations of property data that are suitable for a safe estimation of consistent Twu α-function parameters: updated parameter values for the translated-consistent tc-PR and tc-RK cubic equations of state, J. Chem. Eng. Data 63 (2018) 3980-3988, https://doi.org/10.1021/acs.jced.8b00640.

[66] C.H. Twu, D. Bluck, J.R. Cunningham, J.E. Coon, A cubic equation of state with a new alpha function and a new mixing rule, Fluid Phase Equilib. 69 (1991) 33-50, https://doi.org/10.1016/0378-3812(91)90024-2.

[67] X. Chen, H. Li, An improved volume-translated SRK equation of state dedicated to accurate determination of saturated and single-phase liquid densities, Fluid Phase Equilib. 521 (2020) 112724, https://doi.org/10.1016/j.fluid. 2020.112724.

[68] X. Chen, H. Li, Improved prediction of saturated and single-phase liquid densities of water through volume-translated SRK EOS, Fluid Phase Equilib. 528 (2021) 112852, https://doi.org/10.1016/j.fluid.2020.112852.

[69] H.H. Rachford Jr., J.D. Rice, Procedure for use of electronic digital computers in calculating flash vaporization hydrocarbon equilibrium, J. Petrol. Tech. 4 (1952) 327-328, https://doi.org/10.2118/952327-G.

[70] Q.L. Ma, G.J. Chen, C.Y. Sun, Vapor-liquid-liquid-hydrate phase equilibrium calculation for multicomponent systems containing hydrogen, Fluid Phase Equilib. 338 (2013) 87-94, http://dx.doi.org/10.1016/j.fluid.2012.11.002.

[71] I. Soreide, C.H. Whitson, Peng-Robinson predictions for hydrocarbons, CO_2, N_2, and H_2S with pure water and NaCl brine, Fluid Phase Equilib. 77 (1992) 217-240, https://doi.org/10.1016/0378-3812(92)85105-H.

[72] A.M. Abudour, S.A. Mohammad, R.L. Robinson Jr., K.A.M. Gasem, Generalized binary interaction parameters for the Peng-Robinson equation of state, Fluid Phase Equilib. 383 (2014) 156-173, https://doi.org/10.1016/j.fluid.2014.10.006.

[73] A. Aasen, M. Hammer, G. Skaugen, J.P. Jakobsen, O. Wilhelmsen, Thermodynamic models to accurately describe the PVTxy-behavior of water/carbon dioxide mixtures, Fluid Phase Equilib. 442 (2017) 125-139, http://dx.doi.org/10.1016/j.fluid.2017.02.006.

[74] J.W. Gibbs, The collected works of J. Willard Gibbs, Nature 124 (1929) 119-120.

[75] M.M. Mooijer-van den Heuvel, Phase behaviour and structural aspects of ternary clathrate hydrate systems. The role of additives, Ph.D. Thesis, Chemical Engineering, Delft University of Technology, Netherlands, 2004.

[76] G. Venkatarathnam, L.R. Oellrich, Identification of the phase of a fluid using partial derivatives of pressure, volume, and temperature without reference to saturation properties: Applications in phase equilibria calculations, Fluid Phase Equilib. 301 (2011) 225-233, http://dx.doi.org/10.1016/j.fluid.2010.12.001.

[77] G.G. Simeoni, T. Bryk, F.A. Gorelli, M. Krisch, G. Ruocco, M. Santoro, T. Scopigno, The Widom line as the crossover between liquid-like and gas-like behaviour in supercritical fluids, Nature Phys. 6 (2010) 503-507, https://doi.org/10.1038/nphys16830.

[78] D. Le Quang, B. Bouillot, J.M. Herri, P. Glenat, P. Duchet-Suchaux, Experimental procedure and results to measure the composition of gas hydrate, during crystallization and at equilibrium, from N_2-CO_2-CH_4-C_2H_6-C_3H_8-C_4H_{10} gas mixtures, Fluid Phase Equilib. 413 (2016) 10-21, https://doi.org/10.1016/j.fluid.2015.10.022.

[79] J.M. Herri, A. Bouchemoua, M. Kwaterski, A. Fezoua, Y. Ouabbas, A. Cameirao, Gas hydrate equilibria for CO_2-N_2 and CO_2-CH_4 gas mixtures—Experimental studies and thermodynamic modelling, Fluid Phase Equilib. 301 (2011) 171-190, https://doi.org/10.1016/j.fluid.2010.09.041.

[80] S.M. Babakhani, B. Bouillot, S. Ho-Van, J. Douzet, J.M. Herri, A review on hydrate composition and capability of thermodynamic modeling to predict hydrate pressure and composition, Fluid Phase Equilib. 472 (2018) 22-38, https://doi.org/10.1016/j.fluid.2018.05.007.

[81] Y.H. Sun, S.L. Li, G.B. Zhang, W. Guo, Y.H. Zhu, Hydrate phase equilibrium of CH_4+N_2+CO_2 gas mixtures and cage occupancy behaviors, Ind. Eng. Chem. Res. 56 (2017) 8133-8142, https://doi.org/10.1021/acs.iecr.7b01093.

[82] S. Li, G. Zhang, Z. Dai, S. Jiang, Y. Sun, Concurrent decomposition and replacement of marine gas hydrate with the injection of CO_2-N_2, Chem. Eng. J. 420 (2021) 129936, https://doi.org/10.1016/j.cej.2021.1299363.

[83] M. Khurana, Z. Yin, P. Linga, A Review of clathrate hydrate nucleation, ACS Sustainable Chem. Eng. 5 (2017) 11176-11203, https://doi.org/10.1021/acssuschemeng.7b03238.

[84] W. Ke, T.M. Svartaas, D. Chen, A review of gas hydrate nucleation theories and growth models, J. Nat. Gas. Sci. Eng. 61 (2019) 169-196, https://doi.org/10.1016/j.jngse.2018.10.021.

[85] H.J. Ng, Hydrate phase composition for multicomponent gas mixtures, Ann. N. Y. Acad. Sci. 912 (2000) 1034-1039, https://doi.org/10.1111/j.1749-6632.2000.tb06858.x.

[86] M.K. Hsieh, W.Y. Ting, Y.P. Chen, P.C. Chen, S.T. Lin, L.J. Chen, Explicit pressure dependence of the Langmuir adsorption constant in the van der Waals-Platteeuw model for the equilibrium conditions of clathrate hydrates, Fluid Phase Equilib. 325 (2012) 80-89, https://doi.org/10.1016/j.fluid.2012.04.012.

Supplementary Material

1. Van der Waals-Platteeuw Model

The classical van der Waals-Platteeuw (vdW-P) model is defined as [1],

$$\frac{\mu_w^H - \mu_w^W}{RT} = \frac{\Delta\mu_w^0}{RT_0} + \int_{P_0}^{P} \frac{\Delta v_w^{\beta-W}}{R\overline{T}} dP - \int_{T_0}^{T} \frac{\Delta h_w^{\beta-W}}{RT^2} dT + \sum_k \lambda_k \ln\left(1 - \sum_i \theta_{ik}\right) - \ln a_w \qquad \text{(5-S1)}$$

where T and P denote temperature and pressure; R denotes the universal gas constant; the superscript 0 refers to the triple point of water; the superscripts H, β, and W refer to the hydrate with filled lattice, the assumed hydrate with empty lattice, and the aqueous water, respectively. When a hydrate phase is formed, the chemical potential of water in the hydrate should be less than the chemical potential of water in the aqueous phase (i.e., $\mu_w^H - \mu_w^W < 0$). At equilibrium, the chemical potentials of water in the hydrate and the aqueous phases are equal (i.e., $\mu_w^H - \mu_w^W = 0$). In addition, $\Delta\mu_w^0$ denotes the difference between the chemical potential of water in the empty hydrate lattice and the chemical potential of water in the aqueous phase at the triple point. The triple-point temperature and pressure (T_0 and P_0) were set to 273.16 K and 611.2 Pa, respectively, in this study. Moreover, $\Delta v_w^{\beta-W}$ denotes the difference in the molar volume of water between the empty lattice and the aqueous phase; $\overline{T}$ denotes the average temperature between T and T_0. Besides, $\Delta h_w^{\beta-W}$ represents the difference in the molar enthalpy of water between the empty lattice and the aqueous phase. The value of $\Delta h_w^{\beta-W}$ is determined using the following equations [1,2],

$$\Delta h_w^{\beta-W} = \Delta h_w^0 + \int_{T_0}^{T} \Delta C_p dT \qquad \text{(5-S2)}$$

where Δh_w^0 denotes the difference in molar enthalpy between pure liquid water and the empty hydrate lattice at the triple point; ΔC_p denotes the difference in heat capacity, which is typically a temperature-dependent function as [2],

$$\Delta C_p = -38.13 + 0.141(T - T_0) \tag{5-S3}$$

Table 5-S1 shows the values of $\Delta\mu_w^0$, Δh_w^0, and $\Delta v_w^{\beta-W}$ for the hydrate structures I and II in the vdW-P hydrate model [3].

Table 5-S1 Thermodynamic parameters used in vdW-P hydrate model [3].

Hydrate structure	$\Delta\mu_w^0$ (J/mol)	Δh_w^0 (J/mol)	$\Delta v_w^{\beta-W}$ (J/mol)
Structure I	1297	-4620.5	4.6
Structure II	937	-4984.5	5

In **Eq. 5-S1**, λ_k denotes the number of k cavity per water molecule in the unit cell, that is, λ_k represents the ratio of water molecules over the type k cavity in the hydrate phase. For type I hydrate structure, λ_1=1/23 (small cavity) and λ_2=3/23 (large cavity). For type II hydrate structure, λ_1=2/17 (small cavity) and λ_2=1/17 (large cavity). In addition, θ_{ik} denotes the probability of a cage k being occupied by a guest molecule i and is determined using the following equation [1],

$$\theta_{ik} = \frac{C_{ik} f_i}{1 + \sum_i C_{ik} f_i} \tag{5-S4}$$

where f_i is the fugacity of the hydrate-forming gas i obtained using an equation of state (EOS); C_{ik} is the Langmuir constant. The Lennard-Jones-Devonshire cell theory is used to calculate the Langmuir constant using the following equation [1-4],

$$C_{ik} = \frac{4\pi}{k_B T} \int_0^{R_k - a} \exp\left(-\frac{w_{ik}(r)}{k_B T}\right) r^2 dr \tag{5-S5}$$

where k_B denotes the Boltzmann constant; $w_{ik}(r)$ denotes the potential energy for the interaction between the guest molecule and the water molecule from the cavity; r is the

radial distance of the guest molecule from the cavity center. Assuming a spherical core, the Kihara potential can aid in determining $w_{ik}(r)$ using the following equations [1-4],

$$w_{ik}(r) = 2z\varepsilon\left[\frac{\sigma^{12}}{R_k^{11} r}\left(\delta^{10} + \frac{a}{R_k}\delta^{11}\right) - \frac{\sigma^{6}}{R_k^{5} r}\left(\delta^{4} + \frac{a}{R_k}\delta^{5}\right)\right] \tag{5-S6}$$

$$\delta^n = \frac{1}{n}\left[\left(1 - \frac{r}{R_k} - \frac{a}{R_k}\right)^{-n} - \left(1 + \frac{r}{R_k} - \frac{a}{R_k}\right)^{-n}\right] \tag{5-S7}$$

where z is the total quantity of water molecules in cavity k; R_k and a are the radii of the cavity and the hydrate-forming molecule, respectively. The value of n can be 4, 5, 10, or 11. ε, σ, and a represent the gas-dependent Kihara potential parameters. Our previous study has developed a new procedure for fitting the Kihara potential parameters in vdW-P model [5]. **Table 5-S2** summarizes the Kihara potential parameters in vdW-P model used in this work.

Table 5-S2 Kihara potential parameters in vdW-P hydrate model used in this study [5].

Guest gas	a (Å)	σ (Å)	ε/k_B (K)
CH_4	0.3834	3.1898	156.7348
C_2H_6	0.5651	3.3603	177.2618
C_3H_8	0.6502	3.7644	228.8093
iC_4H_{10}	0.8706	3.5599	237.3476
nC_4H_{10}	0.9379	3.5263	197.2445
CO_2	0.6805	2.9826	172.1648
N_2	0.3526	2.9416	133.4185

In the final term of **Eq. 5-S1**, a_w is the water activity in aqueous phase. Since the solubilities of gases in water are very small, a_w is assumed to be equal to the molar fraction of water in aqueous phase, which is close to unity [2].

2. Equation of State for Fugacity Calculations

The current study employs the volume translated Peng-Robinson (vt-PR) EOS to determine the fugacity of components [6,7]. The vt-PR EOS is represented using the following equation [6],

$$P = \frac{RT}{v-b} - \frac{a}{(v+t)(v+b+2t)+(b+t)(v-b)} \tag{5-S8}$$

where v is molar volume in PR EOS; t is the volume translated term to improve the density calculations over a wide temperature and pressure range; a and b are PR EOS parameters representing the attractive force and repulsive force between the molecules, respectively. The values of a and b in PR EOS can be expressed using the following equations [6,7],

$$a = 0.457535\frac{R^2T_c^2}{P_c}\alpha(T) \tag{5-S9}$$

$$b = 0.077796\frac{RT_c}{P_c} - t \tag{5-S10}$$

where T_c and P_c are critical temperature and critical pressure, respectively; $\alpha(T)$ is the so-called α-function. This study adopts the Twu α-function updated by Pina-Martinez et al. because of its good performances in reproducing thermodynamic properties [6,8],

$$\alpha(T) = T_r^{N(M-1)}\exp[L(1-T_r^{MN})] \tag{5-S11}$$

where T_r is reduced temperature (i.e., $T_r = \frac{T}{T_c}$); L, M, and N are the compound-dependent parameters. **Table 5-S3** summarizes the thermodynamic parameters and α-function parameters of components used in this study [6].

Table 5-S3. Thermodynamic parameters and α-function parameters of components used in this study [6].

Components	T_c (K)	P_c (MPa)	L	M	N
H_2O	647.096	22.064	0.3872	0.8720	1.9668
CH_4	190.564	4.5992	0.1473	0.9075	1.8243
C_2H_6	305.322	4.872	0.3041	0.8694	1.3340

C_3H_8	369.83	4.248	0.7212	0.9076	0.7830
iC_4H_{10}	407.80	3.640	1.0649	0.9876	0.5812
nC_4H_{10}	425.12	3.796	0.4120	0.8488	1.3282
CO_2	304.21	7.383	0.1784	0.8590	2.4107
N_2	126.21	3.390	0.1242	0.8898	2.0130

In the vt-PR EOS adopted in this study, the volume translated term for gases is expressed as [9],

$$t = v - c_1\left(\frac{RT_c}{P_c}\right) - \delta_c\left(\frac{1}{c_2 + c_3 d}\right) \tag{5-S12}$$

where c_1, c_2 and c_3 are the fluid-dependent parameters; δ_c is the volume shift at critical point in PR EOS; d is the dimensionless distance in PR EOS. The expressions of δ_c and d are given as,

$$d = -\frac{v^2}{RT_c}\left(\frac{\partial P}{\partial v}\right)_T = \frac{v^2}{RT_c}\left[\frac{RT}{(v-b)^2} - \frac{2a(v+b)}{\left(v^2 + 2bv - b^2\right)^2}\right] \tag{5-S13}$$

$$\delta_c = \frac{RT_c}{P_c}\left(Z_c - Z_c^{EXP}\right) = v_c - v_c^{EXP} \tag{5-S14}$$

where Z_c and v_c are the critical compressibility factor and critical molar volume in PR EOS, respectively; Z_c^{EXP} and v_c^{EXP} are the experimental critical compressibility factor and critical molar volume, respectively.

The volume translated term for water is expressed as [10],

$$t = v - c_1\left(\frac{RT_c}{P_c}\right) - \delta_c\left(\frac{1}{c_2 + c_3\left(d + c_5\left(P_r - 1\right)\right)^{c_4}}\right) \tag{5-S15}$$

where c_4 and c_5 are another two fluid-dependent parameters; P_r is reduced pressure (i.e., $P_r = \frac{P}{P_c}$). **Table 5-S4** summarizes the parameters in volume translated term of components used in this study [9,10].

Table 5-S4. Parameters in volume translated term of components used in this study [9,10].

Components	c_1	c_2	c_3	c_4	c_5
H_2O	0.02056	1.04894	1.89448	0.74355	-0.29850
CH_4	-0.00195	0.79540	2.13497	-	-
C_2H_6	0.00270	0.85431	2.59463	-	-
C_3H_8	0.00492	0.89221	2.75570	-	-
iC_4H_{10}	0.00554	0.89812	2.61896	-	-
nC_4H_{10}	0.00594	0.93036	2.60453	-	-
CO_2	0.00608	0.92912	2.65917	-	-
N_2	-0.00252	0.75199	2.19566	-	-

The fugacity of pure gas can be further calculated using tc-PR EOS based on the following equation [11,12],

$$f = P\exp\left(Z - 1 - \ln(Z-B) - \frac{A}{2\sqrt{2}B}\ln\left[\frac{Z+\left(1+\sqrt{2}\right)B}{Z+\left(1-\sqrt{2}\right)B}\right] - \frac{tP}{RT}\right) \tag{5-S16}$$

where $A = \frac{aP}{R^2T^2}$ and $B = \frac{(b+t)P}{RT}$, and Z is the compressibility factor calculated using the following equation [11,12],

$$Z^3 - (1-B)Z^2 + \left(A - 3B^2 - 2B\right)Z - \left(AB - B^2 - B^3\right) = 0 \tag{5-S17}$$

For mixtures, the fugacity of each compound is calculated using the following equation [11,12],

$$f_i = y_i P\exp\left(\frac{B_i}{B}(Z-1) - \ln(Z-B) + \frac{A}{2\sqrt{2}B}\left(\frac{B_i}{B} - \frac{2}{A}\sum_{j=1}^{N} y_i A_{ij}\right)\ln\left[\frac{Z+\left(1+\sqrt{2}\right)B}{Z+\left(1-\sqrt{2}\right)B}\right] - \frac{t_i P}{RT}\right) \tag{5-S18}$$

where the subscript i denotes the pure compound i in the mixture and y_i is the molar fraction of the pure compound i in a given phase. The terms A and B are obtained using the following equations [11,12],

$$A = \sum_{i=1}^{N}\sum_{j=1}^{N} y_i y_j A_{ij} \tag{5-S19}$$

$$B = \sum_{i=1}^{N} y_i B_i \tag{5-S20}$$

$$A_{ij} = \left(1 - k_{ij}\right)\sqrt{A_i A_j} \tag{5-S21}$$

where k_{ij} denotes the empirical "binary interaction parameters (BIPs)". The BIPs may affect the robustness and accuracy of multiphase equilibrium calculations [13]. After many careful trials, the values of k_{ij} used in the example calculations of **Cases 1** and **2** were determined and summarized in **Tables 5-S5** and **5-S6**. In the multiphase equilibrium calculations of **Cases 3** and **4**, the correlations for BIPs provided by Soreide and Whitson [13,14] were used to calculate the fugacities of components.

Table 5-S5. BIPs between the components in the $H_2O/C_2H_6/C_3H_8$ mixture.

Component	H_2O	C_2H_6	C_3H_8
H_2O	0	0.2	0.1
C_2H_6	0.2	0	0.022
C_3H_8	0.1	0.022	0

Table 5-S6. BIPs between the components in the $H_2O/CH_4/CO_2$ mixture.

Component	H_2O	CH_4	CO_2
H_2O	0	0.16	0.45
CH_4	0.16	0	0.1
CO_2	0.45	0.1	0

3. Detailed Results for Example Calculations

Tables 5-S7 and 5-**S8** present the experimental data and the calculation results for gas fractions in hydrate phase and vapor phase yielded by the new VLAH four-phase equilibrium algorithm for $H_2O/CH_4/CO_2$ mixtures (**Case 2** in the manuscript). **Tables 5-S9** and **5-S10** present the experimental data and the calculation results for gas fractions in hydrate phase and vapor phase yielded by the new VLAH four-phase equilibrium algorithm for water/natural gas mixtures (**Case 4** in the manuscript).

Table 5-S7. Calculation results in reproducing gas fractions in vapor phase and hydrate phase yielded by the new VLAH four-phase equilibrium algorithm for $H_2O/CH_4/CO_2$ mixtures against the experimental data (free-water) from Belandria et al. [15]

T (K)	P (MPa)	Experimental data for gas fractions in vapor phase		Experimental data for gas fractions in hydrate phase		Predicted gas fractions in vapor phase		Predicted gas fractions in hydrate phase		AAD% for predicted gas fractions in vapor phase		AAD% for predicted gas fractions in hydrate phase	
		CO_2	CH_4	CO_2	CH_4	CO_2	CH_4	CO_2	CH_4	CO_2	CH_4	CO_2	CH_4
273.6	1.844	0.345	0.655	0.549	0.451	0.4068	0.5932	0.5678	0.4322	17.91	9.43	3.43	4.18

273.6	1.941	0.288	0.712	0.392	0.608	0.3732	0.6268	0.5354	0.4646	29.57	11.96	36.59	23.59
273.6	2.048	0.22	0.78	0.294	0.706	0.3591	0.6409	0.5235	0.4765	63.21	17.83	78.06	32.51
273.6	1.51	0.63	0.37	0.884	0.116	0.7089	0.2911	0.8166	0.1834	12.53	21.34	7.62	58.08
273.6	1.607	0.545	0.455	0.801	0.199	0.6601	0.3399	0.7823	0.2177	21.11	25.29	2.33	9.38
275.2	2.583	0.166	0.834	0.338	0.662	0.2041	0.7959	0.3293	0.6707	22.98	4.57	2.58	1.32
275.2	2.123	0.384	0.616	0.65	0.35	0.4553	0.5447	0.6059	0.3941	18.56	11.57	6.79	12.61
275.2	2.22	0.302	0.698	0.586	0.414	0.4113	0.5887	0.5649	0.4351	36.19	15.66	3.60	5.10
275.2	2.4	0.228	0.772	0.366	0.634	0.3688	0.6312	0.5256	0.4744	61.76	18.24	43.61	25.18
275.2	1.792	0.657	0.343	0.831	0.169	0.7271	0.2729	0.8238	0.1762	10.66	20.42	0.87	4.26
275.2	1.865	0.565	0.435	0.752	0.248	0.6888	0.3112	0.7969	0.2031	21.92	28.47	5.97	18.10
276.1	2.813	0.179	0.821	0.264	0.736	0.2172	0.7828	0.3422	0.6578	21.35	4.66	29.64	10.63
276.1	3.025	0.134	0.866	0.239	0.761	0.1530	0.8470	0.2561	0.7439	14.19	2.20	7.15	2.25
276.1	3.027	0.096	0.904	0.238	0.762	0.1592	0.8408	0.2655	0.7345	65.86	6.99	11.55	3.61
276.1	2.318	0.405	0.595	0.644	0.356	0.4735	0.5265	0.6178	0.3822	16.92	11.51	4.07	7.37
276.1	2.503	0.315	0.685	0.4	0.6	0.3923	0.6077	0.5419	0.4581	24.55	11.29	35.48	23.65
276.1	2.69	0.232	0.768	0.312	0.688	0.3668	0.6332	0.5203	0.4797	58.12	17.56	66.78	30.28
276.1	1.985	0.669	0.331	0.877	0.123	0.7291	0.2709	0.8219	0.1781	8.98	18.15	6.28	44.76
276.1	2.174	0.579	0.421	0.784	0.216	0.6598	0.3402	0.7729	0.2271	13.95	19.19	1.41	5.12
278.1	3.631	0.139	0.861	0.225	0.775	0.1820	0.8180	0.2871	0.7129	30.96	5.00	27.60	8.01
278.1	3.802	0.103	0.897	0.148	0.852	0.1544	0.8456	0.2513	0.7487	49.88	5.73	69.81	12.13
278.1	3.037	0.323	0.677	0.457	0.543	0.4266	0.5734	0.5633	0.4367	32.08	15.31	23.26	19.57
278.1	3.319	0.233	0.767	0.273	0.727	0.3782	0.6218	0.5208	0.4792	62.30	18.93	90.75	34.08
278.1	2.58	0.609	0.391	0.786	0.214	0.7058	0.2942	0.7970	0.2030	15.90	24.76	1.40	5.16
280.2	4.486	0.147	0.853	0.307	0.693	0.2066	0.7934	0.3075	0.6925	40.57	6.99	0.18	0.08
280.2	4.655	0.108	0.892	0.245	0.755	0.1752	0.8248	0.2685	0.7315	62.27	7.54	9.59	3.11
280.2	4.109	0.235	0.765	0.42	0.58	0.3980	0.6020	0.5254	0.4746	69.37	21.31	25.09	18.17
280.2	3.481	0.49	0.51	0.788	0.212	0.6938	0.3062	0.7787	0.2213	41.59	39.96	1.18	4.38
282.2	5.767	0.114	0.886	0.276	0.724	0.1909	0.8091	0.2762	0.7238	67.48	8.68	0.07	0.03
					Overall					34.92	14.85	20.78	14.71

Table 5-S8. Calculation results in reproducing gas fractions in vapor phase and hydrate phase yielded by the new VLAH four-phase equilibrium algorithm for $H_2O/CH_4/CO_2$ mixtures against the experimental data (free-water) from Le Quang et al. [16]

T (K)	*P* (MPa)	Experimental data for gas fractions in vapor phase		Experimental data for gas fractions in hydrate phase		Predicted gas fractions in vapor phase		Predicted gas fractions in hydrate phase		AAD% for predicted gas fractions in vapor phase		AAD% for predicted gas fractions in hydrate phase	
		CO_2	CH_4	CO_2	CH_4	CO_2	CH_4	CO_2	CH_4	CO_2	CH_4	CO_2	CH_4
276.55	3.33	0.127	0.874	0.318	0.682	0.1435	0.8565	0.2441	0.7559	13.02	2.01	23.25	10.84
277.55	3.53	0.134	0.866	0.319	0.681	0.1555	0.8445	0.2539	0.7461	16.04	2.48	20.41	9.56
278.05	3.71	0.141	0.859	0.32	0.68	0.1583	0.8417	0.2556	0.7444	12.30	2.02	20.13	9.47
278.95	4.03	0.151	0.849	0.32	0.68	0.1696	0.8304	0.2663	0.7337	12.34	2.19	16.77	7.89
279.95	4.45	0.163	0.837	0.317	0.683	0.1812	0.8188	0.2763	0.7237	11.16	2.17	12.84	5.96
280.95	4.93	0.175	0.825	0.296	0.704	0.1932	0.8068	0.2859	0.7141	10.42	2.21	3.41	1.43
275.35	2.91	0.12	0.88	0.292	0.708	0.1330	0.8670	0.2309	0.7691	10.80	1.47	20.92	8.63
275.65	2.97	0.129	0.871	0.282	0.718	0.1354	0.8646	0.2328	0.7672	4.93	0.73	17.44	6.85
276.75	3.18	0.135	0.865	0.283	0.717	0.1635	0.8365	0.2676	0.7324	21.13	3.30	5.44	2.15

277.65	3.47	0.147	0.853	0.27	0.73	0.1735	0.8265	0.2774	0.7226	18.06	3.11	2.74	1.01
278.35	3.8	0.162	0.838	0.227	0.773	0.1596	0.8404	0.2553	0.7447	1.46	0.28	12.48	3.67
					Overall					11.97	1.99	14.17	6.13

Table 5-S9. Calculation results in reproducing gas fractions in vapor phase yielded by the new VLAH four-phase equilibrium algorithm for water/natural gas mixtures against the experimental data (free-water) from Mahabadian et al. [17]

T (K)	P (MPa)	Experimental data for gas mole fractions in vapor phase							Predicted gas mole fractions in vapor phase							%AAD for calculated gas mole fractions in vapor phase						
		N_2	CO_2	CH_4	C_2H_6	C_3H_8	iC_4H_{10}	nC_4H_{10}	N_2	CO_2	CH_4	C_2H_6	C_3H_8	iC_4H_{10}	nC_4H_{10}	N_2	CO_2	CH_4	C_2H_6	C_3H_8	iC_4H_{10}	nC_4H_{10}
277.45	2.785	0.0183	0.0157	0.923	0.039	0.0016	0.0001	0.0019	0.0212	0.0174	0.9375	0.0197	0.0011	0.0001	0.0027	15.71	10.66	1.57	49.52	31.29	33.20	40.99
279.45	2.875	0.0174	0.015	0.918	0.043	0.0042	0.0002	0.0021	0.0180	0.0180	0.9206	0.0366	0.0030	0.0002	0.0031	3.18	19.86	0.28	14.78	28.33	6.32	49.26
281.45	3.019	0.0167	0.0148	0.906	0.05	0.0096	0.0007	0.0025	0.0166	0.0179	0.9039	0.0504	0.0071	0.0005	0.0032	0.84	20.87	0.23	0.81	26.50	33.95	27.93
282.95	3.149	0.0163	0.0148	0.894	0.055	0.016	0.0013	0.0028	0.0159	0.0177	0.8930	0.0565	0.0122	0.0009	0.0032	2.41	19.72	0.11	2.74	23.51	34.07	12.63
284	3.241	0.0162	0.0148	0.884	0.059	0.0218	0.0018	0.003	0.0155	0.0176	0.8856	0.0589	0.0174	0.0013	0.0031	4.18	18.73	0.18	0.11	20.25	27.55	3.32
287.2	6.205	0.0163	0.0169	0.902	0.05	0.0108	0.0009	0.0027	0.0168	0.0189	0.9044	0.0481	0.0069	0.0005	0.0033	3.25	11.77	0.27	3.83	36.57	45.66	22.67
288.25	6.405	0.0159	0.0163	0.895	0.054	0.0148	0.0012	0.0029	0.0162	0.0185	0.8952	0.0542	0.0107	0.0008	0.0032	1.63	13.70	0.02	0.28	27.37	33.74	11.44
289.25	6.601	0.0154	0.0157	0.885	0.059	0.0211	0.0018	0.003	0.0156	0.0182	0.8866	0.0579	0.0160	0.0012	0.0031	1.61	15.93	0.18	1.86	24.37	31.41	4.77

Table 5-S10. Calculation results in reproducing gas fractions in hydrate phase yielded by the new VLAH four-phase equilibrium algorithm for water/natural gas mixtures against the experimental data (free-water) from Ng [18].

T (K)	P (MPa)	Experimental data for gas mole fractions in hydrate phase						Predicted gas mole fractions in vapor phase						%AAD for calculated gas mole fractions in vapor phase					
		CH_4	C_2H_6	C_3H_8	iC_4H_{10}	nC_4H_{10}	CO_2	CH_4	C_2H_6	C_3H_8	iC_4H_{10}	nC_4H_{10}	CO_2	CH_4	C_2H_6	C_3H_8	iC_4H_{10}	nC_4H_{10}	CO_2
284.3	2.07	0.581	0.074	0.206	0.107	0.031	-	0.5989	0.0559	0.2114	0.1102	0.0236	-	3.09	24.45	2.60	2.98	23.87	-
292.6	6.89	0.617	0.089	0.181	0.087	0.027	-	0.6567	0.0712	0.1771	0.0722	0.0228	-	6.43	19.97	2.16	16.97	15.66	-
282.8	2.07	0.584	0.076	0.265	0.044	0.018	0.011	0.6051	0.0613	0.2688	0.0426	0.0123	0.0100	3.61	19.39	1.43	3.25	31.59	9.19
291.7	6.89	0.621	0.077	0.238	0.039	0.011	0.01	0.6633	0.0709	0.2148	0.0297	0.0118	0.0096	6.81	7.98	9.76	23.86	7.08	3.94

References

[1] J.H. van der Waals, J.C. Platteeuw, Clathrate solutions, Adv. Chem. Phys. 2 (1959) 1-57, https://doi.org/10.1002/9780470143483.ch1.

[2] W.R. Parrish, J.M. Prausnitz, Dissociation pressures of gas hydrates formed by gas mixtures, Ind. Eng. Chem. Process Des. Dev. 11 (1972) 26-35, https://doi.org/10.1021/i260041a006.

[3] P.B. Dharmawardhana, W.R. Parrish, E.D. Sloan, Experimental thermodynamic parameters for the prediction of natural gas hydrate dissociation conditions, Ind. Eng. Chem. Fundam. 19 (1980) 410-414, https://doi.org/10.1021/i160076a015.

[4] X. Chen, H. Li, New pragmatic strategies for optimizing Kihara potential parameters used in van der Waals-Platteeuw hydrate model, Chem. Eng. Sci. 248 (2022) 117213, https://doi.org/10.1016/j.jngse.2015.04.003.

[5] V. McKoy, O. Sinanoglu, Theory of dissociation pressures of some gas hydrates, J. Chem. Phys. 38 (1963) 2946-2956, https://doi.org/10.1063/1.1733625.

[6] A. Pina-Martinez, Y. Le Guennec, R. Privat, J. Jaubert, P.M. Mathias, Analysis of the combinations of property data that are suitable for a safe estimation of consistent Twu α-function parameters: updated parameter values for the translated-consistent tc-PR and tc-RK cubic equations of state, J. Chem. Eng. Data 63 (2018) 3980-3988, https://doi.org/10.1021/acs.jced.8b00640.

[7] D.Y. Peng, D.B. Robinson, A new two-constant equation of state, Ind. Eng. Chem. Fundam. 15 (1976) 59-64, https://doi.org/10.1021/i160057a011.

[8] C.H. Twu, D. Bluck, J.R. Cunningham, J.E. Coon, A cubic equation of state with a new alpha function and a new mixing rule, Fluid Phase Equilib. 69 (1991) 33-50, https://doi.org/10.1016/0378-3812(91)90024-2.

[9] X. Chen, H. Li, An improved volume-translated SRK equation of state dedicated to accurate determination of saturated and single-phase liquid densities, Fluid Phase Equilib. 521 (2020) 112724, https://doi.org/10.1016/j.fluid. 2020.112724.

[10] X. Chen, H. Li, Improved prediction of saturated and single-phase liquid densities of water through volume-translated SRK EOS, Fluid Phase Equilib. 528 (2021) 112852, https://doi.org/10.1016/j.fluid.2020.112852.

[11] J.D. van der Waals, Continuity of the gaseous and liquid state of matter, Ph.D. thesis, Leiden, 1873.

[12] H.W. Curtis, R.B. Michael, Phase behavior, SPE Monograph Series 20, 2000.

[13] R. Li, H. Li, Improved three-phase equilibrium calculation algorithm for water/hydrocarbon mixtures, Fuel 244 (2019) 517-527, https://doi.org/10.1016/j.fuel.2019.02.026.

[14] I. Soreide, C.H. Whitson, Peng-Robinson predictions for hydrocarbons, CO_2, N_2, and H_2S with pure water and NaCl brine, Fluid Phase Equilib. 77 (1992) 217-240, https://doi.org/10.1016/0378-3812(92)85105-H.

[15] V. Belandria, A. Eslamimanesh, A.H. Mohammadi, P. Theveneau, H. Legendre, D. Richon, Compositional analysis and hydrate dissociation conditions measurements for carbon dioxide + methane + water system, Ind. Eng. Chem. Res. 50 (2011) 5783-5794, https://doi.org/10.1021/ie101959t.

[16] D. Le Quang, B. Bouillot, J.M. Herri, P. Glenat, P. Duchet-Suchaux, Experimental procedure and results to measure the composition of gas hydrate, during crystallization and at equilibrium, from N_2-CO_2-CH_4-C_2H_6-C_3H_8-C_4H_{10} gas mixtures, Fluid Phase Equilib. 413 (2016) 10-21, https://doi.org/10.1016/j.fluid.2015.10.022.

[17] M.A. Mahabadian, A. Chapoy, B. Burgass, B. Tohidi, Development of a multiphase flash in presence of hydrates: Experimental measurements and validation with the CPA equation of state, Fluid Phase Equilib. 414 (2016) 117-132, http://dx.doi.org/10.1016/j.fluid.2016.01.009.

[18] H.J. Ng, Hydrate phase composition for multicomponent gas mixtures, Ann. N. Y. Acad. Sci. 912 (2000) 1034-1039, https://doi.org/10.1111/j.1749-6632.2000.tb06858.x.

CHAPTER 6 CONCLUSIONS, CONTRIBUTIONS, AND RECOMMENDATIONS

6.1. Conclusions and Scientific Contributions to the Literature

This study develops a series of advanced VT-EOSs to achieve more accurate volumetric calculations for water and hydrocarbons. To improve the modeling of gas-mixture hydrate equilibria, a new procedure for fitting the Kihara potential parameters in the vdW-P hydrate model has been proposed. Finally, on the basis of the improved thermodynamic models, a multiphase equilibrium calculation algorithm for water/hydrocarbons systems in the presence of gas hydrates is developed.

Chapter 2:

In this work, a new volume translation in SRK EOS is developed to improve the calculation accuracy of saturated and single-phase liquid volumes. To acutely capture the variation of residuals between the measured molar volumes and the calculated ones by CEOS, two fluid-dependent parameters related to distance function have been added to the traditional one fluid-dependent parameter VT-model. As a result, the calculation errors for the saturated and single-phase liquid volumes of different compounds yielded by the newly developed 3-parameter VT-SRK EOS are usually lower than 1%. Besides, a fairly good generalization of the fluid-dependent parameters in the newly proposed VT-model has been obtained for hydrocarbons. Finally, the improved VT-model has been extended to mixtures through the conventional mixing rules, demonstrating that the VT-SRK EOS also performs well in the density predictions for hydrate-forming gas-mixtures.

Chapter 3:

In this chapter, we propose an improved VT-SRK EOS to provide more accurate volumetric prediction for water. First, we adopt an additional fluid-dependent parameter as the power of the dimensionless distance and propose a 4-parameter VT-model. The overall average absolute percentage deviation in reproducing the saturated liquid molar volume of water yielded by the proposed 4-parameter VT-SRK EOS is 0.26%. Then through coupling the 4-parameter VT-model with the translated distance function proposed in this study, a 5-parameter VT-SRK EOS is developed for water. This 5-parameter VT-SRK EOS provides a more accurate determination of the single-phase liquid volume of water over a wide temperature/pressure range. Moreover, we extend the 5-parameter VT-model to mixtures through the conventional mixing rules, demonstrating that the VT-SRK EOS also performs well in the density predictions for water/hydrocarbons systems that may form gas hydrates.

Chapter 4:

This work provides a new pragmatic procedure for fitting Kihara potential parameters in the vdW-P hydrate model. To account for the differences between hydrate structures I and II, this procedure optimizes the Kihara potential parameters in the vdW-P hydrate model based on the experimental hydrate equilibrium data of both pure gases and binary-gas mixtures. Thus, the newly fitted Kihara potential parameters perform well in modeling pure-gas hydrates and also predict gas-mixture hydrate equilibria with good robustness and accuracy. Furthermore, the vdW-P hydrate model coupled with the newly fitted Kihara potential parameters is capable of accurately detecting the hydrate structure transitions and cage occupancy behaviors.

Chapter 5:

In this work, we develop a multiphase equilibrium calculation algorithm for water/hydrocarbons systems in the presence of gas hydrates. In contrast to the conventional framework adopting the simultaneous stability analysis and flash calculation, this new multiphase equilibrium calculation algorithm is formulated in a stage-wise manner. In the developed algorithm, we propose a new criterion for determining the onset of hydrate dissociation and provide a series of material-balance equations involving hydrates. The performance of the new algorithm has been examined by different water/hydrocarbons systems. The calculation results demonstrate that this algorithm is able to determine the multiphase equilibria involving vapor phase, hydrocarbon-rich liquid phase, aqueous phase and gas hydrate phase over a wide range of pressure and temperature conditions. In addition, this algorithm can also provide reliable predictions of the phase fractions and phase compositions of gas hydrate systems.

6.2. Suggested Future Work

- In this study, the new VT-models are developed for SRK EOS. It is worthwhile trying to improve the VT-models for other EOSs as well, such as PC-SAFT EOS and CPA EOS. The performance of the newly proposed VT-models in predicting the densities of complicated mixtures should be further verified with experimental data.
- The present study has primarily focused on optimizing the Kihara potential parameters in the classical vdW-P hydrate model for six gases (i.e., CH_4, C_2H_6, C_3H_8, iC_4H_{10}, CO_2, and N_2) by considering hydrate structures I and II. It is critical to expand the database in future studies to include additional hydrate-forming gases

(such as O_2, H_2S, and n-C_4H_{10}) and upgrade the fitting procedure to include other hydrate structures (such as structure H).

- Although this new VLAH four-phase equilibrium calculation algorithm has been validated by several example calculations, we cannot guarantee that we can always converge to the correct multiphase equilibria for all other water/hydrocarbons systems at different temperature/pressure conditions. This is partly because the mixing rules and BIPs used in the algorithm may yield no equivalent fugacities between aqueous phase and non-aqueous phases (Li and Li, 2019). In the future, we hope to avoid this non-convergence problem through adopting more advanced mixing rules.
- The experimental data about the multiphase equilibria involving hydrates are insufficient. The newly developed framework should be further verified by more upcoming experimental data.

References

Li, R., Li, H., 2019. Improved three-phase equilibrium calculation algorithm for water/hydrocarbon mixtures. Fuel 244: 517-527.

BIBLIOGRAPHY

Aalto, M., Keskinen, K.I., Aittamaa, J., Liukkonen, S., 1996. An improved correlation for compressed liquid densities of hydrocarbons. Part 2. Mixtures. Fluid Phase Equilib. 114: 21-35.

Aasen, A., Hammer, M., Skaugen, G., Jakobsen, J.P., Wilhelmsen, O., 2017. Thermodynamic models to accurately describe the PVTxy-behavior of water/carbon dioxide mixtures. Fluid Phase Equilib. 442: 125-139.

Abramson, E.H., Brown, J.M., 2004. Equation of state of water based on speeds of sound measured in the diamond-anvil cell. Geochim. Cosmochim. Ac. 68: 1827-1835.

Abudour, A.M., Mohammad, S.A., Robinson, R.L., Gasem, K.A.M., 2012. Volume-translated Peng-Robinson equation of state for saturated and single-phase liquid densities. Fluid Phase Equilib. 335: 74-87.

Abudour, A.M., Mohammad, S.A., Robinson, R.L., Gasem, K.A.M., 2013. Volume-translated Peng-Robinson equation of state for liquid densities of diverse binary mixtures. Fluid Phase Equilib. 349: 37-55.

Adisasmito, S., Frank, R.J., Sloan Jr., E.D., 1991. Hydrates of carbon dioxide and methane mixtures. Chem. Eng. Data, 3: 68-71.

Adisasmito, S., Sloan Jr., E.D., 1992. Hydrates of hydrocarbon gases containing carbon dioxide. J. Chem. Eng. Data 37: 343-349.

Aghajanloo, M., Taheri, Z., Behbahani, T.J., Mohammadi, A.H., Ehsani, M.R., Heydarian, H., 2020. Experimental determination and thermodynamic modeling of clathrate hydrate stability conditions in methane + hydrogen sulfide + water system. J. Nat. Gas Sci. Eng. 83: 103549.

Allal, A., Boned, C., Baylaucq, Q., 2001. Free volume viscosity model for fluids in the dense and gaseous states. Phys. Rev. E 64: 011203.

Anderson, B.J., Tester, J.W., Trout, B.L., 2004. Accurate potentials for argon-water and methane-water interactions via ab initio methods and their application to clathrate hydrates. J. Phys. Chem. B 108: 18705-18715.

Anderson, G.K., 2003. Enthalpy of dissociation and hydration number of carbon dioxide hydrate from the Clapeyron equation. J. Chem. Thermodyn. 35: 1171-1183.

Amani, M.J., Dehdari, L., Ghamartale, A., 2019. Modelling density and excess volume of hydrocarbon + water mixtures near the critical region. Fluid Phase Equilib. 492: 55-66.

Archer, D.G., Wang, P., 1990. The dielectric constant of water and Debye-Hückel limiting law slopes. J. Phys. Chem. Ref. Data 19: 371-411.

Avlonitis, D., 1988. Multiphase equilibria in oil-water hydrate forming systems. M.Sc. Thesis, Heriot-Watt University, Edinburgh, Scotland.

Babakhani, S.M., Bouillot, B., Ho-Van, S., Douzet, J., Herri, J.M., 2018. A review on hydrate composition and capability of thermodynamic modeling to predict hydrate pressure and composition. Fluid Phase Equilib. 472: 22-38.

Babakhani, S.M., Bouillot, B., Douzet, J., Ho-Van, S., Herri, J.M., 2018. PVTx measurements of mixed clathrate hydrates in batch conditions under different crystallization rates: Influence on equilibrium. J. Chem. Thermodyn. 122: 73-84.

Baled, H., Enick, R.M., Wu, Y., McHugh, M.A., Burgess, W., Tapriyal, D., Morreale, B.D., 2012. Prediction of hydrocarbon densities at extreme conditions using volume-translated SRK and PR equations of state fit to high temperature, high pressure PVT data. Fluid Phase Equilib. 317: 65-76.

Ballard, A.L, Sloan, E.D. Jr., 2002. The next generation of hydrate prediction I. Hydrate standard states and incorporation of spectroscopy. Fluid Phase Equilib. 194-197: 371-383.

Ballard, A.L., Sloan Jr., E.D., 2002. The next generation of hydrate prediction: An overview. J. Supramol. Chem. 2: 385-392.

Ballard, A.L., Sloan, E.D. Jr., 2004. The next generation of hydrate prediction Part III. Gibbs energy minimization formalism. Fluid Phase Equilib. 218: 15-31.

Ballard, A.L., Sloan, E.D. Jr., 2004. The next generation of hydrate prediction IV. A comparison of available hydrate prediction programs. Fluid Phase Equilib. 216: 257-270.

Bamberger, A., Sieder, G., Maurer, G., 2000. High-pressure (vapor+liquid) equilibrium in binary mixtures of (carbon dioxide+water or acetic acid) at temperatures from 313 to 353 K. J. Supercrit. Fluid. 17: 97-110.

Bandyopadhyay, D., Mohan, S., Ghosh, S.K., Choudhury, N., 2013. Correlation of structural order, anomalous density, and hydrogen bonding network of liquid water. J. Phys. Chem. B 117: 8831-8843.

Barkan, E.S., Sheinin, D.A., 1993. A general technique for the calculation of formation conditions of natural gas hydrates. Fluid Phase Equilib. 86: 111-136.

Barr-David, F., Dodge, B.F., 1959. Vapor-liquid equilibrium at high pressures. The systems ethanol-water and 2-propanol-water. Chem. Eng. Data 4: 107-121.

Barrufet, M.A., Liu, H., Rahman, S., Wu, C., 1996. Simultaneous vapor-liquid-liquid equilibria and phase molar densities of a quaternary system of propane + pentane + octane + water. J. Chem. Eng. Data 41: 918-922.

Bavoh, C.B., Khan, M.S., Lal, B., Ghaniri, N.I.B.A., Sabil, K.M., 2018. New methane hydrate phase boundary data in the presence of aqueous amino acids. Fluid Phase Equilib. 478: 129-133.

Bavoh, C.B., Partoon, B., Lal, B., Keong, L.K., 2017. Methane hydrate-liquid-vapour-equilibrium phase condition measurements in the presence of natural amino acids. J. Nat. Gas Sci. Eng. 37: 425-434.

Bazant, M.Z., Trout, B.L., 2001. A method to extract potentials from the temperature dependence of Langmuir constants for clathrate-hydrates. Phys. A 300: 139-173.

Beg, S.A., Tukur, N.M., Al-Harbi, D.K., 1995. Densities and excess volumes of cyclohexane + hexane between 298.15 K and 473.15 K. Fluid Phase Equilib. 113: 173-184.

Beg, S.A., Tukur, N.M., Al-Harbi, D.K., Hamad, E.Z., 1995. Densities and excess volumes of benzene + hexane between 298.15 and 473.15 K. J. Chem. Eng. Data 40: 74-78.

Belandria, V., Eslamimanesh, A., Mohammadi, A.H., Theveneau, P., Legendre, H., Richon, D., 2011. Compositional analysis and hydrate dissociation conditions measurements for carbon dioxide + methane + water system. Ind. Eng. Chem. Res. 50: 5783-5794.

Belandria, V., Mohammadi, A.H., Richon, D., 2010. Phase equilibria of clathrate hydrates of methane + carbon dioxide: New experimental data and predictions. Fluid Phase Equilib. 296: 60-65.

Bell, I.H., Welliquet, J., Mondejar, M.E., Bazyleva, A., Quoilin, S., Haglind, F., 2019. Application of the group contribution volume translated Peng-Robinson equation of state to new commercial refrigerant mixtures. Int. J. Refrig. 103: 316-328.

Belosludov, V.R., Bozhko, Y.Y., Subbotin, O.S., Belosludov, R.V., Zhdanov, R.K., Gets, K.V., Kawazoe, Y., 2018. Influence of N_2 on formation conditions and guest distribution of mixed CO_2 + CH_4 gas hydrates. Molecules 23: 3336.

Beltran, J.G., Servio, P., 2008. Equilibrium studies for the system methane + carbon dioxide + neohexane + Water. J. Chem. Eng. Data 53: 1745-1749.

Ben-Naim, A., 1970. Application of an approximate Percus-Yevick equation for liquid water. J. Chem. Phys. 52: 5531.

Bhawangirkar, D.R., Adhikari, J., Sangwai, J.S., 2018. Thermodynamic modeling of phase equilibria of clathrate hydrates formed from CH_4, CO_2, C_2H_6, N_2 and C_3H_8, with different equations of state. J. Chem. Thermodyn. 117: 180-192.

Bishnoi, P.R., Dholabhai, P.D., 1993. Experimental study on propane hydrate equilibrium conditions in aqueous electrolyte solutions. Fluid Phase Equilib. 83: 455-462.

Bishnoi, P.R., Dholabhai, P.D., 1999. Equilibrium conditions for hydrate formation for a ternary mixture of methane, propane and carbon dioxide, and a natural gas mixture in the presence of electrolytes and methanol. Fluid Phase Equilib. 158-160: 821-827.

Bishnoi, P.R., Gupta, A.K., Englezos, P., Kalogerakis, N., 1989. Multiphase equilibrium flash calculations for systems containing gas hydrates. Fluid Phase Equilib. 53: 97-104.

Bouchafaa, W., Dalmazzone, D., 2011. Thermodynamic equilibrium data for mixed hydrates of CO_2-N_2, CO_2-CH_4 and CO_2-H_2 in pure water and TBAB solutions. Presented in: 7th International Conference on Gas Hydrates, Edinburgh, United Kingdom.

Breland, E., Englezos, P., 1996. Equilibrium hydrate formation data for carbon dioxide in aqueous glycerol solutions. J. Chem. Eng. Data 41: 11-13.

Bruusgaard, H., Beltran, J.G., Servio, P., 2008. Vapor-liquid water-hydrate equilibrium data for the system N_2 + CO_2 + H_2O, J. Chem. Eng. Data 53: 2594-2597.

Bruusgaard, H., Beltran, J.G., Servio, P., 2010. Solubility measurements for the CH_4 + CO_2 + H_2O system under hydrate-liquid-vapor equilibrium. Fluid Phase Equilib. 296: 106-109.

Buleiko, V.M., Grigoriev, B.A., Mendoza, J., 2018. Calorimetric investigation of hydrates of pure isobutane and iso- and normal butane mixtures. Fluid Phase Equilib. 462: 14-24.

Burgess, W.A., Gamwo, I.K., Enick, R.M., McHugh, M.A., 2018. Viscosity models for pure hydrocarbons at extreme conditions: A review and comparative study. Fuel 218: 89-111.

Burgess, W.A., Tapriyal, D., Gamwo, I.K., Morreale, B.D., McHugh, M.A., Enick, R.M., 2012. Viscosity models based on the free volume and frictional theories for systems at pressures to 276 MPa and temperatures to 533 K. Ind. Eng. Chem. Res. 51: 16721-16733.

Cardoso, S.G., Costa, G.M.N., Vieira de Melo, S.A.B., 2016. Assessment of the liquid mixture density effect on the prediction of supercritical carbon dioxide volume expansion of organic solvents by Peng-Robinson equation of state. Fluid Phase Equilib. 425: 196-205.

Carson, D.B., Katz, D.L., 1942. Natural gas hydrates. Trans. AIME 146: 150-158.

Chandran, J., Salih, A., 2019. A modified equation of state for water for a wide range of pressure and the concept of water shock tube. Fluid Phase Equilib. 483: 182-188.

Chapman, W.G., Gubbins, K.E., Jackson, G., Radosz, M., 1989. SAFT: Equation-of-state solution model for associating fluids. Fluid Phase Equilib. 52: 31-38.

Chapman, W.G., Gubbins, K.E., Jackson, G., Radosz, M., 1990. New reference equation of state for associating liquids. Ind. Eng. Chem. Res. 29: 1709-1721.

Chapman, W.G., Jackson, G., Gubbins, K.E., 1988. Phase equilibria of associating fluids: Chain molecules with multiple bonding sites. Mol. Phys. 65: 1067-1079.

Chapoy, A., Burgass, R., Tohidi, B., Alsiyabi, I., 2015. Hydrate and phase behavior modeling in CO_2-rich pipelines. J. Chem. Eng. Data 60: 447-453.

Chapoy, A., Haghighi, H., Burgass, R., Tohidi, B., 2012. On the phase behaviour of the (carbon dioxide + water) systems at low temperatures: Experimental and modelling. J. Chem. Thermodyn. 47: 6-12.

Chazallon, B., Pirim, C., 2018. Selectivity and CO_2 capture efficiency in CO_2-N_2 clathrate hydrates investigated by in-situ Raman spectroscopy. Chem. Eng. J. 342: 171-183.

Chen, L., Sun, C., Chen, G., Nie, Y., Sun, Z., Liu, Y., 2009. Measurements of hydrate equilibrium conditions for CH_4, CO_2, and $CH_4 + C_2H_6 + C_3H_8$ in various systems by step-heating method. Chinese J. Chem. Eng. 17: 635-641.

Chen, X., Li, H., 2020. An improved volume-translated SRK equation of state dedicated to accurate determination of saturated and single-phase liquid densities. Fluid Phase Equilib. 521: 112724.

Chen, X., Li, H., 2021. Improved prediction of saturated and single-phase liquid densities of water through volume-translated SRK EOS. Fluid Phase Equilib. 528: 112852.

Chen, X., Li, H., 2022. New pragmatic strategies for optimizing Kihara potential parameters used in van der Waals-Platteeuw hydrate model. Chem. Eng. Sci. 248: 117213.

Chen, G.J., Guo, T.M., 1998. A new approach to gas hydrate modelling. Chem. Eng. J. 71: 145-151.

Chima-Maceda, J.M., Esquivel-Mora, P., Pimentel-Rodas, A., Galicia-Luna, L.A., Castro-Arellano, J.J., 2019. Effect of 1-propanol and TBAB on gas hydrates dissociation conditions for CO_2 + hexane + water systems. J. Chem. Eng. Data 64: 4775-4780.

Cho, C.H., Urquidi, J., Singh, S., Park, S.C., Robinson, G.W., 2002. Pressure effect on the density of water. J. Phys. Chem. A 106: 7557-7561.

Chong, Z.R., Yang, S.H.B., Babu, P., Linga, P., Li, X.S., 2016. Review of natural gas hydrates as an energy resource: Prospects and challenges. Appl. Energ. 162: 1633-1652.

Chou, G.F., Prausnitz, J.M., 1989. A phenomenological correction to an equation of state for the critical region. AIChE J. 35: 1487-1496.

Chueh, P.L., Prausnitz, J.M., 1967. Vapor-liquid equilibria at high pressures: Calculation of critical temperatures, volumes, and pressures of nonpolar mixtures. AIChE J. 13: 1107-1113.

Cipollina, A., Anselmo, R., Scialdone, O., Filardo, G., Galia, A., 2007. Experimental P-T-ρ measurements of supercritical mixtures of carbon dioxide, carbon monoxide, and hydrogen and semiquantitative estimation of their solvent power using the solubility parameter concept. J. Chem. Eng. Data 52: 2291-2297.

Circone, S., Kirby, S.H., Stern, L.A., 2005. Direct measurement of methane hydrate composition along the hydrate equilibrium boundary. J. Phys. Chem. B 109: 9468-9475.

Cismondi, M., Cruz, J., Gomez, M.J., Montoya, G.F., 2015. Modelling the phase behavior of alkane mixtures in wide ranges of conditions: New parameterization and predictive correlations of binary interactions for the RKPR EOS. Fluid Phase Equilib. 403: 49-59.

Civan, F., 2007. Critical modification to the Vogel-Tammann-Fulcher equation for temperature effect on the density of water. Ind. Eng. Chem. Res. 46: 5810-5814.

Clarke, M., Bishnoi, P.R., 2001. Determination of the activation energy and intrinsic rate constant of methane gas hydrate decomposition. Can. J. Chem. Eng. 79: 143-147.

Cole, W.A., Stephen, P., 1990. Flash calculations for gas hydrates: A rigorous approach. Chem. Eng. Sci. 45: 569-573.

Collett, T.S., 2002. Energy resource potential of natural gas hydrates. AAPG Bull. 86: 1971-1992.

Curtis, H.W., Michael, R.B., 2000. Phase Behavior. SPE Monograph Series 20.

Dahbag, M.B., Zirrahi, M., Hassanzadeh, H., 2019. Solubility and liquid density of ammonia/athabasca bitumen mixtures at temperatures up to 463 K: Measurements and modeling. J. Chem. Eng. Data 64: 3592-3597.

Dai, M.L., Sun, Z.G., Li, J., Li, C.M., Huang, H.F., 2020. Effect of n-dodecane on equilibrium dissociation conditions of carbon dioxide hydrate. J. Chem. Thermodyn. 148: 106144.

Deaton, W.M., Frost Jr., E.M., 1946. Gas hydrates and their relation to the operation of natural-gas pipe lines. U.S. Bureau of Mines Monograph 8.

De Menezes, D.E.S, Filho, P.A.P., Fuentes, M.D.R., 2020. Phase equilibrium for methane, ethane and carbon dioxide hydrates at pressures up to 100 MPa through high-pressure microcalorimetry: Experimental data, analysis and modeling. Fluid Phase Equilib. 518: 112590.

De Menezes, D.E.S., Sum, A.K., Desmedt, A., Filho, P.A.P., Fuentes, M.D.R., 2019. Coexistence of sI and sII in methane-propane hydrate former systems at high pressures. Chem. Eng. Sci. 208: 115149.

De Roo, J.L., Peters, C.J., Lichtenthaler, R.N., Diepen, G.A.M., 1983. Occurrence of methane hydrate in saturated and unsaturated solutions of sodium chloride and water in dependence of temperature and pressure. AIChE J. 29: 651-657.

De Sant'Ana, H.B., Ungerer, P., De Hemptinne, J.C., 1999. Evaluation of an improved volume translation for the prediction of hydrocarbon volumetric properties. Fluid Phase Equilib. 154: 193-204.

De Sant'Ana, H.B., Ungerer, P., Batut, C., 1998. Measurement and prediction of volumetric and transport properties of reservoir fluids at high pressure. Oil Gas Sci. Tech. 53: 265-281.

Dharmawardhana, P.B., Parrish, W.R., Sloan, E.D., 1980. Experimental thermodynamic parameters for the prediction of natural gas hydrate dissociation conditions. Ind. Eng. Chem. Fundam. 19: 410-414.

Dholabhai, P.D., Bishnoi, P.R., 1994. Hydrate equilibrium conditions in aqueous electrolyte solutions: Mixtures of methane and carbon dioxide. J. Chem. Eng. Data 39: 191-194.

Dholabhai, P.D., Kalogerakis, N., Bishnoi, P.R., 1993. Equilibrium conditions for carbon dioxide hydrate formation in aqueous electrolyte solutions. J. Chem. Eng. Data 38: 650-654.

Dholabhai, P.D., Parent, J.S., Bishnoi, P.R., 1996. Carbon dioxide hydrate equilibrium conditions in aqueous solutions containing electrolytes and methanol using a new apparatus. Ind. Eng. Chem. Res. 35: 819-823.

Dholabhai, P.D., Parent, J.S., Bishnoi, P.R., 1997. Equilibrium conditions for hydrate formation from binary mixtures of methane and carbon dioxide in the presence of electrolytes, methanol and ethylene glycol. Fluid Phase Equilib. 141: 235-246.

Diamond, L.W., 1994. Salinity of multivolatile fluid inclusions determined from clathrate hydrate stability. Geochim. Cosmochim. Acta 58: 19-41.

Dickens, G.R., Quinby-Hunt, M.S., 1994. Methane hydrate stability in seawater. Geophys. Res. Lett. 21: 2115-2118.

Du, G., Hu, J., 2016. An equation of state for accurate thermodynamic modeling of water and carbon dioxide from triple points to 647 K and 100-200 MPa. Int. J. Greenh. Gas Con. 49: 94-107.

Du, Y.H., Guo, T.M., 1990. Prediction of hydrate formation for systems containing methanol. Chem. Eng. Sci. 45: 893-900.

Dyadin, Y., Aladko, E., 1996. Decomposition of the methane hydrate up to 10 Kbar. Presented in: Second International Conference on Natural Gas Hydrates, Toulouse, France.

Dymond, J.H., Malhotra, R., 1988. The Tait equation: 100 years on. Int. J. Thermophys. 9: 941-951.

Economou, I.G., Donohue, M.D., 1992. Equation of state with multiple associating sites for water and water-hydrocarbon mixtures. Ind. Eng. Chem. Res. 31: 2388-2394.

Elgibaly, A.A., Elkamel, A.M., 1998. A new correlation for predicting hydrate formation conditions for various gas mixtures and inhibitors. Fluid Phase Equilib. 152: 23-42.

Englezos, P., 1993. Clathrate hydrates. Ind. Eng. Chem. Res. 32: 1251-1274.

Englezos, P., Bishnoi, P.R., 1991. Experimental study on the equilibrium ethane hydrate formation conditions in aqueous electrolyte solutions. Ind. Eng. Chem. Res. 30: 1655-1659.

Englezos, P., Hall, S., 1994. Phase equilibrium data on carbon dioxide hydrate in the presence of electrolytes, water soluble polymers and montmorillonite. Can. J. Chem. Eng. 72: 887-893.

Englezos, P., Ngan, Y.T., 1993. Incipient equilibrium data for propane hydrate formation in aqueous solutions of sodium chloride, potassium chloride and calcium chloride. J. Chem. Eng. Data 38: 250-253.

Falabella, B.J., 1975. A study of natural gas hydrates. Ph.D. Thesis, University of Massachusetts, USA.

Falabella, B.J., Vanpee, M., 1974. Experimental determination of gas hydrate equilibrium below the ice point. Ind. Eng. Chem. Fundamen. 13: 228-231.

Fan, S., Li, Q., Nie, J., Lang, X., Wen, Y., Wang, Y., 2013. Semiclathrate hydrate phase equilibrium for CO_2/CH_4 gas mixtures in the presence of tetrabutylammonium halide (bromide, chloride, or fluoride). J. Chem. Eng. Data 58: 3137-3141.

Fan, S., You, S., Wang, Y., Lang, X., Yu, C., Wang, S., Li, Z., Li, W., Liu, Y., Zhou, Z., 2019. Hydrate phase equilibrium of CH_4-rich binary and ternary gas mixtures in the presence of tetra-n-butyl ammonium bromide. J. Chem. Eng. Data 64: 5929-5934.

Fan, S.S., Chen, G.J., Ma, Q.L., Guo, T.M., 2000. Experimental and modeling studies on the hydrate formation of CO_2 and CO_2-rich gas mixtures. Chem. Eng. J. 78:173-178.

Fan, S.S., Guo, T.M., 1999. Hydrate formation of CO_2-rich binary and quaternary gas mixtures in aqueous sodium chloride solutions. J. Chem. Eng. Data 44: 829-832.

Ferrari, P.F., Guembaroski, A.Z., Neto, M.A.M., Morales, R.E.M., Sum, A.K., 2016. Experimental measurements and modelling of carbon dioxide hydrate phase equilibrium with and without ethanol. Fluid Phase Equilib. 413: 176-183.

Firoozabadi, A., 2015. Thermodynamics and applications of hydrocarbons energy production. McGraw-Hill Education.

Florusse, L.J., Peters, C.J., Schoonman, J., Hester, K.C., Koh, C.A., Dec, S.F., Marsch, K.M., Sloan, E.D., 2004. Stable low-pressure hydrogen clusters stored in a binary clathrate hydrate. Science 306: 469-471.

Freer, E.M., Selim, M.S., Sloan Jr., E.D., 2001. Methane hydrate film growth kinetics. Fluid Phase Equilib. 185: 65-75.

French, M., Mattsson, T.R., Nettelmann, N., Redmer, R., 2009. Equation of state and phase diagram of water at ultrahigh pressures as in planetary interiors. Phys. Rev. B 79: 054107.

Frey, K., Modell, M., Tester, J.W., 2013. Density-and-temperature-dependent volume translation for the SRK EOS: 2. Mixtures. Fluid Phase Equilib. 343: 13-23.

Frey, K., Tester, J.W., Modell, M.,2009. Density-and-temperature-dependent volume translation for the SRK EOS: 1. Pure fluids. Fluid Phase Equilib. 279: 56-63.

Fu, D., Li, X., 2007. Investigation of vapor-liquid nucleation for water and heavy water by density functional theory. J. Phys. Chem. C 111: 13938-13944.

Fuentevilla, D.A., Anisimov, M.A., 2006. Scaled equation of state for supercooled water near the liquid-liquid critical point. Phys. Rev. Lett. 97: 195702.

Galloway, T.J., Ruska, W., Chappelear, P.S., Kobayashi, R., 1970. Experimental measurement of hydrate numbers for methane and ethane and comparison with theoretical values. Ind. Eng. Chem. Fundam. 9: 237-243.

Gasem, K.A.M., Gao, W., Pan, Z., Robinson Jr., R.L., 2001. A modified temperature dependence for the Peng-Robinson equation of state. Fluid Phase Equilib. 181: 113-125.

Gayet, P., Dicharry, C., Marion, G., Graciaa, A., Lachaise, J., Nesterov, A., 2005. Experimental determination of methane hydrate dissociation curve up to 55 MPa by using a small amount of surfactant as hydrate promoter. Chem. Eng. Sci. 60: 5751-5758.

Ghoderao, P.N.P., Dalvi, V.H., Narayan, M., 2018. A four-parameter cubic equation of state for pure compounds and mixtures. Chem. Eng. Sci. 190: 173-189.

Ghoderao, P.N.P., Dalvi, V.H., Narayan, M., 2019. A four parameter cubic equation of state with temperature dependent covolume parameter. Chinese J. Chem. Eng. 27: 1132-1148.

Gibbs, J.W., 1929. The collected works of J. Willard Gibbs. Nature 124: 119-120.

Gonzalez, B., Calvar, N., Gomez, E., Dominguez, A., 2007. Density, dynamic viscosity, and derived properties of binary mixtures of methanol or ethanol with water, ethyl acetate, and methyl acetate at T=(293.15, 298.15, and 303.15) K. J. Chem. Thermodynamics 39: 1578-1588.

Gorucu, S.E., Johns, R.T., 2016. Robustness of three-phase equilibrium calculations. J. Petrol. Sci. Eng. 143: 72-85.

Gross, J., Sadowski, G., 2001. Perturbed-chain SAFT: An equation of state based on a perturbation theory for chain molecules. Ind. Eng. Chem. Res. 40: 1244-1260.

Guo, P., Tu, H., Wang, Z., Wang, Q., 2017. Calculation of thermodynamic properties of water by the CPA equation of state. Nat. Gas Ind. B 4: 305-310.

Gupta, A., Lachance, J., Sloan Jr., E.D., Koh, C.A., 2008. Measurements of methane hydrate heat of dissociation using high pressure differential scanning calorimetry. Chem. Eng. Sci. 63: 5848-5853.

Gupta, A.K., 1988. Steady state simulation of chemical processes. Ph.D. Thesis, University of Calgary, Calgary, Canada.

Gupta, A.K., Raj Bishnoi, P., Kalogerakis, N., 1991. A method for the simultaneous phase equilibria and stability calculations for multiphase reacting and non-reacting systems. Fluid Phase Equilib. 63: 65-89.

Habasaki, J., 2019. Heterogeneous-homogeneous transition and anomaly of density in SPC/E water examined by molecular dynamics simulations. Physica A 527: 121391.

Handa, Y.P., Tse, J.S., 1986. Thermodynamic properties of empty lattices of structure I and structure II clathrate hydrates. J. Phys. Chem. 90: 5917-5921.

Hankinson, R.W., Thomson, G.H., 1979. A new correlation for saturated densities of liquids and their mixtures. AIChE J. 25: 653-663.

Hansen, C.M., 2004. 50 years with solubility parameters-past and future. Prog. Org. Coat. 51: 77-84.

Harrington, S., Poole, P.H., Sciortino, F., Stanley, H.E., 1997. Equation of state of supercooled water simulated using the extended simple point charge intermolecular potential. J. Chem. Phys. 107: 7443.

Hashimoto, S., Sasatani, A., Matsui, Y., Sugahara, T., Ohgaki, K., 2008. Isothermal phase equilibria for methane + ethane + water ternary system containing gas hydrates. Open Thermodyn. J. 2: 100-105.

Haugen, K.B., Firoozabadi, A., Sun, L., 2011. Efficient and robust three-phase split computations. AIChE J. 57: 2555-2565.

Heidaryan, E., Fuentes, M.D.R., Filho, P.A.P., 2019. Equilibrium of methane and carbon dioxide hydrates below the freezing point of water: Literature review and modeling. J. Low Temp. Phys. 194: 27-45.

Herri, J.M., Bouchemoua, A., Kwaterski, M., Fezoua, A., Ouabbas, Y., Cameirao, A., 2011. Gas hydrate equilibria for CO_2-N_2 and CO_2-CH_4 gas mixtures—Experimental studies and thermodynamic modelling. Fluid Phase Equilib. 301: 171-190.

Hoang, H., Galliero, G., 2016. Predictive Tait equation for non-polar and weakly polar fluids: Applications to liquids and liquid mixtures. Fluid Phase Equilib. 425: 143-151.

Hoang, H., Galliero, G., Montel, F., Bickert, J., 2015. Tait equation in the extended corresponding states framework: Application to liquids and liquid mixtures. Fluid Phase Equilib. 387: 5-11.

Holder, G.D., Corbin, G., Papadopoulos, K.D., 1980. Thermodynamic and molecular properties of gas hydrates from mixtures containing methane, argon, and krypton. Ind. Eng. Chem. Fundam. 19: 282-286.

Holder, G.D., Godbole, S.P., 1982. Measurement and prediction of dissociation pressures of isobutane and propane hydrates below the ice point. AIChE J. 28: 930-934.

Holder, G.D., Grigoriou, G.C., 1980. Hydrate dissociation pressures of (methane + ethane + water) existence of a locus of minimum pressures. J. Chem. Thermodyn. 12: 1093-1104.

Holder, G.D., Hand, J.H., 1982. Multiple-phase equilibria in hydrates from methane, ethane, propane and water mixtures. AIChE J. 28: 440-447.

Holder, G.D., Kamath, V.A., 1984. Hydrates of (methane + cis-2-butene) and (methane + trans-2-butene). J. Chem. Thermodyn. 16: 399-400.

Holder, G.D., Zetts, S.P., Pradhan, N., 1988. Phase behavior in systems containing clathrate hydrates: A review. Rev. Chem. Eng. 5: 1-70.

Holten, V., Qiu, C., Guillerm, E., Wilke, M., Ricka, J., Frenz, M., Caupin, F., 2017. Compressibility anomalies in stretched water and their interplay with density anomalies. J. Phys. Chem. Lett. 8: 5519-5522.

Hsieh, M.K., Ting, W.Y., Chen, Y.P., Chen, P.C., Lin, S.T., Chen, L.J., 2012. Explicit pressure dependence of the Langmuir adsorption constant in the van der Waals-Platteeuw model for the equilibrium conditions of clathrate hydrates. Fluid Phase Equilib. 325: 80-89.

Huang, S.H., Radosz, M., 1990. Equation of state for small, large, polydisperse, and associating molecules. Ind. Eng. Chem. Res. 29: 2284-2294.

Ilani-Kashkouli, P., Hashemi, H., Basdeo, A., Naidoo, P., Ramjugernath, D., 2019. Hydrate dissociation data for the systems (CO_2/CH_4/Ar) + water with (TBAF/TBAA/TBPB/$TBANO_3$ and cyclopentane). J. Chem. Eng. Data 64: 2542-2549.

Ilani-Kashkouli, P., Mohammadi, A.H., Naidoo, P., Ramjugernath, D., 2016. Thermodynamic stability conditions for semi-clathrate hydrates of CO_2, CH_4, or N_2 with tetrabutyl ammonium nitrate ($TBANO_3$) aqueous solution. J. Chem. Thermodyn. 96: 52-56.

Jager, M.D., Ballard, A.L., Sloan, E.D. Jr., 2003. The next generation of hydrate prediction II. Dedicated aqueous phase fugacity model for hydrate prediction. Fluid Phase Equilib. 211: 85-107.

Jager, M.D., Sloan, E.D., 2001. The effect of pressure on methane hydration in pure water and sodium chloride solutions. Fluid Phase Equilib. 185: 89-99.

Jarrahian, A., Nakhaee, A., 2019. Hydrate-liquid-vapor equilibrium condition of N_2+CO_2+H_2O system: Measurement and modeling. Fuel 237: 769-774.

Jaubert, J.N., Privat, R., Le Guennec, Y., Coniglio, L., 2016. Note on the properties altered by application of a Peneloux-type volume translation to an equation of state. Fluid Phase Equilib. 419: 88-95.

Javanmardi, J., Babaee, S., Eslamimanesh, A., Mohammadi, A.H., 2012. Experimental measurements and predictions of gas hydrate dissociation conditions in the presence of methanol and ethane-1,2-diol aqueous solutions. J. Chem. Eng. Data 57: 1474-1479.

Jeffery, C.A., Austin, P.H., 1999. A new analytic equation of state for liquid water. J. Chem. Phys. 110: 484-496.

Jhaveri, J., Robinson, D.B., 1965. Hydrates in the methane-nitrogen system. Can. J. Chem. Eng. 43: 75-78.

Ji, W.R., Lempe, D.A., 1997. Density improvement of the SRK equation of state. Fluid Phase Equilib. 130: 49-63.

Jing, J., Yin, R., Zhu, G., Xue, J., Wang, S., Wang, S., 2019. Viscosity and contact angle prediction of low water-containing heavy crude oil diluted with light oil. J. Petrol. Sci. Eng. 176: 1121-1134.

John, V.T., Papadopoulos, K.D., Holder, G.D., 1985. A generalized model for predicting equilibrium conditions for gas hydrates. AIChE J. 31: 252-259.

Kakati, H., Mandal, A., Laik, S., 2015. Phase stability and kinetics of $CH_4 + CO_2 + N_2$ hydrates in synthetic seawater and aqueous electrolyte solutions of NaCl and $CaCl_2$. J. Chem. Eng. Data 60: 1835-1843.

Kamari, A., Hashemi, H., Babaee, S., Mohammadi, A.H., Ramjugernath, D., 2017. Phase stability conditions of carbon dioxide and methane clathrate hydrates in the presence of KBr, $CaBr_2$, $MgCl_2$, HCOONa, and HCOOK aqueous solutions: Experimental measurements and thermodynamic modelling. J. Chem. Thermodyn. 115: 30-317.

Kang, S.P., Lee, H., Lee, C.S., Sung, W.M., 2001. Hydrate phase equilibria of the guest mixtures containing CO_2, N_2 and tetrahydrofuran. Fluid Phase Equilib. 185: 101-109.

Kastanidis, P., Romanos, G.E., Michalis, V.K., Economou, I.G., Stubos, A.K., Tsimpanogiannis, I.N., 2016. Development of a novel experimental apparatus for hydrate equilibrium measurements. Fluid Phase Equilib. 424: 152-161.

Kastanidis, P., Romanos, G.E., Stubos, A.K., Economou, I.G., Tsimpanogiannis, I.N., 2017. Two- and three-phase equilibrium experimental measurements for the ternary $CH_4 + CO_2 + H_2O$ mixture. Fluid Phase Equilib. 451: 96-105.

Kataoka, Y., 1987. Studies of liquid water by computer simulations. V. Equation of state of fluid water with Carravetta-Clementi potential. J. Chem. Phys. 87: 589-598.

Katz, D.L., 1945. Prediction of conditions for hydrate formation in natural gases. Trans. AIME 160: 140-149.

Kay, W.B., 1970. Vapor-liquid equilibrium relations of binary systems. The propane-n-alkane systems. n-butane and n-pentane. J. Chem. Eng. Data 15: 46-52.

Ke, W., Svartaas, T.M., Chen, D., 2019. A review of gas hydrate nucleation theories and growth models. J. Nat. Gas. Sci. Eng. 61: 169-196.

Khan, M.N., Warrier, P., Peters, C.J., Koh, C.A., 2018. Advancements in hydrate phase equilibria and modeling of gas hydrates systems. Fluid Phase Equilib. 463: 48-61.

Khan, M.S., Lal, B., Shariff, A.M., Mukhtar, H., 2019. Ammonium hydroxide ILs as dual-functional gas hydrate inhibitors for binary mixed gas (carbon dioxide and methane) hydrates. J. Mol. Liq. 274: 33-44.

Khan, M.S., Partoon, B., Bavoh, C.B., Lal, B., Mellon, N.B., 2017. Influence of tetramethylammonium hydroxide on methane and carbon dioxide gas hydrate phase equilibrium conditions. Fluid Phase Equilib. 440: 1-8.

Kharrat, M., Dalmazzone, D., 2003. Experimental determination of stability conditions of methane hydrate in aqueous calcium chloride solutions using high pressure differential scanning calorimetry. J. Chem. Thermodyn. 35: 1489-1505.

Khurana, M., Yin, Z., Linga, P., 2017. A Review of clathrate hydrate nucleation. ACS Sustainable Chem. Eng. 5: 11176-11203.

Kim, H.M., Schultz, A.J., Kofke, D.A., 2012. Virial equation of state of water based on Wertheim's association theory. J. Phys. Chem. B 116: 14078-14088.

Kim, N.J., Lee, J.H., Cho, Y.S., Chun, W., 2010. Formation enhancement of methane hydrate for natural gas transport and storage. Energy 35: 2717-2722.

King, M.B., Mubarak, A., Kim, J.D., Bott, T.R., 1992. The mutual solubilities of water with supercritical and liquid carbon dioxide? J. Supercrit. Fluid. 5: 296-302.

Klauda, J.B., Sandler, S.I., 2000. A fugacity model for gas hydrate phase equilibria. Ind. Eng. Chem. Res. 39: 3377-3386.

Klauda, J.B., Sandler, S.I., 2003. Phase behavior of clathrate hydrates: A model for single and multiple gas component hydrates. Chem. Eng. Sci. 58: 27-41.

Knierbein, M., Held, C., Holzl, C., Horinek, D., Paulus, M., Sadowski, G., Sternemann, C., Nase, J., 2019. Density variations of TMAO solutions in the kilobar range: Experiments, PC-SAFT predictions, and molecular dynamics simulations. Biophys. Chem. 253: 106222.

Kobayashi, R., Katz, D.L., 1949. Methane hydrate at high pressure. J. Pet. Technol. 1: 66-70.

Koh, C.A., Sloan, E.D., 2007. Natural gas hydrates: Recent advances and challenges in energy and environmental applications. AIChE J. 53: 1636-1643.

Koh, C.A., Sum, A.K., Sloan, E.D., 2012. State of the art: Natural gas hydrates as a natural resource. J. Nat. Gas Sci. Eng. 8: 132-138.

Kontogeorgis, G.M., Privat, R., Jaubert, J., 2019. Taking another look at the van der Waals equation of state-almost 150 years later. J. Chem. Eng. Data 64: 4619-4637.

Kontogeorgis, G.M., Voutsas, E.C., Yakoumis, I.V., Tassios, D.P., 1996. An equation of state for associating fluids. Ind. Eng. Chem. Res. 35: 4310-4318.

Kraska, T., Gubbins, K.E., 1996. Phase equilibria calculations with a modified SAFT equation of state. 2. Binary mixtures of n-alkanes, 1-alkanols, and water. Ind. Eng. Chem. Res. 35: 4738-4746.

Kubota, H., Shimizu, K., Tanaka, Y., Makita, T., 1984. Thermodynamic properties of R13 ($CCIF_3$), R23 (CHF_3), R152A ($C_2H_4F_2$), and propane hydrates for desalination of sea water. J. Chem. Eng. Japan 17: 423-429.

Kubota, H., Tanaka, Y., Makita, T., 1987. Volumetric behavior of pure alcohols and their water mixtures under high pressure. Int. J. Thermophysics 8: 47-70.

Kumar, R., Linga, P., Moudrakovski, I., Ripmeester, J.A., Englezos, P., 2008. Structure and kinetics of gas hydrates from methane/ethane/propane mixtures relevant to the

design of natural gas hydrate storage and transport facilities. AIChE J. 54: 2132-2144.

Kummamuru, N.B., Perreault, P., Lenaerts, S., 2021. A new generalized empirical correlation for predicting methane hydrate equilibrium conditions in pure water. Ind. Eng. Chem. Res. 60: 3474-3483.

Kunz, O., Wagner, W., 2012. The GERG-2008 wide-range equation of state for natural gases and other mixtures: an expansion of GERG-2004. J. Chem. Eng. Data 57: 3032-3091.

Kurihara, H., Minoura, T., Takeda, K., Kojima, K., 1995. Isothermal vapor-liquid equilibria for methanol+ethanol+water, methanol+water, and ethanol+water. J. Chem. Eng. Data 40: 679-684.

Larson, S.D., 1955. Phase studies of the two-component carbon dioxide-water system involving the carbon dioxide hydrate. Ph.D. Thesis, University of Illinois, USA.

Laugier, S., Rivollet, F., Richon, D., 2007. New volume translation for cubic equations of state. Fluid Phase Equilib. 259: 99-104.

Le Guennec, Y., Lasala, S., Privat, R., Jaubert, J.N., 2019. A consistency test for α-functions of cubic equations of state. Fluid Phase Equilib. 427: 513-538.

Le Quang, D., Bouillot, B., Herri, J.M., Glenat, P., Duchet-Suchaux, P., 2016. Experimental procedure and results to measure the composition of gas hydrate, during crystallization and at equilibrium, from N_2-CO_2-CH_4-C_2H_6-C_3H_8-C_4H_{10} gas mixtures. Fluid Phase Equilib. 413: 10-21.

Lee, J.W., Kim, D.Y., Lee, H., 2006. Phase behavior and structure transition of the mixed methane and nitrogen hydrates. Korean J. Chem. Eng. 23: 299-302.

Lee, S., Chien, M.C.H., 1984. A new multicomponent surface tension correlation based on scaling theory. Presented at the SPE/DOE Fourth Symposium on Enhanced Oil Recovery, Tulsa Oklahoma.

Lee, S., Lee, Y., Lee, J., Lee, H., Seo, Y., 2013. Experimental verification of methane-carbon dioxide replacement in natural gas hydrates using a differential scanning calorimeter. Environ. Sci. Technol. 47: 13184-13190.

Lee, S., Lee, Y., Park, S., Kim, Y., Cha, I., Seo, Y., 2013. Stability conditions and guest distribution of the methane + ethane + propane hydrates or semiclathrates in the presence of tetrahydrofuran or quaternary ammonium salts. J. Chem. Thermodyn. 65: 113-119.

Lee, Y., Lee, S., Lee, J., Seo, Y., 2014. Structure identification and dissociation enthalpy measurements of the CO_2 + N_2 hydrates for their application to CO_2 capture and storage. Chem. Eng. J. 246: 20-26.

Lee, Y.J., Kawamura, T., Yamamoto, Y., Yoon, J.H., 2012. Phase equilibrium studies of tetrahydrofuran (THF) + CH_4, THF + CO_2, CH_4 + CO_2, and THF + CO_2 + CH_4 hydrates. J. Chem. Eng. Data 57: 3543-3548.

Legoix, L.N., Ruffine, L., Deusner, C., Haeckel, M., 2018. Experimental study of mixed gas hydrates from gas feed containing CH_4, CO_2 and N_2: Phase equilibrium in the presence of excess water and gas exchange. Energies 11: 1984.

Li, H., 2022. Multiphase equilibria of complex reservoir fluids, Springer.

Li, R., Li, H., 2019. Improved three-phase equilibrium calculation algorithm for water/hydrocarbon mixtures. Fuel 244: 517-527.

Li, S., Zhang, G., Dai, Z., Jiang, S., Sun, Y., 2021. Concurrent decomposition and replacement of marine gas hydrate with the injection of CO_2-N_2. Chem. Eng. J. 420: 129936.

Li, S., Wang, J., Lv, X., Ge, K., Jiang, Z., Li, Y., 2020. Experimental measurement and thermodynamic modeling of methane hydrate phase equilibria in the presence of chloride salt. Chem. Eng. J. 395: 125126.

Li, Z., Firoozabadi, A., 2012. General strategy for stability testing and phase-split calculation in two and three phases. SPE J. 17: 1096-1107.

Lin, C.-W., Trusler, J.P.M., 2012. The speed of sound and derived thermodynamic properties of pure water at temperatures between (253 and 473) K and at pressures up to 400 MPa. J. Chem. Phys. 136: 094511.

Lin, H., Duan, Y., 2005. Empirical correction to the Peng-Robinson equation of state for the saturated region. Fluid Phase Equilib. 233: 194-203.

Lin, H., Duan, Y.Y., Zhang, T., Huang, Z.M., 2006. Volumetric property improvement for the Soave-Redlich-Kwong equation of state. Ind. Eng. Chem. Res. 45: 1829-1839.

Linga, P., Kumar, R., Englezos, P., 2007. Gas hydrate formation from hydrogen/carbon dioxide and nitrogen/carbon dioxide gas mixtures. Chem. Eng. Sci. 62: 4268-4276.

Linga, P., Kumar, R., Englezos, P., 2007. The clathrate hydrate process for post and pre-combustion capture of carbon dioxide. J. Hazard. Mater. 149: 625-629.

Linstrom, R.J., Mallard, W.G., 2012. NIST Chemistry WebBook. NIST standard reference subscription database 3n, National Institute of Standards and Technology, Gaithersburg, MD, 20899, http://webbook.nist.gov.

Lim, D., Ro, H., Seo, Y., Seo, Y., Lee, J.Y., Kim, S.J., Lee, J., Lee, H., 2017. Thermodynamic stability and guest distribution of CH_4/N_2/CO_2 mixed hydrates for methane hydrate production using N_2/CO_2 injection. J. Chem. Thermodyn. 106: 16-21.

Long, X., Wang, Y., Lang, X., Fan, S., Chen, J., 2016. Hydrate equilibrium measurements for CH_4, CO_2, and CH_4 + CO_2 in the presence of tetra-n-butyl ammonium bromide. J. Chem. Eng. Data 61: 3897-3901.

Long, Z., Du, J.W., Li, D.L., Liang, D.Q., 2010. Phase equilibria of ethane hydrate in $MgCl_2$ aqueous solutions. J. Chem. Eng. Data 55: 2938-2941.

Long, Z., Zhou, X., Liang, D., Li, D., 2015. Experimental study of methane hydrate equilibria in [EMIM]-NO_3 aqueous solutions. J. Chem. Eng. Data 60: 2728-2732.

Long, Z., Zhou, X., Shen, X., Li, D., Liang, D., 2015. Phase equilibria and dissociation enthalpies of methane hydrate in imidazolium ionic liquid aqueous solutions. Ind. Eng. Chem. Res. 54: 11701-11708.

Lopez-Echeverry, J.S., Reif-Acherman, S., Araujo-Lopez, E., 2017. Peng-Robinson equation of state: 40 years through cubics. Fluid Phase Equilib. 447: 39-71.

Lu, T., Zhang, Y., Li, X.S., Chen, Z.Y., Yan, K.F., 2009. Equilibrium conditions of hydrate formation in the systems of CO_2-N_2-TBAB and CO_2-N_2-THF. Chinese J. Process Eng. 9: 541-544.

Ma, Q.L., Chen, G.J., Sun, C.Y., 2013. Vapor-liquid-liquid-hydrate phase equilibrium calculation for multicomponent systems containing hydrogen. Fluid Phase Equilib. 338: 87-94.

Ma, M., Chen, S., Abedi, J., 2019. Modeling the density, solubility and viscosity of bitumen/solvent systems using PC-SAFT. J. Petrol. Sci. Eng. 139: 1-12.

Maekawa, T., 2001. Equilibrium conditions for gas hydrates of methane and ethane mixtures in pure water and sodium chloride solution. Geochem. J. 35: 59-66.

Maekawa, T., 2010. Equilibrium conditions for carbon dioxide hydrates in the presence of aqueous solutions of alcohols, glycols, and glycerol. J. Chem. Eng. Data 55: 1280-1284.

Maekawa, T., 2014. Equilibrium conditions for clathrate hydrates formed from carbon dioxide or ethane in the presence of aqueous solutions of 1,4-dioxane and 1,3-dioxolane. Fluid Phase Equilib. 384: 95-99.

Maftoon-Azad, L., Elyasi, S., 2015. An analytical equation of state for water and aliphatic alcohols. J. Mol. Liq. 211: 667-674.

Magoulas, K., Tassios, D., 1990. Thermophysical properties of n-alkanes from C1 to C20 and their prediction for higher ones. Fluid Phase Equilib. 56: 119-140.

Mahabadian, M.A., Chapoy, A., Burgass, R., Tohidi, B., 2016. Development of a multiphase flash in presence of hydrates: Experimental measurements and validation with the CPA equation of state. Fluid Phase Equilib. 414: 117-132.

Makogon, T.Y., Sloan Jr., E.D., 1994. Phase equilibrium for methane hydrate from 190 to 262 K. J. Chem. Eng. Data 39: 351-353.

Mangold, F., Pilz, St., Bjelic, S., Vogel, F., 2019. Equation of state and thermodynamic properties for mixtures of H_2O, O_2, N_2, and CO_2 from ambient up to 1000 K and 280 MPa. J. Supercrit. Fluid. 153: 104476.

Mannar, N., Bavoh, C.B., Baharudin, A.H., Lal, B., Mellon, N.B., 2017. Thermophysical properties of aqueous lysine and its inhibition influence on methane and carbon dioxide hydrate phase boundary condition. Fluid Phase Equilib. 454: 57-63.

Mao, W.L., Mao, H.K., Goncharov, A.F., Struzhkin, V.V., Guo, Q.Z., Hu, J.Z., Shu, J.F., Hemley, R.J., Somayazulu, M., Zhao, Y.S., 2002. Hydrogen clusters in clathrate hydrate. Science 297: 2247-2249.

Marshall, B.D., 2018. Mixture equation of state for water with an associating reference fluid. Ind. Eng. Chem. Res. 57: 4070-4080.

Marshall, B.D., 2017. Perturbation theory for water with an associating reference fluid. Phys. Rev. E 96: 052602.

Marshall, D.R., Saito, S., Kobayashi, R., 1964. Hydrates at high pressures: Part I. Methane-water, argon-water, and nitrogen-water systems. AIChE J. 10: 202-205.

Martin, J.J., 1979. Cubic equations of state-which? Ind. Eng. Chem. Fundam. 18: 81-97.

Martin, A., Peters, C.J., 2009. New thermodynamic model of equilibrium states of gas hydrates considering lattice distortion. J. Phys. Chem. C 113: 422-430.

Matheis, J., Muller, H., Lenz, C., Pfitzner, M., Hickel, S., 2016. Volume translation methods for real-gas computational fluid dynamics simulations. J. Supercrit. Fluid 107: 422-432.

Mathias, P.M., Naheiri, T., Oh, E.M., 1989. A density correction for the Peng-Robinson equation of state. Fluid Phase Equilib. 47: 77-87.

Matsui, Y., Ogura, Y., Miyauchi, H., Makino, T., Sugahara, T., Ohgaki, K., 2010. Isothermal phase equilibria for binary hydrate systems of carbon dioxide + ethane and carbon dioxide + tetrafluoromethane. J. Chem. Eng. Data 55: 3297-3301.

Maximino, R.B., 1990. Surface tension and density of binary mixtures of monoalcohols, water and acetonitrile: Equation of correlation of the surface tension. Phys. Chem. Liq. 47: 475-486.

McLeod, H.O., Campbell, J.M., 1961. Natural gas hydrates at pressures to 10,000 psia. J. Pet. Technol. 13: 590-594.

McKoy, V., Sinanoglu, O., 1963. Theory of dissociation pressures of some gas hydrates. J. Chem. Phys. 38: 2946-2956.

Mech, D., Pandey, G., Sangwai, J.S., 2015. Effect of molecular weight of polyethylene glycol on the equilibrium dissociation pressures of methane hydrate system. J. Chem. Eng. Data 60: 1878-1885.

Medeiros, F.A., Segtovich, I.S.V., Barreto Jr., A.G., Tavares, F.W., 2018. Heat of dissociation from statistical thermodynamics: Using calorimetric data to estimate gas hydrate parameters. J. Chem. Thermodyn. 117: 164-179.

Medeiros, F.A., Segtovich, I.S.V., Tavares, F.W., Sum, A.K., 2020. Sixty years of the van der Waals and Platteeuw model for clathrate hydrates-A critical review from its statistical thermodynamic basis to its extensions and applications. Chem. Rev. 120: 13349-13381.

Mei, D.H., Liao, J., Yang, J.T., Guo, T.M., 1996. Experimental and modeling studies on the hydrate formation of a methane + nitrogen gas mixture in the presence of aqueous electrolyte solutions. Ind. Eng. Chem. Res. 35: 4342-4347.

Melnikov, V.P., Nesterov, A.N., Reshetnikov, A.M., Istomin, V.A., 2011. Metastable states during dissociation of carbon dioxide hydrates below 273 K. Chem. Eng. Sci. 66: 73-77.

Melo, E.B., Oliveira, E.T., Martins, T.D., 2020. A neural network correlation for molar density and specific heat of water: Predictions at pressures up to 100 MPa. Fluid Phase Equilib. 506: 112411.

Meragawi, S.E., Diamantonis, N.I., Tsimpanogiannis, I.N., Economou, I.G., 2016. Hydrate-fluid phase equilibria modeling using PC-SAFT and Peng-Robinson equations of state. Fluid Phase Equilib. 413: 209-219.

Michalis, V.K., Tsimpanogiannis, I.N., Stubos, A.K., Economou, I.G., 2016. Direct phase coexistence molecular dynamics study of the phase equilibria of the ternary methane-carbon dioxide-water hydrate system. Phys. Chem. Chem. Phys. 18: 23538-23548.

Michel, S., Hooper, H.H., Prausnitz, J.M., 1989. Mutual solubilities of water and hydrocarbons from an equation of state. Need for an unconventional mixing rule. Fluid Phase Equilib. 45: 173-189.

Michelsen, M.L., 1982. The isothermal flash problem. Part I Stability. Fluid Phase Equilib. 9: 1-19.

Michelsen, M.L., 1982. The isothermal flash problem. Part II. Phase-split calculation. Fluid Phase Equilib. 9: 21-40.

Michelsen, M.L., 1991. Calculation of hydrate fugacities. Chem. Eng. Sci. 46: 1192-1193.

Michelsen, M.L., 1994. Calculation of multiphase equilibrium. Comput. Chem. Eng. 18: 545-550.

Michelsen, M.L., Mollerup, J., 2004. Thermodynamic modelling: Fundamentals and computational aspects. Tie-Line Publications.

Miller, B., Strong, E.R., 1946. Hydrate storage of natural gas. Am. Gas Assoc. Mon. 28: 63-67.

Miller, S.L., Smythe, W.D., 1970. Carbon dioxide clathrate in the martian ice cap. Science 170: 531-533.

Mohammadi, A.H., Afzal, W., Richon, D., 2008. Experimental data and predictions of dissociation conditions for ethane and propane simple hydrates in the presence of distilled water and methane, ethane, propane, and carbon dioxide simple hydrates in the presence of ethanol aqueous solutions. J. Chem. Eng. Data 53: 73-76.

Mohammadi, A.H., Anderson, R., Tohidi, B., 2005. Carbon monoxide clathrate hydrates: Equilibrium data and thermodynamic modeling. AIChE J. 51: 2825-2833.

Mohammadi, A.H., Eslamimanesh, A., Richon, D., 2013. Semi-clathrate hydrate phase equilibrium measurements for the CO_2 + H_2/CH_4 + tetra-n-butylammonium bromide aqueous solution system. Chem. Eng. Sci. 94: 284-290.

Mohammadi, A.H., Richon, D., 2013. Clathrate hydrate phase equilibria for carbonyl sulfide, hydrogen sulfide, ethylene, or propane + water system below water freezing point. Chem. Eng. Commun. 200: 1635-1644.

Mohammadi, A.H., Tohidi, B., Burgass, R.W., 2003. Equilibrium data and thermodynamic modeling of nitrogen, oxygen, and air clathrate hydrates. J. Chem. Eng. Data 48: 612-616.

Moine, E., Pina-Martinez, A., Jaubert, J., Sirjean, B., Privat, R., 2019. I-PC-SAFT: An industrialized version of the volume-translated PC-SAFT equation of state for pure components, resulting from experience acquired all through the years on the parameterization of SAFT-type and cubic models. Ind. Eng. Chem. Res. 58: 20815-20827.

Monnery, W.D., Svrcek, W.Y., Satyro, M.A., 1998. Gaussian-like volume shifts for the Peng-Robinson equation of state. Ind. Eng. Chem. Res. 37: 1663-1672.

Mooijer-van den Heuvel, M.M., 2004. Phase behaviour and structural aspects of ternary clathrate hydrate systems. The role of additives. Ph.D. Thesis, Chemical Engineering, Delft University of Technology, Netherlands

Mooijer-van den Heuvel, M.M., Peters, C.J., de Swaan Arons, J., 2002. Gas hydrate phase equilibria for propane in the presence of additive components. Fluid Phase Equilib. 193: 245-259.

Mooijer-van den Heuvel, M.M., Witteman, R., Peters, C.J., 2001. Phase behaviour of gas hydrates of carbon dioxide in the presence of tetrahydropyran, cyclobutanone, cyclohexane and methylcyclohexane. Fluid Phase Equilib. 182: 97-110.

Moradia, G., Khosravani, E., 2013. Modeling of hydrate formation conditions for CH_4, C_2H_6, C_3H_8, N_2, CO_2 and their mixtures using the PRSV2 equation of state and obtaining the Kihara potential parameters for these components. Fluid Phase Equilib. 338: 179-187.

Morita, K., Nakano, S., Ohgaki, K., 2000. Structure and stability of ethane hydrate crystal. Fluid Phase Equilib. 169: 167-175.

Mottahedin, M., Varaminian, F., Mafakheri, K., 2011. Modeling of methane and ethane hydrate formation kinetics based on non-equilibrium thermodynamics. J. Non-Equilib. Thermodyn. 36: 3-22.

Mu, L., von Solms, N., 2018. Hydrate thermal dissociation behavior and dissociation enthalpies in methane-carbon dioxide swapping process. J. Chem. Thermodyn. 117: 33-42.

Muller, E.A., Gubbins, K.E., 1995. An equation of state for water from a simplified intermolecular potential. Ind. Eng. Chem. Res. 34: 3662-3673.

Munck, J., Skjold-Jorgensen, S., Rasmussen, P., 1988. Computations of the formation of gas hydrates. Chem. Eng. Sci. 43: 2661-2672.

Nagashima, H.D., Ohmura, R., 2016. Phase equilibrium condition measurements in methane clathrate hydrate forming system from 197.3 K to 238.7 K. J. Chem. Thermodyn. 102: 252-256.

Nakamura, T., Makino, T., Sugahara, T., Ohgaki, K., 2003. Stability boundaries of gas hydrates helped by methane—structure-H hydrates of methylcyclohexane and cis-1,2-dimethylcyclohexane. Chem. Eng. Sci. 58: 269-273.

Nakano, S., Moritoki, M., Ohgaki, K., 1998. High-pressure phase equilibrium and Raman microprobe spectroscopic studies on the CO_2 hydrate system. J. Chem. Eng. Data 4: 807-810.

Nakano, S., Moritoki, M., Ohgaki, K., 1999. High-pressure phase equilibrium and Raman microprobe spectroscopic studies on the methane hydrate system. J. Chem. Eng. Data 44: 254-257.

Nakano, S., Yamamoto, K., Ohgaki, K., 1998. Natural gas exploitation by carbon dioxide from gas hydrate fields—high-pressure phase equilibrium for an ethane hydrate system. Proc. Inst. Mech. Eng. A-J. Pow. 212: 159-163.

Nashed, O., Dadebayev, D., Khan, M.S., Bavoh, C.B., Lal, B., Shariff, A.M., 2018. Experimental and modelling studies on thermodynamic methane hydrate inhibition in the presence of ionic liquids. J. Mol. Liq. 249: 886-891.

Nascimento, F.P., Paredes, M.L.L., Pessoa, F.L.P., 2019. Evaluation of the polar contribution in the SAFT-VR Mie equation of state for simultaneous correlation of condensed-phase density, condensedphase speed of sound, saturated density and saturated pressure of pure polar fluids. J. Chem. Thermodyn. 134: 106-118.

Nazarzadeh, M., Moshfeghian, M., 2013. New volume translated PR equation of state for pure compounds and gas condensate systems. Fluid Phase Equilib. 337: 214-224.

Nema, Y., Ohmura, R., Senaha, I., Yasuda, K., 2017. Quadruple point determination in carbon dioxide hydrate forming system. Fluid Phase Equilib. 441: 49-53.

Ng, H.J., 2000. Hydrate phase composition for multicomponent gas mixtures. Ann. N. Y. Acad. Sci. 912: 1034-1039.

Ng, H.J., Petrunia, J.P., Robinson, D.B., 1977-1978. Experimental measurement and prediction of hydrate forming conditions in the nitrogen-propane-water system. Fluid Phase Equilib. 1: 283-291.

Ng, H.J., Robinson, D.B., 1976. The measurement and prediction of hydrate formation in liquid hydrocarbon-water systems. Ind. Eng. Chem. Fundamen. 15: 293-298.

Ng, H.J., Robinson, D.B., 1985. Hydrate formation in systems containing methane, ethane, propane, carbon dioxide or hydrogen sulfide in the presence of methanol. Fluid Phase Equilib. 21: 145-155.

Nichita, D.V., Broseta, D., Montel, F., 2007. Calculation of convergence pressure/temperature and stability test limit loci of mixtures with cubic equations of state. Fluid Phase Equilib. 261: 176-184.

Nixdorf, J., Oellrich, L.R., 1997. Experimental determination of hydrate equilibrium conditions for pure gases, binary and ternary mixtures and natural gases. Fluid Phase Equilib. 139: 325-333.

Obanijesu, E.O., Barifcani, A., Pareek, V.K., Tade, M.O., 2014. Experimental study on feasibility of H_2 and N_2 as hydrate inhibitors in natural gas pipelines. J. Chem. Eng. Data 59: 3756-3766.

Obeidat, A., Badarneh, M., 2019. New estimations of vapor density and surface tension of water at low temperatures using scaled model. J. Mol. Liq. 287: 110952.

Ohgaki, K., Makihara, Y., Takano, K., 1993. Formation of CO_2 hydrate in pure and sea waters. J. Chem. Eng. Japan 26: 558-564.

Ohgaki, K., Takano, K., Sangawa, H., Matsubara, T., Nakano, S., 1996. Methane exploitation by carbon dioxide from gas hydrates—Phase equilibria for CO_2-CH_4 mixed hydrate system. J. Chem. Eng. Japan 29: 478-483.

Okuno, R., Johns, R.T., Sepehrnoori, K., 2010. Three-phase flash in compositional simulation using a reduced method. SPE J. 15: 689-703.

Olseni, M.B., Majumdar, A., Bishnoi, P.R., 1999. Experimental studies on hydrate equilibrium-carbon dioxide and its systems. Int. J. Soc. of Mat. Eng. Resour. 7: 17-23.

Pahlavanzadeh, H., Hassan, H., Pourranjbar, M., 2020. Hydrate dissociation conditions of CH_4 in the presence of $TBANO_3$ and cyclopentane promoter mixture: Thermodynamic modeling and experimental measurement. J. Chem. Eng. Data 65: 1927-1935.

Pahlavanzadeh, H., Khanlarkhani, M., Mohammadi, A.H., 2016. Clathrate hydrate formation in (methane, carbon dioxide or nitrogen + tetrahydropyran or furan +

water) system: Thermodynamic and kinetic study. J. Chem. Thermodyn. 92: 168-174.

Palma, A.M., Queimada, A.J., Coutinho, J.A.P., 2017. Improved prediction of water properties and phase equilibria with a modified cubic plus association equation of state. Ind. Eng. Chem. Res. 56: 15163-15176.

Palma, A.M., Queimada, A.J., Coutinho, J.A.P., 2018. Using a volume shift in perturbed-chain statistical associating fluid theory to improve the description of speed of sound and other derivative properties. Ind. Eng. Chem. Res. 57: 11804-11814.

Palma, A.M., Queimada, A.J., Coutinho, J.A.P., 2019. Using volume shifts to improve the description of speed of sound and other derivative properties with cubic equations of state. Ind. Eng. Chem. Res. 58: 8856-8870.

Palmer, D.A., Fernandez-Prini, R., Harvey, A.H., 2004. Aqueous systems at elevated temperatures and pressures. Academic Press.

Pallares, G., Gonzalez, M.A., Abascal, J.L.F., Valeriani, C., Caupin, F., 2016. Equation of state for water and its line of density maxima down to -120 MPa. Phys. Chem. Chem. Phys. 18: 5896.

Pan, H., Connolly, M., Tchelepi, H., 2019. Multiphase equilibrium calculation framework for compositional simulation of CO_2 injection in low-temperature reservoirs. Ind. Eng. Chem. Res. 58: 2052-2070.

Paranjpe, S.G., Patil, S.L., Kamath, V.A., Godbole, S.P., 1989. Hydrate equilibria for binary and ternary mixtures of methane, propanes isobutane, and n-butane: Effect of salinity. SPE Res. Eng. 4: 446-454.

Parrish, W.R., 1984. Compressed liquid densities of ethane-propane mixtures between 10 and 49°C at pressures up to 9.6 MPa. Fluid Phase Equilib. 18: 279-297.

Parrish, W.R., Prausnitz, J.M., 1972. Dissociation pressures of gas hydrates formed by gas mixtures. Ind. Eng. Chem. Process Des. Dev. 11: 26-35.

Partoon, B., Sabil, K.M., Roslan, H., Lal, B., Keong, L.K., 2016. Impact of acetone on phase boundary of methane and carbon dioxide mixed hydrates. Fluid Phase Equilib. 412: 51-56.

Patel, N.C., Teja, A.S., 1982. A new cubic equation of state for fluids and fluid mixtures. Chem. Eng. Sci. 37: 463-473.

Patil, S.L., 1987. Measurements of multiphase gas hydrates phase equilibria: Effect of inhibitors and heavier hydrocarbon components. M.Sc. Thesis, University of Alaska, Anchorage, Alaska, USA.

Pecar, D., Dolecek, V., 2003. Isothermal compressibilities and isobaric expansibilities of pentane, hexane, heptane and their binary and ternary mixtures from density measurements. Fluid Phase Equilib. 211: 109-127.

Pedersen, K.S., Christensen, P.L., Shaikh, J.A., 2014. Phase behavior of petroleum reservoir fluids. CRC Press, 2 edition.

Peneloux, A., Rauzy, E., Freze, R., 1982. A consistent correction for Redlich-Kwong-Soave volumes. Fluid Phase Equilib. 8: 7-23.

Penoncello, S.G., 2018. Thermal energy systems: Design and analysis. CRC Press.

Peng, D.Y., Robinson, D.B., 1976. A new two-constant equation of state. Ind. Eng. Chem. Fundam. 15: 59-64.

Pina-Martinez, A., Le Guennec, Y., Privat, R., Jaubert, J., Mathias, P.M., 2018. Analysis of the combinations of property data that are suitable for a safe estimation of consistent Twu α-function parameters: Updated parameter values for the translated-consistent tc-PR and tc-RK cubic equations of state. J. Chem. Eng. Data 63: 3980-3988.

Pina-Martinez, A., Privat, R., Jaubert, J., Peng, D.Y., 2019. Updated versions of the generalized Soave α-function suitable for the Redlich-Kwong and Peng-Robinson equations of state. Fluid Phase Equilib. 485: 264-269.

Pitzer, K.S., Sterner, S.M., 1994. Equations of state valid continuously from zero to extreme pressures for H_2O and CO_2. J. Chem. Phys. 101: 3111-3116.

Platteeuw, J.C., van der Waals, J.H., 1958. Thermodynamic properties of gas hydrates. Mol. Phys. 1: 91-96.

Queimada, A.J., Miqueu, C., Marrucho, I.M., Kontogeorgis, G.M., Coutinho, J.A.P., 2005. Modeling vapor-liquid interfaces with the gradient theory in combination with the CPA equation of state. Fluid Phase Equilib. 228-229: 479-485.

Quinones-Cisnero, S.E., Zeberg-Mikkelsen, C.K., Stenby, E.H., 2001. The friction theory for viscosity modeling: extension to crude oil systems. Chem. Eng. Sci. 56: 7007-7015.

Rachford Jr., H.H., Rice, J.D., 1952. Procedure for use of electronic digital computers in calculating flash vaporization hydrocarbon equilibrium. J. Petrol. Tech. 4: 327-328.

Rackett, H.G., 1970. Equation of state for saturated liquids. J. Chem. Eng. Data 15: 514-517.

Reamer, H.H., Selleck, F.T., Sage, B.H., 1952. Some properties of mixed paraffinic and olefinic hydrates. J. Pet. Technol. 4: 197-202.

Ripmeester, J.A., Ratcliffe, C.I., 1998. The diverse nature of dodecahedral cages in clathrate hydrates as revealed by ^{129}Xe and ^{13}C NMR spectroscopy: CO_2 as a small-cage guest. Energy Fuels 12: 197-200.

Roberts, C.J., Debenedetti, P.G., Stillinger, F.H., 1990. Equation of state of the energy landscape of SPC/E water. J. Phys. Chem. B 103: 10258-10265.

Roberts, O.L., Brownscombe, E.R., Howe, L.S., 1940. Constitution diagrams and composition of methane and ethane hydrates. Oil Gas J. 39: 37-40.

Robinson, D.B., Metha, B.R., 1971. Hydrates in the propane-carbon dioxide-water system. J. Can. Pet. Technol. 10: 33-35.

Ross, M.J., Toczylkin, L.S., 1992. Hydrate dissociation pressures for methane or ethane in the presence of aqueous solutions of triethylene glycol. J. Chem. Eng. Data 37: 488-491.

Ruffine, L., Trusler, J.P.M., 2010. Phase behaviour of mixed-gas hydrate systems containing carbon dioxide. J. Chem. Thermodyn. 42: 605-611.

Rouher, O.S., Barduhn, A.J., 1969. Hydrates of iso- and normal butane and their mixtures. Desalination 6: 57-73.

Sabil, K.M., Nashed, O., Lal, B., Ismail, L., Japper-Jaafar, A., 2015. Experimental investigation on the dissociation conditions of methane hydrate in the presence of imidazolium-based ionic liquids. J. Chem. Thermodyn. 84: 7-13.

Sabil, K.M., Nasir, Q., Partoon, B., Seman, A.A., 2014. Measurement of H-L_W-V and dissociation enthalpy of carbon dioxide rich synthetic natural gas mixtures. J. Chem. Eng. Data 59: 3502-3509.

Sabil, K.M., Witkamp, G.J., Peters, C.J., 2010. Estimations of enthalpies of dissociation of simple and mixed carbon dioxide hydrates from phase equilibrium data. Fluid Phase Equilib. 290: 109-114.

Sadeq, D., Iglauer, S., Lebedev, M., Smith, C., Barifcani, A., 2017. Experimental determination of hydrate phase equilibrium for different gas mixtures containing methane, carbon dioxide and nitrogen with motor current measurements. J. Nat. Gas. Sci. Eng. 38: 59-73.

Salim, P.H., Trebble, M.A., 1991. A modified Trebble-Bishnoi equation of state: Thermodynamic consistency revisited. Fluid Phase Equilib. 65: 59-71.

Sami, N.A., Das, K., Sangwai, J.S., Balasubramanian, N., 2013. Phase equilibria of methane and carbon dioxide clathrate hydrates in the presence of (methanol + $MgCl_2$) and (ethylene glycol + $MgCl_2$) aqueous solutions. J. Chem. Thermodyn. 65: 198-203.

Sanchez-Valle, C., Mantegazzi, D., Bass, J.D., Reusser, E., 2013. Equation of state, refractive index and polarizability of compressed water to 7 GPa and 673 K. J. Chem. Phys. 138: 054505.

Saul, A., Wagner, W., 1989. A fundamental equation for water covering the range from the melting line to 1273 K at pressures up to 25000 MPa. J. Phys. Chem. Ref. Data 18: 1537-1564.

Schechter, D.S., Guo, B., 1998. Parachors based on modern physics and their uses in IFT prediction of reservoir fluids. SPE Reserv. Eval. Eng. 1: 207-217.

Schneider, G.R., Farrar, J., 1968. Nucleation and growth of ice crystals. U.S. Dept. of Interior, Office of Saline Water, Research Development Report, No. 292.

Schmid, B., Gmehling, J., 2010. From van der Waals to VTPR: The systematic improvement of the van der Waals equation of state. J. Supercrit. Fluid. 55: 438-447.

Schottler, M., Redmer, R., French, M., 2013. Low-density equation of state for water from a chemical model. Contrib. Plasm. Phys. 53: 336-346.

Segtovich, I.S.V., Barreto, A.G. Jr., Tavares, F.W., 2016. Simultaneous multiphase flash and stability analysis calculations including hydrates. Fluid Phase Equilib. 413: 196-208.

Segtovich, I.S.V., Barreto, A.G. Jr., Tavares, F.W., 2016. Phase diagrams for hydrates beyond incipient condition - Complex behavior in methane/propane and carbon dioxide/iso-butane hydrates. Fluid Phase Equilib. 426: 75-82.

Seider, W.D., Widagdo, S., 1996. Multiphase equilibria of reactive systems. Fluid Phase Equilib. 123: 283-303.

Seo, Y.T., Kang, S.P., Lee, H., Lee, C.S., Sung, W.M., 2000. Hydrate phase equilibria for gas mixtures containing carbon dioxide: A proof-of-concept to carbon dioxide recovery from multicomponent gas stream. Korean J. Chem. Eng. 17: 659-667.

Servio, P., Lagers, F., Peters, C., Englezos, P., 1999. Gas hydrate phase equilibrium in the system methane-carbon dioxide-neohexane and water. Fluid Phase Equilib. 158-160: 795-800.

Sfaxi, I.B.A., Belandria, V., Mohammadi, A.H., Lugo, R., Richon, D., 2012. Phase equilibria of CO_2 + N_2 and CO_2 + CH_4 clathrate hydrates: Experimental measurements and thermodynamic modelling. Chem. Eng. Sci. 84: 602-611.

Shi, J., Li, H., 2016. Criterion for determining crossover phenomenon in volume-translated equation of states. Fluid Phase Equilib. 430: 1-12.

Shi, J., Li, H., Pang, W., 2018. An improved volume translation strategy for PR EOS without crossover issue. Fluid Phase Equilib. 470: 164-175.

Shi, L.L., Liang, D.Q., Li, D.L., 2014. Phase equilibrium conditions for simulated landfill gas hydrate formation in aqueous solutions of tetrabutylammonium nitrate. J. Chem. Thermodyn. 68: 322-326.

Shibue, Y., 2000. A modified rackett equation applied to water and aqueous NaCl and KCl solutions. J. Chem. Eng. Data 45: 523-529.

Simeoni, G.G., Bryk, T., Gorelli, F.A., Krisch, M., Ruocco, G., Santoro, M., Scopigno, T., 2010. The Widom line as the crossover between liquid-like and gas-like behaviour in supercritical fluids. Nature Phys. 6: 503-507.

Sirino, T.H., Marcelino Neto, M.A., Bertoldi, D., Morales, R.E.M., Sum, A.K., 2018. Multiphase flash calculations for gas hydrates systems. Fluid Phase Equilib. 475: 45-63.

Sloan, E.D., 2000. Clathrate hydrates: The other common solid water phase. Ind. Eng. Chem. Res. 39: 3123-3129.

Sloan, E.D., 2003. Fundamental principles and applications of natural gas hydrates. Nature 426: 353-359.

Sloan, E.D., Koh, C.A., 2008. Clathrate hydrates of natural gases. CRC Press/Taylor & Francis.

Smith, C., Pack, D., Barifcani, A., 2017. Propane, n-butane and i-butane stabilization effects on methane gas hydrates. J. Chem. Thermodyn. 115: 293-301.

Smits, P.J., Economou, I.G., Peters, C.J., Arons, J.S., 1994. Equation of state description of thermodynamic properties of near-critical and supercritical water. J. Phys. Chem. 98: 12080-12085.

Soave, G., 1972. Equilibrium constants from a modified Redlich-Kwong equation of state. Chem. Eng. Sci. 27: 1197-1203.

Sofyan, Y., Ghajar, A.J., Gasem, K.A.M., 2003. Multiphase equilibrium calculations using Gibbs minimization techniques. Ind. Eng. Chem. Res. 42: 3786-3801.

Song, K.Y., Kobayashi, R., 1982. Measurement and interpretation of the water content of a methane-propane mixture in the gaseous state in equilibrium with hydrate. Ind. Eng. Chem. Fundam. 21: 391-395.

Soreide, I., Whitson, C.H., 1992. Peng-Robinson predictions for hydrocarbons, CO_2, N_2, and H_2S with pure water and NaCl brine. Fluid Phase Equilib. 77: 217-240.

Span, R., Wagner, W., 1996. A new equation of state for carbon dioxide covering the fluid region from the triple-point temperature to 1100 K at pressures up to 800 MPa. J. Phys. Chem. Ref. Data 25: 1509-1596.

Spencer, C.F., Danner, R.P., 1972. Improved equation for prediction of saturated liquid density. J. Chem. Eng. Data 17: 236-241.

Starling, K.E., Savidge, J.L., 1992. Compressibility factors of natural gas and other related hydrocarbon gases. American Gas Association, Transmission Measurement Committee Report No. 8.

Subramanian, S., Kini, R.A., Dec, S.F., Sloan Jr., E.D., 2000. Evidence of structure II hydrate formation from methane-ethane mixtures. Chem. Eng. Sci. 55: 1981-1999.

Sugahara, K., Tanaka, Y., Sugahara, T., Ohgaki, K., 2002. Thermodynamic stability and structure of nitrogen hydrate crystal. J. Supramol. Chem. 2: 365-368.

Sum, A.K., Burruss, R.C., Sloan Jr., E.D., 1997. Measurement of clathrate hydrates via raman spectroscopy. J. Phys. Chem. B 101: 7371-7377.

Sum, A.K., Koh, C.A., Sloan, E.D., 2009. Clathrate hydrates: From laboratory science to engineering practice. Ind. Eng. Chem. Res. 48: 7457-7465.

Sun, D., Ripmeester, J., Englezos, P., 2016. Phase equilibria for the $CO_2/CH_4/N_2/H_2O$ system in the hydrate region under conditions relevant to storage of CO_2 in depleted natural gas reservoirs. J. Chem. Eng. Data 61: 4061-4067.

Sun, S., Zhao, J., Yu, D., 2018. Dissociation enthalpy of methane hydrate in salt solution. Fluid Phase Equilib. 456: 92-97.

Sun, S.C., Liu, C.L., Meng, Q.G., 2015. Hydrate phase equilibrium of binary guest-mixtures containing CO_2 and N_2 in various systems. J. Chem. Thermodyn. 84: 1-6.

Sun, T., Takbiri-Borujeni, A., Nourozieh, H., Gu, M., 2019. Application of Peng-Robinson equation of state for modelling the multiphase equilibrium properties in Athabasca bitumen/ethane mixtures. Fuel 252: 439-447.

Sun, Y.H., Li, S.L., Zhang, G.B., Guo, W., Zhu, Y.H., 2017. Hydrate phase equilibrium of $CH_4+N_2+CO_2$ gas mixtures and cage occupancy behaviors. Ind. Eng. Chem. Res. 56: 8133-8142.

Sun, Y., Jiang, S., Li, S., Wang, X., Peng, S., 2021. Hydrate formation from clay bound water for CO_2 storage. Chem. Eng. J. 406: 126872.

Sun, Y., Zhang, G., Li, S., Jiang, S., 2019. CO_2/N_2 injection into $CH_4+C_3H_8$ hydrates for gas recovery and CO_2 sequestration. Chem. Eng. J. 375: 121973.

Sun, Z.G., Fan, S.S., Shi, L., Guo, Y.K., Guo, K.H., 2001. Equilibrium conditions hydrate dissociation for a ternary mixture of methane, ethane, and propane in aqueous solutions of ethylene glycol and electrolytes. J. Chem. Eng. Data 46: 927-929.

Svartas, T., Fadnes, F., 1992. Methane hydrate equilibrium data for the methane-water-methanol system up to 500 bara. Presented in: The Second International Offshore and Polar Engineering Conference. San Francisco, California, USA.

Takenouchi, S., Kennedy, G.C., 1965. Dissociation pressures of the phase $CO_2 \cdot 5\ 3/4\ H_2O$. J. Geol. 73: 383-390.

Tassin, N.G., Reartes, S.B.R., Cismondi, M., 2019. New correlations for prediction of high-pressure phase equilibria of n-alkane mixtures with the RKPR EoS: Back from the use of l_{ij} (repulsive) interaction parameters. J. Chem. Eng. Data 64: 2093-2109.

Tavasoli, H., Feyzi, F., 2015. Compositional data calculation of vapor-aqueous-hydrate systems in batch operations by a new algorithm. J. Nat. Gas. Sci. Eng. 24: 473-488.

Teng, H., Yamasaki, A., Chun, M.-K., Lee, H., 1997. Solubility of liquid CO_2 in water at temperatures from 278K to 293K and pressures from 6.44 MPa to 29.49 MPa and densities of the corresponding aqueous solutions. J. Chem. Thermodynamics 29: 1301-1310.

Thakore, J.L., Holder, G.D., 1987. Solid vapor azeotropes in hydrate-forming systems. Ind. Eng. Chem. Res. 26: 462-469.

Thomson, G.H., Brobst, H.R., Hankinson, R.W., 1982. An improved correlation for densities of compressed liquids and liquid mixtures. AIChE J. 28: 671-676.

Tohidi, B., Danesh, A., Burgass, R.W., and Todd, A.C., 1996. Measurement and prediction of hydrate-phase equilibria for reservoir fluids. SPE Prod. Fac. 11: 69-76.

Tohidi, B., Danesh, A., Todd, A.C., 1995. Modeling single and mixed electrolyte-solutions and its applications to gas hydrates. Chem. Eng. Res. Des. 73: 464-472.

Tohidi, B., Danesh, A., Todd, A.C., Burgass, R.W., Ostergaard, K.K., 1997. Equilibrium data and thermodynamic modelling of cyclopentane and neopentane hydrates. Fluid Phase Equilib. 138: 241-250.

Tsai, J.C., Chen, Y.P., 1998. Application of a volume-translated Peng-Robinson equation of state on vapor-liquid equilibrium calculations. Fluid Phase Equilib. 145: 193-215.

Tsimpanogiannis, I.N., Papadimitriou, N.I., Stubos, A.K., 2012. On the limitation of the van der Waals-Platteeuw-based thermodynamic models for hydrates with multiple occupancy of cavities. Mol. Phys. 110: 1213-1221.

Tsonopoulos, C., Heidman, J.L., 1986. High-pressure vapor-liquid equilibria with cubic equation of state. Fluid Phase Equilib. 29: 391-411.

Twu, C.H., Bluck, D., Cunningham, J.R., Coon, J.E., 1991. A cubic equation of state with a new alpha function and a new mixing rule. Fluid Phase Equilib. 69: 33-50.

Twu, C.H., 1988. A modified Redlich-Kwong equation of state for highly polar, supercritical systems. Presented at the Proceedings of the International Symposium on Thermodynamics in Chemical Engineering and Industry, Beijing China.

Unruh, C.H., Katz, D.L., 1949. Gas hydrates of carbon dioxide-methane mixtures. J. Pet. Technol. 1: 83-86.

Valderrama, J.O., Alfaro, M., 2000. Liquid volumes from generalized cubic equations of state: Take it with care. Oil Gas Sci. Technol. 55: 523-531.

Valoerrama, J.O., Cisternas, L.A., 1986. A cubic equation of state for polar and other complex mixtures. Fluid Phase Equilib. 29: 431-438.

Valtz, A., Chapoy, A., Coquelet, C., Paricaud, P., Richon, D., 2004. Vapour-liquid equilibria in the carbon dioxide-water system, measurement and modelling from 278.2 to 318.2 K. Fluid Phase Equilib. 226: 333-344.

Van Cleeff, A., Diepen, G.A.M., 1960. Gas hydrates of nitrogen and oxygen. Rec. Trav. Chim. 79: 582-586.

van der Waals, J.D., 1873. Continuity of the gaseous and liquid state of matter. Ph.D. thesis, Leiden.

van der Waals, J.H., Platteeuw, J.C., 1959. Clathrate solutions. Adv. Chem. Phys. 2: 1-57.

Veesam, S.K., Punnathanam, S.N., 2019. VdWP-FL: An improved thermodynamic theory for gas hydrates with free-energy contributions due to hydrate lattice flexibility. J. Phys. Chem. C 123: 26406-26414.

Venkatarathnam, G., Oellrich, L.R., 2011. Identification of the phase of a fluid using partial derivatives of pressure, volume, and temperature without reference to saturation properties: Applications in phase equilibria calculations. Fluid Phase Equilib. 301: 225-233.

Verdier, S., Duong, D., Andersen, S.I., 2005. Experimental determination of solubility parameters of oils as a function of pressure. Energy Fuels 19: 1225-1229.

Verma, V.K., 1974. Gas hydrates from liquid hydrocarbon-water systems. Ph.D. Thesis, Department of Chemical Engineering, University of Michigan, USA.

Vins, V., Jager, A., Span, R., Hruby, J., 2016. Model for gas hydrates applied to CCS systems part I. Parameter study of the van der Waals and Platteeuw model. Fluid Phase Equilib. 427: 268-281.

Vlahakis, J.G., Chen, H.S., Suwandi, M.S., Barduhn, A.J., 1972. The growth rate of ice crystals: Properties of carbon dioxide hydrate, a review of properties of 51 gas hydrates. Syracuse U, Research and Development Report, No. 830.

Wagner, W., Pruβ, A., 2002. The IAPWS formulation 1995 for the thermodynamic properties of ordinary water substance for general and scientific use. J. Phys. Chem. Ref. Data 31: 387-535.

Wang, Z., Zhang, J., Sun, B., Chen, L., Zhao, Y., Fu, W., 2017. A new hydrate deposition prediction model for gas-dominated systems with free water. Chem. Eng. Sci. 163: 145-154.

Wang, Z., Zhao, Y., Zhang, J., Wang, X., Yu, J., Sun, B., 2018. Quantitatively assessing hydrate-blockage development during deepwater-gas-well testing. SPE J. 23: 1166-1183.

Ward, Z.T., Deering, C.E., Marriott, R.A., Sum, A.K., Sloan, E.D., Koh, C.A., 2015. Phase equilibrium data and model comparisons for H_2S hydrates. J. Chem. Eng. Data 60: 403-408.

Watson, P., Cascella, M., May, D., Salerno, S., Tassios, D., 1986. Prediction of vapor pressures and saturated molar volumes with a simple cubic equation of state. 2. The Van der Waals-711 EOS. Fluid Phase Equilib. 27: 35-52.

Wendland, M., Hasse, H., Maurer, G., 1999. Experimental pressure−temperature data on three- and four-phase equilibria of fluid, hydrate, and ice phases in the system carbon dioxide−water. J. Chem. Eng. Data 44: 901-906.

Whitson, C.H., Michelsen, M.L., 1989. The negative flash. Fluid Phase Equilib. 53: 51-71.

Wilcox, W.I., Carson, D.B., Katz, D.L., 1941. Natural gas hydrates. Ind. Eng. Chem. 33: 662-665.

Wiryana, S., Slutsky, L.J., Brown, J.M., 1970. The equation of state of water to 200ºC and 3.5 GPa: Model potentials and the experimental pressure scale. Earth Planet. Sci. Lett. 163: 123-130.

Wu, B.J., Robinson, D.B., Ng, H.J., 1976. Three- and four-phase hydrate forming conditions in methane + isobutane + water. J. Chem. Thermodyn. 8: 461-469.

Wu, J., Prausnitz, J.M., 1998. Phase equilibria for systems containing hydrocarbons, water, and salt: An extended Peng-Robinson equation of state. Ind. Eng. Chem. Res. 37: 1634-1643.

Xu, Z.C., Liang, D.Q., 2014. Equilibrium data of (tert-butylamine + CO_2) and (tert-butylamine + N_2) clathrate hydrates. J. Chem. Eng. Data 59: 476-480.

Xiao, K., Zou, C., Yang, Y., Zhang, H., Li, H., Qin, Z., 2020. A preliminary study of the gas hydrate stability zone in a gas hydrate potential region of China. Energy Sci. Eng. 8: 1080-1091.

Yasuda, K., Ohmura, R., 2008. Phase equilibrium for clathrate hydrates formed with methane, ethane, propane, or carbon dioxide at temperatures below the freezing point of water. J. Chem. Eng. Data, 53: 2182-2188.

Yang, S.O., Cho, S.H., Lee, H., Lee, C.S., 2001. Measurement and prediction of phase equilibria for water + methane in hydrate forming conditions. Fluid Phase Equilib. 185: 53-63.

Yoon, J.-H., Chun, M.-K., Lee, H., 2002. Generalized model for predicting phase behavior of clathrate hydrate. AIChE J. 48: 1317-1330.

Yoon, J.-H., Yamamoto, Y., Komai, T., Kawamura, T., 2004. PSRK method for gas hydrate equilibria: I. Simple and mixed hydrates. AIChE J. 50: 203-214.

Young, A.F., Pessoa, F.L.P., Ahon, V.R.R., 2017. Comparison of volume translation and co-volume functions applied in the Peng-Robinson EoS for volumetric corrections. Fluid Phase Equilib. 435: 73-87.

Yu, Y., Zhou, S., Li, X., Wang, S., 2016. Effect of graphite nanoparticles on CO_2 hydrate phase equilibrium. Fluid Phase Equilib. 414: 23-28.

Zang, X., Liang, D., 2017. Phase equilibrium data for semiclathrate hydrate of synthesized binary CO_2/CH_4 gas mixture in tetra-n-butylammonium bromide aqueous solution. J. Chem. Eng. Data 62: 851-856.

Zang, X., Liang, D., 2018. Phase equilibrium data for the hydrates of synthesized ternary $CH_4/CO_2/N_2$ biogas mixtures. J. Chem. Eng. Data 63: 197-201.

Zang, X., Wan, L., Liang, D., 2019. Investigation of the hydrate formation process in fine sediments by a binary CO_2/N_2 gas mixture. Chinese J. Chem. Eng. 27: 2157-2163.

Zeberg-Mikkelsen, C.K., 2001. Viscosity study of hydrocarbon fluids at reservoir conditions, Ph.D. thesis, Technical University of Denmark.

Zhang, J., Wang, Z., Liu, S., Zhang, W., Yi, J., Sun, B., 2019. Prediction of hydrate deposition in pipelines to improve gas transportation efficiency and safety. Appl. Energ. 253: 113521.

Zhang, J., Wang, Z., Sun, B., Sun, X., Liao, Y., 2019. An integrated prediction model of hydrate blockage formation in deep-water gas wells. Int. J. Heat Mass Tran. 140: 187-202.

Zhang, Y.D., Wang, D., Yang, J.P., Tian, L., Wu, L., 2016. Research on the hydrate formation in the process of gas phase CO_2 pipeline transportation. Int. J. Heat Technol. 34: 339-344.

Zheng, R., Fan, Z., Li, X., Negahban, S., 2021. Phase boundary of CH_4, CO_2, and binary CH_4-CO_2 hydrates formed in NaCl solutions. J. Chem. Thermodyn. 154: 106333.

Zhong, D., Englezos, P., 2012. Methane separation from coal mine methane gas by tetra-n-butyl ammonium bromide semiclathrate hydrate formation. Energy Fuels 26: 2098-2106.